

**A COMPARATIVE STUDY ON SIZE SEGREGATED  
ULTRAFINE PARTICLE CONCENTRATION AND ITS  
TEMPORAL DISTRIBUTION IN URBAN AND  
BACKGROUND REGIONS**

**By**

**VIGNESH MOHAN**

**Environmental Science & Engineering**

Submitted

*In fulfilment of the requirements of the degree*

**of**

**DOCTOR OF PHILOSOPHY**

**to**



**Department of Environmental Science & Engineering  
DELHI TECHNOLOGICAL UNIVERSITY  
DELHI-110042, INDIA  
NOVEMBER 2025**

**A COMPARATIVE STUDY ON SIZE SEGREGATED  
ULTRAFINE PARTICLE CONCENTRATION AND ITS  
TEMPORAL DISTRIBUTION IN URBAN AND  
BACKGROUND REGIONS**

**A Thesis Submitted  
In Fulfilment of the Requirements  
for the Award of the Degree  
of**

**DOCTOR OF PHILOSOPHY**  
by

**VIGNESH MOHAN**  
(2K20/PHDEN/05)

**Under the Supervision of**

**Dr. Rajeev Kumar Mishra**

**Associate Professor, Department of Environmental Science & Engineering  
Delhi Technological University**

**And**

**Dr. Vijay Kumar Soni**

**Scientist - F**

**India Meteorological Department**



**To the  
Department of Environmental Science & Engineering  
DELHI TECHNOLOGICAL UNIVERSITY  
(Formerly Delhi College of Engineering)  
Shahbad Daultpur, Main Bawana Road, Delhi-110042, India  
November, 2025**

**©DELHI TECHNOLOGICAL UNIVERSITY-2025**  
**ALL RIGHTS RESERVED**



# DELHI TECHNOLOGICAL UNIVERSITY

(Formerly Delhi College of Engineering)

Shahbad Daultapur, Main Bawana Road, Delhi-110042

## DECLARATION

I hereby declare that the research work presented in this thesis entitle **“A comparative study on size segregated ultrafine particle concentration and its temporal distribution in urban and background regions”** is original and carried out by me under the supervision of Dr. Rajeev Kumar Mishra, Associate Professor, Department of Environmental Science & Engineering, Delhi Technological University, Delhi, and Dr. Vijay Kumar Soni, Scientist - F, India Meteorological Department, Delhi, being submitted for the award of Ph.D. degree to Delhi Technological University, Delhi, India. The content of this thesis has not been submitted either in part or whole to any other university or institute for the award of any degree or diploma.

Date:     /     / 2025

(Vignesh Mohan)

Place: DTU, Delhi.

2K20/PHDEN/05





# DELHI TECHNOLOGICAL UNIVERSITY

(Formerly Delhi College of Engineering)

Shahbad Daultpur, Main Bawana Road, Delhi-110042

## CERTIFICATE

Date: - / /2025

This is to certify that the Ph.D thesis entitled, “**A comparative study on size segregated ultrafine particle concentration and its temporal distribution in urban and background regions**”, being submitted by Mr. Vignesh Mohan for the fulfilment of the requirements for the award of the degree of Doctor of Philosophy in Environmental Science & Engineering, to the Department of Environmental Science & Engineering, Delhi Technological University, Delhi, India, is a bonafide record of original research work carried out by him under my guidance and supervision. The results embodied in this thesis have not been submitted to any other university or institution for the award of any degree or diploma.

Dr. Rajeev Kumar Mishra  
Supervisor  
Delhi Technological University  
Delhi – 110042

Dr. Vijay Kumar Soni  
Co-supervisor  
India Meteorological Department  
Delhi – 110003



# **DELHI TECHNOLOGICAL UNIVERSITY**

(Formerly Delhi College of Engineering)

Shahbad Daultpur, Main Bawana Road, Delhi-110042

## **PLAGIARISM VERIFICATION**

Title of the Thesis: **A comparative study on size segregated ultrafine particle concentration and its temporal distribution in urban and background regions.**

Total Pages:

Name of the Scholar: VIGNESH MOHAN

Supervisor (s)

(1) Dr. Rajeev Kumar Mishra

(2) Dr. Vijay Kumar Soni

Department \_\_\_\_\_

This is to report that the above thesis was scanned for similarity detection. Process and outcome is given below:

Software used: Turnitin, Similarity Index: \_\_\_\_\_, Total Word Count: \_\_\_\_\_

Date: \_\_\_\_\_

**Candidate's Signature**

**Signature of Supervisor(s)**



# DELHI TECHNOLOGICAL UNIVERSITY

(Formerly Delhi College of Engineering)

Shahbad Daultpur, Main Bawana Road, Delhi-42

## CANDIDATE'S DECLARATION


I, VIGNESH MOHAN hereby declare that the research work presented in this thesis entitled **“A comparative study on size segregated ultrafine particle concentration and its temporal distribution in urban and background regions”** in fulfilment of the requirement of the award of Degree of Doctor of Philosophy, submitted in the Department of Environmental Science & Engineering, Delhi Technological University is authentic record of my on work carried out during the period from August 2020 to December 2025 under the supervision of Dr. Rajeev Kumar Mishra, Associate Professor, Department of Environmental Science & Engineering, Delhi Technological University, Delhi and co-supervision of Dr. Vijay Kumar Soni, Scientist - F, India Meteorological Department, Delhi.

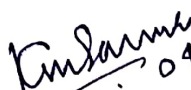
The matter present in this thesis has not been submitted either in part or whole to any other university or institute for the award of any degree or diploma.

  
Candidate's Signature

(Vignesh Mohan)

This is to certify that the student has incorporated all the corrections suggested by the examiners in the thesis, and the statement made by the candidate is correct to the best of our knowledge.

  
04-11-2025  
Signature of Supervisor(s)

  
04.11.2025  
Signature of the External Examiner

(Prof. Kiranmay Sarma GGSIPU -Delhi)

**Dedicated**

**To**

**My Parents**

**Sh. Mohan B,**

**Mrs. Usha Nandhini M**

**And**

**Our home's special little one**

**"Nihan"**

## ACKNOWLEDGEMENTS

I would like to express my appreciation to the people who have helped me the most during my research work. First and foremost, I am deeply grateful to my research supervisor, Dr. Rajeev Kumar Mishra, and co-supervisor Dr. Vijay Kumar Soni for their nonstop guidance, enduring patience, and nurturing support throughout this research, without which successful completion would not have been possible. It has been an honor to be associated with such a great supervisor and learn from his experience.

I accord my heartfelt thanks to Dr. Geeta Singh, Head, and Prof. Anil Kumar Haritash, DRC Chairman, Department of Environmental Science & Engineering, Delhi Technological University. I extend my thanks to other faculty members from Environmental Science & Engineering. I extend my thanks to the members of the India Meteorological Department for their support, which helped me to learn many things throughout my research.

I am grateful to my colleagues, Dr. Amrit Kumar, Dr. Shailendra Kumar Yadav, Dr. Abhinav Pandey, Dr. Amit Krishan, Ms. Monika Sharma, Mr. Ravi Pratap Singh Jadon, Mr. Anil Maan, Mr. Abhishek Kumar Yadav, Mr. Vishu Tomar, and Ms. Shweta Meena for providing me with critical comments and suggestions and all those who interacted and exchanged ideas with me in completing the research. I extend my thanks to my friend and colleague, Dr. Kanagaraj Rajagopal. Since 2011, we have travelled together up to now. I would like to take a moment to express my sincere gratitude for your valuable help and guidance.

I want to extend special thanks to the immense contribution made by my family, especially my brother (Suriya Prakash) and sister-in-law (Abinaya), who not only encouraged and supported me but also stood by me like a pillar and gave me constant motivation. All my family members have shown enormous patience during this process and have cheerfully sacrificed the time that rightfully belonged to them. I extend special thanks to my sister (Sathyavidhya), who helped me during my Ph.D.

Last but not least, I pay my everlasting thanks and gratitude to all my friends and the Almighty who were always there to guide me eternally and help me to become who I am.

## LIST OF PUBLICATIONS

### Research Publication

1. **Vignesh Mohan**, Vijay Kumar Soni, Rajeev Kumar Mishra (2024). “Analysing the impact of day-night road traffic variation on ultrafine particle number size distribution and concentration at an urban site in the megacity Delhi”. Atmospheric Pollution Research. <https://doi.org/10.1016/j.apr.2024.102065>.
2. **Vignesh Mohan**, Vijay Kumar Soni, Rajeev Kumar Mishra (2024). “Geographical variability of ultrafine particle concentrations in urban and background regions in India”. Urban Climate. <https://doi.org/10.1016/j.uclim.2024.102066>.
3. Kanagaraj Rajagopal, **Vignesh Mohan**, Monika Sharma, Shailendra Kumar Yadav, Veerendra Sahu, Rajeev Kumar Mishra, Sneha Gautam, Bhola Ram Gurjar & Prashant Kumar (2025). “Impact of the odd-even scheme on particulate matter reduction in Delhi traffic intersections”. Particulate Science and Technology. <https://doi.org/10.1080/02726351.2025.2558979>.
4. **Vignesh Mohan**, Rajeev Kumar Mishra, Vijay Kumar Soni (2024). “Air Quality Analysis in Desert Region in the Northern State of India: GIS Based Approach”. Journal of the Indian Society of Remote Sensing. <https://doi.org/10.1007/s12524-024-02073-z>.
5. Kanagaraj Rajagopal, **Vignesh Mohan**, Rajeev Kumar Mishra (2024). “Are Delhi residents exposed to lesser particle number concentration due to the firework ban in the city?”. Air Quality, Atmosphere & Health. <https://doi.org/10.1007/s11869-024-01532-3>.
6. **Vignesh Mohan**, Rajeev Kumar Mishra (2022). “A picture of Delhi’s regional air quality during diminished anthropogenic activities in the COVID era”. Arabian Journal of Geosciences. <https://doi.org/10.1007/s12517-022-10567-8>.
7. Shailendra Kumar Yadav, Raghav Sharma, Sankalp Kumar, Aviral Agarwal, **Vignesh Mohan**, Rajeev Kumar Mishra, Ankita Shukla (2021). “Urban air pollution reduction: evidence from phase-wise analysis of COVID-19 pandemic lockdown”. Arabian Journal of Geosciences. <https://doi.org/10.1007/s12517-021-07777-x>.

**Communicated / about to communicate**

1. **Vignesh Mohan**, Amit Kumar Yadav, Vijay Kumar Soni, Rajeev Kumar Mishra. “Rapid growth of new particle formation events in Delhi: Insights from field measurements and varying meteorological parameters”.
2. **Vignesh Mohan**, Kanagaraj Rajagopal, Shailendra Kumar Yadav, S. Ramachandran, Vijay Kumar Soni, Rajeev Kumar Mishra. “Phenomenology of the size distribution and number concentration trends of Delhi, India, using 3 years of data of the urban roadside environment”.
3. Shailendra Kumar Yadav, Monika Sharma, Kanagaraj Rajagopal, **Vignesh Mohan**, Veerendra Sahu, Rajeev Kumar Mishra, Bholaram Gurjar. “Investigating the effects of Delhi's odd-even vehicle restriction policy on particle number concentration”.

### **Conference**

1. **Vignesh Mohan**, Rajeev Kumar Mishra, Vijay Kumar Soni (2024). “Analysing the particle number concentration in day-night traffic variation during the winter period in the megacity Delhi”. International Conference on Sustainable Development in Air and Waste Management, Department of Civil Engineering, AMU, Aligarh, on 20<sup>th</sup> - 21<sup>st</sup> December 2024.
2. **Vignesh Mohan**, Rajeev Kumar Mishra, Vijay Kumar Soni (2023). Seasonal and Temporal Distribution of urban fine particulates and associated health risk analysis: A long-term measurement (2018 - 2020) analysis in megacity Delhi. 8<sup>th</sup> Indian International Conference on Air Quality Management (IICAQM 2023), Indian Institute of Science (IISC) Bangalore, on 6<sup>th</sup> - 8<sup>th</sup> December 2023.
3. Shailendra Kumar Yadav, Monika Sharma, Kanagaraj Rajagopal, **Vignesh Mohan**, Veerendra Sahu, Rajeev Kumar Mishra, Bholaram Gurjar (2024). Investigating the effects of Delhi’s odd-even vehicle restriction policy on particle number concentration. International Conference on Waste Recycling and Environmental Technology (WRET-2024), Department of Environmental Science, Babasaheb Bhimrao Ambedkar University (A Central University), Lucknow, India, on 8<sup>th</sup> - 9<sup>th</sup> February 2024.



## ABSTRACT

In developing countries like India, air pollutants have become a serious issue. Industrialization and urbanization have greatly boosted the Indian economy. On the other hand, they have also brought about a drastic change in the environment. Due to various natural and anthropogenic activities, different pollutants are released into the atmosphere. Air pollution is still a major problem faced by the whole world, resulting in 6.2 million deaths throughout the world and 6,20,000 premature deaths in India alone. The alarming increase in air pollutants, with its intensity on the higher side, has resulted in numerous health issues and lung diseases, including chronic respiratory disorders, pneumonia, acute asthma, and shortness of breath. Although technological advancements have improved our understanding of ultrafine particles and air quality, many environmental conditions and scientific problems remain unresolved. Ultrafine particles in the atmosphere are formed due to natural and anthropogenic activities, including photochemical reactions and combustion processes. Atmospheric aerosols persist in solid or liquid form and significantly impact a region's air quality, contributing to climate change and affecting human health. The concentration of the ultrafine particles in a region is highly dependent on the intensity of the emission sources, represented by the number concentration. The ultrafine particle concentration is quantified in terms of particle number concentration (PNC) per unit volume of air, expressed as the number of particles per cubic centimeter ( $\text{cm}^3$ ). Ultrafine particles are considered a universal carrier of a wide variety of toxic chemicals to humans. The deposition of particles in the human respiratory system varies based on the size of the particles, which are categorized into nucleation, Aitken, and accumulation modes. Also, the concentration of these particles signifies the emission sources in a particular region. These can enter the deeper regions of the respiratory system, such as the alveoli, and can be transported to the circulatory system, allowing them to reach any organ in the body. This study analyzes the year-long measurements of particle number size distribution (10.21-1090.23 nm) in 2022 in the urban traffic corridor of the megacity Delhi. The study examined particle number concentration in the ultrafine (<100 nm) and accumulation (100-1000 nm) ranges during both day and night, in terms of the source's intensity, emission patterns, and local meteorological conditions. Further, the ultrafine particles (< 100 nm) are separated into three mode size fractions

( $N_{nuc}$ ,  $N_{atk}$ , and  $N_{acc}$ ) were also considered, and the data set was analyzed for the different meteorological periods and day and night time in terms of sources and type of emission (from CNG, petrol, and diesel vehicular exhaust) and meteorology. Nucleation mode particles ( $N_{nuc}$ , 10-30 nm) contributed ~50% during the daytime in the summer period due to increased fresh traffic emissions. During the daytime, particle concentration was dominated by smaller sizes, such as nucleation mode particles ( $N_{nuc}$ , 30-100 nm), while at nighttime, the particles were found in the Aitken and Accumulation ( $N_{acc}$ , 100-1000 nm) modes.  $N_{nuc}$  and  $N_{atk}$  were reduced by ~45% and 4% at night, while  $N_{acc}$  increased by ~34%. The mean normalized particle number size distribution confirmed these findings, showing clearly that  $N_{nuc}$  dominated during the daytime, especially during peak rush hours, and at night, particle concentration increased up to the size of 300 nm particles. The particle number size distribution and the changes experienced in the percentage concentration of the different particle size ranges highlight the role of engine exhaust emissions in the atmospheric particles contributed in urban areas. The study's findings help identify the intensity and behavior of different sources during the day and nighttime, which can inform policy formulation and decision-making to mitigate air quality and its associated health impacts.

The study measured and analysed the particle number concentration of particles ranging from 10 nm to 800 nm in urban and background sites. The aim of the study is to estimate the role of anthropogenic sources in urban regions in terms of number concentration. The study finds that the particle number concentration in an urban site is ~8 times higher than in the background sites. At the urban site, the Aitken and Nucleation modes contributed more to the total particle concentration, whereas at the background site, it was the Aitken and Accumulation modes. The annual average concentrations at the urban and background sites were  $2.5 \times 10^4$ ,  $2.9 \times 10^3 \text{ cm}^{-3}$ , respectively. Aitken-mode particles dominated both in the urban and background sites, with the lowest concentrations observed in the summer ( $6.4 \times 10^2 \text{ cm}^{-3}$ ) and monsoon periods ( $1.09 \times 10^2 \text{ cm}^{-3}$ ), respectively. The diurnal concentration illustrates the role of transportation emissions at the urban site and the natural process of particle condensation at the background site. The long-range transportation of sources indicates that during the winter and autumn seasons, the westerly and north-westerly winds bring biomass burning emissions smoke to the urban region, which is less visible

in the background conditions.

Road traffic emissions are often identified as the leading source of ultrafine particles in urban environments. However, recent international studies have revealed that in cities with elevated solar radiation, the occurrence of new particle formation events may also significantly contribute to the levels of ultrafine particles. To assess the frequency and effects of these events, a comprehensive study was carried out in Delhi from January to December 2022. The analysis showed that the highest mean concentration of total particle number concentration ( $N_{\text{tot}}$ ) followed the order of Post-Monsoon > Winter > Monsoon > Summer. The Aitken particle contribution ( $N_{\text{atk}}$ ) to  $N_{\text{tot}}$  was approximately 52% on event days and 46% on non-event days. Throughout the year, 23 new particle formation (NPF) events were identified, accounting for 6% of the total days, which included 2 nocturnal and 21 midday occurrences. During the nocturnal events, ammonia levels increased by about 34%, which aids in the growth of newly formed particles. The remaining NPF events predominantly occurred during daylight hours, when solar radiation was a crucial factor in particle generation. The highest growth rates were observed in winter ( $12.07 \pm 1.07 \text{ nm h}^{-1}$ ), while the condensation sink (cs) was highest in the post-monsoon period ( $0.087 \pm 0.039 \text{ s}^{-1}$ ). The presence of larger pre-existing particles during the post-monsoon season appeared to hinder formation rates but enhance particle growth. An increase in particle numbers was associated with a decrease in the condensation sink throughout the day. Winds from the northwest direction were conducive to new particle formation, coinciding with increased solar radiation and temperature, alongside a decrease in relative humidity. In summary, although traffic remains the predominant source of ultrafine particles (UFP) in urban areas, urban nucleation events also represent a significant source of UFP. A future decline in traffic-related particle concentrations is expected; however, an increase in nucleation events in urban areas is likely due to the reduced capacity of urban condensation sinks.

The festival of Diwali, characterized by extensive fireworks displays in India, significantly contributes to the increase of atmospheric particles over a brief period, thereby compromising air quality. Implementing short-term measures, such as prohibiting the use of firecrackers during these celebrations, can enhance urban air quality. This study examined particle number concentrations ranging from 10 nm to

1000 nm during the years 2021 and 2022. A notable decrease in particle number concentration was recorded, dropping from  $3.8 \times 10^4 \text{ cm}^{-3}$  to  $3.1 \times 10^4 \text{ cm}^{-3}$ , following the ban on firecrackers in Delhi. The concentration range shifted from  $10^5 \text{ cm}^{-3}$  to  $10^4 \text{ cm}^{-3}$ . The analysis of various size categories, Nucleation (10 nm to 30 nm), Aitken (30 nm to 100 nm), and Accumulation (100 nm to 1000 nm), revealed that on Diwali day, Accumulation mode particles accounted for approximately 60% to 83% of the total particle number concentration. Furthermore, the total inhalable particle concentration exposure on Diwali day was reduced by about 18%, equating to 1.6 million particles per day. The findings of this study indicate that significant reductions in emissions within urban environments can be achieved through effective policy implementation and active citizen engagement. Lowering particle emissions is crucial for enhancing air quality, minimizing health risks, and promoting sustainability. The overarching sustainability objectives emphasize the necessity of clean air for all, while health improvements in polluted areas represent achievable interim goals through the execution of appropriate mitigation strategies, which also contribute to combating climate change.

## TABLE OF CONTENTS

<i>Declaration</i> .....	<i>i</i>
<i>CERTIFICATE</i> .....	<i>ii</i>
<i>ACKNOWLEDGEMENTS</i> .....	<i>vi</i>
<i>LIST OF PUBLICATIONS</i> .....	<i>vii</i>
<i>Abstract</i> .....	<i>x</i>
<i>TABLE OF CONTENTS</i> .....	<i>xiv</i>
<i>LIST OF FIGURES</i> .....	<i>xviii</i>
<i>LIST OF TABLES</i> .....	<i>xxiii</i>
<i>LIST OF ABBREVIATIONS</i> .....	<i>xxiv</i>
CHAPTER – 1 .....	1
INTRODUCTION .....	1
1.1. Introduction .....	1
1.2. Objectives of the study .....	4
1.2.1 Novelty and significance of the study .....	4
1.2.2 Policy relevance and societal importance .....	5
1.3. Thesis structure .....	5
1.4. Summary .....	7
CHAPTER - 2 .....	8
LITERATURE REVIEW .....	8
2.1 Introduction .....	8
2.2 UFPs definition, size range and mode classification .....	12
2.3 Sources of ultrafine particle number concentration .....	14
2.3.1 Forest fires .....	15
2.3.2 Volcanic eruption .....	17
2.3.3 Marine aerosols .....	20
2.3.4 Industrial emissions .....	22
2.3.5 Transport sector .....	23
2.3.6 Indoor ultrafine particles .....	25
2.4 Particle number concentration in roadside-microenvironment .....	29
2.5 Particle number concentration in regional background .....	32
2.6 Comparison between the urban regions and other regions .....	33

2.7 Role of meteorological parameter in particle number concentration -----	35
2.8 New particle formation in different microenvironments -----	36
2.9 Ultrafine particle in Indian scenarios -----	40
2.10 Health impact of ultrafine particles -----	42
2.11 Summary -----	45
CHAPTER - 3 -----	47
METHODOLOGY -----	47
3.1 Introduction -----	47
3.2 Site selection -----	49
3.3 Instrumentation -----	55
3.3.1 Particle monitoring instruments -----	55
3.3.2 Gaseous monitoring instruments -----	58
3.3.3 Weather monitoring instruments -----	61
3.4 HYSPLIT trajectory -----	62
3.5 Limitations of the study -----	66
3.6 Statistics and equations -----	66
3.6.1 Statistics analysis -----	66
3.6.2 Calculation of particle number size distribution -----	66
3.6.3 Calculation of polar plot -----	67
3.7 New particle formation event and calculation -----	68
3.7.1 Event classification -----	68
3.7.2 Calculation of the growth rate -----	68
3.7.3 Calculation of the condensation sink -----	69
3.7.4 Calculation of the coagulation sink -----	69
3.8 Summary -----	70
CHAPTER – 4 -----	71
RESULTS AND DISCUSSION -----	71
4.1 Introduction -----	71
4.2 Year-long calendar plot for urban and background regions -----	72
4.3 Traffic emissions and meteorological factors -----	74
4.4 Particle number concentration and its variation -----	79

4.4.1 Particle number concentration of different particle sizes during day and nighttime in urban site -----	79
4.4.2 Variation in particle number concentration in an urban and a background site --- -----	81
4.4.3 Diurnal variations of mode particle number concentration in the urban and background sites-----	84
4.5 Mode contributions to the total particle number concentration-----	86
4.5.1 Contribution from different mode particles in urban site -----	86
4.5.2 Particle number contribution during the winter period in urban site -----	88
4.6 Particle number size distribution-----	90
4.6.1 Particle number size distribution during day and nighttime in urban site -----	90
4.6.2 Particle number size distribution during day and nighttime in winter period ---	92
4.6.3 Particle size distribution in an urban and a background site -----	94
4.6.4 Correlation between the number concentration with particulate matter, gaseous, and meteorological parameters -----	96
4.7 Role of meteorological parameters -----	98
4.7.1 Influence of meteorology on the particle number concentration and its size distribution in urban site -----	98
4.7.2 Impact of meteorological conditions on particle number concentration during winter period -----	100
4.7.3 Role of wind speed and direction on particle dispersion in urban and background site -----	101
4.7.4 Long-range dispersion pattern in urban and background site -----	103
4.7.5 Diurnal variation of meteorological conditions in urban and background site --- -----	105
4.8 Role of new particle formation in urban microenvironment -----	108
4.8.1 Overview of the new particle formation events -----	108
4.8.2 Nocturnal new particle events in Delhi -----	110
4.8.3 Other new particle events in Delhi -----	113
4.8.4 Diurnal variation in event and non-event days -----	119
4.8.5 Role of meteorological parameters in NPF event days -----	122
4.9 Episodic event during the monitoring period -----	124

4.9.1 Introduction -----	124
4.9.2 Temporal variability of particle number concentration -----	126
4.9.3 Size-resolved particle distribution during diwali -----	128
4.9.4 Different mode particle contribution to the total number particle concentration - -----	130
4.9.5 Hourly analysis of particle contribution -----	132
4.9.6 Percentage variations in size-resolved particle concentration -----	135
4.9.7 Diurnal variation of particle concentration -----	136
4.9.8 Exposure analysis -----	139
4.9.8.1 Inhalable particle assessment -----	139
4.10 Summary -----	141
CHAPTER – 5 -----	142
CONCLUSION -----	142
5.1 General -----	142
5.2 Ultrafine particle number concentration during day and nighttime near selected urban roadside -----	142
5.2.1 Key takeaways from the results -----	143
5.3 Particle number concentration of ultrafine particles in urban and background regions -----	143
5.3.1 Key takeaways from the results -----	144
5.4 Role of micrometeorological parameters in urban and background ultrafine particle number concentration -----	144
5.4.1 Key takeaways from the results -----	146
5.5 Role of new particle formation in urban microenvironment -----	147
5.5.1 Key takeaways from the results -----	148
5.6 Particle number concentration during the diwali period -----	148
5.6.1 Key takeaways from the results -----	149
5.7 Importance of the study -----	150
5.8 Future Prospects of study -----	151
5.9 SDGs alignment -----	151
5.10 Summary -----	152
References -----	153



## LIST OF FIGURES

Figure 2.1. Particle number size and particle mass distribution (Source: Hinds 1999) -----	13
Figure 2.2. Sources of ultrafine particles (Source: Moreno-Ríos et al., 2022) ----	15
Figure 2.3. The ultrafine particle number concentration from forest fire (Sources: Guo et al., 2020) -----	17
Figure 2.4. The ultrafine particle number concentration from volcanic eruption (source: McGuinness, 2008) -----	19
Figure 2.5. The ultrafine particle number concentration from the marine emission (source: Mayer et al., 2020) -----	21
Figure 2.6. The ultrafine particle number concentration from industrial emissions (source: Rivas-Ubach et al., 2019) -----	23
Figure 2.7. The ultrafine particle number concentration from traffic emissions (sources: Li et al., 2023) -----	25
Figure 2.8. Ultrafine particle number concentration from Indoor emissions (Ali et al., 2022) -----	29
Figure 2.9. The ultrafine particle number concentration from roadside microenvironment (Olin et al., 2022) -----	30
Figure 2.10. Deposition of ultrafine particle number concentration in the human body (Goossens et al., 2021) -----	44
Figure 3.1. The interior view of the monitoring site in an urban location, Delhi -	51
Figure 3.2. The exterior view of the monitoring site in an urban location, Delhi -	51
Figure 3.3. The exterior view of the monitoring site in a regional background, Ranichauri -----	53
Figure 3.4. The location map representing the Urban Observatory includes (a) India, (b) Delhi, and (c) monitoring station -----	54
Figure 3.5. The location map representing the Background Observatory includes (a) India, (b) Ranichauri, and (c) Delhi -----	55
Figure 3.6. Schematic diagram of the working principle of SMPS+C -----	57
Figure 3.7. Schematic diagram of the instrument principle (Source: <a href="https://www.grimm-aerosol.com">https://www.grimm-aerosol.com</a> ) -----	57
Figure 3.8. Scanning mobility particle sizer counter (SMPS + C) -----	58

Figure 3.9. NO <sub>x</sub> Analyzer Instrument -----	59
Figure 3.10. SO <sub>2</sub> Analyzer Instrument -----	60
Figure 3.11. CO Analyzer Instrument -----	60
Figure 3.12. Automatic Weather Monitoring -----	61
Figure 3.13. Website of the National Oceanic and Atmospheric Administration (NOAA) -----	62
Figure 3.14. Choosing model inputs from REANALYSIS data -----	63
Figure 3.15. Final data extraction page from NOAA -----	63
Figure 3.16. Extraction of Trajectory data points using HYSPLIT Desktop version -----	64
Figure 3.17. Front page of MeteoInfoMap software -----	64
Figure 3.18. Plotting daily Trajectory data points for one season in MeteoInfoMap -----	65
Figure 3.19. Plotting Weighted Concentration Weighted Trajectory (WCWT) from daily Trajectory data points in MeteoInfoMap -----	65
Figure 4.1. The calendar plot indicated the cumulative daily concentration of N <sub>tot</sub> (10 to 1000 nm particles) for every month (January to December) throughout the year 2022 in the urban region -----	73
Figure 4.2. The calendar plot indicated the cumulative daily concentration of N <sub>tot</sub> (10 to 800 nm particles) for every month (January to December) throughout the year 2017 in the background region -----	74
Figure 4.3. Boxplot represented the concentration of N <sub>nuc</sub> , N <sub>atk</sub> , N <sub>acc</sub> and N <sub>total</sub> in both scenarios (daytime and nighttime) every month (from January to December) during 2022 -----	81
Figure 4.4. Box whisker analysis of N <sub>nuc</sub> , N <sub>atk</sub> , and N <sub>acc</sub> mode particles in an urban and a background site -----	83
Figure 4.5. Diurnal variation of modal particles number concentration in an urban and a background site during the different seasons -----	85
Figure 4.6. Size-segregated particle number contribution in both scenarios ((a) daytime and (b) nighttime)) in every month (from January to December) during 2022 -----	87

Figure 4.7. Different mode particle contribution during (a) daytime and (b) nighttime to the total particles -----	89
Figure 4.8. Monthly average particle number size distributions at both scenarios (daytime and nighttime) every month (from January to December) during 2022 ---	91
Figure 4.9. (A) Particle number size distribution ( $dN/d\log D_p$ in $\text{cm}^{-3}$ ) in the 10 to 1090 nm size range and its (B) normalized during 2022 -----	92
Figure 4.10. Size distribution of the particles during daytime and nighttime throughout the winter period -----	93
Figure 4.11. Monthly size distribution of the particles in the winter period during daytime and nighttime -----	94
Figure 4.12. Particle number size distribution of particles in (a) an urban and (b) a background site during different seasons -----	95
Figure 4.13. Relationship between particle number concentration, particulate matter, gaseous pollutants, and meteorological variables during the daytime ----	97
Figure 4.14. Relationship between particle number concentration, particulate matter, gaseous pollutants, and meteorological variables during the nighttime ---	97
Figure 4.15. Monthly average particle number size distributions at both the scenarios (daytime and nighttime) with an RH lower and higher than 70% every month (from January to December) during 2022 -----	99
Figure 4.16. Polar plot represents the contributions of the different sources for $N_{\text{nuc}}$ , $N_{\text{atk}}$ and $N_{\text{acc}}$ at both scenarios (daytime and nighttime) in every month (from January to December) during 2022 -----	100
Figure 4.17. Polar plot represented the daytime and nighttime concentration of mode particles and total particles -----	101
Figure 4.18. Polar cluster analysis of seasonal total particle concentration in the urban and background sites during different seasons -----	102
Figure 4.19. Back trajectory plots in urban site for the different seasons -----	104
Figure 4.20. Back trajectory plots in background site for the different seasons --	105
Figure 4.21. Diurnal variation of relative humidity and temperature in the urban and background sites during the different seasons -----	106

Figure 4.22. Diurnal variation of particle number concentrations and meteorology (Temperature and relative humidity) in urban and background sites during different seasons -----	108
Figure 4.23. Percentage Contribution represented the three different mode particles ( $N_{nuc}$ , $N_{atk}$ , and $N_{acc}$ ) that contributed to total particle number concentration ( $N_{tot}$ ) during the event, and non-event -----	109
Figure 4.24. Typical nocturnal event of growth particles on 06 July 2022. The mode diameter of the particles is indicated by the black cross symbol -----	112
Figure 4.25. Each individual plot represents a new particle formation event occurring in each season. The black cross symbol represents the model diameter of the particles -----	114
Figure 4.26. Box-wisher plot represented the growth rate of different seasons (Winter, Summer, Monsoon, and Post-Monsoon) -----	117
Figure 4.27. Diurnal profile represents the particle concentration during event and non-event periods (left-side axis), and condensation sink (right-side axis) -----	120
Figure 4.28. Diurnal variation shows four seasons (Winter, Summer, Monsoon, and Post-Monsoon) of non-event (a-d), and event (e-f) periods of particle number concentration (left-side), and condensation sink (right-side) -----	122
Figure 4.29. The polar plot represented the event and non-event days of $N_{nuc}$ in different seasons (Winter, Summer, Monsoon, and Post-Monsoon) -----	123
Figure 4.30. Diurnal plots represent the event and non-event periods of meteorological parameters. The left-side axis shows Relative Humidity (RH), and atmospheric Temperature (AT), The First right-side axis shows wind speed (WS), and the second right-side axis shows Solar Radiation (SR) -----	123
Figure 4.31. Box whisker plot represents the hourly mean concentration of $N_{nuc}$ (10 nm to 30 nm), $N_{atk}$ (30 nm to 100 nm), and $N_{acc}$ (100 nm to 1000 nm) during Diwali 2021 (a), and Diwali 2022 (b) -----	127
Figure 4.32. The daily variation in the hourly averaged concentrations of $N_{nuc}$ (ranging from 10 nm to 30 nm), $N_{atk}$ (spanning 30 nm to 100 nm), and $N_{acc}$ (covering 100 nm to 1000 nm) during Diwali are presented for two distinct periods: (a) Diwali 2021, from October 30 to November 10, and (b) Diwali 2022, from October 19 to October 29 -----	128

Figure 4.33. Particle number size distribution during Diwali 2021, and 2022 ---	129
Figure 4.34. Percentage contribution of mode particles ( $N_{nuc}$ (10 nm to 30 nm), $N_{atk}$ (30 nm to 100 nm), and $N_{acc}$ (100 nm to 1000 nm)) to total particles ( $N_{tot}$ ) during Diwali 2021, and 2022 -----	132
Figure 4.35. Hourly percentage contribution of three mode particles ( $N_{nuc}$ (10 nm to 30 nm), $N_{atk}$ (30 nm to 100 nm), and $N_{acc}$ (100 nm to 1000 nm)) to Total PNC on Pre-Diwali (a), Diwali (b), and Post-Diwali (c) during 2021 -----	133
Figure 4.36. Hourly percentage contribution of three mode particles ( $N_{nuc}$ (10 nm to 30 nm), $N_{atk}$ (30 nm to 100 nm), and $N_{acc}$ (100 nm to 1000 nm)) to Total PNC a) Pre-Diwali, b) Diwali, and c) Post-Diwali during 2022 -----	135
Figure 4.37. Percentage change of three different mode particles ( $N_{nuc}$ (10 nm to 30 nm), $N_{atk}$ (30 nm to 100 nm), and $N_{acc}$ (100 nm to 1000 nm)) in the year 2022 compared to 2021 -----	136
Figure 4.38. Diurnal variation of three mode particles ( $N_{nuc}$ (10 to 30 nm), $N_{atk}$ (30 to 100 nm), and $N_{acc}$ (100 to 1000 nm)) during three days (Pre-Diwali, Diwali, and Post-Diwali) in the year 2021 -----	137
Figure 4.39. Diurnal variation of three mode particles ( $N_{nuc}$ (10 to 30 nm), $N_{atk}$ (30 to 100 nm), and $N_{acc}$ (100 to 1000 nm)) during three days (Pre-Diwali, Diwali, and Post-Diwali) in the year 2022 -----	138
Figure 4.40. Analysis of heat maps depicting the distribution of size-resolved particles and geometric mean diameter (GMD) was conducted during the Diwali of 2021, spanning from October 30 to November 10, and in 2022, from October 19 to October 29 -----	138
Figure 4.41. Total concentration of inhalable particles of varying sizes, specifically $N_{nuc}$ (ranging from 10 nm to 30 nm), $N_{atk}$ (from 30 nm to 100 nm), and $N_{acc}$ (spanning 100 nm to 1000 nm), was calculated for two distinct periods: (a) Diwali 2021, which occurred from October 30 to November 10, and (b) Diwali 2022, taking place from October 19 to October 29 -----	140

## LIST OF TABLES

Table 2.1. Recent literature reviews around the world -----	9
Table 3.1. The geographical areas where observation campaigns were conducted ---	53
Table 4.1. The yearly statistical summary of the particle number concentration during the day and nighttime -----	75
Table 4.2. Statistical values (min, max, mean and SD) for the modal sizes fractions ( $N_{nuc}$ , $N_{atk}$ and $N_{acc}$ ) of the aerosol number size distribution including their geometric mean diameter (GMD) during the day and night-time for each month (from January to December) in 2022 -----	75
Table 4.3. Statistical values (min, max, mean and SD) of meteorological parameters (relative humidity (HR), wind speed (WS), solar radiation (SR) and atmospheric temperature (AT)) during the day and night-time for each month (from January to December) in 2022 -----	77
Table 4.4. Classification of seasonal periods -----	79
Table 4.5. Average mean particle concentration in the urban and background sites during the study period -----	82
Table 4.6. Season-wise average statistics for modal particle number concentration in the urban and background sites during the study period -----	84
Table 4.7. Seasonal-wise average statistical summary of temperature (T), relative humidity (RH), and wind speed (WS) in the urban and background sites during the study period -----	106
Table 4.8. The growth rate for all event days during the monitoring period -----	112
Table 4.9. Statistical mean concentration of gaseous precursors, and meteorological parameters in event and non-event -----	114
Table 4.10. Season-wise mean value of Growth Rate (GR), Condensation Sink (CS), and Coagulation Sink (CoagS) -----	117
Table 4.11. Statistical mean concentration of different mode particles ( $N_{nuc}$ (10 nm to 30 nm), $N_{atk}$ (30 nm to 100 nm), $N_{acc}$ (100 nm to 1000 nm), $N_{total}$ (10 nm to 1000 nm), and Geometric Mean Diameter (GMD) during Diwali 2021, and 2022 -----	129
Table 4.12 Average mean concentration of meteorological parameters (Ambient Temperature (AT), Relative Humidity (RH), and Solar Radiation (SR)) during Pre-Diwali, Diwali, and pre, Post-Diwali in 2021, and 2022 -----	133

## LIST OF ABBREVIATIONS

AGL	Above Ground Level
AIMIL-AWS	Aimil Automatic Weather Station
AM	Anti Meridiem
Amsl	Above the Mean Sea Level
ARL	Air Resource Laboratory
AT	Atmospheric Temperature
BG	Background
CCGS	Canadian Coast Guard Ship
CCN	Cloud Condensation Nuclei
CO <sub>2</sub>	Carbon Dioxide
CS	Condensation Sink
CoagS	Coagulation Sink
cm <sup>3</sup>	Cubic Centimetre
cm <sup>-3</sup>	Per Cubic Centimetre
CMD	Count median Diameters
cm <sup>3</sup> min <sup>-1</sup>	Standard Cubic Centimeters Per Minute
CNG	Compressed Natural Gas
CO	Carbon Monoxide
COPD	Chronic Obstructive Pulmonary Disease
CPCB	Central Pollution Control Board
D	Diwali
DEL	Delhi
DMA	Differential Mobility Analyzer
DMPS	Differential Mobility Particle Sizer
DMS	Dimethyl Sulfide
Dp	Diameter
E	East
ET	Extrathoracic
FEM	Federal Equivalent Method
Fig	Figure
GAW	Global Atmospheric Watch
Gg/yr	Giga Grams Per Year
GMD	Geometric Mean Diameter

GR	Growth Rate
GRAP	Graded Response Action Plan
hrs	Hour
h/d	Hour/day
HDV	Heavy-Duty Vehicle
H <sub>2</sub> SO <sub>4</sub>	Sulfuric Acid
HYD	Hyderabad
HYSPLIT	Hybrid Single Particle Lagrangian Integrated Trajectory
IAQ	Indoor Air Quality
IGP	Indo-Gangetic Plain
IMD	India Meteorological Department
IPN	Inhalable Particulate Matter
IST	Indian Standard Time
km	Kilometer
km <sup>2</sup>	Square kilometer
LDMA	Large Differential Mobility Analyser
LPG	Liquefied Petroleum Gas
LPM	Litre Per Minute
MBL	Mahabaleshwar
m/s	Meter per Second
MSL	Mean Sea Level
MUK	Mukteshwar
n	North
NAAQS	National Ambient Air Quality Standard
N <sub>acc</sub>	Accumulation mode
NaCl	Sodium Chloride
N <sub>atk</sub>	Aitken mode
NCR	National Capital Region
NDL	New Delhi
NH <sub>3</sub>	Ammonia
NH <sub>4</sub> <sup>+</sup>	Ammonium ion
N <sub>nuc</sub>	Nucleation mode
nm	nanometre



nm h <sup>-1</sup>	Nanometer Per Hour
NPG	New Particle Growth
NPF	New Particle Formation
NO	Nitric oxide
NOAA	National Oceanic and Atmospheric Administration
NO <sub>x</sub>	Nitrogen Oxides
NO <sub>2</sub>	Nitrogen Dioxide
O <sub>3</sub>	Ozone
PAHs	Polycyclic Aromatic Hydrocarbons
pb	Lead
PBL	Planetary Boundary Layer
PD	Pre-Diwali
PM	Particulate Matter
PM <sub>10</sub>	PM <sub>10</sub> – Particulate Matter with a diameter of 10 µm
PM <sub>2.5</sub>	PM <sub>2.5</sub> – Particulate Matter with a diameter of 2.5 µm
PM <sub>0.1</sub>	PM <sub>0.1</sub> – Particulate Matter with a diameter of 1 µm
PN	Particle Number
PNC	Particle Number Concentration
PNSD	Particle Number Size Distribution
PoD	Post-Diwali
ppb	Parts Per Billion
ppbv	Parts Per Billion by Volume
ppm	Parts Per Million
ppmv	Parts Per Million by Volume
PSD	Particle Size Distribution
PUL	Pulmonary
RB	Background
RH	Relative Humidity
RNC	Ranichauri
s <sup>-1</sup>	Per Second
SD	Standard Deviation
SDGs	Sustainable Development Goals
SJTU	Shanghai Jiao Tong University

SMPS+C	Scanning Mobility Particle Sizer with Condensation Particle Counter
SO <sub>2</sub>	Sulfur Dioxide
SUB	Suburban
SR	Solar Radiation
SVOCs	Semi-Volatile Organic Compounds
TB	Tracheobronchial
Total	Total Particle Number Concentration
TRAP	Traffic-Related Air Pollution
UFP	Ultrafine Particles
USA	United States of the America
USEPA	United States Environmental Protection Agency
UVF	Ultraviolet Fluorescent
VOCs	Volatile Organic Compounds (VOCs)
Vog	Volcanic Smog
WD	Wind Speed
WHO	World Health Organization
WRAS	Wide-Range Aerosol Spectrometer
W/m <sup>2</sup>	Watt Per Square Meter
WS	Wind Speed
%	Percentage
°C	Degree Celsius
#/min	Per Minute
µg/m <sup>3</sup>	Microgram Per cubic Meter
µg/h	Microgram Per Hour
µm	Micrometer

## **CHAPTER - 1**

### **INTRODUCTION**

#### **1.1 Introduction**

In developing countries like India, air pollutants have become a serious issue. Industrialization and urbanization have greatly boosted the Indian economy. On the other hand, they have also brought about a drastic change in the environment. Due to various natural and anthropogenic activities, different pollutants are released into the atmosphere, which is often referred to as “air pollution” (Gurjar et al., 2008). Advancements in instrument technology have made the measurement of smaller particles, such as particulate matter and fine particles, possible. The pollutants emitted in the atmosphere are not uniformly distributed and are found to be in different size ranges. The World Health Organization (WHO) globally and the Central Pollution Control Board (CPCB) in India have established guidelines to maintain and regulate air quality standards.

Delhi city is the national capital of India and one of the most polluted cities in the world (Guttikunda & Gurjar, 2012). Due to its continuously deteriorating environmental air quality, it has been persistently ranked among the topmost polluted cities globally in recent years (Apte et al., 2011; Kanawade., 2020a; Kulkarni et al., 2020; Tiwari et al., 2015). The particulate matter concentration in Delhi was almost three times higher than in Beijing and ten times higher than that of Washington, DC (WHO, 2014). Various factors, including vehicular emissions, biomass burning, fossil fuel combustion, diesel generators, construction activities, and road dust emissions, contribute to the higher concentration of particulate matter in Delhi (Kumar et al., 2011; Mishra et al., 2016; Pant et al., 2015). The transportation sector contributes approximately 29% of PM<sub>10</sub> and 45% of PM<sub>2.5</sub> emissions (Sahu et al., 2011). The urban centers where half of the world's population resides have been demanding a cleaner environment due to the increasing disturbances in air quality (Gurjar et al., 2008). Air pollution is still a major problem faced by the whole world, resulting in 6.2 million deaths throughout the world and 6,20,000 premature deaths in India alone (WHO, 2020). The alarming increase in air pollutants, with its intensity on the higher side, has resulted in numerous health issues and lung diseases, including chronic respiratory disorders, pneumonia, acute asthma, and shortness of breath (Baldauf et al., 2013).

Any development is appreciated until it is harmful to humans and their safety. To ensure this, regular monitoring of ambient air quality and the development of new strategies for upcoming sources of emissions should be made a priority, especially in developing urban areas.

Delhi is reported to have 29 planned industrial areas and 5 factory complexes, encompassing a range of industries, including food and beverages, metals and alloys, leather and leather products, chemicals, and paper (Mohan & Mishra, 2022). Fuels like diesel are used for both industrial and transportation purposes. Industrial uses include power backup systems, mobile phone towers, and other miscellaneous applications, while transportation uses cover cars, utility vehicles, heavy-duty vehicles, and more. Compressed Natural Gas (CNG) is used to run public transportation in cities, and diesel, CNG, Liquefied Petroleum Gas (LPG), and gasoline are used for private vehicles. In recent times, reports have shown that several brick kilns are operated in several areas around Delhi (Guttikunda & Gurjar, 2012). For cooking purposes, nearly 90% of households use LPG as their primary fuel. Not only LPG but also firewood, coal, cow dung cake, biogas, crop residues, and electricity are used as fuel for cooking. According to Mishra et al. (2019), the emission and increase of particulate matter are due to the day-to-day use of road transportation (30.25 Gg/yr). Not only road transportation, but also dust (18.25 Gg/yr) generation, residential emissions (18.65 Gg/yr), and industrial emissions (16.29 Gg/yr) are key contributors to the higher level of particulate matter. Guttikunda & Calori (2013) found that domestic emissions, transportation, and power plants, the three major contributors, are responsible for the rise in particulate matter.

Although technological advancements have improved our understanding of ultrafine particles and air quality, many environmental conditions and scientific problems remain unresolved (Pant et al., 2015). The particulate matter in the atmosphere significantly alters climatic and weather patterns, and it also poses several health risks (Trechera et al., 2023). Sebastian et al. (2022) stated that ultrafine particles are defined as those particles that persist in the atmosphere in any state that is solid or liquid. Since there is no precise division of the particle number concentration, they are classified into three modes: Nucleation ( $N_{nuc}$ , 10 to 30 nm), Aitken ( $N_{atk}$ , 30 to 100 nm), and Accumulation mode ( $N_{acc}$ , 100 to 1000 nm). Nucleation and Aitken mode

come under the ultrafine particles since they are less than 100 nm (Damayanti et al., 2023; Giemsa et al., 2021; Harrison, 2020; Kittelson et al., 2022; Liang et al., 2020; Lorelei de Jesus et al., 2020; Yadav et al., 2021). There are still challenges within research communities in categorizing ultrafine particles with appropriate measurement standards, specifically regarding the upper and lower size cut points, and establishing relevant metrics, such as number, mass, volume, and surface area. A particle with a diameter smaller than 100 nm is considered to be an ultrafine particle. However, the number concentration of ultrafine particles contributes disproportionately to the mass of particulate matter in the ambient air (Damayanti et al., 2023; Thén & Salma, 2022; Zhou et al., 2020). Some natural and anthropogenic activities, such as combustion processes and photochemical reactions, are the primary contributors to the presence of ultrafine particles in the atmosphere. The ultrafine particles have extended lifespans in the atmosphere with higher potential to travel long distances (Belkacem et al., 2020; Harrison et al., 2019), contributing to a lesser extent to the mass concentration but prominently to the particle number concentration (Austin et al., 2021; Chen et al., 2022; Mikkonen et al., 2020). The concentration of the ultrafine particles (UFP) in a region is represented by the number of concentrations and is also dependent on the intensity of the emission source. Additionally, the size of the particle plays a significant role in determining the source type, specifically whether the particle is anthropogenic or natural (Chatain et al., 2021). The total Particle Number Concentration (PNC) is often driven by UFP since UFP accounts for more than 80% of total PNC (Giemsa et al., 2021; Harrison, 2020).

The Ultrafine particle concentration is typically measured by the particle number concentration (PNC), per unit volume of air ( $\text{cm}^{-3}$ ). According to particulate matter (PM) guidelines, ambient air quality in a given region is assessed based on the mass concentration of particles with aerodynamic diameters below specific thresholds, typically expressed in micrograms per cubic meter ( $\mu\text{g}/\text{m}^3$ ) (Damayanti et al., 2022; Kalkavouras et al., 2020; Won et al., 2020). With the help of Particle Size Distribution (PSD), it is easy to classify the size-dependent mechanisms that govern a particle's transportation, transformation, and fate in the urban environment, and also makes it possible through the measurement of urban aerosol (Kompalli et al., 2020; Wu & Boor, 2021). The spatiotemporal variability of UFP is highly influenced by the complex

interplay of various factors, including regional sources, local sources, meteorological conditions, and aerosol dynamic processes. Recent research from diverse regions, landscapes, and various cities around the world has shown that the ultrafine particle number dominates the total particle number concentration (PNC) with noticeable increases during periods of higher solar radiation.

People living in and around urban areas are exposed to higher levels of air pollution that exceed the values recommended by the WHO (Su et al., 2021). Over the past five years, several studies have highlighted the adverse effects of air pollution or particular contaminants on the respiratory system (Goossens et al., 2021; Takegawa et al., 2021). Due to their extremely small size, the ultrafine particles can penetrate deep into the respiratory system. Once entering the alveoli in the lungs, they can easily enter the circulatory system and potentially can reach any organ of the body. Also, their ultra-fine size allows the possibility of translocation to the brain via the olfactory nerve (Gani et al., 2020; Pirhadi et al., 2020).

## **1.2 Objectives of the study**

Given the importance of particle concentration in various contexts and its significant contribution to air pollution, this research has been conducted with the following objectives.

- 1) To investigate the temporal behavior and concentration of UFP during Day and Night-time near selected urban roadside.
- 2) To compare and analyze the particle number concentration of ultrafine particles in urban and background regions.
- 3) To investigate the role of micrometeorological parameters in urban and background ultrafine particle number concentration.

### **1.2.1 Novelty and significance of the study**

Previous studies have examined ultrafine particle (UFP) concentrations in various Indian urban regions; however, most of them have been limited to short-term campaigns, single-site observations, or measurements focused solely on total particle number concentrations without detailed size segregation. There remains a lack of comparative research that characterizes size-segregated UFP dynamics across both urban and background environments within Delhi.

This thesis addresses this gap by conducting a detailed comparative analysis of particle number size distributions (10.23-1090.21 nm) between an urban roadside and an urban background site. The study uniquely explores the temporal variability of UFPs during day-night periods and examines how micrometeorological parameters influence the size-resolved behavior of particles. Through this approach, the work provides new insights into the source characteristics and atmospheric processes that govern the formation and transformation of UFPs in Delhi's complex urban atmosphere.

These novel aspects directly align with the stated research objectives and advance current understanding of ultrafine particle behavior in developing megacities, providing valuable inputs for future air quality management and policy interventions.

### **1.2.2 Policy relevance and societal importance**

The outcomes of this research hold direct relevance for urban air quality management and environmental policy in Delhi. Understanding the size-segregated behavior of ultrafine particles (10.23-1090.21 nm) across urban and background environments provides critical evidence for designing effective mitigation strategies. Insights into temporal variations and meteorological influences can support the development of targeted emission control measures, particularly for traffic-related and combustion sources that contribute significantly to UFP formation.

Moreover, since UFPs pose significant health risks due to their ability to penetrate deep into the respiratory system and enter the bloodstream, the results of this study can inform public health policies and exposure management frameworks. The findings thus contribute to strengthening scientific support for ongoing initiatives by agencies such as the Central Pollution Control Board (CPCB) and the Delhi Pollution Control Committee (DPCC) in developing evidence-based standards and interventions to improve urban air quality.

### **1.3 Thesis structure**

The thesis is organized into five comprehensive chapters, each structured to contribute to a coherent narrative that supports the study's objectives. Below is a detailed outline of each chapter:

**Chapter 1** serves as the introductory framework for the thesis, divided into three main sections. The first section provides background information, providing an

overview of the research topic and establishing its relevance. The second section then clearly articulates the research objectives, explaining the specific aims and objectives that guide the study. The chapter concludes with an overview of the thesis structure, providing readers with a roadmap for this chapter. This structured introduction sets the stage by contextualizing the study and its importance within the broader academic and practical fields.

**Chapter 2** is a comprehensive literature review that draws on relevant sources to provide an in-depth understanding of the research area. This chapter synthesizes existing research from various academic, industry, and theoretical perspectives, identifying both established knowledge and gaps in the literature. This section not only provides context but also supports the thesis by highlighting the need for further research into the specific aspects this study seeks to address. By critically examining multiple perspectives, the chapter establishes a strong theoretical foundation, ensuring that the study is well-informed and carefully designed.

**Chapter 3** outlines the research design and methodology, detailing the strategic approach employed in conducting the research. This chapter describes the research methods selected, including the methods and instruments used for data collection, analysis, and fieldwork. Each method is discussed in detail, explaining its relevance to the study objectives and how it was implemented in practice. This chapter provides transparency into the research process by highlighting the rationale for choosing certain methodologies over others. This careful selection of methods is necessary to obtain accurate and reliable results and also facilitates the validation of the study findings, demonstrating a systematic and reproducible approach.

**Chapter 4** presents an analysis and discussion of the data collected using the methods described in Chapter 3. It critically examines the results, interpreting them in the context of the research objectives and questions. This chapter constitutes the analytical core of the thesis, where the data are transformed into meaningful insights. Key trends, patterns, and findings are identified and discussed, highlighting their implications for the field of study. This chapter not only reports the findings but also situates them within a broader field by linking the findings to the literature reviewed in Chapter 2. This critical appraisal of the findings strengthens the study's contribution and offers new insights into the topic.



**Chapter 5** concludes the thesis by summarizing the main findings and providing a final reflection on the study's impact. It discusses the results of the data analysis, synthesizing key ideas that address the research questions. Additionally, this chapter offers recommendations for future research by identifying areas where further investigation could expand on the findings presented here. Chapter 5 highlights the broader implications of the study, aligning it with the Sustainable Development Goals, positioning it as a springboard for ongoing research in the field, and offering suggestions to other researchers who may continue to study related topics.

#### **1.4 Summary**

In the Introduction section, a comprehensive examination of air pollution is presented, addressing its origins, properties, and general dynamics within the environment. The concept of ultrafine particles (UFPs) is introduced, detailing their definition, primary sources, and distinctive behaviors that differentiate them from other forms of particulate matter. The Objective section clearly articulates the study's aims, providing a focused framework for the research. In the Thesis Structure section, the organization of the thesis is outlined, offering a detailed overview of each chapter and clarifying the specific topics and content addressed, thereby guiding the reader through the progression of the study.

Overall, Chapter 1 establishes the scientific context and rationale for investigating ultrafine particles in urban environments. By defining key concepts and presenting the research objectives, this chapter provides the foundation for the subsequent chapters. Chapter 2 builds upon this introduction by presenting a detailed literature review that synthesizes current knowledge and identifies gaps in the understanding of ultrafine particles. Chapter 3 uses these insights to develop the methodology for data collection and analysis. Chapter 4 then presents the results and discussion based on the applied methodology, while Chapter 5 concludes the thesis by summarizing the findings, highlighting their implications, and suggesting future research directions. This clear progression ensures that each chapter logically flows from the preceding one, maintaining coherence and continuity throughout the thesis.

## **CHAPTER – 2**

### **LITERATURE REVIEW**

#### **2.1 Introduction**

The air pollution constantly endangers people's health and quality of life, and it is one of the environmental issues being researched globally. "The presence in the outdoor atmosphere of one or more contaminants, such as features and quantities of dust, fumes, gas, mist, odor, smoke, or vapor, to be detrimental to human, plant, animal life, or property" is the Engineers Joint Council's definition of air pollution. Additionally, their existence could irrationally obstruct one's ability to appreciate life and property comfortably (Gloss. Air Pollution., 1980). There are various differences that can be made depending on the particle size and physical state. First, gaseous chemicals and particulate matter (PM) are the two primary categories of pollutants that may be identified based on their composition (Manisalidis et al., 2020; Tiotiu et al., 2020). Ozone, nitrogen oxides, carbon monoxide (CO), polyaromatic hydrocarbons (PAHs), carbon dioxide (CO<sub>2</sub>), volatile organic compounds (VOCs), and heavy metals are among the gaseous chemicals that contribute to air pollution (Manisalidis et al., 2020). Particulate matter, which includes both liquid and solid particles, comes in second (Goossens et al., 2021).

Particulate matter (PM), a complex mixture of chemical and biological components, is a primary source of air pollution (Moreno-Ríos et al., 2022). Particles range in size from nanometers (nm) to microns (μm), with three categories: coarse, fine, and ultrafine; PM<sub>10</sub> particles have an aerodynamic diameter between 2500 and 10000 nm, PM<sub>2.5</sub> particles have an aerodynamic diameter between 100 and 2500 nm, and PM<sub>0.1</sub> particle have an aerodynamic diameter of less than 100 nm (Clifford et al., 2018; Jeong et al., 2017). We know more about PM<sub>2.5</sub> exposures than UFP exposures for several reasons. A primary cause is the absence of extensive monitoring networks. Under the Clean Air Act, the U.S. EPA regulates seven criteria pollutants (PM<sub>2.5</sub>, PM<sub>10</sub>, NO<sub>2</sub>, O<sub>3</sub>, CO, SO<sub>2</sub>, Pb) and a network of over 4,000 stations across the country measures the ambient concentrations of these pollutants. More than 20 years' worth of continuous measurements (for example, hourly) of specific pollutants are available in numerous locations. High spatial resolution national exposure estimates have been derived from these data (Kim et al., 2020). They also enable the quantification of long-

term declines in pollutant concentrations in both urban and rural areas. Since UFP does not meet the standards for pollution, there is no extensive monitoring network, and only a small amount of monitoring data is available (Presto et al., 2021). The few studies on UFPs around the world are summarized in Table 2.1. The PM<sub>2.5</sub> includes ultrafine particles (UFP) as a subset. Although alternative definitions exist (e.g., particles less than 200 nm), the term UFP is typically defined as particles smaller than 100 nm (Kwon et al., 2020; Ostro et al., 2015). UFP typically makes up a small portion of PM<sub>2.5</sub> bulk because of their small size, but they predominate in terms of total number concentrations. A typical stand-in for UFP is total particle number concentration (PNC). There are worries that the health effects of UFP exposure differ from those of PM<sub>2.5</sub> mass. According to toxicological research, UFP may have different health impacts than PM<sub>2.5</sub> (Presto et al., 2021). According to Solomon. (2019), unlike bigger particles, UFP can enter the lungs' alveolar area profoundly, which tends to deposit less effectively due to their size. This is attributed to their rapid diffusion and relatively slow clearance mechanisms, which enable UFPs to interact with lung lining cells and potentially translocate intact to other areas of the body.

Table 2.1. Recent literature reviews around the world.

S. No	Authors	Year	Title	Remarks
1.	(Dröge et al., 2024)	2024	Influence of a large commercial airport on the ultrafine particle number concentration in a distant residential area under different wind conditions and the impact of the COVID-19 pandemic	<ul style="list-style-type: none"> <li>• The particle number concentration was measured in a low-traffic residential area, approximately 7 km from Frankfurt Airport, using a Condensation Particle Counter in a long-term study. Additionally, the particle size distribution was determined using a Fast Mobility Particle Sizer.</li> <li>• The particle number concentrations exhibited high variations throughout the entire measurement period and even within a single day.</li> <li>• A maximum 24 h-mean of 24,120 cm<sup>-3</sup> was detected. Very high particle number concentrations were measured, particularly when the wind came from the direction of the airport. In this case, the particle size distribution showed a maximum in the particle size range of 5-15 nm.</li> </ul>
2.	(Rajagopal et al., 2024a)	2024	Seasonal variation of particle number	<ul style="list-style-type: none"> <li>• Concentrations of UFP (particles of size between 10 and 100 nm) and</li> </ul>

			concentration in a busy urban street with exposure assessment and deposition in human respiratory tract	<p>accumulation mode (<math>N_{acc}</math>) (particles of size <math>&gt;100</math> and up to <math>1000</math> nm) are analyzed over a highly polluted megacity, Delhi, in conjunction with vehicular flow density, during peak (morning and evening) and non-peak hours.</p> <ul style="list-style-type: none"> <li>• UFP contributes to <math>\geq 60\%</math> of the total particle concentration during autumn and the monsoon.</li> <li>• UFP concentrations are approximately <math>50,000</math> particles per <math>cm^3</math> in winter, decreasing to around <math>25,000</math> particles during the monsoon. <math>N_{acc}</math> are about <math>20,000</math> (winter) and <math>10,000</math> (monsoon) particles per <math>cm^3</math>.</li> <li>• UFP concentration and <math>N_{acc}</math> during peak hours are at least twice as high as those obtained in non-peak hours, confirming the dominant influence of emissions from vehicular exhaust in the study region.</li> </ul>
3.	(Vörösmarty et al., 2024)	2024	Attribution of aerosol particle number size distributions to main sources using an 11-year urban dataset	<ul style="list-style-type: none"> <li>• The study was conducted in Budapest, using a flow-switching-type differential mobility particle sizer system that operates in an electrical mobility diameter range of <math>6</math> to <math>1000</math> nm.</li> <li>• Six sources were identified in Budapest.</li> <li>• The mean relative contributions of traffic emissions (<math>60\%</math>) indicate that on-road motor vehicles were the leading source of particle numbers.</li> <li>• The nucleation was responsible for <math>24\%</math> of the PNC annually, as a lower estimate.</li> <li>• It exhibited a compound character consisting of photochemically induced nucleation and traffic-related nucleation.</li> <li>• Its contributions were the highest in spring and the lowest in winter.</li> </ul>
4.	(Garcia-Marlès et al., 2024)	2024	Inter-annual trends of ultrafine particles in urban Europe	<ul style="list-style-type: none"> <li>• The study was conducted in 15 European cities and 1 in the USA (12 urban background (UB), 5 traffic (TR), 3 suburban background (SUB), and 1 regional background (RB) sites) were evaluated.</li> <li>• The non-parametric Theil-Sen's method was used to detect monotonic trends. Meta-analyses were conducted to examine the overall trends and those specific to different environments.</li> <li>• The results showed significant decreases in <math>NO</math>, <math>NO_2</math>, <math>BC</math>, <math>CO</math>, and particle concentrations in the Aitken (<math>25-100</math> nm) and the Accumulation (<math>100-800</math> nm) modes, suggesting a positive impact of the implementation of EURO 5/V and</li> </ul>

				6/VI vehicle standards on European air quality.
5.	(Krecl et al., 2024a)	2024	Long-term trends of black carbon and particle number concentrations and their vehicle emission factors in Stockholm	<ul style="list-style-type: none"> <li>The study analyzed BC and PN (particle diameter <math>D_p &gt; 4</math> nm) concentrations in Stockholm spanning the years 2013-2019 (BC) and 2009-2019 (PN), measured at street canyon and rooftop sites to assess the effectiveness of the implemented policies.</li> <li>Combining these data with inverse dispersion modeling, the study estimated BC and PN emission factors (<math>EF_{BC}</math> and <math>EF_{PN}</math>) for the mixed fleet, reflecting real-world driving conditions.</li> <li>The pollutants exhibited decreasing trends at both sites; however, PN concentrations remained high at the canyon site, exceeding the World Health Organization (WHO) recommendations.</li> <li>BC concentrations declined more rapidly than PN concentrations, showing a -9.4% and -4.9% annual decrease at the canyon and -7.2% and -0.5% at the rooftop site in the years 2013-2019. The <math>EF_{BC}</math> and <math>EF_{PN}</math> trends indicated that mitigation strategies for reducing particulate emissions in on-road vehicles were successful over the study period.</li> <li>Stricter Euro emission regulations, especially with diesel particulate filters (DPF) in Euro 5, 6, and VI vehicles, led to a 66% decrease in <math>EF_{BC}</math> and 55% in <math>EF_{PN}</math>.</li> </ul>
6.	(Trechera et al., 2023)	2023	Phenomenology of ultrafine particle concentrations and size distribution across urban Europe	<ul style="list-style-type: none"> <li>The study was conducted from 2017–2019 using hourly particle number size distributions (PNSD) from 26 sites in Europe and 1 in the US were evaluated, focusing on 16 urban background (UB) and 6 traffic (TR) sites in the framework of Research Infrastructures services reinforcing air quality monitoring capacities in European URBAN &amp; industrial areas (RIURBANS) project.</li> <li>The primary objective was to describe the phenomenology of urban ultrafine particles (UFPs) in Europe, with a particular focus on air quality.</li> <li>The varying lower size detection limits made it difficult to compare PN concentrations (PNC), particularly <math>PN_{10-25}</math>, from different cities. PNCs follow a <math>TR &gt; UB &gt; Suburban (SUB)</math> order.</li> </ul>
7.	(Kalaiaresan et al., 2024)	2023	Particle Number Size Distribution in Three Different	<ul style="list-style-type: none"> <li>This study was conducted in three different microenvironments in London (indoor, IN; traffic intersection, TI; park, PK), measuring particles in the range of</li> </ul>

			Microenvironments of London	6-10,000 nm using an electrical low-pressure impactor. <ul style="list-style-type: none"> <li>• Mean PNCs were <math>1.68 \pm 1.03 \times 10^4 \text{ #cm}^{-3}</math>, <math>7.00 \pm 18.96 \times 10^4 \text{ #cm}^{-3}</math>, and <math>0.76 \pm 0.95 \times 10^4 \text{ #cm}^{-3}</math> at IN, TI, and PK, respectively.</li> <li>• The PNDs were high for nucleation-mode particles at the TI site, especially during peak traffic hours.</li> <li>• Wind speeds ranging from 0 to 6 <math>\text{ms}^{-1}</math> exhibit higher PNCs for nucleation and accumulation mode particles at TI and PK sites.</li> </ul>
8.	(Rajagopal et al., 2023)	2023	Roadside measurements of nanoparticles and their dynamics in relation to traffic sources in Delhi: Impact of restrictions and pollution events	<ul style="list-style-type: none"> <li>• This study analyzes nanoparticle (10 to 1090 nm) during different emission scenarios, seasonal and meteorological conditions in two phases: April to June 2021 (Period I) and October to November 2021 (Period II).</li> <li>• Period I experienced around 31% less concentration of particles (<math>\sim 2.4 \times 10^4 \text{ cm}^{-3}</math>) due to lockdown restrictions, and, on the other hand, particle concentration increased by 35% compared to normal conditions due to the sudden rise in firework emissions in Period II.</li> <li>• Except for the post-Diwali phase (<math>10^4 \text{ cm}^{-3}</math> to <math>10^5 \text{ cm}^{-3}</math>), the concentrations lie between <math>10^3 \text{ cm}^{-3}</math> and <math>10^5 \text{ cm}^{-3}</math>. The Aitken modes contribute 10-30% of the total concentration in both periods.</li> </ul>

## 2.2 UFP's definition, size range, and mode classification

Many researchers classify UFPs based on their size within the term of the mode. The modal classification approach is primarily utilized in aerosol science, which deals with the natural UFP; however, in several studies, it's been used to classify anthropogenic UFP. The victimization of this modal approach for UFP helps to grasp their formation and interaction, as particles of various modes (sizes) have distinct characteristics, formation mechanisms, sources, and interactions with different particles (Kumar et al., 2010). Although there is no strict definition of classification based on size range, particle size distribution is generally classified into three groups: the Nucleation mode, Aitken mode, and Accumulation mode, which may reflect their formation process and origin (Damayanti et al., 2023). The particle number size and particle mass distribution are depicted in Fig.2.1.

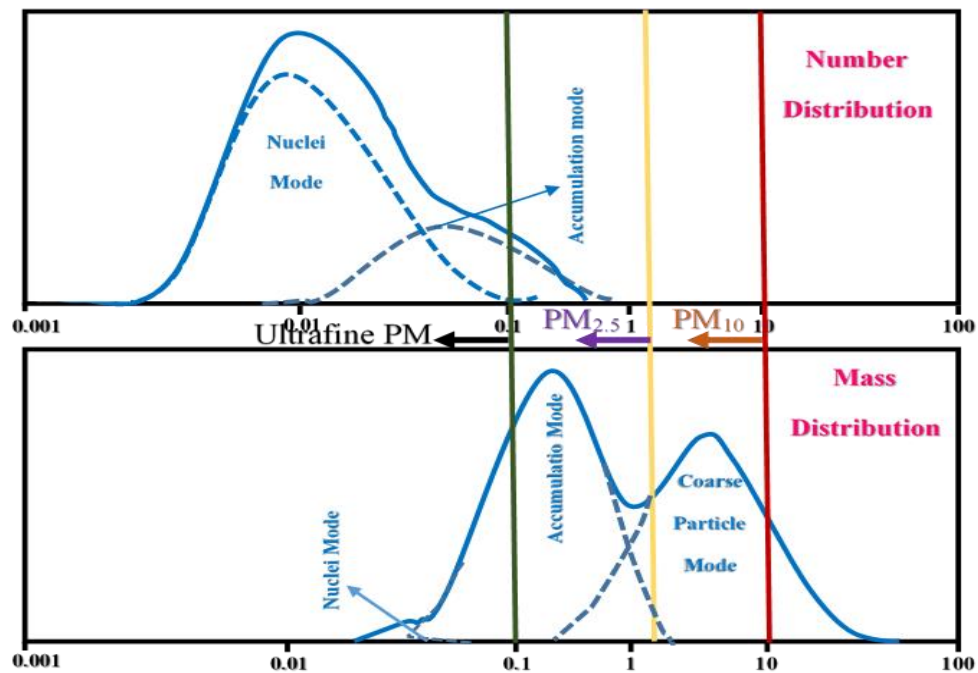


Figure 2.1. Particle number size and particle mass distribution (Source: Hinds 1999).

- **Nucleation mode** includes particles having a size of < 30 nm. Some studies have employed different ranges for nucleation mode, depending on the study's aim and the instrument used. Lingard outlines nucleation mode as particle size 3-20 nm (Lingard et al., 2006), whereas Wallace defines them as particles having a size range of 1-10 nm (Wallace, 2009). On the other hand, Charron defines it as a particle having a size range of 18-33 nm (Charron et al., 2008). These particles are shaped because of the results of nucleation and coagulation of the gases discharged from the tailpipe. It is found that nucleation mode particles dominate the PNC within the early stages of UFP formation, and therefore their number concentration remains high near the source (Lingard et al., 2006). Additionally, according to Kulmala et al. (2012) and Yadav et al. (2019), nucleation mode particles are divided into two categories: narrow nucleation mode (<10 nm) and broad nucleation mode (> 10 nm).
- **Aitken mode** doesn't have a very defined boundary layer. It consists of a particle between nucleation mode and accumulation mode. Some studies have defined Aitken mode as a particle with a size of 10-100 nm or as a particle with a size of 20-90 nm, 33-90 nm, or 30-100 nm (Charron et al., 2008; Lingard et al., 2006; Wallace, 2009). It acts as a transition mode between

nucleation mode and accumulation mode. Due to this uncertainty, Aitken mode particles are generally not considered alone and are termed with the accumulation mode as Aitken-accumulation mode particles. These particles are formed both through nucleation and accumulation (Kumar et al., 2010).

- **Accumulation mode** encompasses particles with a size range of 90-1000 nm (Kulmala et al., 2004; Lingard et al., 2006). Some studies have also defined accumulation particles as particle sizes 90-120 nm (Charron et al., 2008), and 100-1000 nm (Wallace, 2009). Accumulation mode particles are formed when the nucleation mode particles start accumulating over the larger size particles (mainly soot); thus, accumulation mode is also referred to as soot mode particles. Accumulation mode particles are also released directly into the air as the by-product of fuel burning in the internal combustion engine (Kumar et al., 2010).

### **2.3 Sources of ultrafine particle number concentration**

Dynamic formation processes, including nucleation, condensation, and coagulation of gas-phase chemicals, result in the production of ultrafine particles (UFPs) (Ramírez et al., 2020). Due to the release of biogenic volatile organic compounds (VOCs), nucleation often happens in forested environments (Ehn et al., 2014). Gaseous molecules are moved into nucleation mode particles or preexisting particles during condensation. Particle collisions may occur during coagulation, causing two initial particles to merge into a single larger particle. UFPs are deposited when newly nucleated UFPs coagulate easily with other particles (Kwon et al., 2020; Zhao et al., 2015). Because changes in size, shape, surface area, volume, and quantity can happen more quickly in UFP processes than in larger particles, they differ from those in larger particles (Kumar et al., 2016). UFPs are eliminated by dry and wet deposition (Kumar et al., 2011; Muñoz-Salazar et al., 2020), and after formation, they can linger in the air longer than larger particles (Abdel-Shafy & Mansour, 2016). The amount of pollutants varies depending on the contribution of each source and the location. The main sources of emissions are depicted in Fig.2.2.



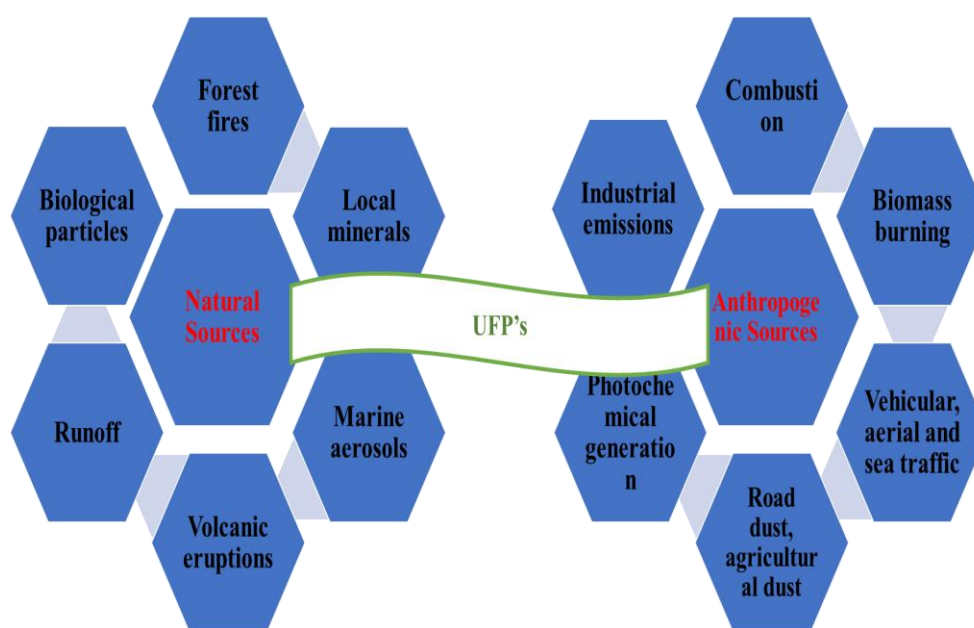


Figure 2.2. Sources of ultrafine particles (Source: Moreno-Ríos et al., 2022).

These sources might be man-made or natural (Mishra et al., 2016). According to Kumar et al. (2016), PM is either released directly into the atmosphere as primary particles or is formed there as a result of photochemical reactions producing new particles and gaseous precursors that change into secondary particles. Forest fires, volcanic eruptions, marine aerosols, local minerals, and runoff are examples of natural sources of UFPs (Dalmora et al., 2016; Kronbauer et al., 2013). However, the primary anthropogenic sources of UFPs include vehicle traffic, biomass burning (such as agricultural burning, forest fires, and waste disposal), combustion of gas, coal, or hydrocarbons, and industrial emissions (Keuken et al., 2015). Tire wear and tear from car brakes, air traffic (Kecorius et al., 2016; Møller et al., 2020; Stacey, 2019), seaports, marine transportation (Agudelo-Castañeda et al., 2019), domestic wood stoves (Marabini et al., 2017), outside burning, kitchens (Chen et al., 2017), and cigarette smoking (Goel & Kumar, 2015) are some of the various sources of ultrafine particles.

### 2.3.1 Forest fires

Due to hotter and drier summers worldwide, climate change is expected to increase the frequency and severity of wildland fires (Miezić et al., 2022; Westerling et al., 2006; Westerling, 2016). Large and mega-fires, also known as unprecedented and devastating wildfires, are a common occurrence in various parts of the world, such

as Australia, some sections of the United States of America, and Southern European countries (Dupuy et al., 2020; Ganteaume et al., 2021; Oliveira et al., 2020; Teixeira et al., 2024; Tyukavina et al., 2022). Significant volumes of gaseous and particulate matter (PM) are released into the atmosphere during forest fires. The aerosol particles from forest fires are depicted in Fig.2.3. Because wildfire plumes in metropolitan areas contain a high concentration of organic species and poisonous black carbon, they have a significant impact on ambient population exposure and health. There have been significant changes in the photolysis rates and photochemical production of secondary aerosols, as well as in the cooling and warming of the lower atmosphere, associated with the ability of biomass-burning aerosols to scatter or absorb solar radiation, depending on their chemical composition and mixing state (Baylon et al., 2018; Forrister et al., 2015; Popovicheva et al., 2014; Wong et al., 2019). A large portion of global emissions from burning biomass is caused by regional burning, such as that which occurs in agriculture and during wildfires that regularly decimate forested areas. When long-range transport occurs, which can extend thousands of kilometers downwind, or during peri-urban forest fire events, the smoke from wildfires burning biomass can cause a significant decline in air quality in urban areas (Adam et al., 2020; Filonchyk et al., 2022; Saxena et al., 2021). Climate change can be attributed to forest fires and their major impact on atmospheric chemistry.

According to research by Stohl et al. (2007), air pollution in the European Arctic can be considerably changed by agricultural fires in Eastern Europe. It is acknowledged that emissions from burning wood have a significant role in both the oxidative potential of PM and PAHs (Polycyclic Aromatic Hydrocarbons) (Guascito et al., 2023; Kaskaoutis et al., 2024; Nim et al., 2023; Paraskevopoulou et al., 2019). Significant amounts of particulate matter released by forest fires interact with solar radiation, altering the physicochemical properties of the atmosphere (Lazaridis et al., 2008). Additionally, through changes in air characteristics and the absorption of solar radiation, aerosols from forest fires can have a negative impact on the surrounding climate (Dumka et al., 2022; Yang et al., 2022; Zhu et al., 2022). Furthermore, wildfire aerosols may act as cloud condensation nuclei (CCN) (Bougiatioti et al., 2016; Wang et al., 2022) due to their strong hygroscopic nature and long-range atmospheric

transport. This could modify cloudiness and rainfall, which in turn affects the regional climate (Ding et al., 2021; Hodnebrog et al., 2016).

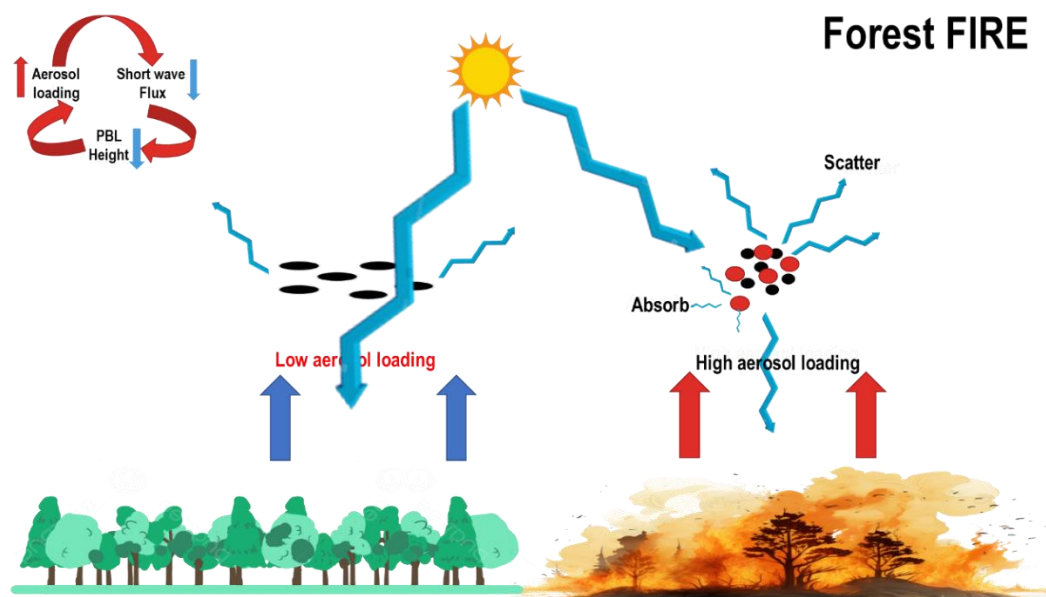


Figure 2.3. The ultrafine particle number concentration from a forest fire (Source: Guo et al., 2020).

Prescribed burns and controlled forest fires are two common methods for managing forests and preventing wildfires. Wildfire mitigation is a global concern. Due to the challenges of determining their temporal and spatial distribution, forest and agricultural biomass fire emissions are less well quantified in the literature than emissions from other anthropogenic sources (Bein et al., 2008; Hays et al., 2005). Moreover, the amount of smoke produced varies from year to year by a factor of ten or more. Burning is a multi-step process that yields distinct compounds at each stage. The resultant charred material is non-uniform and challenging to quantify mathematically. This feature could lead to notable discrepancies in air pollution levels between predicted and observed values. Exposure to black carbon emissions from wildfires has been directly associated in several recent studies with unfavorable cardiovascular outcomes, including elevated hypertension and ischemic illness (Ljungman et al., 2019; Pullabhotla & Souza, 2022).

### 2.3.2 Volcanic eruption

Volcanic aerosols contain ultrafine particles (UFPs), which are a crucial yet often overlooked component. The ultrafine particles from volcanic eruptions are

depicted in Fig.2.4. These particles, which have dimensions of less than 100 nanometers, have a significant impact on the atmosphere, the environment, and human health. Fine ash, sulfur dioxide (SO<sub>2</sub>), and other volcanic gases that condense into aerosols in the atmosphere are commonly found in UFPs formed by volcanic eruptions (Horwell & Baxter, 2006). Large ambient SO<sub>2</sub> concentrations have been observed downwind from volcano plumes in studies that have documented the impact of volcanoes on air quality (Businger et al., 2015; Carn et al., 2017; Cuesta-Mosquera et al., 2018, 2020; Schäfer et al., 2011; Silva et al., 2020). Volcanoes can release a significant number of particles into the atmosphere, ranging from nano (<50 nm) to coarse (PM<sub>10</sub>) (Trejos et al., 2021). A wide range of adverse environmental consequences, including deterioration of air quality, alterations in the climate, and impacts on human health, could result from UFP emissions into the atmosphere. One of the primary environmental impacts of UFPs from volcanic eruptions is their influence on air quality.

Volcanic smog, often known as "vog," is caused by the reaction of gases and ash released by volcanoes into the atmosphere (Longo & Yang, 2008b). Ultrafine sulfur particles, which are highly concentrated in vog, can pose serious health risks, particularly to those who live downwind of the eruption. According to studies, inhaling vog, especially ultrafine particles, can exacerbate respiratory disorders such as bronchitis, asthma, and other pulmonary ailments (Longo et al., 2008a). These particles are particularly harmful to human health due to their small size, which enables them to penetrate the lungs deeply. Significant contributions from ultrafine volcanic particles are also made to atmospheric processes. According to Textor et al. (2006), they can act as cloud condensation nuclei (CCN), which are tiny particles that collect condensation of water vapor to create cloud droplets. Due to their ability to function as CCN, UFPs influence precipitation patterns, cloud formation, and cloud albedo (reflectivity). Increased CCN levels in the atmosphere have the potential to alter cloud dynamics, potentially affecting local weather and climate trends. For example, a rise in CCN may cause clouds to have smaller droplets, which reflect more sunlight and are less likely to precipitate. This could change the patterns of rainfall and have a cooling effect on the Earth's surface. Volcanic eruptions' ultrafine particles have short-term air effects, but they can also have longer-term climate effects. Depending on the

size of the eruption, these particles, particularly sulfur-rich aerosols, can linger suspended in the stratosphere for months or even years (Robock, 2000). Once in the stratosphere, they disperse solar energy, resulting in a cooling effect on the entire planet. Large volcanic eruptions, such as the 1991 explosion of Mount Pinatubo, have been shown in the past to have caused a detectable drop in global temperature due to the dispersion of sulfur aerosols, including ultrafine particles (Robock, 2000). These years-long cooling impacts have a big impact on the world's climate systems. The distinct physical and chemical properties of ultrafine volcanic particles are also important, as they influence their potential toxicity and atmospheric persistence. According to studies, these particles exhibit a broad range of morphologies, varying from spherical to highly irregular shapes, and can remain suspended in the air for extended periods due to their small size (Durant et al., 2010, 2012).

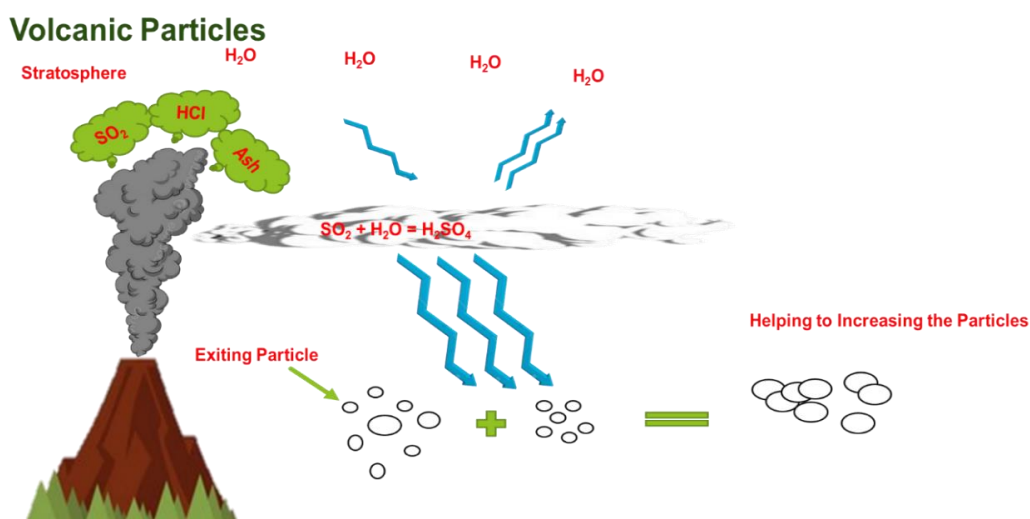


Figure 2.4. The ultrafine particle number concentration from a volcanic eruption (Source: McGuinness, 2008).

In summary, ultrafine particles from volcanic eruptions, which are vital and have a significant impact on the environment, climate, and human health, are found in volcanic aerosols. Due to their long-term persistence in the stratosphere, these particles have the ability to induce global cooling, contribute to the formation of vog, and alter atmospheric processes as nuclei for cloud condensation. Their small size, unique form, and chemical composition make them incredibly deadly and persistent, underscoring the need for further research into their effects on both local and global levels.

### 2.3.3 Marine aerosols

Marine aerosols are a diverse group of particles found in the atmosphere over oceans, playing a critical role in atmospheric chemistry, weather, and climate regulation. They originate from both natural and anthropogenic sources, impacting the Earth's radiative balance, cloud formation, and even global climate processes. Understanding the composition and sources of marine aerosols is crucial for evaluating their impact on the environment and human health. The most abundant natural source of marine aerosols is sea salt, which is generated when wind-driven waves break at the ocean surface, causing bubbles to burst and eject small droplets of seawater into the atmosphere (Wang et al., 2023). These droplets evaporate, leaving behind salt particles, primarily composed of sodium chloride (NaCl), along with other sea salts like magnesium, calcium, and potassium. Sea salt aerosols are a key component of the marine boundary layer, particularly in coastal and open-ocean regions, where they contribute to cloud condensation nuclei (CCN), thereby influencing cloud formation and albedo.

Collins et al. (2017) conducted their study throughout the Canadian Arctic during shipboard expeditions aboard the research icebreaker Canadian Coast Guard Ship (CCGS) Amundsen in the summers of 2014 and 2016. Ambient aerosol concentrations with particle diameters larger than 4 nm were measured using an ultrafine condensation particle counter (UCPC; Model 3776, TSI Inc.), while particle number size distributions in the 10-430 nm range were determined using a scanning mobility particle sizer (SMPS; Model 3080/3787, TSI Inc.). The particle number concentrations (diameter > 4 nm) ranged from  $10^1$  to  $10^4$  cm<sup>-3</sup> and were recorded across both seasons, with occurrences of concentrations exceeding  $10^3$  cm<sup>-3</sup> being more prevalent in 2016. Burkart et al. (2017) noted that the minimum  $N_{\text{tot}}$  was recorded at 1 cm<sup>-3</sup> in one second; at the same time, the maximum value was recorded at 10,000 cm<sup>-3</sup>. Another significant phenomenon in the marine atmosphere is new particle formation (NPF) (Vaattovaara et al., 2006). This process involves the conversion of gaseous precursors into new aerosol particles through nucleation and subsequent growth. In marine environments, NPF often occurs when gases like sulfuric acid and oxidized organic vapors condense into tiny particles. Sulfuric acid, derived from the oxidation of dimethyl sulfide (DMS), plays a central role in this process, particularly in remote

ocean regions where anthropogenic influences are minimal. However, new particle formation can also be influenced by anthropogenic emissions, increasing the complexity of aerosol dynamics in marine environments (Saliba et al., 2020).

Ship emissions represent one of the most prominent anthropogenic sources of marine aerosol pollution (Eyring et al., 2005). Ships release a variety of pollutants into the atmosphere, including particulate matter (PM), nitrogen oxides (NO<sub>x</sub>), and sulfur dioxide (SO<sub>2</sub>). UFPs exhibited concentrations ranging from 35 to 50 × 10<sup>3</sup> cm<sup>-3</sup>, with approximately 65 to 70% of these attributed to emissions from ships, primarily associated with SO<sub>2</sub> (Di Natale & Carotenuto, 2015; González et al., 2011). Primary particles released by vessels comprise a diverse combination of elemental and organic carbon, sulfate that has condensed into ash (Kasper et al., 2007), and trace metals such as vanadium and nickel. Additionally, the emission of volatile organic compounds and sulfur dioxide leads to the generation of secondary particles through nucleation and condensation processes (Petzold & Schönlinner, 2004). Due to these characteristics, the particle size distribution within the exhaust plume of ships can range from the nucleation mode to the coarse mode, specifically from 0.005 μm to over 3 μm (Kasper et al., 2007). The ultrafine particles from marine emissions are depicted in Fig.2.5.

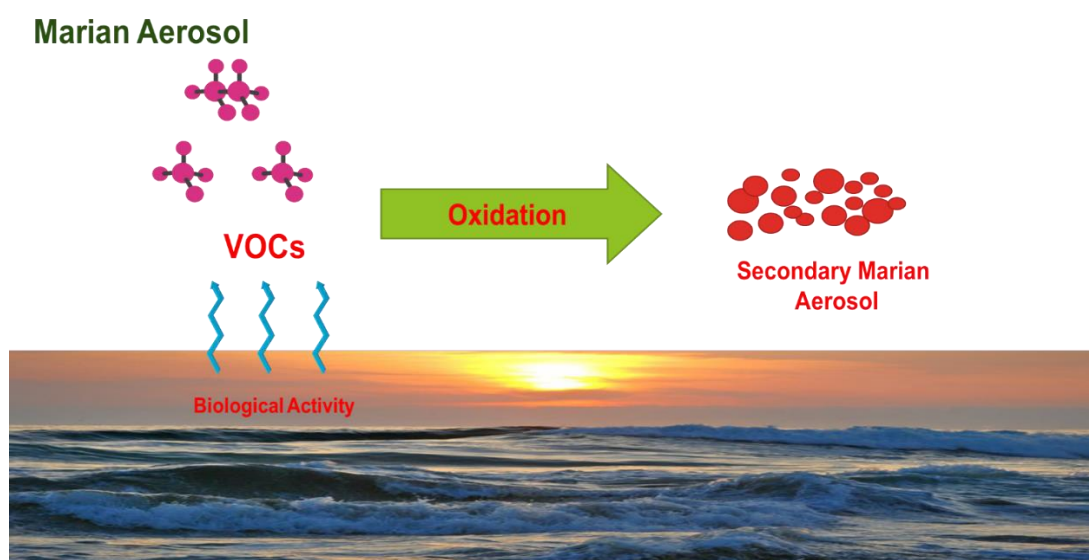


Figure 2.5. The ultrafine particle number concentration from the marine emission (Source: Mayer et al., 2020).

### 2.3.4 Industrial emissions

The ultrafine particles, defined as a diameter ( $D_p$ ) of less than  $< 100$  nanometers, are believed to pose increased toxicological risks due to their significantly larger surface area relative to larger particles (Silva et al., 2010). While it is established that ultrafine particles in the ambient environment primarily originate from vehicle exhaust and the nucleation of secondary particles, there is limited knowledge regarding the levels and prevalence of ultrafine particle concentrations in occupational settings (Machaczka et al., 2021). Industrial activities that involve high temperatures, such as galvanizing, welding of metals and plastics, soldering, and plasma spraying, have been identified as sources of elevated ultrafine particle emissions compared to ambient air quality. The ultrafine particles from industries are depicted in Fig.2.6. The study conducted within the UK industrial sector utilized portable condensation particle counters (TSI P-Trak Model 8525 and, in earlier stages, the TSI Porta count Model 8010) and scanning mobility particle sizer (SMPS; TSI Model 3071A). The number concentrations can exceed  $5 \times 10^5$  particles per cubic centimeter. In contrast, ambient levels typically range from  $10^3$  to  $10^4$  particles per cubic centimeter (Wake et al., 2002).

In workplaces, ultrafine particles are generated through processes characterized by high temperatures, combustion, and mechanical operations that involve substantial energy (Biswas & Wu, 2005). Everyday activities that produce these particles include welding, engine operation, and grinding. The review indicated that ultrafine particle concentrations in various industrial sectors surpass the usual urban background levels. The highest average concentrations were observed in welding, machine shops, the basic metal industry, and other industrial sectors, with values ranging from approximately  $0.7$  to  $4.7 \times 10^6 \text{ cm}^{-3}$ , which is about 60 to 450 times greater than the background levels found in typical non-occupational urban environments. This finding aligns with expectations, as high-temperature processes, machine tooling, and engine operations are prevalent in these industries. Notably, the maximum concentration recorded was in the metal industry, specifically in facilities processing beryllium metal and alloys, where a concentration of  $1739 \times 10^6 \text{ cm}^{-3}$  was documented during a process involving the reduction of magnesium from beryllium hydroxide in a fluoride furnace area. This concentration is alarmingly high, leading the



authors to recommend prohibiting access to the area (McCawley et al., 2001; Viitanen et al., 2017).

## Industry

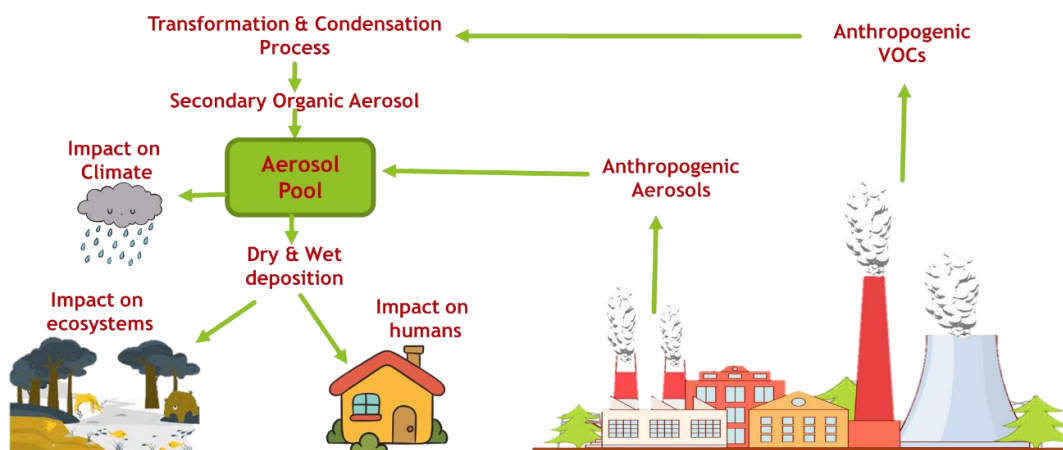


Figure 2.6. The ultrafine particle number concentration from industrial emissions (Source: Rivas-Ubach et al., 2019).

### 2.3.5 Transport sector

Air quality in urban environments has faced significant challenges in recent decades, primarily due to a range of human activities, including demolition and construction, industrial operations, vehicular emissions, and biomass combustion. The rise in vehicle numbers is frequently cited as a significant contributing factor by various researchers (Amato et al., 2011; Bergbäck et al., 2001; Sörme et al., 2001). Ultra-fine particles, defined as those smaller than 300 nm in diameter, account for over 99% of total particulate emissions. It is noteworthy that while the lower size limit is significant, any upper limit exceeding 300 nm has minimal impact on the estimation of ultrafine particles (UFPs). In Europe, the proportion of nanoparticle emissions attributed to road traffic ranges from approximately 32% in Greece to about 97% in Luxembourg. The leading emitters of particulate matter in the European Union include France, Spain, Germany, Italy, the UK, and Poland, collectively responsible for nearly three-quarters (approximately 72%) of the total traffic-related particulate emissions in the region (Kumar et al., 2014; Trejos et al., 2021). Particle number concentration (PNC) serves as the primary metric for characterizing UFPs and assessing their associated exposure risks. Established measurement technologies for PNC, based on

particle number size distribution (PNSD), have been effectively implemented. Observations of PNSD indicate that in most global cities, the count median diameters (CMD) are typically below 100 nm, suggesting that UFPs are the predominant contributors to PNC in urban settings. The primary sources of UFPs are primarily attributed to internal combustion engines, including those in gasoline and diesel vehicles, as well as emissions from ships and airplanes. A recent comprehensive review indicated that traffic-related emissions are the leading source of PNC in over 94.4% of cities, based on a synthesis of 245 studies examining PNC globally. Additionally, secondary UFPs resulting from new particle formation (NPF) events can lead to significant increases in PNC, often by one to two orders of magnitude (Wang et al., 2023). Fresh particles released from vehicle exhausts typically display a bimodal distribution, characterized by a nucleation ( $N_{\text{nuc}} < 20$  nm) and a carbonaceous mode (50-200 nm). Sulfuric acid droplets, which are produced during the exhaust's dilution and chilling operations, make up the majority of the nucleation mode. These droplets are then covered in condensed sulfate and/or hydrocarbons. The rates of nucleation mode development can be influenced by several variables, including the exhaust after-treatment system, fuel mixture, lubricating oil, and ambient conditions. A part of the material in the nucleation mode is semi-volatile, and the temperature and relative humidity of the surrounding air, along with the dilution circumstances, affect how quickly it forms. The carbonaceous mode, which spans from 50 to 200 nm, is primarily composed of soot, absorbed organic substances, and other trace elements produced within the engine and emitted directly in a solid form (González et al., 2011). The ultrafine particles from traffic emissions are depicted in Fig.2.7.

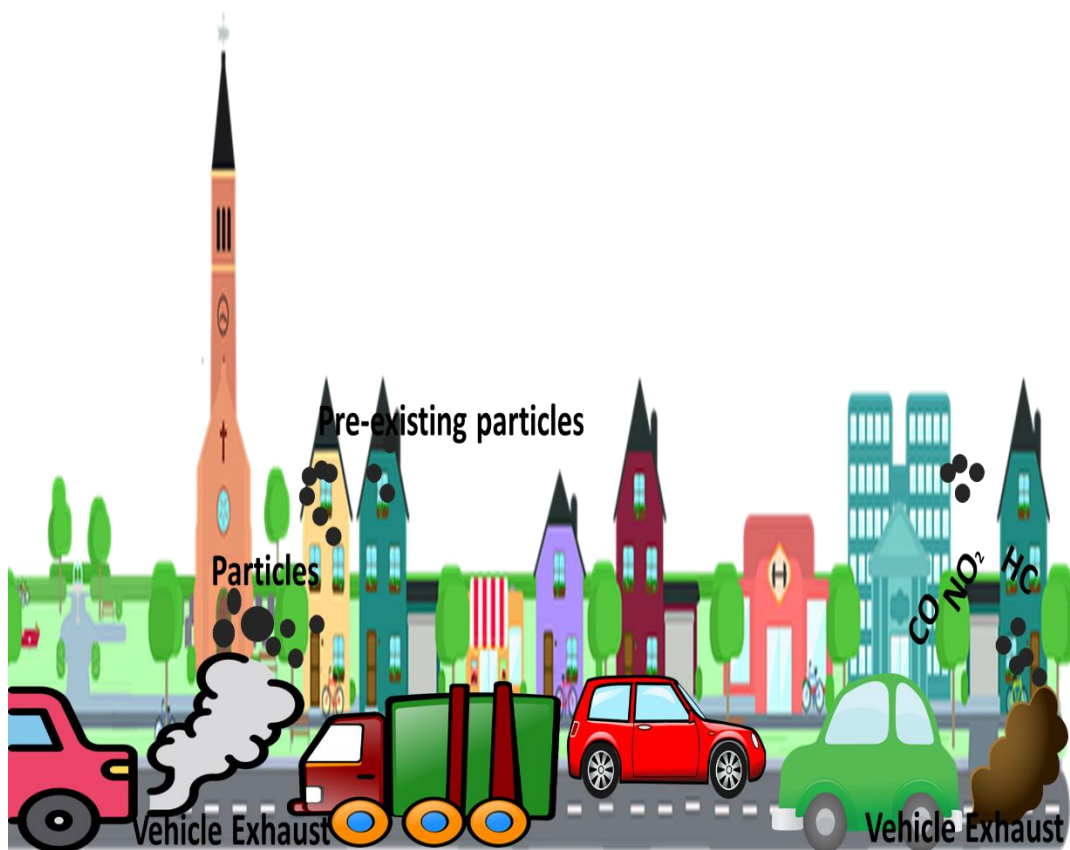


Figure 2.7. The ultrafine particle number concentration from traffic emissions (Source: Li et al., 2023).

### 2.3.6 Indoor ultrafine particles

Daily exposure to ambient air pollution is unavoidable; however, individuals spend most of their time in indoor spaces (Bekö et al., 2015). In developed nations, it is estimated that people spend approximately 80% to 90% of their time in indoor microenvironments (Franck et al., 2003; Klepeis et al., 2001), where pollutant concentrations can be nearly two to five times greater than those found outdoors (Ali et al., 2022; Hassan et al., 2015; Ubaid Ali et al., 2019). This suggests that indoor particulate matter plays a significant role in determining human exposure to PM (Marval & Stronville, 2022). Consequently, indoor air quality (IAQ) has a significant influence on health, potentially posing greater risks than outdoor pollution (Cincinelli & Martellini, 2017).

Indoor aerosols comprise a combination of outdoor aerosols that infiltrate buildings with specific size-resolved efficiencies, as well as particles produced indoors

through daily human activities (Azimi & Stephens, 2020). Notable sources of ultrafine particles (UFP) in indoor settings include combustion activities (such as cooking, tobacco smoking, and candle use), operation of various devices (including printers, photocopiers, heaters, and vacuum cleaners), as well as other occupant activities (Mazaheri et al., 2016; Morawska et al., 2017; Quang et al., 2013). Additionally, a considerable portion of indoor UFP arises from secondary formations (Morawska et al., 2009; Reche et al., 2014; Rossignol et al., 2013). In both residential and commercial buildings, nearly any activity can serve as a potential source of  $PM_{0.1}$ . Numerous studies have examined the UFP emissions associated with routine activities, including cooking, smoking, candle burning, cleaning, using sprays, ironing, electric heating, vacuuming, and digital and 3D printing (Diapouli et al., 2011; Géhin et al., 2008; Wallace & Ott, 2011). Among these, cooking and combustion-related activities (for example, using an electric stove or oven, smoking, or lighting a candle or match) are identified as the most significant sources of UFPs (Afshari et al., 2005). These activities can generate particles at a rate of  $2.02 \times 10^{12}$  #/min, ranging from  $7.86 \times 10^{12}$  #/min to  $5.25 \times 10^{13}$  #/min (He et al., 2004; Hussein et al., 2006). Zhang et al. (2010) found that individuals are exposed to significantly elevated levels of ultrafine particles (UFPs) during cooking, with concentrations reaching up to 550 times higher than ambient levels. Non-combustion sources, such as electric radiators, fan heaters, and hair dryers, that involve heated surfaces can produce UFP levels comparable to those from combustion sources, particularly when dust is present on their surfaces. The UFP generation rate from these sources is measured at  $2.75 \times 10^{11}$  particles per minute, falling within a range of  $7 \times 10^8$  to  $8.84 \times 10^{11}$  particles per minute (Afshari et al., 2005; Hussein et al., 2006; Wallace & Ott, 2011). Among the identified indoor UFP sources, a clean iron operated without steam generates the least particles, with a rate of  $7 \times 10^8$  particles per minute (Afshari et al., 2005). In office environments, standard printers can emit particles at a rate of up to  $1.38 \times 10^{12}$  particles per minute (Géhin et al., 2008; Wang et al., 2017), while 3D printers are capable of generating particles at a rate of  $2 \times 10^{11}$  particles per minute (Marval & Tronville, 2022). Various studies have evaluated the relative contributions of indoor sources to UFP concentrations compared to outdoor air (Bekö et al., 2015; Isaxon et al., 2015; Weichenthal et al., 2007; Zhao et al., 2020, 2021).

In residential settings, it is consistently noted that indoor sources significantly contribute to UFP levels. On average, the contributions from indoor emissions are comparable to those from outdoor air. However, episodic emissions from activities such as cooking can lead to temporary spikes in concentration, during which indoor sources prevail. In instances of heavy indoor source usage, such as frequent candle burning, indoor emissions can dominate even when averaged over time. Since many episodic emissions coincide with occupant activities, the impact of indoor emissions on exposure is heightened beyond their average contribution to indoor concentrations (Wierzbicka et al., 2015). Additionally, indoor sources have been identified in other environments, including schools (Morawska et al., 2009) and offices (Tang et al., 2012). However, the influence of indoor emissions in these contexts is generally less significant than in residential areas (Morawska et al., 2017). Weichenthal et al. (2007) conducted measurements of particle number concentrations in 36 Canadian homes during the evening and overnight periods of the heating season. Their findings indicated that the average concentrations during the evening hours (16:00 - 24:00) and overnight hours (24:00 - 08:00) were  $21.6 \times 10^3 \text{ cm}^{-3}$  and  $6.6 \times 10^3 \text{ cm}^{-3}$ , respectively. In a separate study, Zhao et al. (2020) observed particle number size distributions (10-800 nm) at 40 households in Berlin and Leipzig over a cumulative duration of 497 days, reporting average household exposures of approximately  $2,00,000 \text{ particles/cm}^3 \times \text{h/d}$ . Additionally, restaurants were found to exhibit increased indoor ultrafine particle (UFP) concentrations due to the emissions from cooking. Ott et al. (2017) conducted a study in Northern California towns while carrying portable continuous monitors that unobtrusively measured ultrafine (down to 10 nm) and fine ( $\text{PM}_{2.5}$ ) particles, and the exposure levels during 73 dining episodes at restaurants. On average, car transportation to and from the restaurant contributed  $17,000 \text{ particles/cm}^3 \times \text{h}$  of exposure, while the dining period itself added another  $72,000 \text{ particles/cm}^3 \times \text{h}$ . It is essential to note that these values represent exposures associated with each dining event, rather than daily averages. In Barcelona, Spain, the average concentration of indoor ultrafine particles (UFPs) was measured at  $15,577 \text{ particles/cm}^3$ , which is significantly lower than the outdoor concentration of  $23,396 \text{ particles/cm}^3$  (Rivas et al., 2014). In Bologna, Italy, the urban environment exhibited a mean UFP concentration ranging from 396 to  $8,287 \text{ particles/cm}^3$  indoors and from 1,446 to

13,988 particles/cm<sup>3</sup> outdoors (Zauli Sajani et al., 2015). Germany experienced severe indoor UFP air pollution, with an exceptionally high particle number concentration (PNC) of 2.3 million particles/cm<sup>3</sup> attributed to an indoor candle burning (Soppa et al., 2019). Similarly, elevated indoor pollution levels were reported in Denmark, Australia, and China, particularly in Heshan City, South China, with concentrations of 2,41,000 particles/cm<sup>3</sup> from candle burning, 1,40,000 particles/cm<sup>3</sup> from classroom art activities, and 1,26,000 particles/cm<sup>3</sup> from the infiltration of outdoor particles (Afshari et al., 2005; Mazaheri et al., 2019; Morawska et al., 2009). This issue is particularly concerning for children, who are more vulnerable to the detrimental effects of air pollution due to their developing respiratory and immune systems, lower body mass index, and distinct respiratory patterns (Burtcher & Schüep, 2012). Furthermore, increased physical activity and rapid inhalation can result in greater exposure to harmful pollutants (Pohl & Abadin, 2008). Given that children spend approximately 25 to 30% of their daily time in educational settings such as nurseries, kindergartens, preschools, and primary schools, the indoor air quality (IAQ) in these environments is a critical factor for their health and well-being (Mejía et al., 2011; Salthammer et al., 2016). Real-time measurements of UFPs were conducted daily from 09:00 to 17:30 in 20 primary schools in Oporto in 2014 (January and April), and 2015 (October and February), across various locations including libraries, canteen classrooms, gyms, and outdoors. Overall, the concentrations of UFPs exhibited significant temporal and spatial variability. Slezakova et al. (2019) reported that the median ultrafine particle (UFP) concentration in classrooms ranged from 1.56 to 16.8 x 10<sup>3</sup> cm<sup>-3</sup>. The ultrafine particles from indoor emission and their deposition areas in the human body are depicted in Fig.2.8.

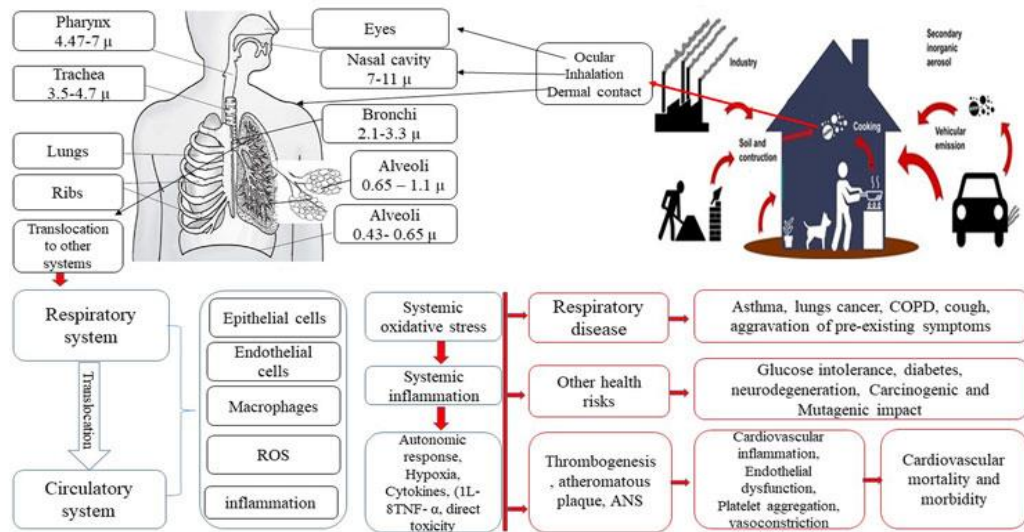


Figure 2.8. Ultrafine particle number concentration from Indoor emissions (Source: Ali et al., 2022).

## 2.4 Particle number concentration at roadside-microenvironment

The World Health Organization's (WHO) recent guidelines emphasized the need for the regular monitoring of particle number concentrations (PNC) due to their detrimental effects on human health. Vehicular sources contribute to particulate matter emissions through both exhaust (from the exhaust pipe) and non-exhaust-type (including brake & tire wear, and road dust). The particles released from exhaust gases and the wear of vehicle components, along with primary and secondary particles of both anthropogenic and natural origins, accumulate daily on road surfaces as road dust (Amato et al., 2009, 2011). Due to the turbulence created by the wheels, road dust with an aerodynamic diameter of less than  $10\ \mu\text{m}$  is resuspended when vehicles travel. The significance of  $\text{PM}_{10}$  emissions lies in their comparability to non-depleted emissions, as evidenced by various studies (Bukowiecki et al., 2010; Harrison et al., 2008; Querol et al., 2001; Trejos et al., 2021). In traffic-dense areas, PN concentrations tend to be elevated, with a predominance of the ultrafine fraction (particles with diameters  $D_p \leq 100\ \text{nm}$ ). Urban environments typically exhibit high PN concentrations due to traffic-related emissions (Krecl et al., 2024). Chen et al. (2022) study presents a long-term trend analysis of particle number concentrations (PNC) in the size range of 11 to 500

nm, based on particle number size distributions (PNSDs) collected in Rochester, NY, from 2005 to 2019. The ultrafine particles from the roadside are depicted in Fig.2.9.

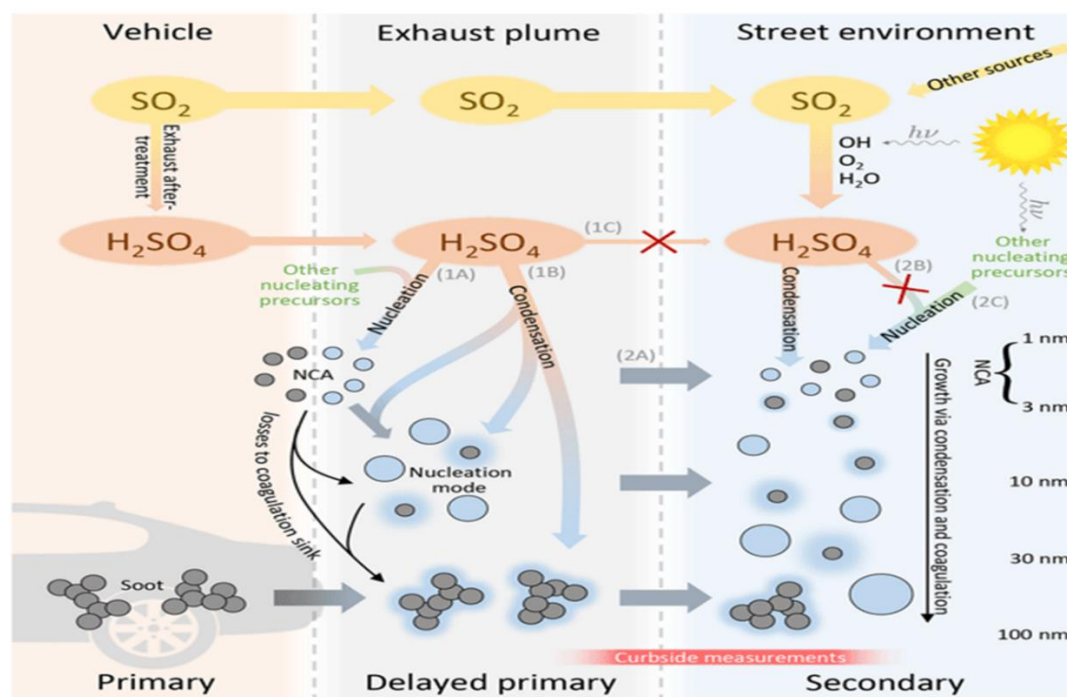


Figure 2.9. The ultrafine particle number concentration from the roadside microenvironment (Source: Olin et al., 2022).

During the years 2013 to 2018, the average concentrations of PNC (4 nm) were  $\sim 1.85 \times 10^4 \text{ cm}^{-3}$ , and PNC (10-410 nm) were  $\sim 6.76 \times 10^3 \text{ cm}^{-3}$ , in the street canyon, which was recorded in Stockholm from 2009 to 2019 (Krecl et al., 2024). Ou et al. (2021) utilized 32 size measurement channels of the FMPS (fast mobility particle sizer) to encompass the particle size range (5.6-560 nm) of ultrafine particles. Study indicated that in Hefei, China, the average number concentration (PN) of aerosol particles within the size range of 5.6-560 nm was  $1.27 \times 10^4 \text{ cm}^{-3}$ , with a predominant concentration of particles smaller than 300 nm, averaging  $1.23 \times 10^4 \text{ cm}^{-3}$ , highlighting the presence of a significant quantity of ultrafine particles in that area. Tremper et al. (2022) reported that during a sampling period at Horley, the average particle concentration was 11,745 particles per  $\text{cm}^{-3}$  at London Gatwick Airport. The emissions observed were primarily from particles smaller than 30 nm. In Beijing, China, particle concentrations ranging from approximately 6 to 150 nm displayed distinct peaks during the morning (06:00 - 12:00) and evening (17:00 - 23:00) hours, attributed to traffic emissions and potentially other sources, along with the growth of emitted



particles (Kontkanen et al., 2020). For instance, Klemm et al. (2022) reported that PN concentrations surged by over  $40,000 \text{ cm}^{-3}$  within just one second while navigating through a traffic circle in a high-traffic area. Dröge et al. (2024) noted that particle number concentrations exhibited significant fluctuations throughout the measurement period, including within individual days, with a maximum 24-hour mean concentration of  $24,120 \text{ cm}^{-3}$  recorded in Frankfurt. Cai et al. (2020) found that in urban and regional locations in China, such as Shanghai, Guangzhou, and Wuxi, the particle lies in the range between  $1.3$  to  $1.8 \times 10^4 \text{ cm}^{-3}$ . These concentrations were found to be 2 to 3 times higher than those recorded at background sites (e.g., Wenling  $5.7 \times 10^3 \text{ cm}^{-3}$  and Changdao  $6.7 \times 10^3 \text{ cm}^{-3}$ ) or in marine environments ( $5.6 \times 10^3 \text{ cm}^{-3}$ ) (Peng et al., 2014). Belkacem et al. (2020) conducted a study along a roadside in Bron, near Lyon, France, in June and July 2019, with sampling performed at 08:15 AM and 05:00 PM. A spectrometer (Model 3091) was used at two distinct heights and various distances from the source, ranging from 6.60 m to 330 m, with a particle size range of 5.6 to 600 nm, adjacent to a heavily trafficked urban roadway. The findings indicated a significant increase in particle number concentration (PNC) with an elevation of less than 2.82 m above the road surface. Measurements were done at two different heights:  $h_1 = 2.03$ , and  $h_2 = 2.82$  m above the pavement. The data revealed that the mean PNC varied between  $1.04 \times 10^4$ , and  $2.70 \times 10^4 \text{ cm}^{-3}$  on the measurement days. The urban study area exhibited a high concentration of nanoparticles, with channel size diameters predominantly in the nucleation mode, primarily around 10.75 nm, reaching values of up to  $5.61 \times 10^3 \text{ cm}^{-3}$  at height  $h_1$  and  $3.23 \times 10^4 \text{ cm}^{-3}$  at height  $h_2$ . This observation can be attributed to the influence of thermal plume rise and the substantial number of buses, as the tailpipe height of a heavy-duty vehicle (HDV) is approximately 2.70 m above the ground.

One important factor to consider in the roadside microenvironment is the presence of traffic intersections. Intersections equipped with traffic signals tend to experience significantly higher peaks of particle number concentrations (PNCs) compared to other roadside locations, categorizing them as pollution hotspots within urban areas. Numerous studies have investigated the particle number distributions (PNDS) and PNC originating from these traffic intersections. A study conducted by Kalaiarasan et al. (2024) examined three distinct microenvironments in a London park

(PK), an indoor setting (IN), and a traffic intersection (TI), focusing on particle sizes ranging from 6 to 10,000 nm. The findings indicated that PNCs at traffic intersections were notably elevated compared to the other locations, with a mean PNC of  $7 \pm 18.96 \times 10^4 \text{ cm}^{-3}$ . The PNDs for nucleation mode ( $N_{\text{nuc}}$ ) particles were particularly high at the traffic intersection, particularly during peak traffic hours. The average particle number concentration (PNC) in nucleation mode ( $N_{\text{nuc}}$ ) at the intersection site ( $\sim 3.1 \pm 9.5 \times 10^4 \text{ cm}^{-3}$ ) was found to be more than 5.5 times and 10.7 times greater than those recorded indoors. This increase in nucleation mode concentrations is likely attributable to exhaust emissions from traffic because particles in this size range are immediately released as supersaturated vapors from automobile tailpipes. Research indicates that traffic intersections in urban areas exhibit approximately 17 times higher PNCs compared to average roadside concentrations (Kumar et al., 2014). Additionally, various tests involving alternative fuel combinations have been conducted, demonstrating a reduction in ultrafine particles during on-road assessments (Yusuf et al., 2021). Furthermore, Kamara & Harrison. (2021) noted that the average particle count on London's Marylebone Road decreased from approximately  $38,000 \text{ cm}^{-3}$  in 2011 to around  $11,000 \text{ cm}^{-3}$  in 2019.

## **2.5 Particle number concentration in regional background**

In regions characterized by a predominantly natural background, the concentration of ultrafine particles (UFPs) is generally lower than that found in urban or industrial settings. These areas are often situated far from significant sources of pollution, including vehicular traffic, manufacturing facilities, and high-density populations, which leads to a reduction in the primary emissions of ultrafine particles. Natural sources, including sea spray, emissions from vegetation, and the long-distance transport of pollutants from other regions, primarily influence the background levels of UFPs. Van De Beek et al. (2021) conducted a study in 2020 that measured ultrafine particles (UFP) ranging from 10 to 300 nm at 20 regional background (RB) locations throughout the Netherlands. The average UFP concentrations recorded at the 20 locations varied between 3814 to 7070 particles/ $\text{cm}^3$ . Additionally, meteorological conditions, including wind speed (WS), temperature (AT), and relative humidity (RH), significantly influence the generation, transformation, and distribution of these particles. Nevertheless, transient events in the atmosphere, such as wildfires or dust

storms, can temporarily increase UFP concentrations. In summary, in these areas, the formation of UFPs is more commonly associated with secondary processes involving the conversion of gases into particles rather than direct emissions.

## **2.6 Comparison between the urban regions and other regions**

The variability of ultrafine particle and particle number size distribution (PNSD) concentrations varies over time in a complex way due to dynamic processes (Harrison et al., 2019; Trechera et al., 2023). Analyzing particle number concentrations across urban and non-urban areas is crucial for understanding the spatial variations in air pollution and its sources. This analysis highlights the significant impact of anthropogenic activities, including vehicular traffic and industrial discharges, which are major contributors to elevated pollution levels in urban areas. Such comparisons are crucial for evaluating the effectiveness of air quality policies, monitoring pollution patterns, and identifying regions that require targeted intervention strategies. In urban areas, particle number concentrations are significantly higher (Austin et al., 2021) than in rural or background areas, primarily due to the proximity of pollution sources, such as automotive emissions, industrial operations, and construction activities. Thén & Salma. (2022) Particle number concentration measurements were conducted in Budapest, Hungary, over nine years, from 2008 to 2021. The annual median value of  $N_{\text{tot}}$  was approximately  $9 \times 10^3 \text{ cm}^{-3}$ . During the summer months in the Eastern United States, gasoline vehicles accounted for 40% of ultrafine particle number emissions, followed by industrial sources at 33%, non-road diesel at 16%, on-road diesel at 10%, and a mere 1% attributed to biomass burning and dust (Posner & Pandis, 2015). In Japan, the primary sources of  $\text{PM}_{0.1}$  emission included automobile exhaust (30%) and coal combustion, likely linked to integrated steelworks (24%) during winter, while in summer, fuel combustion (39%) and automobile exhaust (11%) were the main contributors (Fujitani et al., 2012). Giemsa et al. (2021) conducted a four-week study in Augsburg across various locations in 2017, where traffic-influenced sites and industrial/commercial areas recorded average values exceeding 10,000 ultrafine particles/ $\text{cm}^3$  throughout the measurement period. The highly trafficked Karlstraße location in Augsburg recorded even higher levels, surpassing 34,000 particles/ $\text{cm}^3$ .

Residents living near major roadways may experience increased exposure to traffic-related air pollution (TRAP) in their daily lives, including at home, work, and

school. Such exposures have been linked to a range of adverse health outcomes, including cardiovascular and respiratory diseases, as well as increased rates of premature mortality (Hashad et al., 2024). In contrast, rural and background areas demonstrate significantly lower particle concentrations as they are located far from pollution sources and are more influenced by natural emissions and the long-range transport of pollutants. Gani et al. (2021) conducted a study that integrated long-term fixed-site measurements with mobile monitoring assessments conducted on roads in the San Francisco Bay Area, California, USA. In 2015, a year characterized by nearly complete pollutant coverage across all measurement sites, the annual average particle number concentrations were recorded as follows: near-highway locations (TRAP), 29,900  $\text{cm}^{-3}$ ; urban areas, 11,900  $\text{cm}^{-3}$ ; suburban regions, 10,100  $\text{cm}^{-3}$ ; and rural settings, 3,500  $\text{cm}^{-3}$ . In a subsequent report by Trechera et al. (2023), data from six traffic monitoring sites in Europe, specifically Dresden (DRE\_TR), Helsinki (HEL\_TR), Leipzig (LEI\_TR), London (LND\_TR), and Stockholm (STO\_TR), along with one background site in Ispra (ISP), were analyzed for the years 2017 to 2019. The traffic sites exhibited elevated particle number concentrations (PNCs), ranging from 13,500 to 10,500  $\text{cm}^{-3}$  at the LEI, LEI2, LND, and HEL locations, followed by 8,800 and 5,100  $\text{cm}^{-3}$  at DRE and STO, respectively. Conversely, the suburban (SUB) and rural background (RB) sites demonstrated comparatively lower concentrations, ranging from 7,400 to 4,500  $\text{cm}^{-3}$ . When examining nucleation mode concentrations (10-25 nm), which considered only sites with a lower size limit of  $< 14$  nm for particle number size distribution (PNSD) measurements, the nucleation mode ( $N_{\text{nuc}}$ ) particle concentrations were found to be lower at the SUB (1,000-2,200  $\text{cm}^{-3}$ ) and RB (1,000  $\text{cm}^{-3}$ ) sites, while markedly higher values were recorded at urban background (UB) sites (1,500-4,600  $\text{cm}^{-3}$ , excluding BIR\_UB, which had 700  $\text{cm}^{-3}$ ) and traffic sites (3,600-6,700  $\text{cm}^{-3}$ , excluding STO\_TR, which had 1,600  $\text{cm}^{-3}$ ). Aitken mode concentrations (25-100 nm) were observed to range from 2800 to 6800 particles per cubic centimeter at TR sites, while UB sites recorded concentrations between 2100 and 5900 particles per cubic centimeter, SUB sites showed values from 2600 to 4100 particles per cubic centimeter, and RB sites had a concentration of 4100 particles per cubic centimeter. Cheung et al. (2022) conducted a study in urban and suburban

regions of Guangzhou, South China, from January to February 2020, before and during the Chinese New Year holiday.

The average particle number concentration (PNC) recorded was  $6.3 \times 10^3 \text{ cm}^{-3}$ , and  $9.7 \times 10^3 \text{ cm}^{-3}$ , respectively. The average particle number concentration recorded was  $6.3 \times 10^3 \text{ cm}^{-3}$ , and  $9.7 \times 10^3 \text{ cm}^{-3}$ , respectively. In a study conducted by Chatain et al. (2021) in Strasbourg, France (20-800 nm) during the winter of 2019, the average PNC concentration throughout the campaign was found to be  $6.8 \times 10^3 \text{ particles/cm}^3$  for the urban background site and  $8.4 \times 10^3 \text{ particles/cm}^3$  for the roadside site. While the concentrations at the roadside site were almost an order of magnitude lower than those typically found at roadside sites, which are approximately  $10^5 \text{ particles/cm}^3$ , the concentrations at both locations are comparable to the average levels seen at urban background sites, which typically range from  $10^3$  to  $10^4 \text{ particles/cm}^3$ . Additionally, studies indicate that roadside sites exhibit particle levels that are two to ten times higher than those at urban background sites. Zheng et al. (2021) reported that the 0.3-0.5  $\mu\text{m}$  size range reached concentrations of approximately  $1.65 \times 10^8$  and  $1.10 \times 10^8 \text{ particles/cm}^3$  at roadside locations and background locations in Shanghai Jiao Tong University (SJTU), respectively.

## **2.7 Role of meteorological parameter in particle number concentration**

Meteorological parameters such as wind speed, wind direction, solar radiation, atmospheric temperature, and relative humidity play a crucial role in the behavior and concentration of ultrafine particles (UFPs) in the atmosphere (Zhang et al., 2016a). The dispersion and transport of UFPs are influenced by wind direction and speed; higher wind speeds often result in more dilution and lower particle concentrations in a given area. Kalaiarasan et al. (2024) reported that nucleation mode ( $N_{\text{nuc}}$ ) particles exhibited elevated concentrations at wind speeds between 4 and 6 m/s, approximately ~13 times greater than the lower concentrations observed at wind speeds of 10-12 m/s. Generally, as wind speed increases, the concentration across all particle modes decreases. Conversely, accumulation mode ( $N_{\text{acc}}$ ) particles demonstrated higher concentrations at lower wind speeds (ws). For example, the particle number concentrations (PNCs) were notably recorded highest at a wind speed of 0 to 2 m/s, with a significant reduction in PNCs as the wind speed increased, reflecting a threefold difference compared to the lowest PNCs recorded in the 10 to 12 m/s range. On

the other hand, Belkacem et al. (2020) conducted a study in June and July 2019 near a roadside in Bron, close to Lyon, France, with sampling times at 08:15 AM and 05:00 PM. The fourth day of measurement exhibited higher concentration levels, attributed to the wind blowing towards the monitoring location. Conversely, the third day recorded the lowest particle concentration levels, which were influenced by a higher wind speed (WS) of 15.2 m/s directed away from the monitoring sample site. Conversely, low wind speeds can lead to the accumulation of UFPs, particularly in urban environments where emissions from vehicles and industrial activities are high. Solar radiation affects the photochemical reactions in the atmosphere, which can lead to the formation of secondary organic aerosols, contributing to the overall particle number concentration (Zhang, et al., 2016b).

Atmospheric temperature impacts the atmosphere's stability; higher temperatures can enhance vertical mixing, dispersing particles more effectively, while lower temperatures can lead to temperature inversions that trap pollutants near the ground (Zhang, et al., 2016b). At a distance exceeding 300 meters from the source (Day – (D8)), the concentration of particles with a diameter greater than 246 nm approached zero, likely due to the elevated ambient temperature of approximately 30°C (Belkacem et al., 2020). These meteorological factors are essential for understanding and predicting UFP concentrations, making them critical for air quality management and public health studies. Relative humidity influences the hygroscopic growth of particles (Klemm et al., 2022), causing them to absorb water and increase in size, which can affect their optical properties and atmospheric lifetime (Flueckiger & Petrucci, 2024). To compare and forecast UFP dynamics and help scientists and policymakers comprehend and lessen the effects of UFP pollution on the environment and public health, meteorological data is therefore crucial. By examining meteorological factors alongside UFP concentrations, researchers can more accurately model UFP behavior, predict pollution events, and design effective intervention strategies (WHO, 2016).

## **2.8 New particle formation in different microenvironments**

New Particle Formation (NPF) is a universal atmospheric phenomenon involving the transformation of gaseous precursors into solid or liquid particles through nucleation and subsequent growth processes (Dada et al., 2017, 2020). Such

particles substantially contribute to the global submicron aerosol population, influencing both direct (scattering/absorption of solar radiation) and indirect (cloud condensation and microphysical properties) radiative effect (Buenrostro Mazon et al., 2016; Cheung et al., 2022; Meskhidze et al., 2019; Ou et al., 2021; Sebastian et al., 2022; Yadav, Kompalli, et al., 2021; Yu et al., 2020; Zhang et al., 2018). These newly formed particles typically originate in the nucleation mode ( $D_p < 25$  nm) and can grow into Aitken ( $25 < D_p < 100$  nm) and accumulation ( $100 < D_p < 1000$  nm) modes (Kulmala et al., 2012). NPF events have been observed in various environments (coastal, inland, rural, urban, forest, boundary layer, and mountain areas) around the world (Dinoi et al., 2023; Größ et al., 2018; Ou et al., 2021). In this study, these foundational NPF concepts guided our interpretation of particle number size distributions. Specifically, the identification of nucleation and growth modes in the observed data was used to characterize NPF events and to evaluate their temporal variability and potential sources under the regional atmospheric conditions. Research has indicated that the occurrence of NPF events is influenced by several factors, including the characteristics and size of the precursor vapor, the concentration of pre-existing particles, local meteorological conditions (such as temperature, relative humidity, solar radiation, and wind), and the prevailing atmospheric circumstances (Brines et al., 2015). It is recognized that multiple pathways may simultaneously play a role in NPF mechanisms, with their relative importance varying by region and likely changing over time.

The method by which atmospheric ultrafine particles are formed is intricate and multifaceted. Sulfuric acid is usually included, though ions may also be present. Still, this is not always the case. These particles can arise through a mechanism known as new particle formation (NPF). The first step in this process is the formation of molecular clusters, which then enlarge. A thorough study of neutral and charged cluster densities, their chemical makeup, and the gaseous components that contribute to their formation and evolution is necessary to understand the early stages of atmospheric aerosol generation. Stable nuclei, which are frequently too small (less than 2 nm) to be picked up by present measurement methods, are first created during the process. After that, gaseous components such as volatile organic compounds (VOCs) and semi-volatile organic compounds (SVOCs) contribute to either

heterogeneous or homogeneous condensation, which both create new nuclei. The process of coagulation, which involves the collision of two particles to form a single particle, then occurs. When newly created ultrafine particles come into contact with other particles, they tend to coagulate rapidly. In the context of solid particles, this coagulation is typically referred to as agglomeration, resulting in clusters known as agglomerates (Marval & Tronville, 2022). Numerous studies often yield conflicting results regarding the relative contributions of various new particle formation (NPF) pathways, even within the same region, making it difficult to identify the predominant NPF pathway for most areas (Zhao et al., 2021). New particle formation appears to be more pronounced in urban settings compared to background environments. Long-term measurements indicate that the annual frequency of NPF in the Mediterranean region ranges from 10% to 36% (Baalbaki et al., 2021). In urban Beijing, research by Deng et al. (2020) revealed that NPF event days and undefined days constituted 37% and 6% of the total days, respectively. Yuan et al. (2015) recorded a total of 26 NPF events over a 120-day measurement period, a frequency that was slightly lower than that observed in other Chinese cities. According to Xiao et al. (2015), there were 13 event days during a 62-day campaign. Additionally, a study by Gao et al. (2012) indicated that new particles formed through homogeneous nucleation occurred on 42.7% of the days during a two-month study period in Beijing (Vu et al., 2015).

A research study conducted by Saha et al. (2018) in Pittsburgh, Pennsylvania, from 2001 to 2002, indicated that nucleation occurred on approximately 50% of the observed days. In contrast, from 2016 to 2017, this occurrence was noted on roughly 27% of the days. Furthermore, Pushpawela et al. (2018) investigated the subtropical urban environment of Brisbane, Australia, where they documented 236 new particle formation (NPF) events over a 485-day period. Baalbaki et al. (2021) reported that during a year-long measurement campaign comprising 365 days, 207 event days were identified, accounting for 56.7% of the total days. In Spain, around 23 NPF events were recorded at urban sites, as noted by Casquero-Vera et al. (2020). Additionally, Jose et al. (2021) examined the monthly and seasonal variations in aerosol particle size distribution in Delhi from December 2011 to January 2013, finding that NPF events were less frequent in this region. From the wide-range aerosol spectrometer (WRAS), out of 222 days of a dataset, only 17 new particle formation (NPF) events were



recorded. Siingh et al. (2018) identified 109 new particle formation (NPF) events from March 8, 2010, to December 31, 2012. During a two-month lockdown study, the frequency of NPF events was approximately 41%, as reported by (Yadav et al., 2021). Sebastian et al. (2022) conducted a study in 2022 across various microenvironments in India, revealing that out of 586 observation days, the new particle formation (NPF) events were recorded in 21 days, accounting for 3.9% at Ranichauri (RNC). In Mukteshwar (MUK), around ~ 440 observation days, NPF occurred 13 days, representing 2.9%. At Mahabaleshwar (MBL), NPF events were noted on 16 days out of 281 valid observation days, representing 5.9%. In Hyderabad (HYD), there were 38 days of NPF events out of 270 valid observation days, which equates to 16.3%. The NPF events at Thiruvananthapuram (TVM) had 23 valid observations out of 133 days, corresponding to a 16.6% occurrence rate. Finally, at Delhi (DEL), NPF events occurred on 39 days from 139 valid observation days, accounting for 28.1%. Additionally, several studies have identified new particle formation in urban and regional backgrounds. For instance, Wang et al. (2023) documented 52 simultaneous NPF events in the North China Plain spanning both urban and regional background locations, from March to November 2008. Furthermore, Kalkavouras et al. (2020) reported 35 days of NPF events occurring simultaneously in Athens (urban) and Finokalia (regional background), all associated with air masses from the Northern sector, indicating the presence of regional events across a wider geographical area characterized by a low condensation sink (CS).

Approximately 877 days were identified as new particle formation (NPF) events during a 20-year observational study conducted in a boreal forest at the SMEAR II station (Dada et al., 2017). The variation in the number of events was influenced by several factors, including geographical characteristics, emission patterns, atmospheric aerosol concentrations, pre-existing aerosol particles, and significant considerations related to the classification methodology of NPF. In Madrid, Gómez-Moreno et al. (2011) recorded 63 events annually over a period of more than two years (from October 2006 to December 2008) in an urban background environment. Limited research has also been conducted in industrial areas. Sipilä et al. (2021) noted that concentrated emissions of sulfur dioxide (SO<sub>2</sub>) from smelting operations can convert

into sulfuric acid ( $\text{H}_2\text{SO}_4$ ) in sufficient amounts to promote new particle formation, even in conditions of low solar radiation in Russia.

## 2.9 Ultrafine particles in Indian scenarios

Many urban areas around the world, particularly highly polluted megacities in China with heavy aerosol loadings, have reported frequent and intense UFP readings (Saha et al., 2018). Over the past decade, numerous experimental and numerical studies have significantly enhanced our understanding of the emission, production, dispersion, exposure, and health effects of ultrafine particles (UFPs). A few emerging Asian cities, where the majority of the world's urban population resides, the majority of this research has been conducted in European cities, but there are very few studies on the concentrations of UFP in India's metropolitan areas (Agarwal & Aggarwal, 2023; Bhandari et al., 2020; Gani et al., 2020; Jose et al., 2021; Kanawade et al., 2014b; Kompalli et al., 2020; Sarangi et al., 2015; Sebastian et al., 2022). Few studies have been conducted in various microenvironments and locations in India. In Delhi, not many studies have been conducted (Mönkkönen, et al., 2004a; Mönkkönen, et al., 2004b). In Delhi, India, Şahin et al. (2022) conducted a small study spanning three seasons. The average total PN levels were  $18.91 \times 10^3 \text{ cm}^{-3}$  in the summer,  $29.35 \times 10^3 \text{ cm}^{-3}$  in the fall, and  $36.73 \times 10^3 \text{ cm}^{-3}$  in the winter. However, Gani et al. (2020) found a somewhat higher concentration. According to measurements taken in 2017, the average PN levels in Delhi were  $52.50 \times 10^3 \text{ cm}^{-3}$  in winter,  $43.40 \times 10^3 \text{ cm}^{-3}$  in summer, and  $38 \times 10^3 \text{ cm}^{-3}$  in fall. Apte et al. (2011) reported the ultrafine particle number concentration (PN) inside a common vehicle (auto-rickshaw) in New Delhi for approximately 180 hours of real-time observations, one of the few studies that only provided on-road measurements and found that concentrations of measured were exposure are significantly higher, at about  $280 \times 10^3 \text{ cm}^{-3}$ , respectively.

Ultrafine particles have been documented in a small number of studies during events such as lockdowns, Diwali, and pollution events (Rajagopal et al., 2023; Rajagopal et al., 2024). According to Joshi et al. (2016), the strong lighting of fireworks on the night of the incident may have caused a noticeable increase in aerosol concentration (about  $1.2 \times 10^5/\text{cm}^3$ ) at 22:10 hours. Due to the restricted fireworks burning the day before and after the celebration, similar phenomena (of low intensity) were seen at night on November 12<sup>th</sup> and 14<sup>th</sup>. In 2023, Rajagopal et al. (2023)

observed that tight limits resulted in a 31% decrease in concentration ( $\sim 2.4 \times 10^4 \text{ cm}^{-3}$ ); nevertheless, the abrupt spike in pyrotechnics caused a 35% increase in concentration relative to normal conditions (Period-II). During Diwali 2019, Yadav et al. (2022) did a study in Delhi, India. The geometric mean diameter (GMD) was approximately 44 nm, and the particle number concentration (PNC) was  $1.7 \times 10^5 \text{ cm}^{-3}$ . Comparing the Diwali period before (October 26, 2019) and after (October 28, 2019), the average PNC increase on Diwali day was 138% and 97%, respectively. A study by Yadav et al. (2021) during the lockdown era showed that the mean total number concentrations were between  $\sim 2 - 3.5 \times 10^4 \text{ cm}^{-3}$  and that they gradually increased ( $\sim 26\%$ ) as anthropogenic activities were gradually unlocked. Concurrently, the concentrations of accumulation particles doubled. However, for the majority of the days, ultrafine particles (UFP) (diameter  $< 100 \text{ nm}$ ) dominated (50-88%) the total number concentrations, and several new particle formation (NPF) events led to high (2-5 times) UFP concentrations.

A small number of research studies have been conducted in various locations in India. According to Kanawade et al. (2014a), from September 2007 to July 2011, total particle concentrations in the Indian city of Kanpur reached approximately  $31.9 \times 10^3 \text{ cm}^{-3}$ . According to Babu et al. (2016), in a tropical coastal semi-urban area called Thiruvananthapuram, ultrafine particles accounted for as much as 45% of the total concentration, making them a significant reservoir that would contribute to the larger particles through size transformation. Sebastian et al. (2021) conducted a study in Hyderabad, an urban area, where approximately 63.9% of all observation days resulted in the production of new particles. In 2014, Kanawade et al. (2014b) carried out research in Pune and Kanpur. Pune had a greater total particle number concentration ( $12.2 \times 10^3 \text{ cm}^{-3}$ ) than Kanpur ( $7.9 \times 10^3 \text{ cm}^{-3}$ ).

Studies have also been conducted in India in a few high-altitude locations and mountainous areas. According to Moorthy et al. (2011), the total number concentration at the Hanle station in the Trans-Himalaya throughout the summer and fall of 2009 varied between 80 and  $8000 \text{ cm}^{-3}$ , with an average of  $1150 \text{ cm}^{-3}$ . A study was carried out by Sharma et al. (2011) in the Kullu-Manali region at Mohal and Kothi. The average ultrafine particle density at the Mohal and Kothi sites was  $20369 \pm 1230 \text{ N cm}^{-3}$  and  $14389 \pm 1464 \text{ N cm}^{-3}$ , respectively, at each hour of the day. In 2018, Kompalli

et al. (2018) conducted a campaign during the pre-monsoon (spring) season over a high-altitude locale, Ooty in the Western Ghats, the highest peak in South India. The concentrations of total numbers were between approximately 1000 and 3000  $\text{cm}^{-3}$ , and they significantly increased (2-4 times) during bursts of ultrafine particles (UFPs) (diameter < 100 nm).

According to Sharma et al. (2009), Mohal in the Kullu-Manali region of the Northwestern Himalayas had an annual average of  $18045 \pm 1212$ ,  $16811 \pm 2790$ , and  $15407 \pm 3109 \text{ N cm}^{-3}$  for ultrafine particles of three size categories in 2008. In 2018, Kompalli et al. (2018) used campaign-based ground observations to investigate the ultrafine particle number concentration and size distribution during the pre-monsoon (spring) season over a high-altitude locale, Ooty in the Western Ghats, the highest peak in South India. The concentrations of total numbers are between approximately 1000 and 3000  $\text{cm}^{-3}$ , and they significantly increase (2-4 times) during bursts of ultrafine particles (UFPs) (diameter < 100 nm). There is not much additional research on the coastal regions. In 2013, Nair et al. (2013) carried out research in the Arabian Sea and the northern Bay of Bengal. Overall, total particle values were high ( $>5000 \text{ cm}^3$ ) throughout the northernmost portions of the cruise track across the Arabian Sea and along the Bay of Bengal coast along the Indian, Bangladeshi, and Myanmar mainlands. While total particle values throughout the northern Arabian Sea were greater than  $40,000 \text{ cm}^3$ , the greatest value over the Bay of Bengal was about  $20,000 \text{ cm}^3$ , which occurred close to the coast of Myanmar. On the other hand, NT values were comparatively low over the southern Arabian Sea ( $< 2,500 \text{ cm}^3$ ) and the central Bay of Bengal ( $< 3,000 \text{ cm}^3$ ).

## **2.10 Health impact of ultrafine particles**

Air pollution has emerged as a significant concern in recent years, with increasing evidence highlighting its detrimental effects on the respiratory, cardiovascular, neurological, and reproductive systems. The World Health Organization (WHO) reports that approximately 4.2 million fatalities are linked to ambient air pollution, indicating a profound impact on both public health and overall quality of life. A closer examination reveals that around 3.6 million deaths globally are attributed to pulmonary diseases. Among the primary contributors to air pollution, alongside natural phenomena such as volcanic eruptions and wildfires, is

industrialization. While developed nations strive to mitigate air pollution, developing countries, which require industrial growth, are experiencing rising pollution levels. Consequently, it is estimated that 80% of individuals residing in urban areas are subjected to air pollution concentrations that surpass WHO recommendations. The respiratory system is divided into two principal zones: the conducting zone, responsible for gas transportation, and the respiratory zone, which facilitates gas exchange. The conducting zone includes the trachea and bronchi, extending to the terminal bronchioles, while the respiratory zone encompasses the respiratory bronchioles, alveolar ducts, alveolar sacs, and alveoli. Chronic lung conditions, such as asthma and chronic obstructive pulmonary disease (COPD), arise from inflammation or obstruction of the lungs and represent one of the most significant burdens on global health systems. Air pollution, particularly in the form of particulate matter, can settle in various regions of the lungs based on factors such as particle size, shape, density, and the individual's breathing patterns (Fig.2.10) (Kodros et al., 2018). Particles larger than 10 micrometers typically do not reach the lower airways, as they are filtered out by the nasal passages and upper airways (Glencross et al., 2020).

Conversely, PM<sub>10</sub>, PM<sub>2.5</sub>, and ultrafine particles (UFP) are capable of penetrating the lower airways, with the smallest particles (PM<sub>2.5</sub> and UFP) accumulating in the terminal bronchioles and alveoli, while PM<sub>10</sub> tends to deposit more in the conducting airways (Losacco & Perillo, 2018). Additionally, UFP can diffuse into the systemic circulation through the blood-air barrier, potentially affecting organs such as the heart, liver, spleen, and brain (Losacco & Perillo, 2018). The elimination of these particles occurs through various pathways, contingent upon their deposition sites. The primary mechanisms for clearance are mucociliary transport and the action of airway macrophages (Geiser & Kreyling, 2010). Upon inhalation, pollutants first interact with the bronchial epithelium, which serves as a protective barrier against environmental substances and regulates both innate and adaptive immune responses (Cooper & Loxham, 2019). Furthermore, innate immune components, including alveolar macrophages, play a role in particle clearance through phagocytosis (Glencross et al., 2020). Ultimately, both clearance pathways can lead to oxidative stress and inflammatory responses within the airways, resulting in lung damage (Cooper & Loxham, 2019; Glencross et al., 2020).

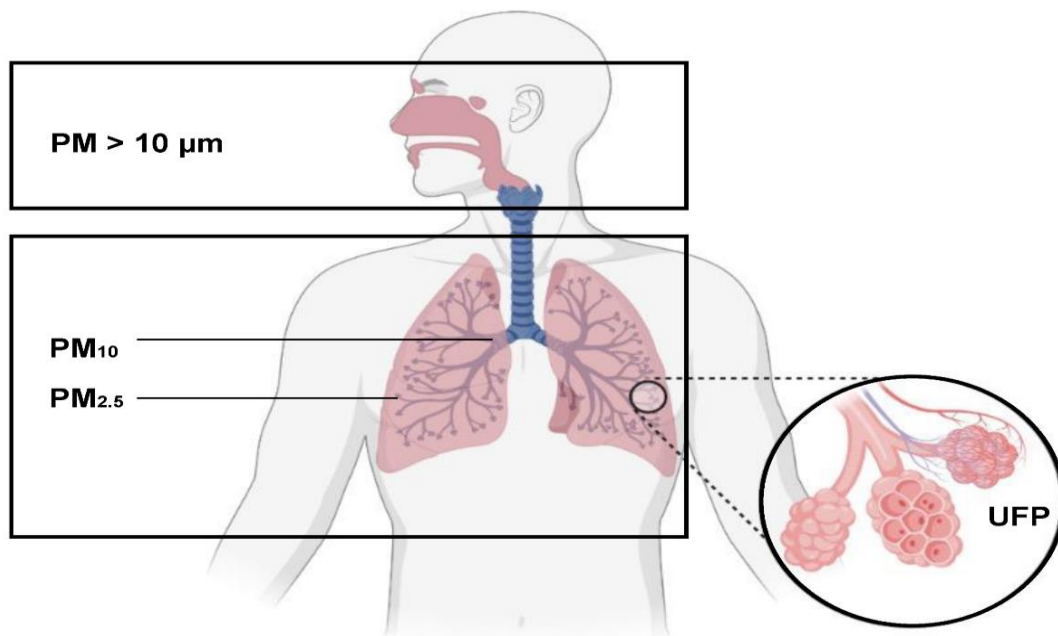


Figure 2.10. Deposition of ultrafine particle number concentration in the human body (Source: Goossens et al., 2021).

Traffic density has been linked to various health impacts. Children residing in areas with high traffic volumes tend to require more medical visits annually due to asthma (English et al., 1999) and exhibit a higher incidence of respiratory symptoms (Ciccone et al., 1998; Oosterlee et al., 1996) compared to those living in regions with lower traffic levels. A study involving nearly 10,000 children in England indicated that the likelihood of wheezing illnesses, including asthma, increased as the distance from a child's home to major roads decreased, with the highest risk observed for children living within 90 meters of such roads (Venn et al., 2002). Additionally, particulate matter generated by traffic has been linked to considerable health hazards (Becker & Soukup, 2003; Ruellan & Cachier, 2001). Recent toxicological and epidemiological research has concentrated on the health effects associated with exposure to ultrafine particles (diameter < 100 nm) (Donaldson et al., 2008; Ibald-Mulli et al., 2002).

To quantify exposure and understand the relationship between ultrafine particles and health, it is essential to assess the concentrations and properties of urban ultrafine particles (Zhu et al., 2004). The study conducted in 2015 along a typical commuting route between urban and suburban regions of Beijing, utilizing four different modes of transportation (63 trips), car, bus, subway, and bicycle, the result

indicated that buses had the highest PNC around  $\sim 35,066 \text{ cm}^{-3}$ , followed by bicycles  $\sim 28,277 \text{ cm}^{-3}$ , cars  $\sim 16,302 \text{ cm}^{-3}$ , and subway  $\sim 13,245 \text{ cm}^{-3}$ . Within the subway system, the highest PNC was recorded at station entrances, followed by transfer tunnels, while cabin areas exhibited the lowest concentrations (Yang et al., 2021). To gain a deeper understanding of the impact of air pollution on human health, it is essential to determine the extent to which inhaled pollutants are deposited within the respiratory tract (Madueño et al., 2022). The particle deposition in various regions of the respiratory tract was observed to decrease in the following order on NPF days: tracheobronchial (TB) > pulmonary (PUL) > extrathoracic (ET), whereas on non-NPF days, the order was PUL > TB > ET (Ma et al., 2022). The total dose rate ranged from  $3 \times 10^9$  to  $65 \times 10^9$  particles/h, with  $\text{PM}_{2.5}$  and  $\text{PM}_{10}$  doses varying between 1 to 22  $\text{g h}^{-1}$  and 9 to 210  $\text{g h}^{-1}$ , respectively, influenced by factors such as gender, activity level, and season. In terms of particle number, the inhaled dose percentages deposited in the alveolar region were 56-76%, tracheobronchial were 16-28%, and head were 7-16%. For the  $\text{PM}_{2.5}$  metric, the corresponding dose rates were 9-41%, 13-19%, and 46-72%, while for  $\text{PM}_{10}$ , the rates were 25-75%, 7-35%, and 15-55%, respectively (Hussein et al., 2022).

## 2.11 Summary

This chapter presented an in-depth review of existing literature on ultrafine particles (UFPs), emphasizing their characteristics, sources, and health implications. It began by defining UFPs (<100 nm) and explaining their classification, as well as their distinctive physical and chemical properties. The review examined both natural and anthropogenic sources of UFPs, including wildfires, marine aerosols, industrial activities, vehicular emissions, and indoor environments. Comparative studies from urban, roadside, and background locations were discussed to highlight the strong spatial variability in UFP number concentrations driven by local emissions and environmental conditions.

The influence of meteorological factors, including wind speed, temperature, humidity, and boundary layer dynamics, on UFP behavior was reviewed in detail, highlighting their significant role in particle dispersion and transformation. Although new particle formation (NPF) processes were also discussed, this was primarily to provide supporting context for understanding secondary UFP generation mechanisms.

The review further incorporated findings from Indian studies to provide a localized perspective on UFP sources, concentrations, and exposure implications.

The reviewed literature reveals that, despite significant progress globally, comprehensive investigations of UFPs in Indian urban and background environments remain limited, particularly in relation to micrometeorological influences. To address this gap, the present study focuses on characterizing ultrafine particle number concentrations, assessing the role of micrometeorological parameters, using observational data collected in both urban and background settings. This synthesis of existing research provides the scientific basis for the methodological framework outlined in the next chapter, where data collection, instrumentation, and analytical procedures are detailed.



## **CHAPTER - 3**

### **METHODOLOGY**

#### **3.1 Introduction**

Air pollution is one of the most pressing environmental issues in India, posing significant health risks to the population (Cash et al., 2023; Nirwan et al., 2024). In India, during the year 2019, around 1.67 million deaths were recorded due to air pollution, which added up to a 17.8% death rate in the whole country (Dandona & Singh, 2021). One of India's megacities, Delhi, is the most densely populated city on the planet. It is known to have 30 million inhabitants living in an area of 1484 km<sup>2</sup> during the year 2020. The greatest problem in all the metropolitan cities in the world is that the ground-level ultrafine Particulate Matter's PM<sub>2.5</sub> (size  $\leq 2.5 \mu\text{m}$ ) is spread in every nook and corner. The air quality is severely compromised due to various factors, including anthropogenic local factors such as fossil fuel, biofuel, and industrial activities, as well as re-suspended dust (Beig et al., 2020). Furthermore, it is also affected by the Earth's unhealthy and polluted air (WHO, 2016), which contains particulate matter (PM<sub>2.5</sub>, particles with aerodynamic diameters  $\leq 2.5 \mu\text{m}$ ). This case often exceeds the normal limit standards set by the WHO and India's ambient air quality for a mean time of 24 hours. The guidelines are the Indian National Ambient Air Quality Standard (NAAQS) of 60  $\mu\text{g}/\text{m}^3$  and the World Health Organization's (WHO) Global Air Quality Guidelines of 15  $\mu\text{g}/\text{m}^3$ . This situation is not the same throughout all the seasons. The situation worsens when it's cold, especially during winter, as the shallow Planetary Boundary Layer (PBL) is doubled, thereby doubling the pollution (Talukdar et al., 2021). In the year 2019, nearly 16,600 deaths occurred in Delhi due to this condition (Mogno et al., 2023; Pandey et al., 2021).

Particulate matter levels in an area are influenced by factors beyond local emission sources. Climatic conditions play a significant role by affecting the concentration, dispersion, and deposition of airborne particles. Additionally, an area's microclimate and local land use patterns are critical in shaping its overall pollution profile. Making sure we understand the spatiotemporal variation of the area being studied is crucial. According to Sharma et al. (2022), there are both natural and man-made sources of particulate matter (PM) in metropolitan environments. The megacity of Delhi and the surrounding regions, known as the National Capital Region (NCR),

have numerous anthropogenic sources, which are a major cause of pollution in these areas. This suggests that we need a clear idea, such as a coordinated emissions reduction strategy, to reduce pollution in the megacity of Delhi. Not only this, but also the local on-road transport in the area is one of the unavoidable factors to consider when calculating the  $PM_{2.5}$  in the air, regardless of the area being considered. Additionally, recent studies on the major problem of pollution due to transportation, particularly during the winter and Post-Monsoon seasons, indicate that vehicular emissions of  $PM_{2.5}$  range from 17 to 30%, with the percentage varying according to the season (Mogno et al., 2023).

Furthermore, Mogno et al. (2023) found that local on-road transport contributes approximately 10% of  $PM_{2.5}$  on a daily basis, rather than over an extended period, and increases in the National Capital Region (NCR) in the regional on-road transport area by 17% throughout Delhi. The largest contributors to  $PM_{2.5}$  in Delhi, on a daily basis, are regional power and transport at 14% and domestic sectors at 11%. This emission is almost entirely dominated at nighttime, compared to the relatively low concentrations during the day. Except for the regions nearest to the National Capital Region (NCR), the longest-range transportation contributes about 40% of the total pollutants. During evening traffic, specifically during peak hours, there is an increase in the diurnal sector, with a mean  $PM_{2.5}$  concentration that is the largest (18%). The above condition is contributed to by the local on-road transportation. This emission is overall dominated by 50% by the contribution of two-wheelers, three-wheelers, and 30% by heavy-duty vehicles, and nonetheless, this is the big picture, which is 60-70% of the total emission of the transport sector of any hour of any day. It is known that the pollutants released into the air bring significant changes in their concentration, depending on the meteorological factors, which are evident on the spatiotemporal scale. Several seasonal meteorological parameters, including temperature, relative humidity (RH), and wind speed, have a significant impact on the concentration of particulate pollution in a given area. Due to variations in meteorological conditions, the concentration of Particulate Matter is higher during the winter season, whereas in summer, the concentration appears to be lower when compared (Chan & Kwok, 2001; Zhang & Cao, 2015). Not only the above factors, but also the speed of the wind in an area, also affects the concentration of the Particulate Matter. The increase and decrease

in concentration of particulate matter are also dependent on the speed and direction of the wind, as these factors determine the direction of dispersion of particulate matter in an area. The PM concentration is not only dependent on the speed but also the direction, says (Noble et al., 2003) in the urban El Paso region of Texas. The concentration of “ultrafine” and “accumulation mode” particles in the urban area of the southerly winds, as compared to northerly winds, is extremely increased just due to the direction (Sharma et al., 2022). The wind speed of Delhi varies from 0.2 to 9 m/s, as stated by (Srivastava et al., 2011). Additionally, he documented that the wind direction is predominantly westerly or north-westerly in Delhi and becomes more northerly in the afternoon.

The requirement for understanding the level of pollution and the quality of the air in developing cities and areas exposed to short-term air pollution appears to center on morbidity for one or a few more days. This is particularly important in the world's fast-growing cities to achieve the maximum benefits of so-called sustainable development (Dutta & Jinsart, 2022; Yadav et al., 2021). Reducing the severity of the human health issue and maintaining it is made more difficult by the rising levels of particulate matter and pollution caused by seasonal local and regional emissions, as well as seasonal weather.

This is now aggravated by the geography of the Indo-Gangetic Plain (Liu et al., 2018). Premature death, disease, and more like this are on the rise due to the increased air pollution. Also, it's the biggest health threat that prevails not only in India but throughout the world. Not only do they pose health threats, such as endangering health and shortening lifespan, but they also have a major impact on the world's economic productivity. The Sustainable Development Goals (SDGs) aim to reduce the burden of deaths and diseases caused by air pollution (Dandona & Singh, 2021). In India, air pollution is increasing the danger and threat to the health of the majority of the population. This threat is not at a moderate level but rather at a very high density (Liu et al., 2018). Due to PM<sub>2.5</sub> exposure, the loss of life expectancy is estimated to be an average of 3.4 years nationwide and up to 6.4 years in the National capital, Delhi.

### **3.2 Site selection**

Since the levels are found to be higher or lower, the site selection is done by selecting two sampling sites for comparison of the levels and values for the study. One

region is a highly urbanized region with a different and complex mixture of particles. The second region is a background region with no complex elements or pollution. A lower concentration of anthropogenic sources can be found here. The station names, along with their short names, latitude, longitude, and geographical details, are depicted in Table 3.1. The location photos are depicted in Fig.3.1-3.3, respectively.

The first region to monitor is the Delhi observatory (Inside the campus of Delhi Technological University), which is located in the northwest part of New Delhi (~ 223 m above the mean sea level (amsl)). Delhi is the capital of India. Also, Delhi is considered to be densely populated and polluted with a higher concentration of Particulate Matter. The Indo-Gangetic Plain (IGP) is located in the vicinity of Delhi. The Himalayas mostly prevent air pollution from escaping to the north, creating a valley effect in the landlocked Indo-Gangetic plain (Kumar et al., 2020; Yadav et al., 2021). The main highway connecting Delhi and Haryana is the Bawana Road, located on the border of Haryana. A large cabin was built 8 meters away from the roadside. The air monitoring instruments were placed inside the cabin at a height of 3.1 m above the road. The major air sampling for this particular location is done through automobiles since the number of automobiles passing this particular area was 1300 vehicles passing per hour on regular days (Rajagopal et al., 2023). This location was surrounded by residential building construction, which was exactly 12 km away from the Bawana industrial area. The detailed depiction is shown in Fig.3.4. One of the main factors taken into consideration while monitoring the air in this particular region was the meteorological factors. Thus, the monitoring of the air conditioning with the meteorological factors taken into consideration was conducted in different weather patterns and the mean  $\pm$  standard deviation of air temperature, wind speed, relative humidity, and solar radiation were  $25.89 \pm 8.35$  °C,  $1.35 \pm 0.83$  m/s and  $59.52 \pm 18.73$  % respectively.



Figure 3.1. The interior view of the monitoring site in an urban location, Delhi.

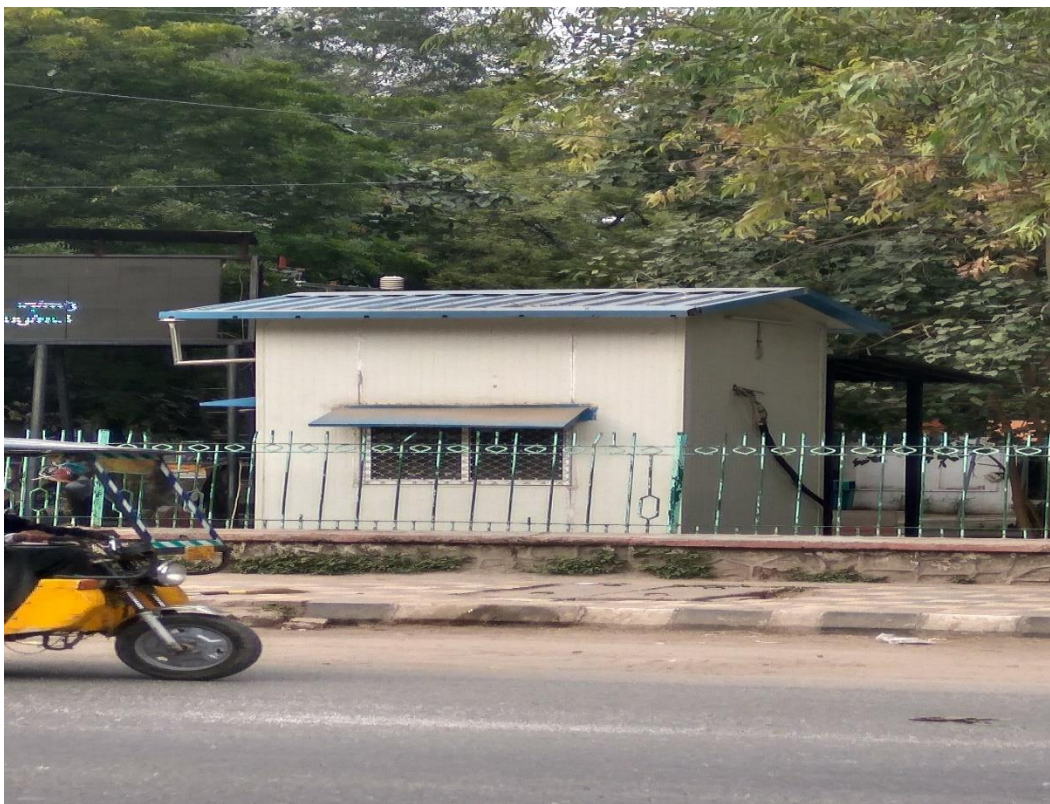


Figure 3.2. The exterior view of the monitoring site in an urban location, Delhi.

The second location considered for monitoring is the Ranichauri Observatory, located in Uttarakhand's Tehri Garhwal district, on the southern slope of the Western Himalayas (~1930 m above mean sea level). This observation is administered by the India Meteorological Department (IMD) under the World Meteorological Organization's Global Atmospheric Watch (GAW) program, as it serves as a climate monitoring station. This station is located away from the significant sources of anthropogenic contamination. So, it is best for the background observation and monitoring. The Ranichauri city is covered by different cities. Srinagar City is located approximately 100 km southeast. From the south, about 70 km away is Rishikesh City. From the west, about 100 km away is Dehradun City. These places are characterized by diverse landforms. They are forest areas, agricultural lands, and small human settlements. This is depicted in a detailed Fig. 3.5. This place, Ranichauri city, is a location that combines two distinct air forms. This is often a mixture of clean air and very polluted air. The source of clean and polluted air flows from the free tropospheric air and the Indo-Gangetic Plain. The location receives the majority of its free tropospheric flow from the north-western area in the winter and after the monsoon season. The pre-monsoon season was dominated by air masses from the contaminated Indo-Gangetic Plain in the southeast, while the monsoon season was dominated by air masses from the west and southeast (Sebastian et al., 2021). The meteorological factors were observed throughout the campaign. The factors were measured under different weather patterns, and the mean  $\pm$  standard deviation of air temperature, wind speed, relative humidity, and solar radiation were  $18.49 \pm 7.02$  °C,  $2.39 \pm 1.42$  m/s, and  $58.67 \pm 22.97\%$ , respectively.





Figure 3.3. The exterior view of the monitoring site in a regional background, Ranichauri.

Table 3.1. The geographical areas where observation campaigns were conducted.

S. No	Station Name	Longitude	Latitude	Code	Area
1.	New Delhi	77.12 °E	28.75 °N	NDL	Urban
2.	Ranichauri	78.08 °E	30.25 °N	RNC	Background

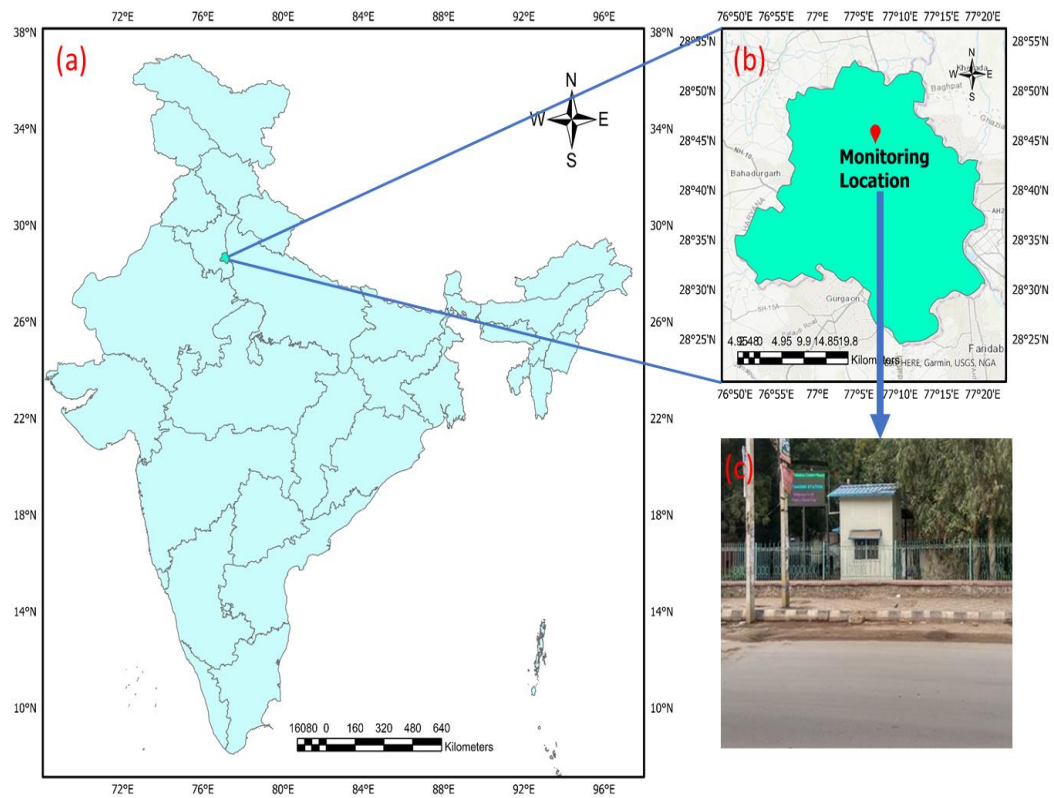


Figure 3.4. The location map representing the Urban Observatory includes (a) India, (b) Delhi, and (c) the monitoring station.



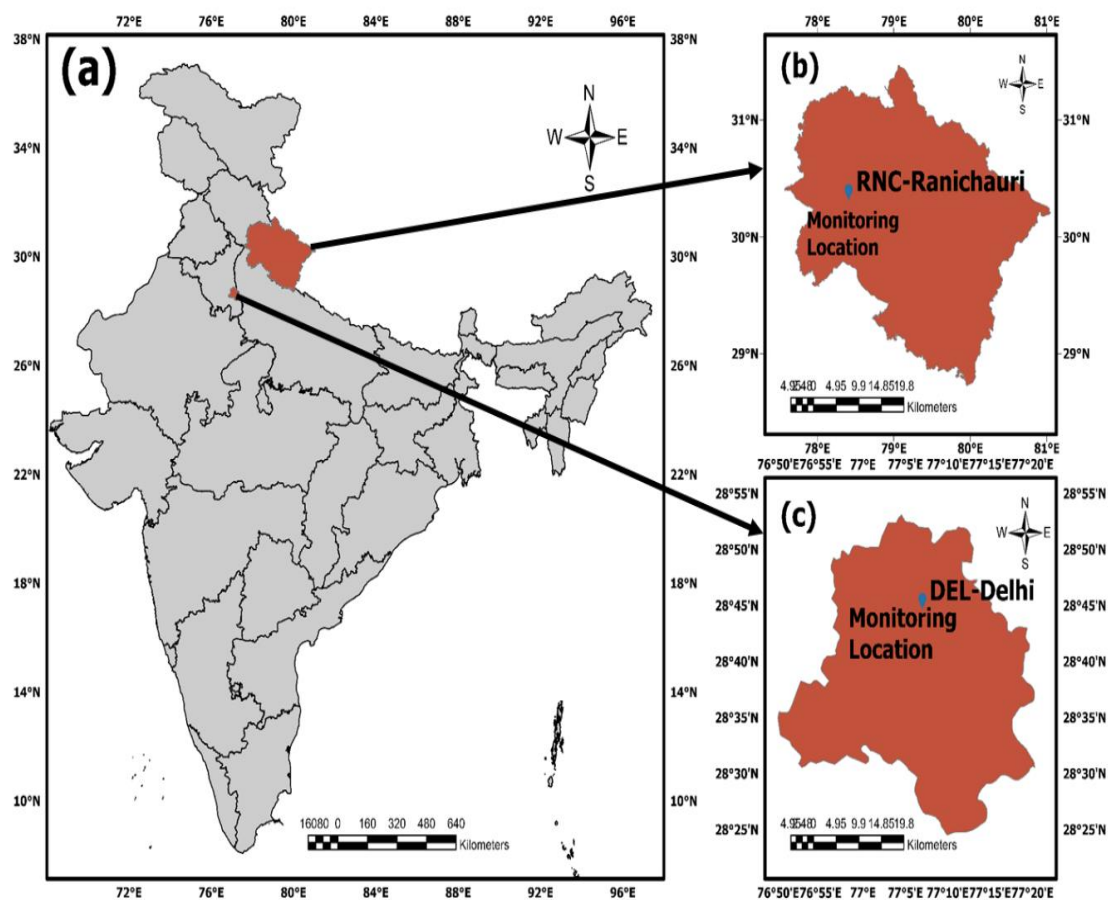


Figure 3.5. The location map representing the Background Observatory includes (a) India, (b) Ranichauri, and (c) Delhi.

### 3.3 Instrumentation

#### 3.3.1 Particle monitoring instruments

The scanning mobility particle sizer with a condensation particle (SMPS + C) (Make: GRIMM Inc., Germany, Model: SMPS + C 5.403) was used to measure the particle number size distributions (PNSD). This was computed using a time interval of approximately seven minutes between each scan. The SMPS + C is operated using the theory of differential mobility analysis. The size-resolved particles in the SMPS configuration are counted using an electrostatic classifier with a long differential mobility analyzer (LDMA) and a condensation particle counter based on n-butanol. Before the particles enter the classifier system, a  $\beta$ -radioactive source (Ni-63) is added to the particles to bring them to an equilibrium charge distribution. After this, the particles are classified based on their electrical mobility. The sample is then passed through a diffusion silica desiccator. The reason behind passing through the silica

desiccator is that it absorbs excessive moisture in the air sample (reduces around ~ 30% RH). Again, this sample is passed through a radioactive material (Am-241) based neutralizer so that the particles attain their equilibrium charge distribution. To ensure there is no excess moisture in the air that is passed through a diffusion dryer made of silica gel was added to the instrument. In addition to this, sensor-based (Aimil-made) weather stations were also used to measure meteorological parameters, including atmospheric relative humidity (RH), temperature (AT), wind direction (WD), wind speed (WS), and solar radiation (SR). The schematic diagram of the instrument's principle and instrument photos are given in Figs. 3.6 to 3.8.

The size distribution of ambient aerosols was measured in the background location. This particle sizer, known as a differential mobility particle sizer (DMPS), measures distinct particles. It is simple to measure the smaller particles with the DMPS because it has a size range of 10-800 nm (30 size bins). The TSI 3772 condensation particle counter and a Vienna-type differential mobility analyzer (DMA) make up the two separate components of the DMPS. A Vienna-type differential mobility analyzer (DMA) categorizes charged particles according to their electrical mobility, while the condensation particle counter counts particles with the required mobility. The entire text's aerosol size information is expressed in terms of electrical mobility diameter because the Differential Mobility Analyser (DMA), which performs the final categorization step, provides results based on electric mobility. For every ten minutes of the procedure, a full aerosol number-size distribution with 30 bins was obtained. The DMPS inlet flow rate was 1 LPM, whereas the sheath air flow rate was 5 LPM. A two-meter-long stainless-steel entrance tube allowed the sample air to enter. Then, the sample air was sucked inside and dried with a Nafion drier to a relative humidity of under 40%. The data inversion took into account diffusion losses in the DMPS's intake and interior.

## SMPS+C

### Measuring Nano-Particles by Magnification: (Problem : too small for light scattering)

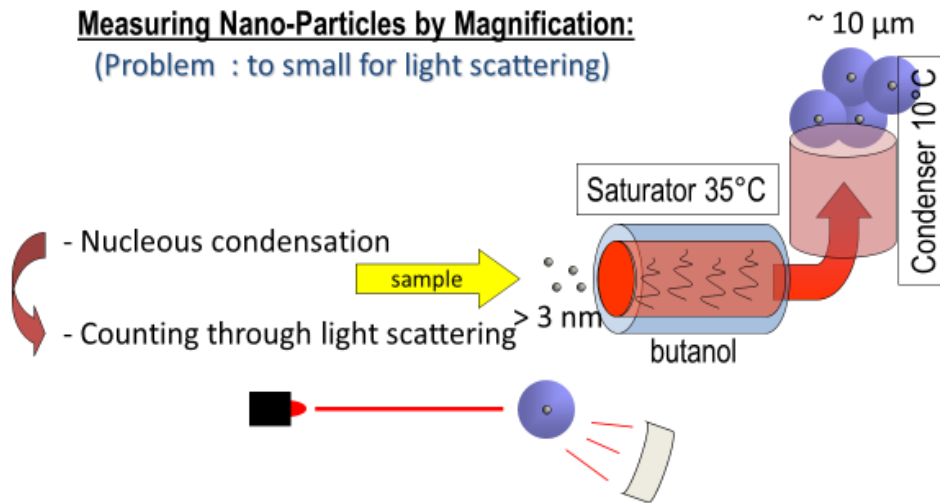


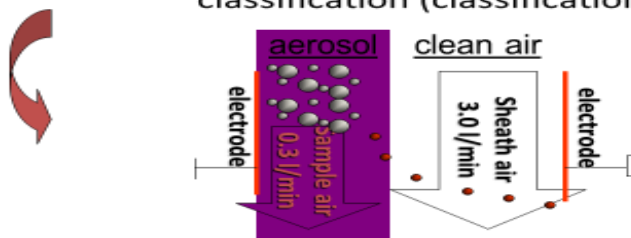
Figure 3.6. Schematic diagram of the working principle of SMPS+C.

## SMPS+C

### Measuring Nano-Particles:

#### Cutting out monodisperse particle distributions:

=> Differentiation due to electrostatic classification (classification between electrodes)



## SMPS+C

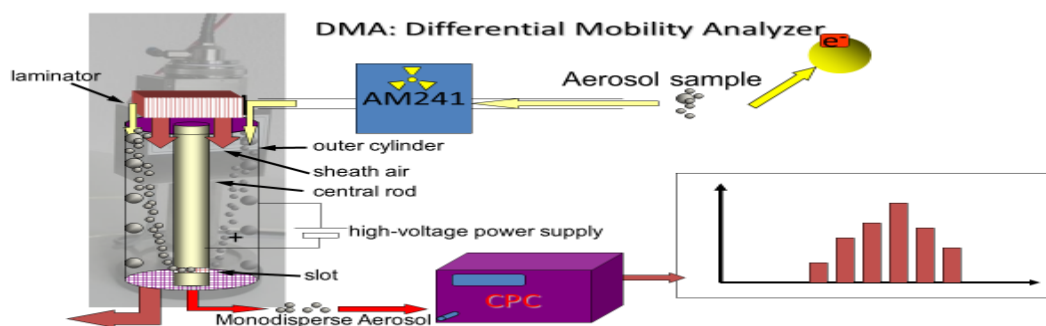


Figure 3.7. Schematic diagram of the instrument principle (Source: <https://www.grimm-aerosol.com>).



Figure 3.8. Scanning mobility particle sizer counter (SMPS + C).

### 3.3.2 Gaseous monitoring instruments

An Ozone Monitor (Model 202, 2B Technologies, Inc., USA) and a NO<sub>2</sub>/NO/NO<sub>x</sub> Monitor (Model 405, 2B Technologies, Inc., USA) with a maximum temporal resolution of one hour can be used to measure Ozone and NO<sub>x</sub> in real-time. Based on the proven method of ultraviolet light absorption at 254 nm, the ozone monitor is made to provide precise measurements of atmospheric ozone across a broad dynamic range, from a detection limit of 1.5 parts per billion by volume (ppbv) to an upper limit of 100 ppmv. In contrast, the NO<sub>x</sub> monitor uses the well-established method of absorption of visible light at 405 nanometres (nm) to provide precise measurements of atmospheric nitrogen dioxide (NO<sub>2</sub>), nitric oxide (NO), and NO<sub>x</sub> (NO + NO<sub>2</sub>) over a dynamic range that extends from a few parts per billion by volume (referred to herein as ppb) up to 10 ppm by volume for NO<sub>2</sub> and 2 ppm for NO. With a sampling flow rate of 1.5 LPM, the Model 405 nm is authorized as a Federal Equivalent Method (FEM) for NO<sub>2</sub> over the range of 0-500 ppb NO<sub>2</sub>. The instrument pictures are depicted in Fig.3.9.

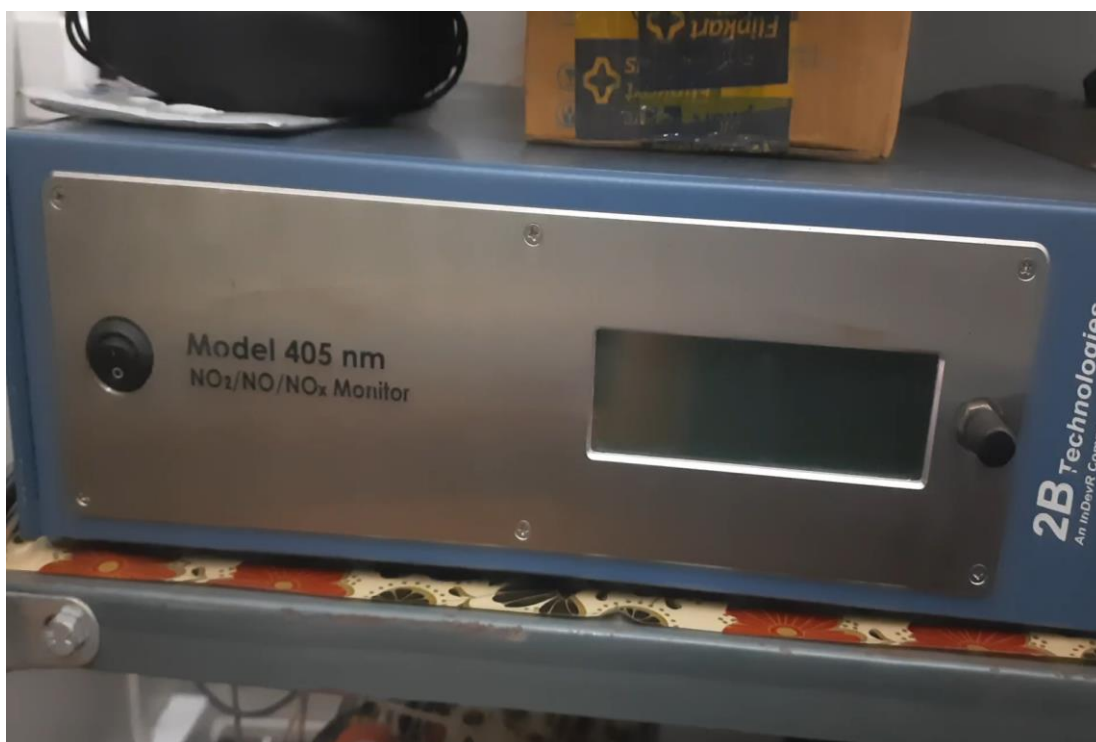


Figure 3.9. NO<sub>x</sub> Analyzer Instrument.

Ambient SO<sub>2</sub> monitor (Model APSA-370, Horiba, Ltd., Japan) can be used for monitoring Sulphur dioxide (SO<sub>2</sub>) in atmospheric air between 0 - 0.5 PPM with a sampling flow rate of 0.7 LPM, and ambient CO monitor (Model APSA-370, Horiba, Ltd., Japan) can be used to measure Carbon monoxide (CO) in atmospheric air between 0 - 100 ppm with the flow rate of 1.5 LPM. Both monitors allow continuous measurement of SO<sub>2</sub> and CO concentrations in the atmosphere. The ambient Sulfur dioxide (SO<sub>2</sub>) monitor operates on the principle of the ultraviolet fluorescent (UVF) Method, and the Carbon monoxide (CO) monitor operates on the principle of the cross-modulation type non-dispersive infrared absorption method. The instrument photos are depicted in Figs. 3.10 and 3.11.





Figure 3.10. SO<sub>2</sub> Analyzer Instrument.



Figure 3.11. CO Analyzer Instrument.

### 3.3.3 Weather monitoring instruments

Furthermore, the Aimil Automatic Weather Station (AIMIL-AWS), a sensor-based system that operates in real-time, is available for measuring meteorological parameters such as temperature (Temp), relative humidity (RH), wind direction (WD), and wind speed (WS). The Vane was connected to a linear infinite potentiometer sensor to detect wind direction, and a 3-cup assembly mounted on a friction-free shaft and connected to a Chopper sensor to measure wind speed. A Standard Platinum RTD element (PT1000 or PT100) installed inside a weather shield, along with a solid-state capacitive type sensor, was also used to monitor the ambient temperature and relative humidity in real-time. The instrument photos are depicted in Fig.3.12.



Figure 3.12. Automatic Weather Monitoring.

### 3.4 HYSPLIT trajectory

The long-range transportation analysis of pollutants is conducted using the Hybrid Single Particle Lagrangian Integrated Trajectory (HYSPLIT) open-source model, developed by the Air Resources Laboratory (ARL) at the National Oceanic and Atmospheric Administration (NOAA). The details extracted from the NOAA website and finally plotted in MeteoInfoMap are given in Figs. 3.13 to 3.19, respectively. The seasonal average trajectories are plotted for a 3-day (-72 hours) back trajectory for every day (24 hours, starting at 00 hours), and clustering is performed for each season. The season has been considered for winter (December to March), summer (April to June), monsoon (July to September), and post-monsoon (October to November) for the years 2022 and 2017 at urban and background sites. The input for the models is taken from REANALYSIS data at a height of 1000 agl (above ground level) for both urban and background sites, used for analyzing back trajectories in MeteoInfoMap.

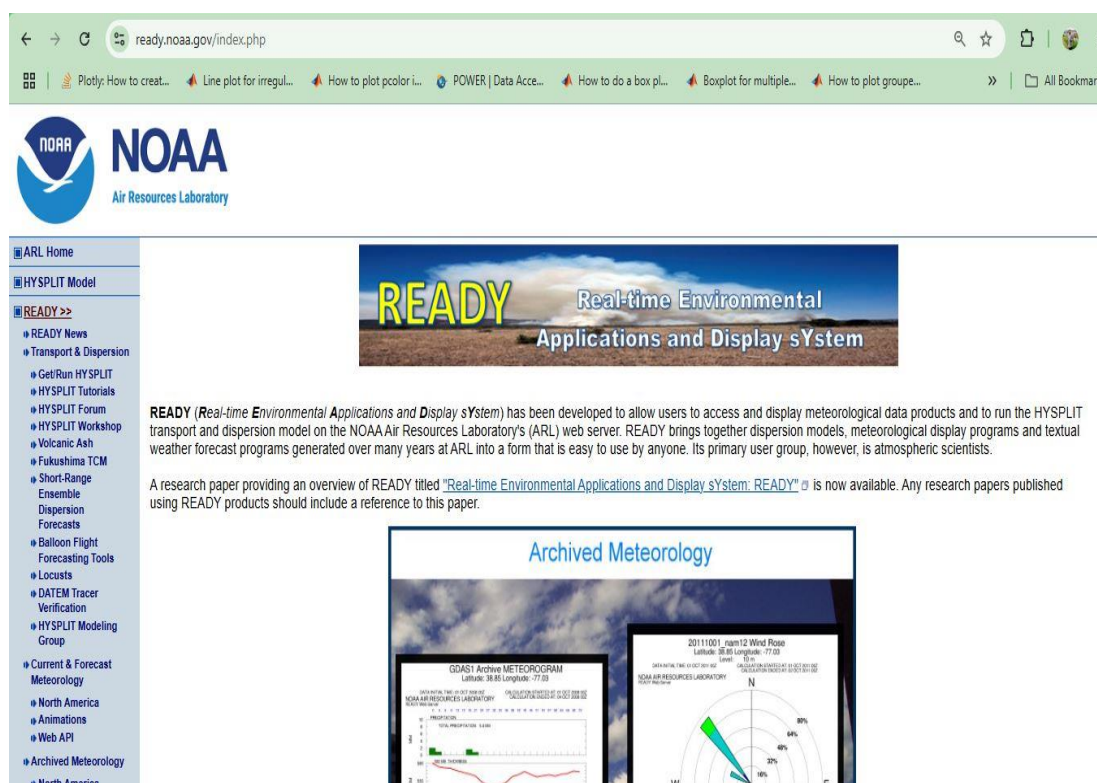


Figure 3.13. Website of the National Oceanic and Atmospheric Administration (NOAA).



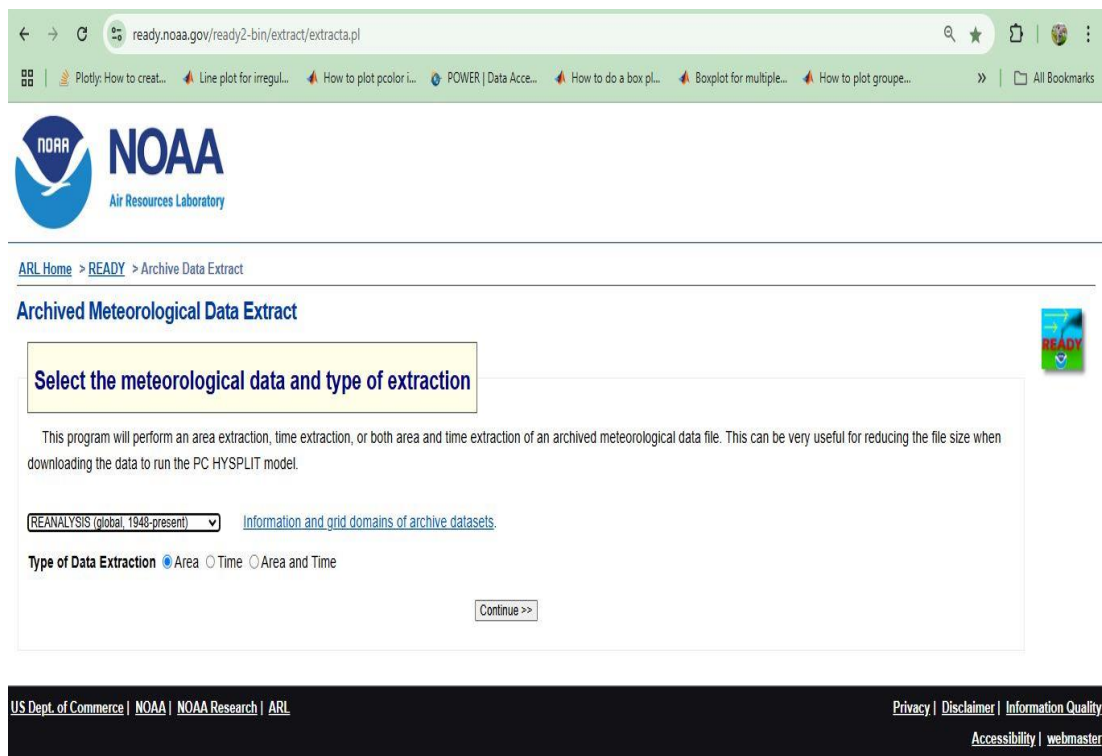


Figure 3.14. Choosing model inputs from REANALYSIS data.

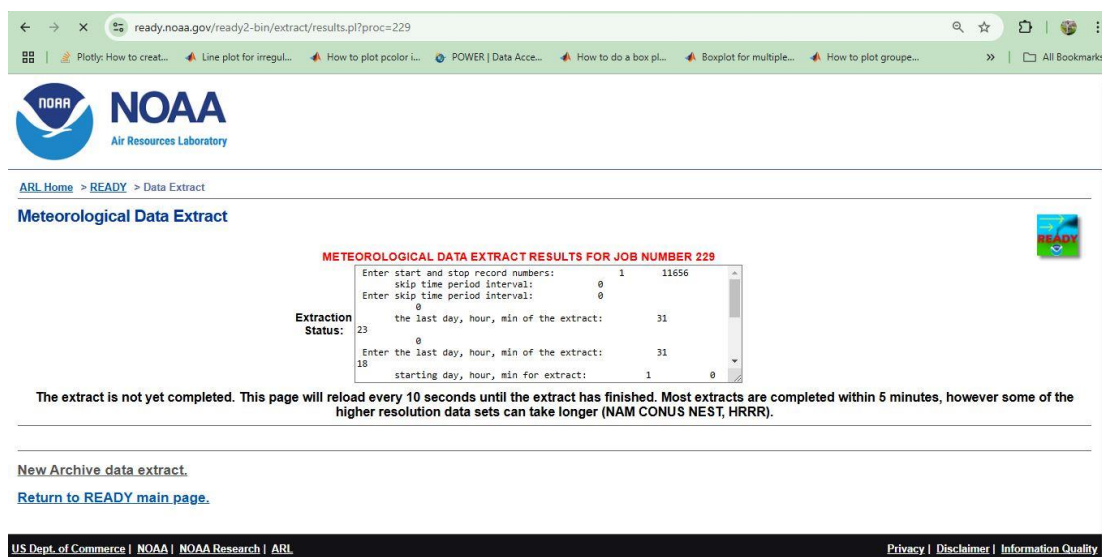


Figure 3.15. Final data extraction page from NOAA.

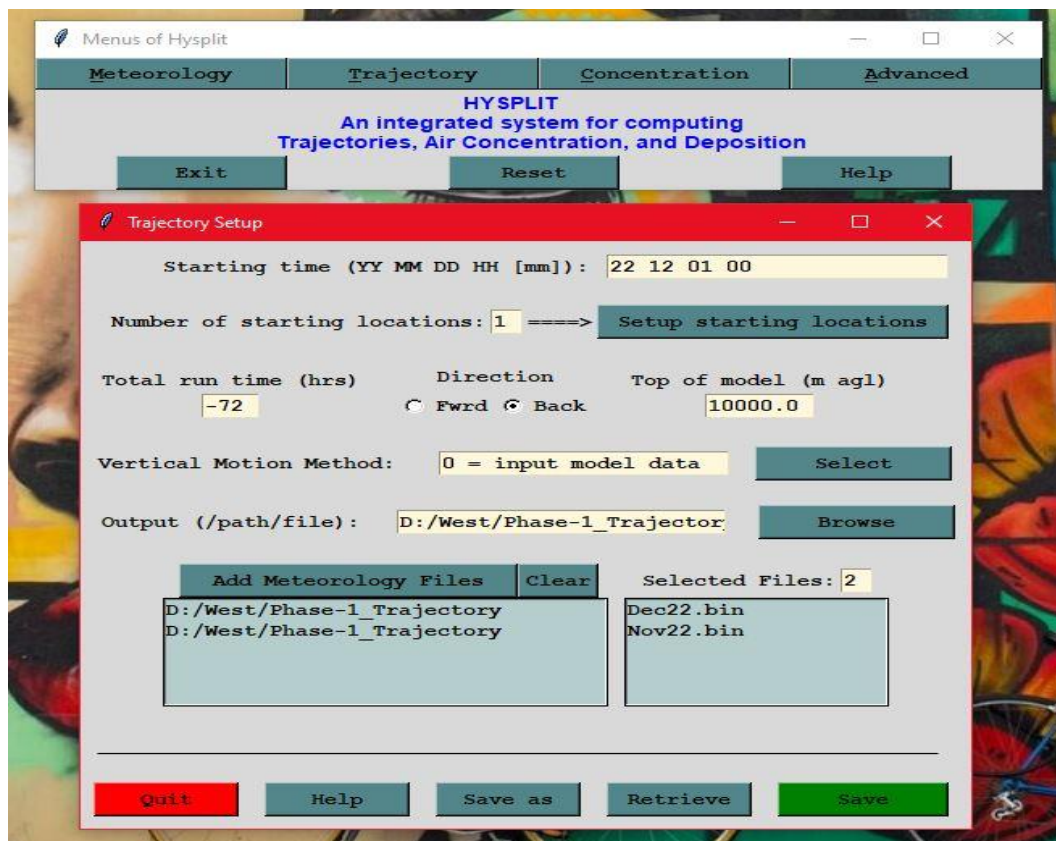


Figure 3.16. Extraction of Trajectory data points using HYSPLIT Desktop version.

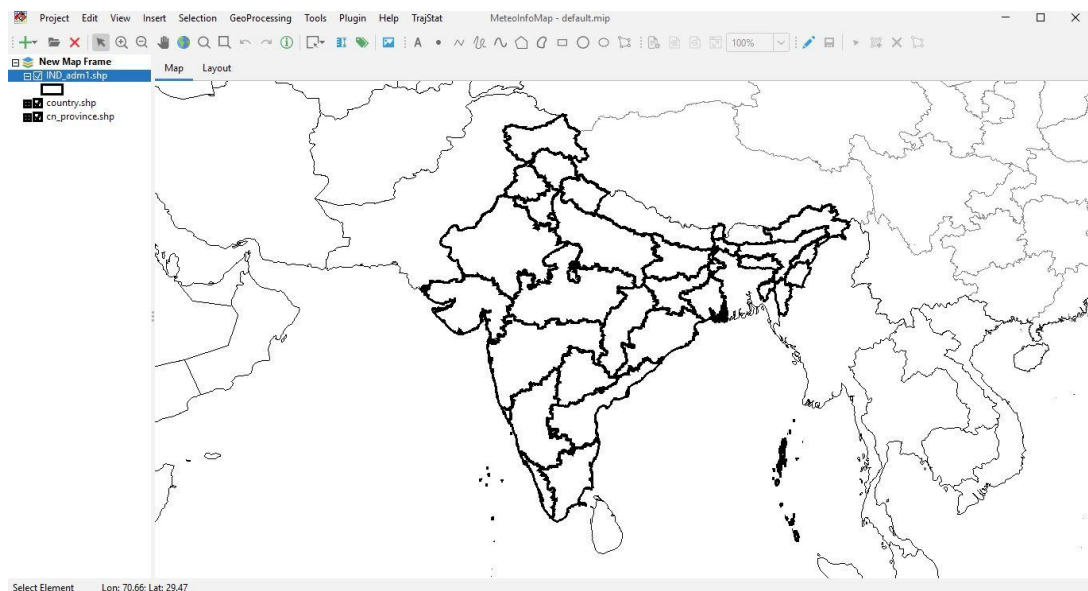


Figure 3.17. Front page of MeteoInfoMap software.

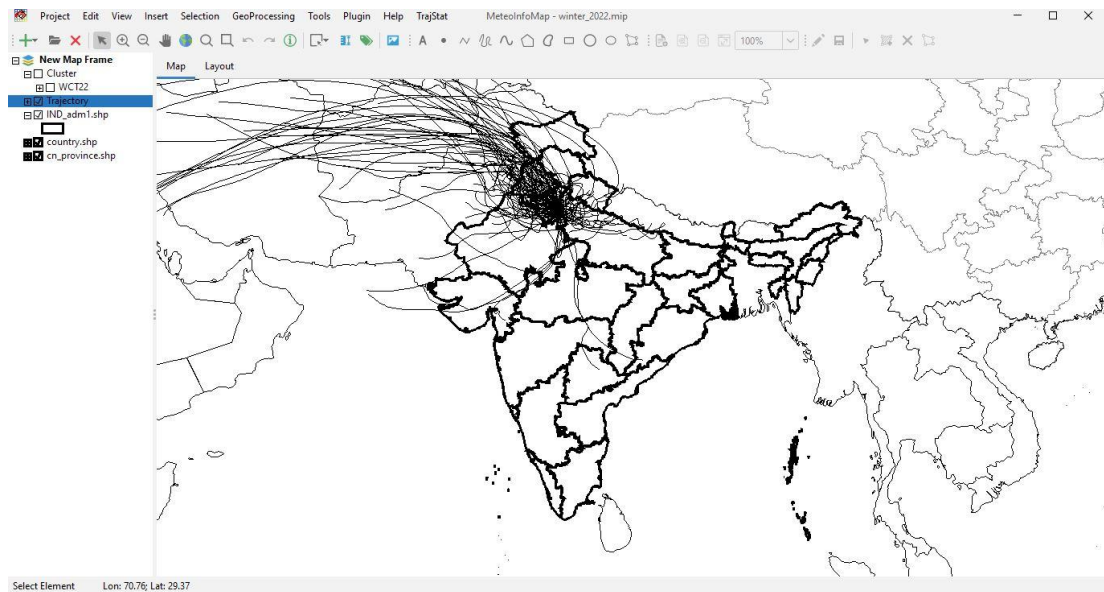


Figure 3.18. Plotting daily Trajectory data points for one season in MeteoinfoMap.

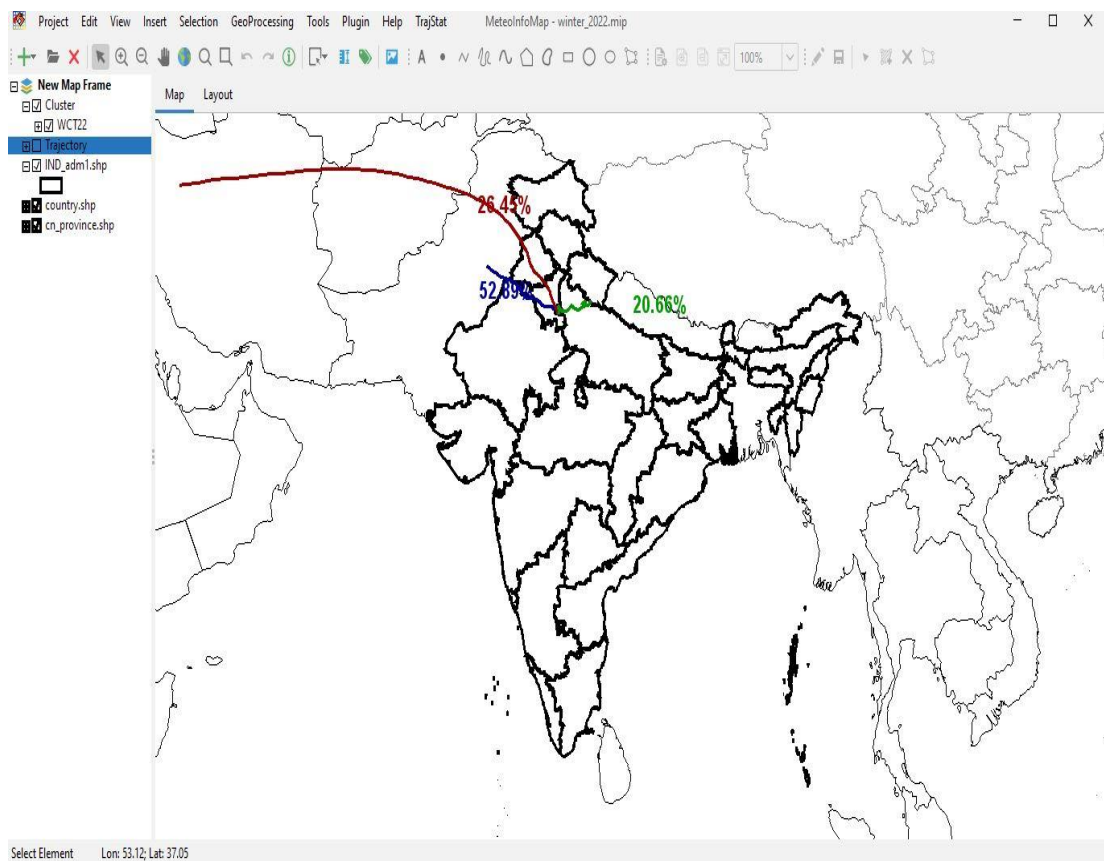


Figure 3.19. Plotting Weighted Concentration Weighted Trajectory (WCWT) from daily Trajectory data points in MeteoinfoMap.

### **3.5 Limitations of the study**

The study measured particle number concentration of particles ranging from 10 to 800 nm in urban and background regions to compare the concentration of sources and type of particles present. Due to the limitations of the resources, the measurements were not done parallelly in both locations. Due to constraints in the instruments, two different instruments that work on the same principle were used for the measurements. These two are considered as limitations of the present study, and still, the data used for analysis were checked for quality checks, and necessary statistical analysis was done to ensure the quality of the data. The significance of the data was tested using the Levene test and F test and found the p-value  $< 0.05$ , so the null hypothesis was rejected.

### **3.6 Statistics and equations**

#### **3.6.1 Statistics analysis**

The data gathered during the monitoring period were filtered and examined using several statistical methods. Using SPSS and R software, the outliers were removed. At the same time, Levene and F tests were used to test the significance of the data collected. The null hypothesis was rejected when the p-value was  $< 0.05$ . MATLAB, Origin, and R statistical tools were used for data visualization.

The sampling strategy was designed to ensure representativeness across both spatial and temporal scales. Continuous monitoring was conducted at strategically selected sites that capture varying land-use patterns and pollution sources. The data collected during 2017 and 2022 represent over 90% of the total dataset and cover all major seasonal variations, ensuring sufficient temporal representation for trend identification. Although approximately 10% of the data were unavailable due to power fluctuations and maintenance to prevent instrument damage, the remaining dataset was comprehensive and consistent enough to capture the key pollution dynamics and trends with statistical reliability.

#### **3.6.2 Calculation of particle number size distribution**

Statisticians use the method of including the normal concentration to plot the data to avoid this problem ( $dN/d\log D_p$ ). The number of particles in the total range is represented as  $dN$  (or  $\Delta N$ ). The difference in the channel width in the log is denoted as  $d\log D_p$  (or  $\Delta \log D_p$ ). To get  $d\log D_p$ , by taking the log of the upper boundary for each channel and subtracting it from the log of the lower bin boundary (normalizing

for bin width). The normalized concentration value is obtained by dividing the concentration by the bin width; this value is independent of the bin width.

$$dN/d\log D_p = \frac{dN}{d\log D_p} = \frac{dN}{\log D_{p,u} - \log D_{p,l}} \text{ --- (3.1)}$$

Where,

dN = Particle Concentration

D<sub>p</sub> = Midpoint Particle Diameter

D<sub>p,l</sub> = Lower Channel Diameter

D<sub>p,u</sub> = Upper Channel Diameter

### 3.6.3 Calculation of polar plot

This method was used to create a bivariate polar plot. Data on wind speed, wind direction, and concentration are first divided into bins based on wind speed and direction. Then, for each bin, the mean concentration is calculated. The concentration distribution of the wind is listed with sufficient data, and the testing has been conducted over a wide range. Additionally, we discovered that the wind speed intervals at 30 degrees and the wind direction intervals at 10 degrees provide us with all the necessary information. The available wind direction data is usually rounded to the nearest 10 degrees. Additionally, wind speed is typically measured at the surface between 0 and 20 to 30 m/s. Intervals longer than thirty minutes would be more difficult to justify when considering the accuracy of the sensors' measurements. Binning the data in this manner is not a strict requirement, but when this is followed, it acts as an effective data reduction technique. Also, this method does not affect the fidelity of the plot. Since the inherent wind normally doesn't flow in the same direction in the atmosphere, data is collected over several days, weeks, months, and years to determine the necessary variation. This is then used to construct a bivariate polar plot that does not diffuse and remains stable, neither changing in an unexpected manner with the wind direction nor with the wind speed. Moreover, working with finely resolved bin sizes or directly with the raw data collected does not provide us with the additional information we need.

The wind components, u and v, are calculated, i.e.

$$u = \bar{u} \cdot \sin\left(\frac{2\pi}{\theta}\right), v = \bar{u} \cdot \cos\left(\frac{2\pi}{\theta}\right) \text{-----} (3.2)$$

Where,

u = hourly mean wind speed

$\theta$  = mean wind direction in degrees, with the east at 90 degrees.

### **3.7 New particle formation event and calculation**

#### **3.7.1 Event classification**

The criteria set by Dal Maso et al. (2005), and Kulmala et al. (2012) were followed in this study's manual identification of new particle formation (NPF) occurrences. Every day, the data was visually analyzed for every 24-hour period between midnight and midnight. The appearance of a clearly new particle mode within the nucleation mode size range that lasts for several hours and shows growth indicators is what is known as an NPF event (Kanawade et al., 2014b; Siingh et al., 2013). The particle number size distribution (PNSD) spectrum should also show a distinctive banana-shaped development pattern (Dal Maso et al., 2005; Siingh et al., 2018). The observation days were divided into three categories: event days, non-event days, and indeterminate days based on the proliferation of nucleation mode particles. A characteristic banana pattern shown in the PNSD is indicative of event days, which are defined by the creation and subsequent expansion of nucleation mode particles. Days without nucleation mode particle formation and subsequent development are referred to as non-event days. Lastly, days that do not fit into any of the previously described categories are referred to as undefined days. These consist of, for instance, rapid increases in particle concentration, irregular particle growth, and fragmented events. The data in this research correctly represent a transportation corridor. Four seasons are used to group various months in order to explain the seasonal variations in NPF properties: Winter (December - March), Summer (April - June), Monsoon (July - September), and Post-Monsoon (October and November).

#### **3.7.2 Calculation of the growth rate**

The average growth rate (GR) during the hours of a new particle formation (NPF) event was determined using the mode diameter ( $D_p$ , mode) from the observed Particle Number Size Distribution (PNSD). As explained by Dal Maso et al. (2005)

and Siingh et al. (2013), this was accomplished by using a first-order polynomial line fitting method.

$$GR = \text{Slope of } D_{p,mode} = \frac{dD_{p,mode}}{dt} \text{ --- (3.3)}$$

In this case, dt is the length of the NPF event, and Dp, mode denotes the mode diameter.

### 3.7.3 Calculation of the condensation sink

The following computation was used to calculate the condensation sink (CS), which is defined as the rate at which condensable vapours condense onto pre-existing particles (Dada et al., 2023; Tuovinen et al., 2021).

$$CS = 2\pi D_j \sum_j \beta_{mj} d_j N_j \text{ --- (3.4)}$$

$$\beta_{mj} = \frac{1 + Kn_j}{1 + 0.337Kn_j + \frac{4Kn_j}{3\alpha} + \frac{4Kn_j^2}{3\alpha}} \text{ --- (3.5)}$$

$$Kn_j = \frac{2\lambda_v}{d_j} \text{ --- (3.6)}$$

Where,

D is the diffusion coefficient for sulphuric acid,

$\beta_m$  is the transition correction factor,

$d_j$  is the diameter of a size bin j,

$\lambda_v$  is the mean free path of the sulphuric acid molecule,

Kn is the Knudsen number, and

$\alpha$  is the mass accommodation coefficient (considered as unity).

### 3.7.4 Calculation of the coagulation sink

The equation 7, which was presented by Kulmala et al. (2012), was used to compute the coagulation sink (CoagS):

$$CoagS_{dp} = \int K(dp, d'p)n(d'p)dd'p$$

$$\cong \sum_{d'p=dp}^{d'p=\max} K(dp, d'p)N_{d'p} \text{ --- (3.7)}$$

Where,

$N_{d'p}$  is the particle number concentration with size  $d'p$  and

$K(dp, d'p)$  is the coagulation coefficient of particles with sizes of  $dp$  and  $d'p$ .

### 3.8 Summary

This chapter presents the comprehensive methodological framework adopted to achieve the study's objectives. It described the rationale behind site selection, ensuring the inclusion of both urban and background environments representative of contrasting emission and meteorological conditions. The instrumentation setup was detailed, encompassing particle number monitoring instruments for ultrafine particles (UFPs), gaseous analyzers for key atmospheric pollutants, and meteorological sensors for micrometeorological parameters. The analytical and statistical approaches were outlined to interpret the temporal and spatial variations in UFP concentrations and their relationship with environmental variables. Furthermore, the procedures for identifying new particle formation (NPF) events and calculating parameters such as growth rate, condensation sink, and coagulation sink were included to provide a broader context for understanding UFP dynamics.

The methodological framework established in this chapter forms the foundation for the subsequent data analysis and interpretation. Specifically, Chapter 4 applies these methods to evaluate the temporal variations, diurnal patterns, and meteorological influences on UFP number concentrations across the selected sites, while Chapter 5 integrates these findings to discuss the broader implications, source contributions, and concluding perspectives of the study. By providing a structured and transparent methodological basis, this chapter ensures a coherent transition from conceptual understanding to empirical analysis in the following chapters.



## **CHAPTER – 4**

### **RESULTS AND DISCUSSION**

#### **4.1 Introduction**

Densely populated areas like Delhi have worsened urban air quality because of high-rise concrete structures that restrict air exchanges, high-rise construction canyons on the streets, growing traffic, and other man-made activities. While big cities like Delhi focus on limiting the exposure and health hazards of regulated air pollutants, including both gaseous and particulate pollution, smaller particles are not as significant. Although they make up a relatively small portion of the overall particle mass in the ambient atmosphere, UFP particles having an aerodynamic diameter of less than 100 nm are quite prevalent. Numerous exhaust emissions, most notably from automobile exhaust in cities, release UFPs into the atmosphere. Human health is significantly impacted by UFPs. Because UFPs are smaller, they can deposit more quickly into the deeper part of the lungs and have the capacity to pass through the air-liquid barrier and enter the systemic circulation, which allows them to reach the distant organs. The scarcity of information, data, and thorough research on UFPs as particulate matter, particularly in metropolitan areas, has led to a lack of awareness. While cities struggle to manage the issue of traditional air pollutants that are part of the current regulatory framework, the emergence of uncontrolled pollutants like UFPs has given a new dimension to this already difficult issue.

People generally spend their time in a variety of microenvironments with varying pollutant concentrations and compositions. The concentrations of UFP in various microenvironments vary considerably. The sources of emissions, the type of activity, and the duration spent in each microenvironment are all attributed to the changes in concentration at the various microenvironments. Data gathered from various microenvironments will enhance the estimation of human exposure assessments and aid in understanding the contaminants. Over the past few decades, numerous experimental and numerical investigations have enhanced our understanding of how ultrafine particles are emitted in various microenvironments. Only a small number of these studies have been done in Asian cities; the majority have been done in European cities. This work's overall goal was to create a thorough analysis of various microenvironments using data from continuous monitoring

campaigns of particles with sizes between 10.23-1090.21 nm, and 10-800 nm at two distinct microenvironments (Urban and Background regions). The results of UFP data analysis, focusing on categorization and quantification in the road microenvironment and pure background microenvironment, respectively, are the primary emphasis of this work.

The total particle number concentration (PNC) ( $N_{tot}$ ,  $< 1000$  nm, and  $N_{tot}$ ,  $< 800$  nm) was examined in this study, which considered two distinct mode particle sizes: 10.23-1090.21 nm in urban areas and 10-800 nm in the regional background. For ease of understanding, it is also divided into three different modes. In urban areas, the three mode size range fractions are Nucleation ( $N_{nuc}$ , 10 nm to 30 nm), Aitken ( $N_{atk}$ , 30 nm to 100 nm), and Accumulation ( $N_{acc}$ , 100 nm to 1000 nm) mode particles. The three mode percentage sizes in the regional background are Nucleation ( $N_{nuc}$ , 10 nm to 30 nm), Aitken ( $N_{atk}$ , 30 nm to 100 nm), and Accumulation ( $N_{acc}$ , 100 nm to 800 nm), in that order. To better understand the different microenvironments of particle number concentration (PNC) and particle number size distribution (PNSD), the data collected in the urban area were reduced to only 800 nm in the comparative research between urban and regional resources. The total PNC ( $N_{tot}$ ) of this comparative study was recalculated for the 10 nm to 800 nm size range.

Urban monitoring took place between January 1<sup>st</sup>, 2022, to December 31<sup>st</sup>, 2022, while a regional background study was undertaken between January 1<sup>st</sup>, 2017, to December 31<sup>st</sup>, 2017. The remaining 10% of the data acquired between 2017 and 2022 could not be analyzed due to power fluctuations and instrument maintenance issues. The remaining 90% of the data was available for study. A pure background and a traffic corridor are accurately depicted by the data in this investigation.

#### **4.2 Year-Long calendar plot for urban and background regions**

The calendar plot illustrates the overall duration of the campaign period in terms of days. The calendar plot visually depicts the duration of monitoring days and the average concentration of the parameters using color scaling. The monitoring period included days and concentrations of  $N_{tot}$  from both urban and background regions in the years 2022 and 2017, as shown in Figs. 4.1 and 4.2, respectively. The days for which monitoring was not carried out throughout the year are represented by white spaces in the calendar plot, while the remaining days display a color variation

corresponding to the concentration. The concentration slowly started increasing from October and gradually increased in the months of November, December, January, and till mid-February, which falls under the winter season. This indicates that the concentration was recorded as higher in the winter season when compared to other seasons in urban regions. Meanwhile, in the background regions, the concentration started to increase in the months of February, March, and April.

### DEL-Urban Region

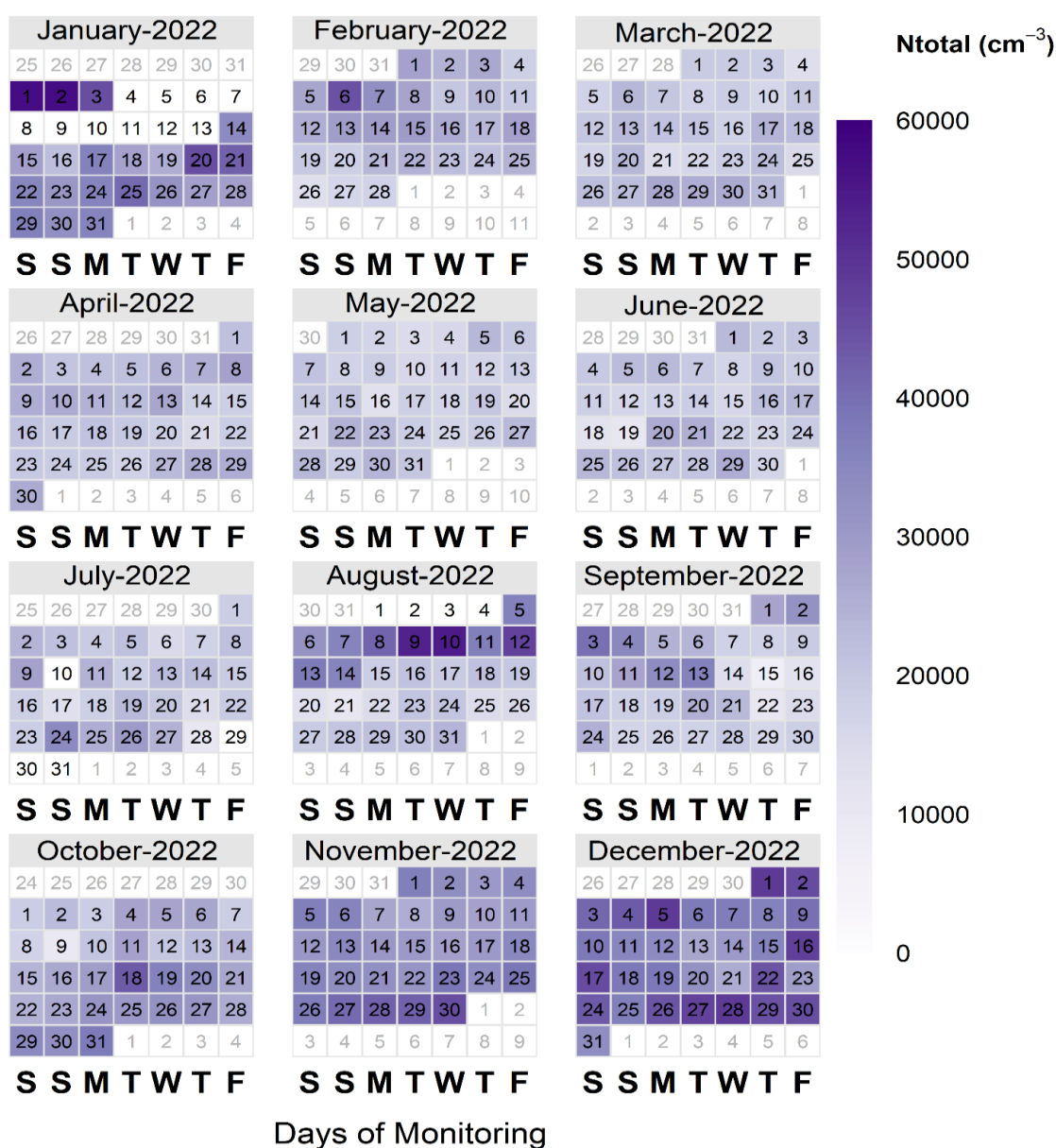


Figure 4.1. Cumulative daily concentration of  $N_{tot}$  (10.23 to 1090.21 nm particles) for every month (January to December) throughout the year 2022 in the urban region.

## RNC-Background Region

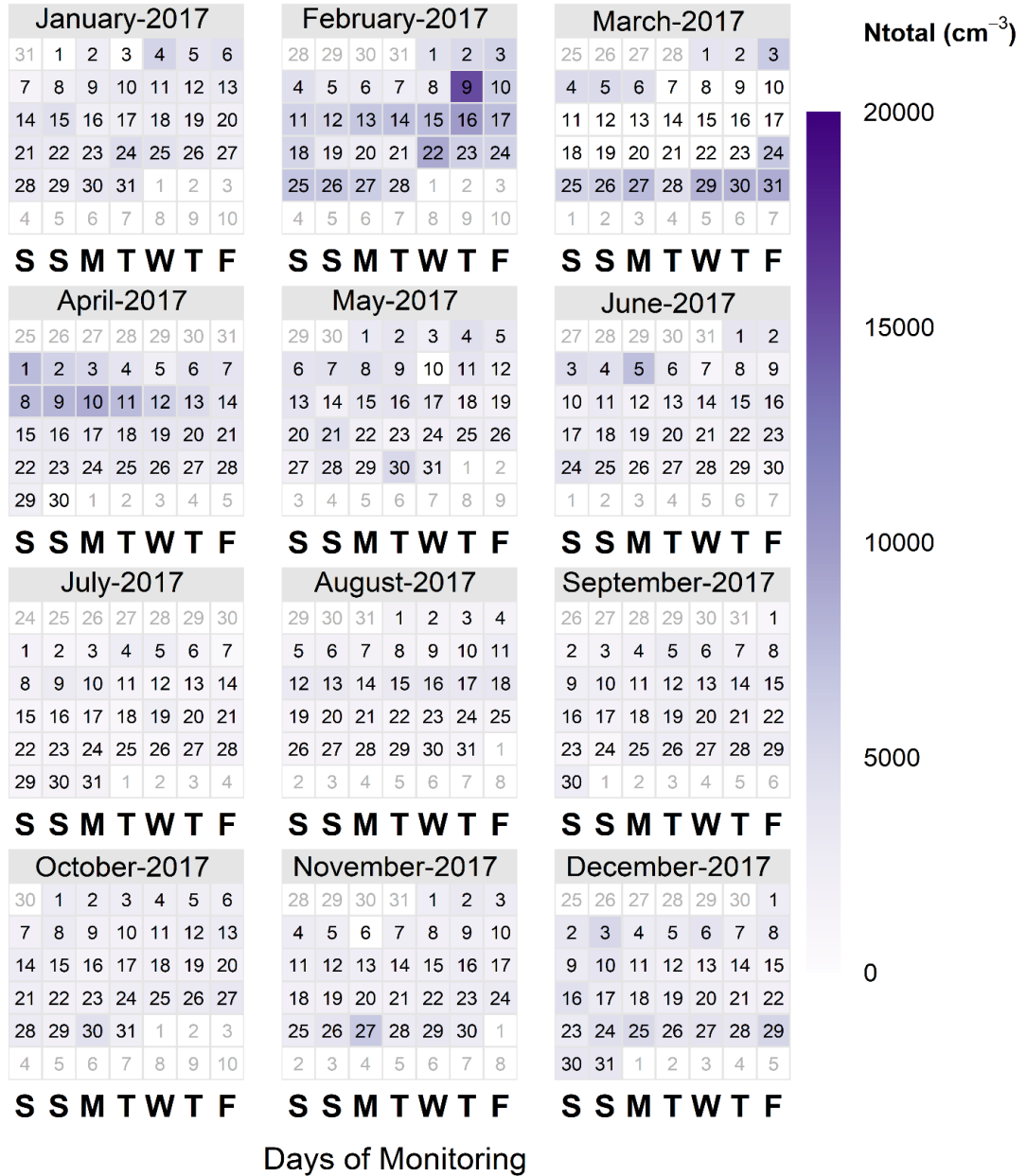


Figure 4.2. Cumulative daily concentration of  $N_{tot}$  (10 to 800 nm particles) for every month (January to December) throughout the year 2017 in the background region.

### 4.3 Traffic emissions and meteorological factors

Pollutant measurements (January-December 2022) in a traffic corridor were analyzed using the total particle concentration ( $N_{tot} < 1000$  nm) as well as the modal size fractions ( $N_{nuc}$  (10-30 nm),  $N_{atm}$  (30-100 nm), and  $N_{acc}$  (100-1000 nm)). Ultrafine

particles (<100 nm) are referred to as  $N_{nuc}$  (10-30 nm) +  $N_{atk}$  (30-100 nm). The study region experiences varying climatic conditions throughout the year, with temperatures ranging from 10 to 38°C during different seasons. Similarly, the relative humidity also varies from season to season, ranging from 28% to 89% in the study area. Consequently, although the emission sources in the study area remain similar throughout the year, seasonal meteorological factors influence the concentration of pollutants in the study area. The particle number concentrations are in agreement with regional emissions from the transportation sector. Likewise, local meteorological conditions, particularly solar radiation, influence the transformation of gases in the atmosphere, driving the formation of secondary pollutants in the study area. The monthly statistical summary of the meteorological parameters and the seasonal periods is provided in Tables 4.2, 4.3, and 4.4.

Table 4.1. The yearly statistical summary of the particle number concentration during the day and nighttime.

	daytime				nighttime			
	$N_{nuc}$	$N_{atk}$	$N_{acc}$	$N_{tot}$	$N_{nuc}$	$N_{atk}$	$N_{acc}$	$N_{tot}$
<b>Min</b>	0	0	0	0	10	67	15	1988
<b>Max</b>	10338	5999	2716	162142	4906	4822	3068	120172
<b>Mean</b>	770	846	313	26955	353	819	481	24375
<b>SD</b>	708	655	280	17381	352	576	383	14606

Table 4.2. Statistical values (min, max, mean and SD) for the modal sizes fractions ( $N_{nuc}$ ,  $N_{atk}$  and  $N_{acc}$ ) of the aerosol number size distribution including their geometric mean diameter (GMD) during the day and night-time for each month (from January to December) in 2022.

Month	Mode	daytime				nighttime			
		Min	Max	Mean	SD	Min	Max	Mean	SD
<b>January</b>	$N_{nuc}$	87	4097	673	605	12	1115	260	218
	$N_{atk}$	292	5234	1412	1026	139	4729	1269	1028
	$N_{acc}$	117	2233	539	361	153	3068	795	521
	$N_{tot}$	10699	115794	37363	22595	5163	117774	35005	22959

	<b>GMD</b>	27	102	65	15	46	135	94	19
<b>February</b>	<b>N<sub>nuc</sub></b>	79	2291	641	433	15	1250	235	229
	<b>N<sub>atk</sub></b>	136	3509	781	573	74	3190	904	615
	<b>N<sub>acc</sub></b>	54	1306	294	198	37	1924	543	338
	<b>N<sub>tot</sub></b>	5014	74960	24092	12763	2389	79818	25138	13314
	<b>GMD</b>	21	107	54	16	29	150	88	25
<b>March</b>	<b>N<sub>nuc</sub></b>	53	2908	685	504	9	1285	226	197
	<b>N<sub>atk</sub></b>	107	1659	608	332	212	2592	670	367
	<b>N<sub>acc</sub></b>	55	821	229	133	151	1597	394	199
	<b>N<sub>tot</sub></b>	4067	54193	21179	10423	6474	58275	19157	8076
	<b>GMD</b>	22	117	49	16	38	141	85	21
<b>April</b>	<b>N<sub>nuc</sub></b>	47	3170	738	465	15	1166	262	210
	<b>N<sub>atk</sub></b>	103	1741	647	331	105	1968	746	377
	<b>N<sub>acc</sub></b>	42	1001	227	152	44	1441	455	237
	<b>N<sub>tot</sub></b>	4886	56847	22332	9166	3309	50478	21775	8595
	<b>GMD</b>	19	108	46	16	41	154	84	23
<b>May</b>	<b>N<sub>nuc</sub></b>	33	4721	660	526	18	1921	329	251
	<b>N<sub>atk</sub></b>	124	2096	618	284	106	1893	620	332
	<b>N<sub>acc</sub></b>	33	658	193	90	38	698	264	135
	<b>N<sub>tot</sub></b>	3559	89397	20295	8911	2907	50816	17375	7839
	<b>GMD</b>	20	122	48	16	26	112	65	18
<b>June</b>	<b>N<sub>nuc</sub></b>	101	3507	844	516	45	2832	445	358
	<b>N<sub>atk</sub></b>	136	2252	596	302	126	2010	654	348
	<b>N<sub>acc</sub></b>	36	531	131	76	49	593	207	103
	<b>N<sub>tot</sub></b>	4728	74826	21221	9305	3250	67884	18250	8945
	<b>GMD</b>	19	83	37	10	28	100	56	15
<b>July</b>	<b>N<sub>nuc</sub></b>	139	5103	886	675	76	4906	376	418
	<b>N<sub>atk</sub></b>	218	3054	749	375	205	2902	634	302
	<b>N<sub>acc</sub></b>	47	468	151	57	48	544	208	93
	<b>N<sub>tot</sub></b>	6401	114950	24144	12505	5617	104198	17104	8925
	<b>GMD</b>	21	98	41	10	26	100	59	14
<b>August</b>	<b>N<sub>nuc</sub></b>	75	8267	1340	1345	58	2530	679	501
	<b>N<sub>atk</sub></b>	141	4418	867	580	196	2035	650	338

	<b>N<sub>acc</sub></b>	44	769	187	114	44	693	217	123
	<b>N<sub>tot</sub></b>	4301	162142	32262	24656	5925	66427	21414	12119
	<b>GMD</b>	20	74	39	11	25	94	49	12
<b>September</b>	<b>N<sub>nuc</sub></b>	47	10338	770	985	32	1721	328	309
	<b>N<sub>atk</sub></b>	132	2526	724	444	74	2071	721	371
	<b>N<sub>acc</sub></b>	20	631	173	100	14	699	258	131
	<b>N<sub>tot</sub></b>	4529	150580	22727	16554	2462	50372	18569	8460
	<b>GMD</b>	17	96	48	15	30	118	66	18
<b>October</b>	<b>N<sub>nuc</sub></b>	45	3328	690	608	21	2874	378	404
	<b>N<sub>atk</sub></b>	120	2490	805	485	66	2526	819	474
	<b>N<sub>acc</sub></b>	31	1690	387	252	20	1937	600	371
	<b>N<sub>tot</sub></b>	7058	74501	26801	14436	1987	67710	26971	13259
	<b>GMD</b>	23	141	64	25	26	170	86	31
<b>November</b>	<b>N<sub>nuc</sub></b>	0	3575	633	569	17	1668	293	276
	<b>N<sub>atk</sub></b>	0	4297	1053	735	115	3291	1027	585
	<b>N<sub>acc</sub></b>	0	1939	592	320	210	2727	934	307
	<b>N<sub>tot</sub></b>	0	97956	33193	18392	11173	93620	34923	12412
	<b>GMD</b>	28	270	76	26	43	236	108	27
<b>December</b>	<b>N<sub>nuc</sub></b>	97	3487	768	643	12	2672	43	437
	<b>N<sub>atk</sub></b>	216	5998	1439	1092	139	4822	1203	899
	<b>N<sub>acc</sub></b>	129	2716	641	402	267	2459	872	477
	<b>N<sub>tot</sub></b>	9088	140537	40885	24747	7673	120172	37849	20841
	<b>GMD</b>	28	121	68	17	36	161	95	25

Table 4.3. Statistical values (min, max, mean and SD) of meteorological parameters (relative humidity (HR), wind speed (WS), solar radiation (SR) and atmospheric temperature (AT)) during the day and night-time for each month (from January to December) in 2022.

<b>Month</b>	<b>Parameter</b>	<b>daytime</b>				<b>nighttime</b>			
		<b>Min</b>	<b>Max</b>	<b>Mean</b>	<b>SD</b>	<b>Min</b>	<b>Max</b>	<b>Mean</b>	<b>SD</b>
<b>January</b>	<b>RH</b>	35.7	95	71.5	15.2	72.1	95	89.7	5.2
	<b>WS</b>	0.2	3.8	1.4	0.7	0.1	4.6	0.9	0.6

	<b>SR</b>	3.1	633.9	163.9	166.6	3	3.8	3.4	0.2
	<b>AT</b>	7.3	22.5	14	3.4	7.4	14.7	10.1	1.5
<b>February</b>	<b>RH</b>	28.5	95.1	56.4	16.8	43.1	95.1	79.8	10.5
	<b>WS</b>	0.1	5.4	1.8	1.1	0.1	5.5	1.2	1
	<b>SR</b>	2.9	680.1	267.4	219.2	2.9	5	3.4	0.2
	<b>AT</b>	8.1	28.2	20	4.7	7.7	21.7	14	2.7
<b>March</b>	<b>RH</b>	22.5	88.6	44.9	12.9	40.1	90.1	67.1	10.5
	<b>WS</b>	0.2	4.7	1.7	0.8	0.2	3.1	1.1	0.6
	<b>SR</b>	2.9	670.7	315.3	225.2	2.9	15.3	3.7	2
	<b>AT</b>	13.3	40.3	29.3	5.6	11.6	30.2	21.8	4
<b>April</b>	<b>RH</b>	20.8	54.1	28.4	6.1	24.1	58.3	40.2	5.8
	<b>WS</b>	0.2	5.1	1.6	0.9	0.1	3.7	1	0.6
	<b>SR</b>	2.8	777.1	347.9	244.4	2.7	41.8	5.2	6.5
	<b>AT</b>	24.3	44.2	36.3	4.4	20.4	36.7	27.9	2.9
<b>May</b>	<b>RH</b>	21.6	77.3	40.6	9.6	27.1	85.2	51.8	10.3
	<b>WS</b>	0.3	7.6	1.7	0.9	0.2	9.1	1.7	1.1
	<b>SR</b>	3.3	746.4	343.4	231.4	2.8	51.4	7.1	10.9
	<b>AT</b>	19.6	46.3	35.8	4.1	19.5	38.1	30.4	3.1
<b>June</b>	<b>RH</b>	21.6	88.2	41.9	15.7	25.6	85.1	49.2	14.7
	<b>WS</b>	0.3	5.4	1.9	0.8	0.3	3.4	1.4	0.6
	<b>SR</b>	3.8	825.5	335.7	254.8	2.9	64.4	7.1	11.4
	<b>AT</b>	24.8	44.9	36.2	4.9	23.6	39	31.8	3.2
<b>July</b>	<b>RH</b>	44.2	87.2	62.9	10.7	52.2	86	73.2	6.5
	<b>WS</b>	0.4	4	1.7	0.7	0.2	3.8	1.3	0.5
	<b>SR</b>	3.3	793.4	264.1	222.6	2.8	56.9	6.2	8.6
	<b>AT</b>	24.8	38.5	32.3	3.1	26.1	35.5	29.8	1.9
<b>August</b>	<b>RH</b>	42.3	86.7	59.3	10	59.1	86.2	72.1	5.7
	<b>WS</b>	0.3	4.3	1.8	0.8	0.2	3.8	1.2	0.6
	<b>SR</b>	3.2	802.9	276.7	209.1	3.1	50.9	5.5	6.4
	<b>AT</b>	25.9	37.9	32.1	2.4	26.1	32.8	29.1	1.3
<b>September</b>	<b>RH</b>	38	88.3	63.4	13.5	57.2	88.4	75.4	8.7



	<b>WS</b>	0.2	4.2	1.5	0.7	0.2	2.6	0.9	0.4
	<b>SR</b>	3.1	724.7	236.5	212.5	3	23.9	4.3	3.1
	<b>AT</b>	23.7	37.7	30.7	3.8	23.5	32.4	27.5	2.4
<b>October</b>	<b>RH</b>	32.5	90.8	56.6	15.5	57.6	90.6	76.1	6.8
	<b>WS</b>	0.1	3.4	1.1	0.6	0.2	3	0.8	0.4
	<b>SR</b>	3.1	654.8	225.3	197.1	3	14.7	4.1	1.7
	<b>AT</b>	18.6	35.7	28.1	4.2	15.9	28.7	22.3	2.6
<b>November</b>	<b>RH</b>	29.4	83.4	50.5	13.1	46.5	85.4	70.8	8.2
	<b>WS</b>	0.2	3	1	0.6	0.1	2.9	0.6	0.4
	<b>SR</b>	3.1	396.3	144.6	126.1	3.2	7.1	3.7	0.5
	<b>AT</b>	11.7	35	24.5	4.7	11.4	25.1	17.6	3.4
<b>December</b>	<b>RH</b>	33.4	94.9	59.6	16.1	52.8	94.9	79.6	8.5
	<b>WS</b>	0.1	3.8	1.1	0.5	0.1	2.3	0.8	0.4
	<b>SR</b>	3.2	296.6	98.8	90.6	3.1	4.2	3.4	0.2
	<b>AT</b>	6.9	28.9	18.1	5.2	7.1	18.3	12.3	2.3

Table 4.4. Classification of seasonal periods.

<b>Season</b>	<b>Start to End day</b>	<b>Month</b>
<b>Winter</b>	01-01-2022 to 14-02-2022 and 01-12-2022 to 31-12-2022	January, February, December
<b>Spring</b>	15-02-2022 to 31-03-2022	February, March
<b>Summer</b>	01-04-2022 to 30-06-2022	April, May, June
<b>Monsoon</b>	01-07-2022 to 15-09-2022	July, August, September
<b>Autumn</b>	16-09-2022 to 30-11-2022	September, October, November

#### 4.4 Particle number concentration and its variation

##### 4.4.1 Particle number concentration of different particle sizes during day and nighttime in urban site

The particle number concentration of the different size fractions varies based on the emission intensity. The different size particles and their seasonal concentration

variations are shown in Fig.4.3. A different pattern in the contribution of the different modal sizes fractions to the  $N_{\text{total}}$  was found throughout the year. Variations were associated with the emitting sources, especially engine exhaust in the study area and aerosol-forming precursors present in the local atmosphere.

The daytime annual mean concentration for  $N_{\text{nuc}}$ ,  $N_{\text{atk}}$  and  $N_{\text{acc}}$  were 770, 846 and 313  $\text{cm}^{-3}$ , respectively (Table 4.1). Similarly, the respective concentrations at night were 353, 819, and 481  $\text{cm}^{-3}$ .  $N_{\text{nuc}}$  reached up to  $1 \times 10^4 \text{ cm}^{-3}$ , being higher during the day than at night due to the impact of traffic emissions on atmospheric particle population. Similarly,  $N_{\text{atk}}$  was found below  $5 \times 10^3 \text{ cm}^{-3}$  throughout the year, influenced by traffic emissions. Compared to the  $N_{\text{nuc}}$  and  $N_{\text{atk}}$ , the  $N_{\text{acc}}$  exhibited a different concentration pattern, with higher concentrations at night than during the day, due to particle coagulation processes. The mean  $N_{\text{acc}}$  also was below  $3 \times 10^3 \text{ cm}^{-3}$ . Consequently, and due to the variations in the modal size fractions, the mean  $N_{\text{total}}$  ranged from 2 to  $4 \times 10^4 \text{ cm}^{-3}$ , being higher during the day than at night, associated with the strongest impact of traffic emissions. The reduction in total particle number concentration during nighttime can also be influenced by the absence of photochemical precursors and the predominance of removal mechanisms such as coagulation and dry deposition. Under stable boundary-layer conditions, smaller particles tend to coagulate or deposit onto surfaces, leading to a decrease in the nucleation- and Aitken-mode concentrations observed after sunset.

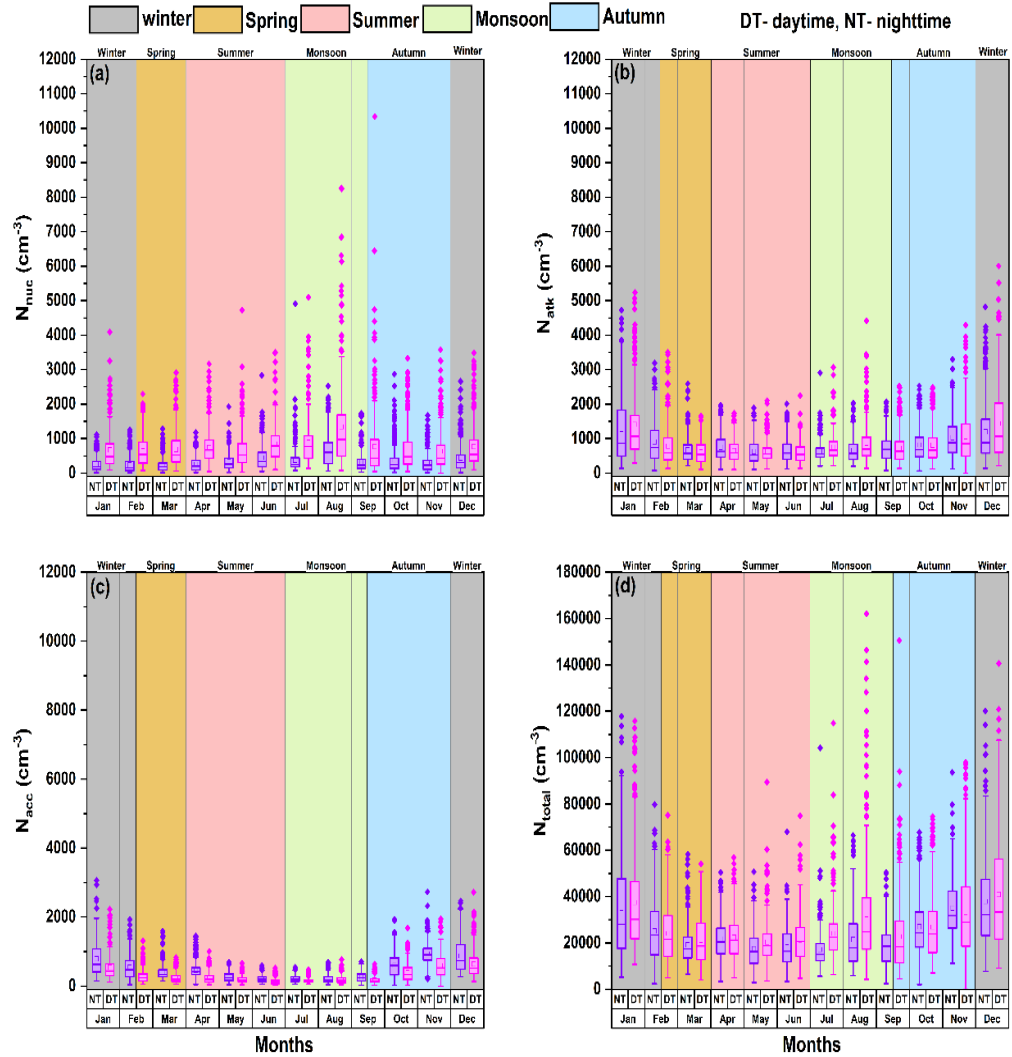


Figure 4.3. Boxplot represented the concentration of  $N_{nuc}$ ,  $N_{atk}$ ,  $N_{acc}$  and  $N_{total}$  in both scenarios (daytime and nighttime) every month (from January to December) during 2022.

Note: Boxes indicate the interquartile range, whiskers represent the 5<sup>th</sup> - 95<sup>th</sup> percentile range, horizontal lines within the boxes indicate the median and the dashes (-) represent the mean.

#### 4.4.2 Variation in particle number concentration in an urban and a background site

The modal particle number concentration, Nucleation ( $N_{nuc}$ , 10 to 30 nm), Aitken ( $N_{atk}$ , 30 to 100 nm), Accumulation ( $N_{acc}$ , 100 to 800 nm), and total particle number concentration ( $N_{tot}$ , < 800 nm) were compared between the two different sites

(urban and background). The analysis shows that  $N_{tot}$  concentration in the urban and background sites were found to be  $2.5 \times 10^4 \text{ cm}^{-3}$  and  $2.9 \times 10^3 \text{ cm}^{-3}$ , respectively (Table 4.5). Trechera et al. (2023) reported 6 cities in European country showed higher PNC ranging from  $1.35 \times 10^4$  to  $1.05 \times 10^4 \text{ # cm}^{-3}$  near the traffic-related site whereas, cities from Italy showed lower concentrations in regional background ranges from  $7.4 \times 10^3$  to  $4.5 \times 10^3 \text{ # cm}^{-3}$ . Similar studies showed that the concentration in the urban site is higher compared with the background site (Rose et al., 2021; Trechera et al., 2023).

Table 4.5. Average mean particle concentration in the urban and background sites during the study period.

	<b>DEL-Urban Site</b>				<b>RNC-Background Site</b>			
	<b><math>N_{nuc}</math></b>	<b><math>N_{atk}</math></b>	<b><math>N_{acc}</math></b>	<b><math>N_{tot}</math></b>	<b><math>N_{nuc}</math></b>	<b><math>N_{atk}</math></b>	<b><math>N_{acc}</math></b>	<b><math>N_{tot}</math></b>
<b>Min</b>	0	0	0	0	0	0	0	0
<b>Max</b>	10338	5999	3422	159194	2047	3573	2110	205780
<b>Mean</b>	577	833	433	25708	42	169	90	2968
<b>SD</b>	608	620	382	16162	85	151	65	3277

The number concentration analysis reveals that in urban regions, the  $N_{atk}$  concentration was found to be higher than  $N_{nuc}$ , and followed by  $N_{acc}$ , but in the background site,  $N_{atk}$  was higher than  $N_{acc}$ , followed by  $N_{nuc}$ , respectively. In urban regions, the higher concentration of  $N_{atk}$  and  $N_{nuc}$  is due to transport-related anthropogenic emissions, with an average of  $5.7 \times 10^2 \text{ cm}^{-3}$ ,  $8.3 \times 10^2 \text{ cm}^{-3}$ , and  $4.3 \times 10^2 \text{ cm}^{-3}$  for  $N_{nuc}$ ,  $N_{atk}$ , and  $N_{acc}$ , similarly for the background site it was  $0.4 \times 10^2 \text{ cm}^{-3}$ ,  $1.6 \times 10^2 \text{ cm}^{-3}$  and  $0.9 \times 10^2 \text{ cm}^{-3}$ . On average, the difference in  $N_{tot}$  between the urban and background sites showed that  $N_{tot}$  was ~8 times higher in the urban site compared to the background one (Chatain et al., 2021).

The Number concentrations in the different geographical regions vary based on the source intensity, types of sources. The size distribution of the particles in urban and background conditions shows the dominance of different size particles in different geographical conditions. In both sites,  $N_{atk}$  showed a higher concentration than other modes, possibly due to the short-lived nature of  $N_{nuc}$  associated with the coagulation

and condensation processes in the atmosphere (Chen et al., 2022; Sun et al., 2019). In the winter season, the maximum  $N_{\text{tot}}$  was observed,  $1.0 \times 10^3 \text{ cm}^{-3}$  in the urban site and  $2.3 \times 10^2 \text{ cm}^{-3}$  in background one (Şahin et al., 2022; Sun et al., 2019) (Fig.4.4). The lowest concentration was observed for  $N_{\text{atk}}$  during the summer ( $6.4 \times 10^2 \text{ cm}^{-3}$ ) in the urban site, while in background one was observed in the monsoon period  $1.06 \times 10^2 \text{ cm}^{-3}$  (Table 4.6). In summer it is usual to find lesser concentration compared to winter due to the meteorology (Kalkavouras et al., 2020). The seasonal average for  $N_{\text{tot}}$  varies from one site to another. In the urban site,  $N_{\text{tot}}$  was higher in post-monsoon ( $3.0 \times 10^4 \text{ cm}^{-3}$ ), followed by winter ( $2.9 \times 10^4 \text{ cm}^{-3}$ ), monsoon ( $2.2 \times 10^4 \text{ cm}^{-3}$ ), and summer ( $2.0 \times 10^4 \text{ cm}^{-3}$ ) (Table 4.6).

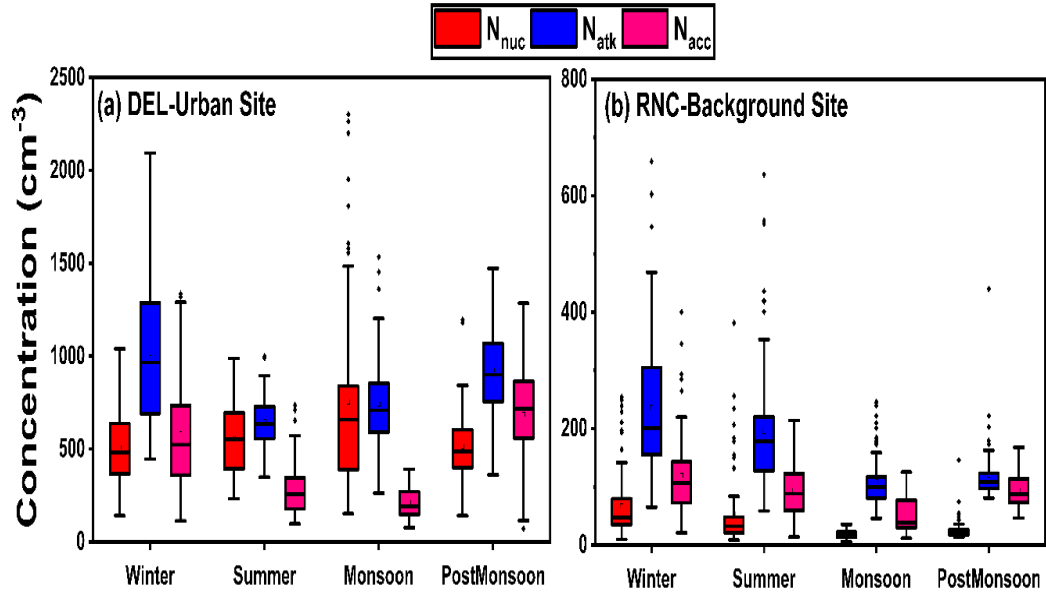


Figure 4.4. Box whisker analysis of  $N_{\text{nuc}}$ ,  $N_{\text{atk}}$ , and  $N_{\text{acc}}$  mode particles in an urban and a background site.

In the urban site,  $N_{\text{nuc}}$  and  $N_{\text{atk}}$  were similar during the summer and monsoon, but in the background site, the modal particle number concentration was as follows:  $N_{\text{atk}} > N_{\text{acc}} > N_{\text{nuc}}$  for all seasons. The variations for  $N_{\text{tot}}$  between the urban and background sites were highest during the monsoon, which was  $\sim 13$  times higher in urban regions, followed by post-monsoon  $\sim 12$  times, winter  $\sim 7$ , and summer  $\sim 6$ . The urban regions with complex emissions emit wide range of particles in different size ranges and also in background conditions the particles are concentrated to particular size range of natural emissions.

Table 4.6. Season-wise average statistics for modal particle number concentration in the urban and background sites during the study period.

Season		DEL-Urban Site				RNC-Background Site			
		N <sub>nuc</sub>	N <sub>atk</sub>	N <sub>acc</sub>	N <sub>tot</sub>	N <sub>nuc</sub>	N <sub>atk</sub>	N <sub>acc</sub>	N <sub>tot</sub>
Winter (Dec to Mar)	Min	10	75	42	2388	0	0	0	0
	Max	4097	5999	3422	140484	1310	3573	2110	205780
	Mean	510	1007	576	29521	64	233	121	4145
	SD	497	834	448	19359	106	197	88	5193
Summer (Apr to Jun)	Min	15	103	37	2906	3	36	9	511
	Max	4722	2253	1608	89387	2047	1969	585	27256
	Mean	562	645	269	20280	54	196	93	3303
	SD	467	332	193	8995	110	153	49	2242
Monsoon (Jul to Sep)	Min	33	74	16	2461	2	19	3	247
	Max	10338	4419	780	159194	258	494	182	6993
	Mean	746	728	213	22778	18	109	51	1728
	SD	878	423	117	15762	19	60	32	899
Post Monsoon (Oct to Nov)	Min	0	0	0	0	6	38	28	863
	Max	3576	4298	3042	97901	583	1632	974	23682
	Mean	513	924	685	30336	26	120	94	2479
	SD	520	592	411	15331	45	102	43	1470

#### 4.4.3 Diurnal variations of mode particle number concentration in the urban and background sites

The diurnal variation of modal particle number concentration in the urban and background sites indicates how the concentration of the particles varies in terms of source during the different seasons. In the urban site, N<sub>nuc</sub> peaked from 8 to 12 hrs in the morning due to the fresh engine exhaust emissions, while in the background site during the winter and spring seasons, this peak was shifted (12 to 20 hrs) (Chen et al., 2022; Zhu et al., 2002, 2004). This was due to the increase in the formation of new particles in the atmosphere by gas-to-particle conversion induced by photochemistry and their subsequent growth. N<sub>atk</sub> in the urban site showed a clear double hump model

during the morning (8 to 11 hrs) and evening peak hours (16 to 20 hrs) which was associated with the transport of emissions from urban areas. Globally, this pattern signifies the role of pollution transportation in determining the particle concentration in the urban site (Fig.4.5). The  $N_{acc}$  mode in the urban site followed a similar pattern to that of  $N_{atk}$ .

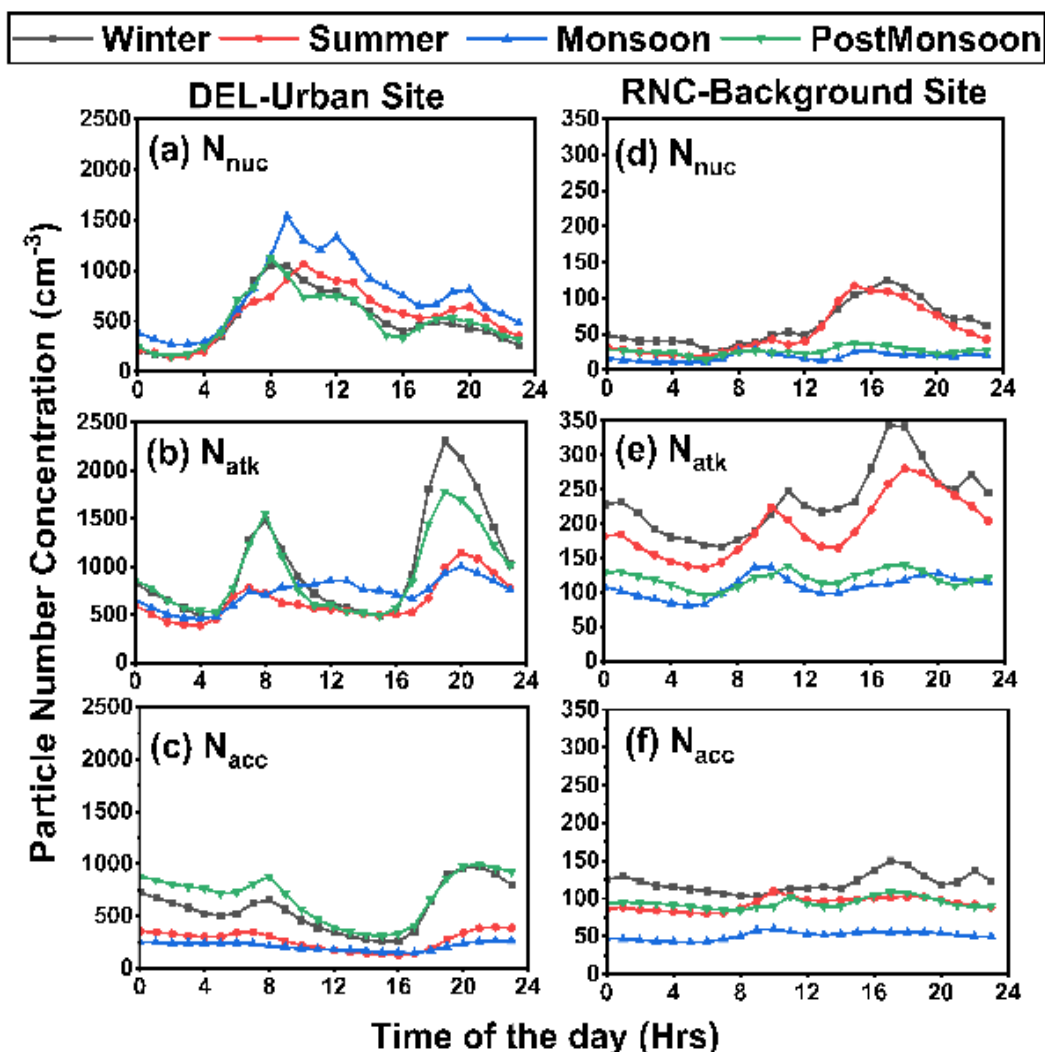


Figure 4.5. Diurnal variation of modal particles number concentration in an urban and a background site during the different seasons.

In the urban site, the  $N_{nuc}$  varied from  $2.5 \times 10^2 \text{ cm}^{-3}$  to  $1.5 \times 10^3 \text{ cm}^{-3}$ , while in the background site, it lies  $< 1 \times 10^3 \text{ cm}^{-3}$ , the evening peak higher due to the  $N_{acc}$  accumulation throughout the day. The  $N_{nuc}$  in monsoons was observed more frequently during the morning hours due to the wet removal of pre-existing larger particles, which promoted an increase in particles fresh from exhaust emissions ( $1.5 \times 10^3 \text{ cm}^{-3}$ ). The

$N_{\text{atk}}$  and  $N_{\text{acc}}$  mode particles showed higher concentration during the winter and post-monsoon periods. The observed enhancement in accumulation-mode concentration during stagnant or low-wind conditions suggests that particle growth through condensation and coagulation dominates over new particle formation. These processes gradually convert smaller particles into larger ones, increasing the accumulation fraction while reducing total particle number. In the background site, the concentration of the three particle modes was higher during winter and summer, followed by post-monsoon and monsoon seasons. The diurnal variation in a region can suggest the pattern of sources in both urban and background conditions. The urban regions show a pattern dominated by the anthropogenic emissions, whereas in the background it was vice versa.

#### **4.5 Mode contributions to the total particle number concentration**

##### **4.5.1 Contribution from different mode particles in urban site**

The particle concentration comparison between day and nighttime showed that  $N_{\text{nuc}}$  was 45.84% lower at night than during the day, while  $N_{\text{atk}}$  only dropped 4%. In contrast, the  $N_{\text{acc}}$  increased by 34% at night. These differences indicated the critical role of vehicular sources and local factors (especially meteorology) on the atmospheric particle population. Similar to diurnal concentrations the contribution of the different size fractions to the total PNC also varied in urban and background conditions. The anthropogenic emissions emit particles in size ranges more in Aitken mode due to the engine exhausts emissions. The profile also based on the emissions source's combustion process. The transportation sources with different fuel usage and combustion processes will also varies during the different hours of the day.



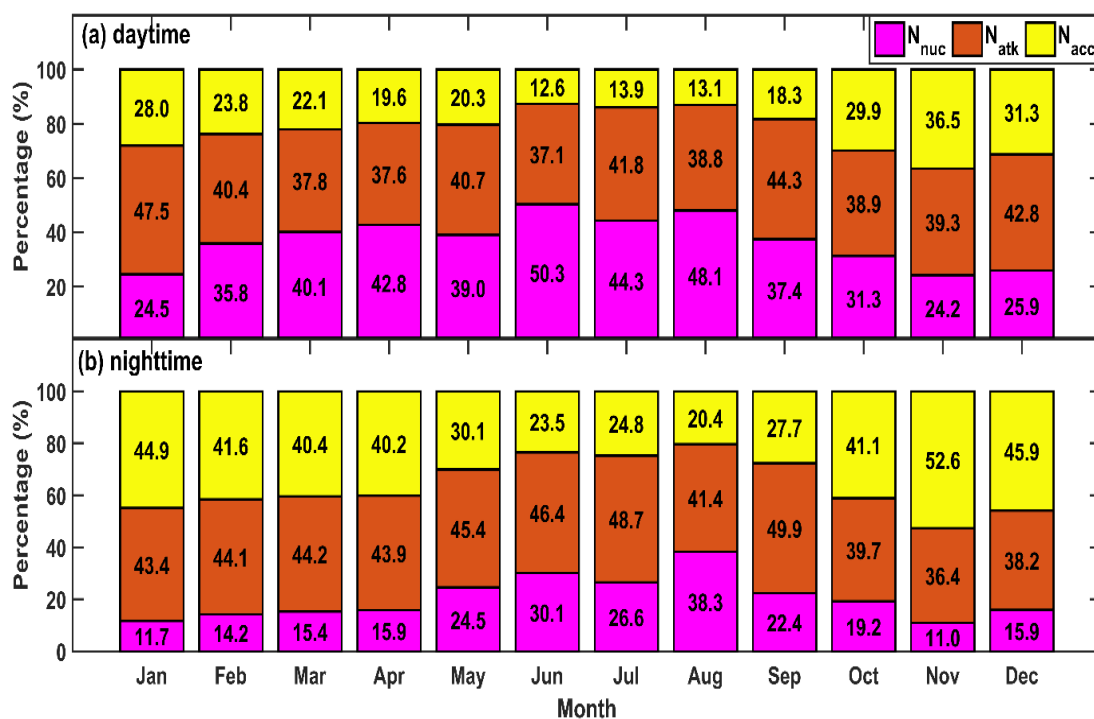


Figure 4.6. Size-segregated particle number contribution in both scenarios ((a) daytime and (b) nighttime)) in every month (from January to December) during 2022.

The  $N_{nuc}$  contribution to the  $N_{tot}$  was the highest during the monsoon period, probably due to clean atmospheric conditions by the washout effect of heavy rain. Following the monsoon period, the second-highest contribution in  $N_{nuc}$  was recorded during the summer season, and the lowest was found in winter, associated with rapid coagulation processes among particles. During the daytime, the contribution of  $N_{nuc}$  seemed to be higher during the summer period (June, July and August), reaching up to 50% of the  $N_{total}$  promoted by fresh emissions and important photochemical activity. However, during the winter period,  $N_{acc}$  had a higher contribution to the  $N_{total}$  due to the growth of particles through coagulation processes, ranging from 30 to 35% (Fig.4.6a). Contrary, during the nighttime, the contribution of  $N_{nuc}$  contribution dropped below 35%, but for the larger-sized particles ( $N_{atk}$  and  $N_{acc}$ ), it was high (Fig.4.6b).  $N_{acc}$  dominated during the night throughout the year except for the summer period when  $N_{atk}$  prevailed high both day and nighttime. This finding is associated with traffic emissions patterns. However, local meteorology influenced atmospheric aerosol transformations, reflected in the increased concentration of the rest of the sizes' fractions. The type of emissions also influenced the aerosol number size distribution.

During the day, most vehicles that pass near the monitoring site were light motor vehicles using petrol and CNG as fuel. These vehicles emitted particles in the ultrafine range, so the contribution of  $N_{\text{nuc}}$  and  $N_{\text{atk}}$  was higher. However, during the nighttime, the vehicular population was dominated by heavy vehicles with diesel-powered engines emitting particles in higher size ranges. This led to an increase in the  $N_{\text{acc}}$ .

#### **4.5.2 Particle number contribution during the winter period in urban site**

The percentage contribution is used to identify the contribution from different mode particles to  $N_{\text{tot}}$ . In February and March,  $N_{\text{nuc}}$  was a particularly large contributor during the day, making up 36 to 40% (Fig.4.7a) of the  $N_{\text{tot}}$  from new emissions and photochemical reactions. Because of their short atmospheric lifetime, the  $N_{\text{nuc}}$  mode particles tend to coagulate with pre-existing particles, causing them to develop into larger particles. On the other hand,  $N_{\text{acc}}$  contributed more to  $N_{\text{tot}}$  at night in all months, which was explained by particle growth through coagulation processes, with values ranging from 40 to 46% (Fig.4.7b). Throughout the study period, the different mode fractions showed different patterns of contribution throughout the day and at night. According to this study,  $N_{\text{nuc}}$  mode particles made up around 32% of  $N_{\text{tot}}$  during the daytime and 15% at nighttime, respectively. On the other hand,  $N_{\text{acc}}$  mode particles made up about 43% at night and 26% during the day. There was no difference in the  $N_{\text{atk}}$  mode between day and night.

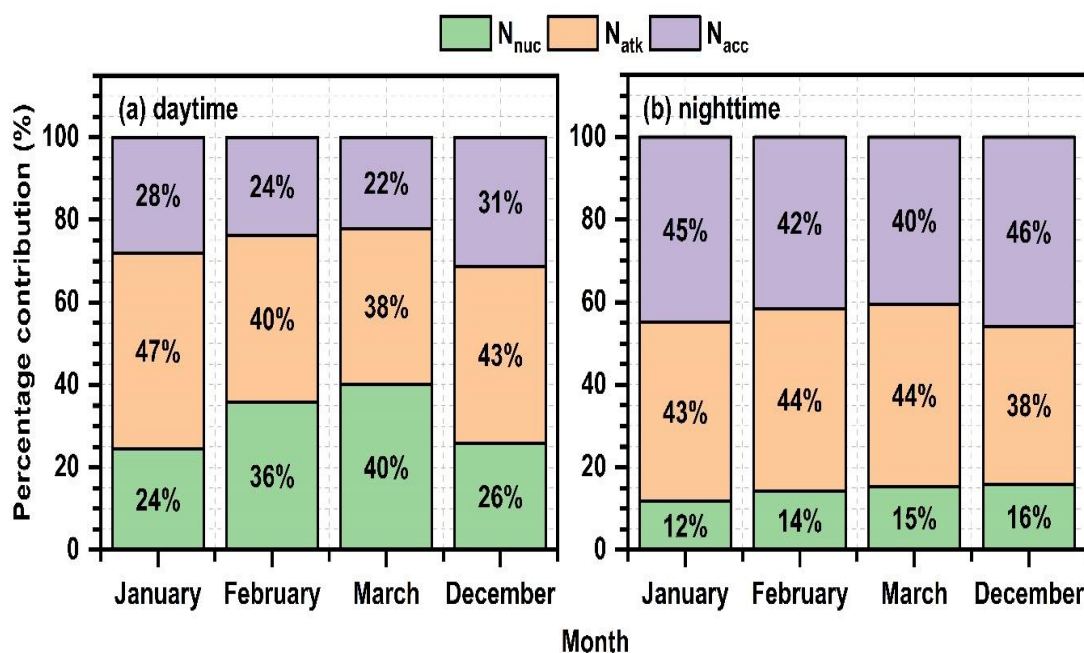


Figure 4.7. Different mode particle contribution during (a) daytime and (b) nighttime to the total particles.

Overnight, the  $N_{nuc}$  contribution dropped to 16%, but the larger particles,  $N_{atk}$  and  $N_{acc}$ , in particular, remained high (Fig.4.7b). On the other hand,  $N_{atk}$  showed high levels both during the day and at night, while  $N_{acc}$  was the most common particle type during the night during the study period. Patterns of transportation emissions are consistent with this discovery. The increase in concentrations of various size fractions further suggests that local meteorological conditions played a significant role in the transformation of atmospheric aerosols. The distribution of aerosol number sizes was also influenced by the type of emissions.  $N_{nuc}$  and  $N_{atk}$  contributed more during the day because most of the vehicles close to the monitoring site were light motor vehicles that ran on gasoline and compressed natural gas (CNG), which released particles mostly in the ultrafine range (Kontkanen et al., 2020; Zhu et al., 2002). At night, however, the mix of cars changed to include heavier diesel-powered vehicles, which produced particles with a wider variety of sizes, raising the  $N_{acc}$ . According to Harrison. (2020), Delhi's diurnal variance shows a major influence from road traffic, especially at night when heavy-duty vehicles enter the city. The winter period with higher emissions and poor air quality in urban regions experiences different contribution profiles compared

to the other seasons. The change in the emission is due to the intensified emissions and influenced by the meteorological conditions.

#### **4.6 Particle number size distribution**

##### **4.6.1 Particle number size distribution during day and nighttime in urban site**

The aerosol number size distribution exhibited a single mode during the winter periods, i.e., in winter (January and December), with a clear peak around 100 nm during both the day and night and a maximum of  $\sim 6 \times 10^4 \text{ cm}^{-3}$  associated with anthropogenic emissions from the vehicles (Fig.4.8) and the rapid particles growth by condensation and coagulation processes (Harrison et al., 2018; Harrison., 2020). In February, March and April, particle concentration was reduced to half compared to the winter periods, being the fresh emissions from the engine exhaust higher during the daytime (Kittelson et al., 2022). This led to the mean concentration of the daytime being higher than the nighttime concentration. At nighttime, a similar pattern was observed in the winter periods due to the condensation processes, recording the maximum particle concentration.

The Geometric Mean Diameter (GMD) concentration also varies based on the emission and intensity of the sources. GMD reached up to 100 nm during the winter and summer months when complex emissions were found. Variations during the day and at night were also observed. The daytime GMD was lower than nighttime, around 20 to 40 nm, reaching a maximum of around 65 nm. During the daytime, gasoline vehicles such as CNG dominate the vehicle density in the study location, contributing to freshly emitted engine exhaust (Chen et al., 2022). However, during the night-time, diesel engine vehicles were dominated, hence, resulting in a higher concentration of particles around 100 nm (Chatain et al., 2021; Damayanti et al., 2023; Şahin et al., 2022; Zhu et al., 2002).

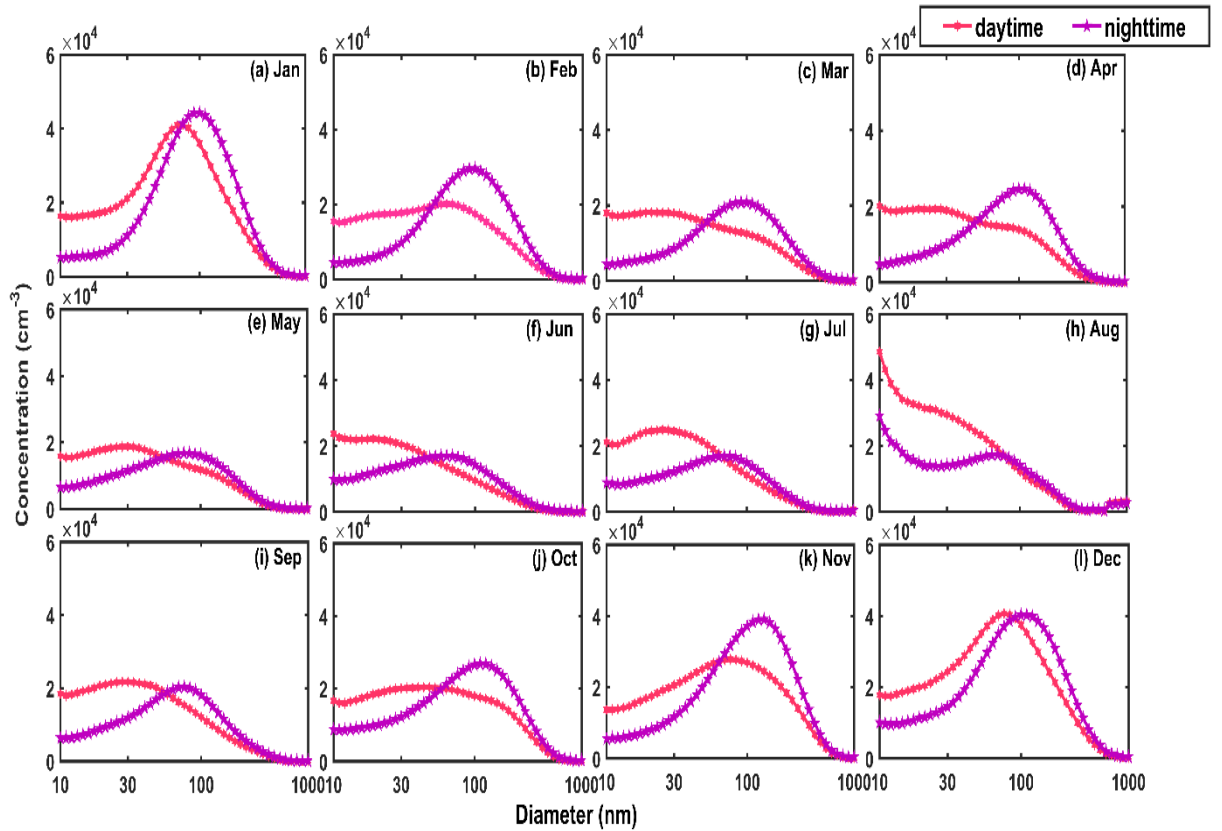


Figure 4.8. Monthly average particle number size distributions at both scenarios (daytime and nighttime) every month (from January to December) during 2022.

Surface plot of the aerosol number size distribution during day and night time in 2022 and its normalized are presented in Fig.4.9. The daytime and nighttime concentrations in 2022 showed that particles around 100 nm were gradually increasing from the evening peak hour to midnight (Fig.4.9A). The normalized mean aerosol number size distribution identified a peak between 10 to 30 nm during the daytime, being directly proportional to the intensity fresh engine exhaust emissions. The  $N_{atk}$  and  $N_{acc}$  (up to 300 nm particles) dominated the  $N_{total}$  at night. This was due to the smaller particles' physical transformation into larger sizes due to the coagulation processes in which they are involved (Yadav et al., 2022). In addition, heavy vehicles dominated the vehicle population at night, emitting particles in larger size ranges than day, such as those of the  $N_{acc}$ .

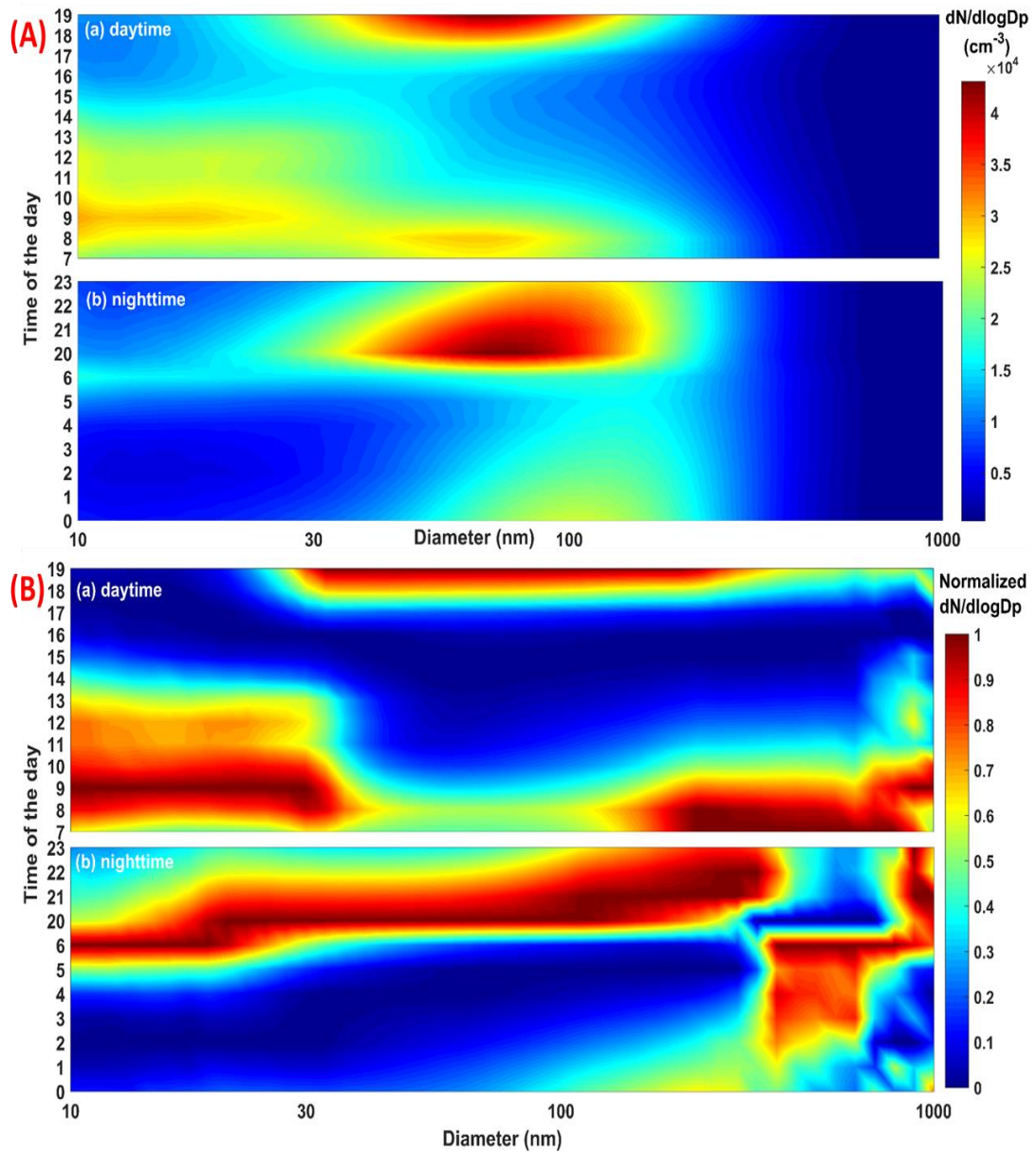


Figure 4.9. (A) Particle number size distribution ( $dN/d\log D_p$  in  $\text{cm}^{-3}$ ) in the 10 to 1090 nm size range and its (B) normalized during 2022.

#### 4.6.2 Particle number size distribution during day and nighttime in winter period

Anthropogenic emissions from vehicles and the quick growth of particles through condensation and coagulation processes are linked to the unimodal pattern of the particle number size distribution, which showed a clear peak near 100 nm at night and a maximum of roughly  $3.3 \times 10^4 \text{ cm}^{-3}$  (Harrison et al., 2018). In contrast to the more intense winter months, particle concentrations were cut in half during February and March. During the day, fresh emissions from engine exhaust were significantly

greater (Kittelson et al., 2022). Condensation mechanisms were responsible for a similar trend that was seen at night as it did during the harsh winter months (Fig.4.11). It is important to highlight that while the average particle concentration was elevated during the daytime compared to nighttime, the most significant peak occurred at night (Fig.4.10). The geometric mean diameter (GMD) also changed according to the strength of the emission sources. In contrast to 90.6 nm during the day, the GMD peaked at 161.6 nm at night. Day and nighttime variations in the emissions' sources were reflected in the GMD concentration. Freshly released engine exhaust, especially from gasoline-powered vehicles, was the main source of the concentration peak during the day, which was detected in the 20 to 40 nm range (Chen et al., 2022). In terms of vehicle density, gasoline vehicles including CNG models dominated the research site during the day. At night, diesel-powered vehicles generate a greater concentration of particles around 100 nm (Chatain et al., 2021; Damayanti et al., 2023; Şahin et al., 2022; Zhu et al., 2004). Heavy-duty vehicles are a major generator of larger-size range particles, such as  $N_{acc}$ , at night.

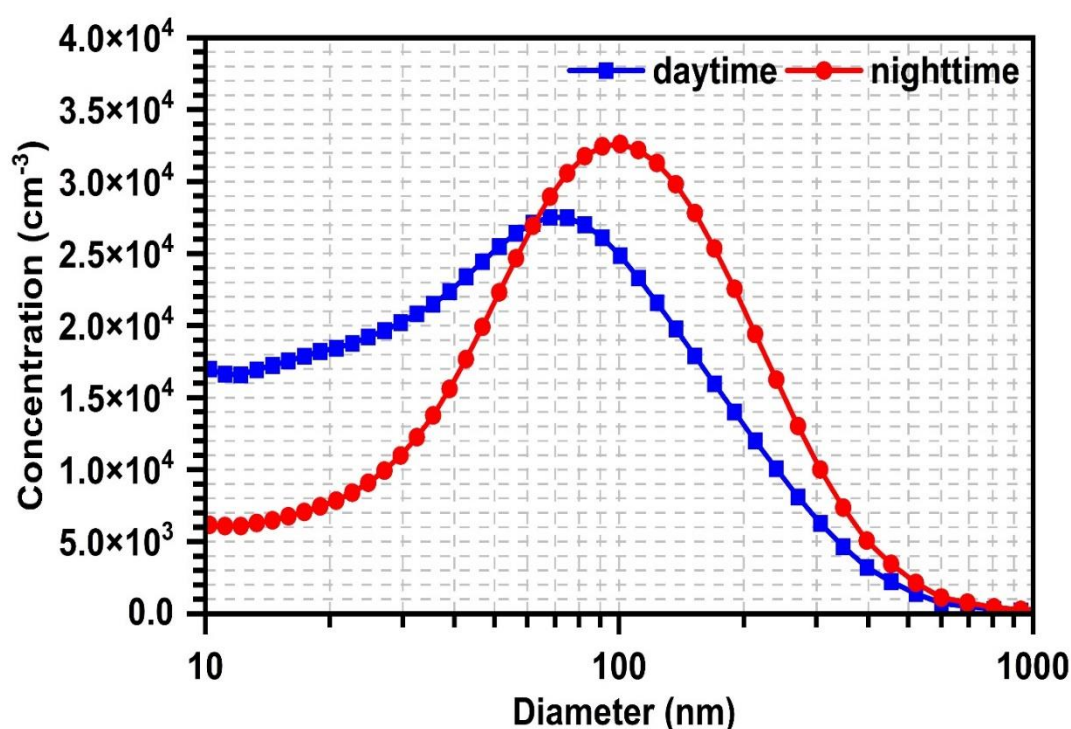


Figure 4.10. Size distribution of the particles during daytime and nighttime throughout the winter period.



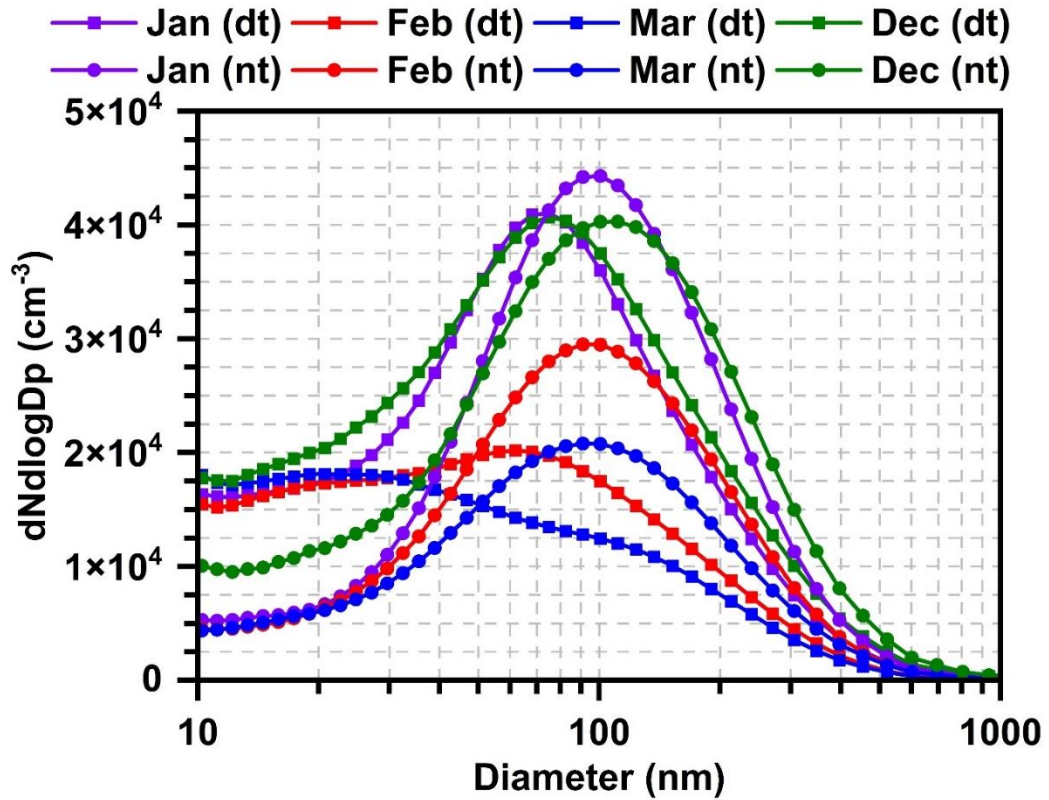


Figure 4.11. Monthly size distribution of the particles in the winter period during daytime and nighttime.

#### 4.6.3 Particle size distribution in an urban and a background site

Aerosol particle number size distribution was used as a tool to identify the sources of the particles. The size distribution pattern varies from the background to the urban site. The size distribution of the particles in urban site showed a single clear peak concentration between 80 and 90 nm, which typically refers to engine exhaust emissions (Chen et al., 2022; Kontkanen et al., 2020) (Fig.4.12). In the background site, particle size distribution ranged gradually increase from 20 to 100 nm due to particle growth, a common phenomenon in this type of sites.

In the urban site, the PNC contribution from the transportation sector is more dominant than other sources (Chen et al., 2022; Gani et al., 2021). The highest concentration was obtained during winter, around  $4 \times 10^4 \text{ cm}^{-3}$ , while the concentration ranged between  $1$  to  $2 \times 10^4 \text{ cm}^{-3}$  in the rest of the seasons. Global studies showed similar behavior during winter (Gani et al., 2021; Şahin et al., 2022). In the background



site, the highest concentration was in winter, followed by summer, post-monsoon and monsoon.

In almost all the seasons, the gradual growth of the particles was observed. The size distribution pattern of the urban site showed that during all the seasons, the concentration of the particles emitted also lies in the range of  $1$  to  $2 \times 10^4 \text{ cm}^{-3}$ , which is the result of direct emission from anthropogenic sources. In the background site, the sub-10 nm particles showed the particle concentration gradually reducing around 10 nm and increasing after 10 nm due to the change of particle phases from gaseous to solid due to the particle formation process. Consequently, the concentration of the size distribution varies from season to season. However, the emission profile remains similar in all the seasons, whereas in the urban site, the size distribution and emission profile change from season to season due to the influence of sources meteorology and the intensity of the sources.

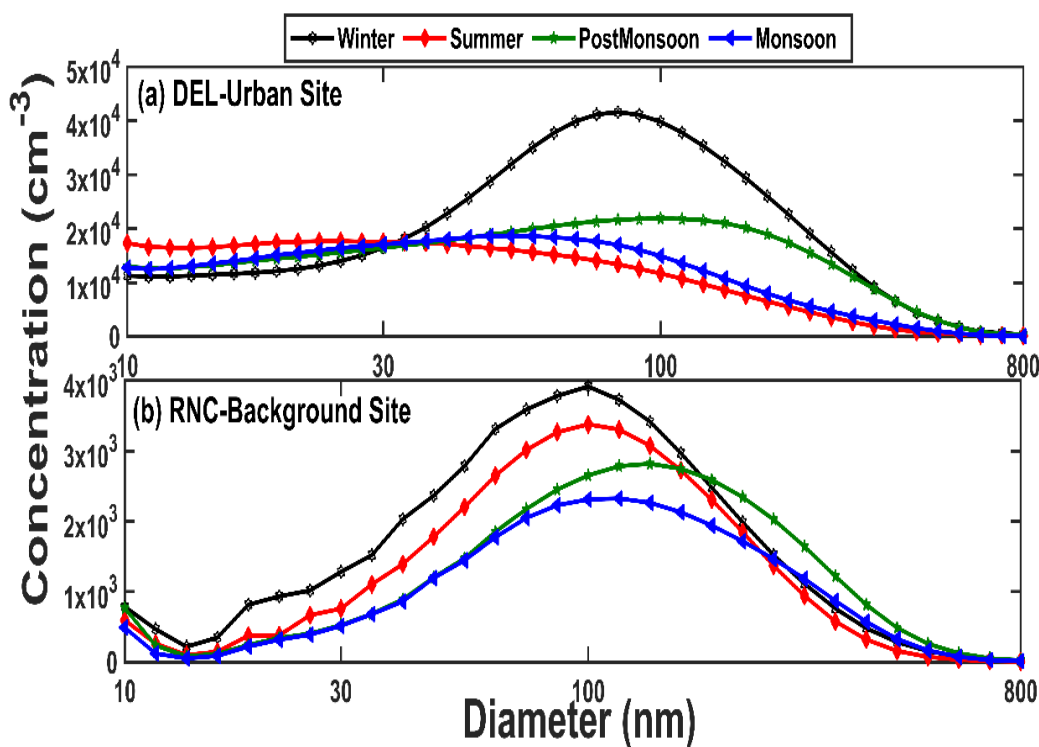


Figure 4.12. Particle number size distribution of particles in (a) an urban and (b) a background site during different seasons.

#### **4.6.4 Correlation between the number concentration with particulate matter, gaseous, and meteorological parameters**

A useful method for evaluating the different contributions of atmospheric processes and emissions that affect air quality, mainly from a variety of sources, is correlation analysis (Yadav et al., 2014a; Yadav et al., 2014b). The particle number concentration, particulate matter, gaseous, and climatic factors were shown to be strongly positively correlated. The significant fresh emission during the day was indicated by the correlation between the  $N_{nuc}$  and  $N_{tot}$ , which was around 0.5 (Fig.4.13). At night, however, a weaker association was noted. At night, the  $N_{acc}$  mode shows a good correlation of about 0.8 (Fig.4.14). Furthermore, there is a strong link between particulate matter and the  $N_{acc}$  mode particles. One major source of PM in urban settings is the  $N_{acc}$  mode particles (Gani et al., 2020). During the day, there was a high connection between the PNC ( $N_{atk}$  and  $N_{acc}$ ) and gaseous ( $NO_2$ ,  $NO_x$ , and CO) in the range of 0.5 to 0.7, indicating that a sizable portion of pollutants originate from vehicle emissions. Because there was not enough sun radiation throughout the winter, there was a significant negative connection found between the PNC and  $O_3$ . During the day, there was a strong link between PNC and relative humidity (RH). Fig.4.13 and Fig.4.14 show that our study location was primarily influenced by local sources. Urban areas are significantly influenced by local sources (Bran & Srivastava, 2017; Pipal et al., 2014).

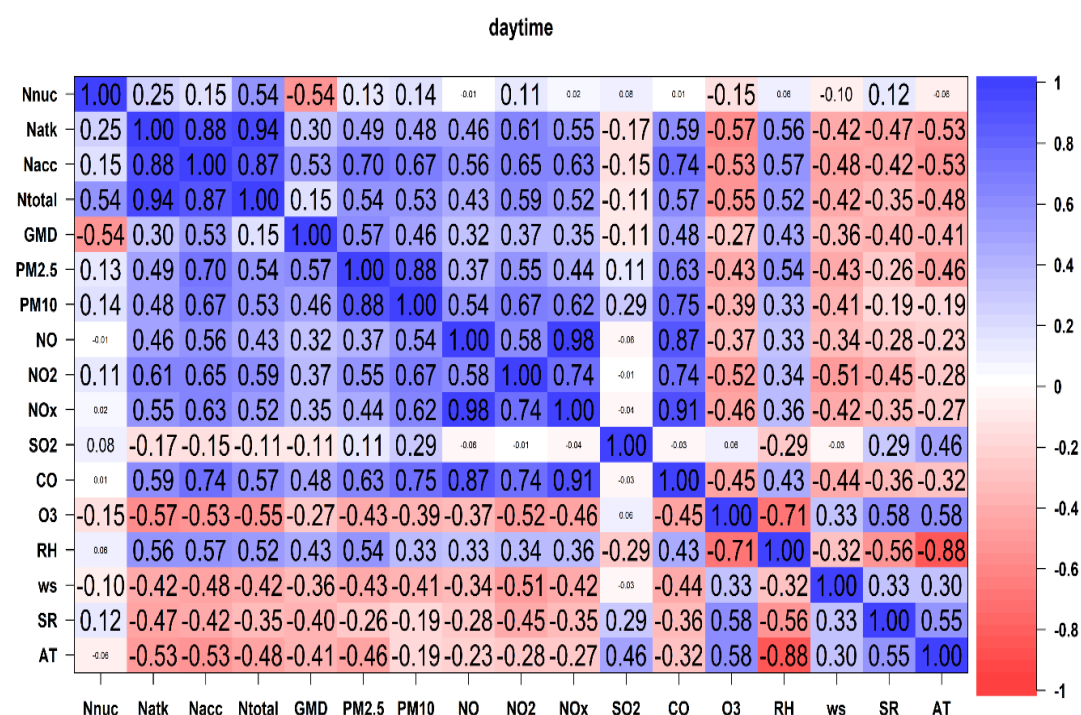


Figure 4.13. Relationship between particle number concentration, particulate matter, gaseous pollutants, and meteorological variables during the daytime.

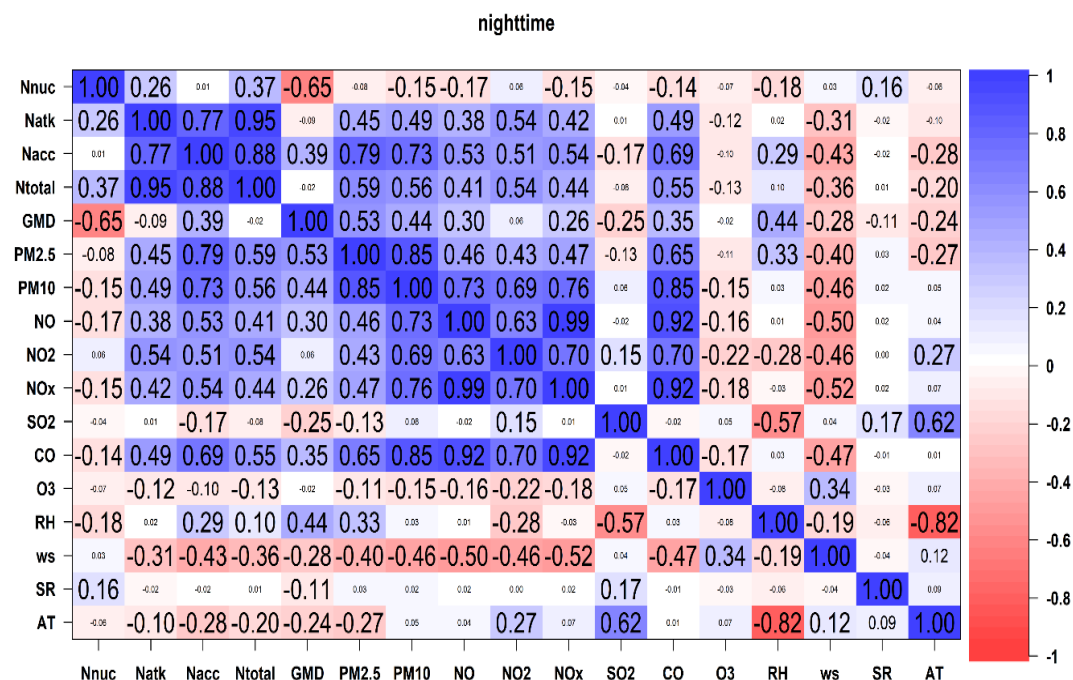


Figure 4.14. Relationship between particle number concentration, particulate matter, gaseous pollutants, and meteorological variables during the nighttime.

## **4.7 Role of meteorological parameters**

### **4.7.1 Influence of meteorology on the particle number concentration and its size distribution in urban site**

The meteorological parameters, such as precipitation, humidity or wind speed, play a significant role in the particles undergoing various transformations, such as condensation and coagulation, affecting the particle concentrations and size. During the summer periods (May to July), the emission pattern was similar to the previous transition periods, but the peak particle concentration was reached during the daytime and not during night-time. In August the size distribution of the particles was similar to winter, due to the influence of humidity. This period falls under the monsoon season, where the higher-size particles are washed away by precipitation, and the lower-size particles undergo more diffusion, resulting in a higher concentration. In the post-monsoon period, such as September to November, the concentration during the daytime remains similar to the previous period, where the lower size particles were found to be in higher concentration. However, the night-time particle concentration was similar to the winter periods. Aerosol number size distribution was studied for relative humidity (RH) higher and lower than 70% (Zhu et al., 2006). The size distribution of the particles showed a higher concentration around 100 nm when RH was higher >70% due to the coagulation processes of the lower-size particles into a larger one (Fig.4.15). This led to the concentration of large particles increased, resulting in a smaller particle number and an increase in its mass.

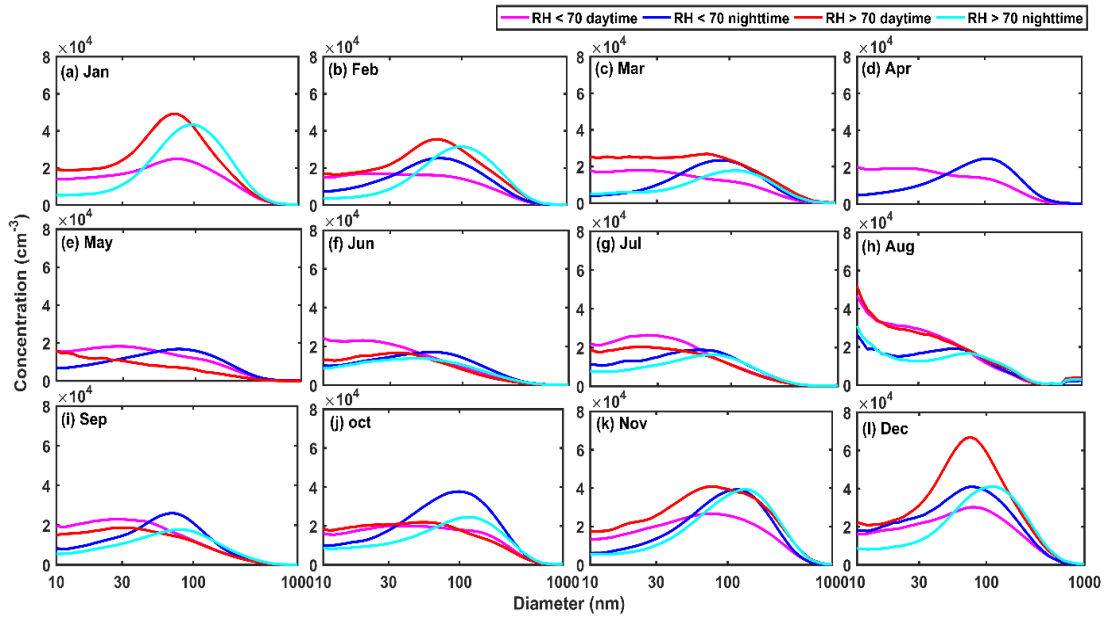


Figure 4.15. Monthly average particle number size distributions at both the scenarios (daytime and nighttime) with an RH lower and higher than 70 % every month (from January to December) during 2022.

The role of the wind speed and direction on aerosol number size distribution have also been studied using an analysis of bivariate polar plots (Fig.4.16). The highest mean wind speed at the site was around 6 m/s, with calm wind periods ( $< 2$  m/s) in which the highest particle concentrations were identified. The wind speed had a higher impact on lower-size particles. Thus, the wind influenced the  $N_{\text{nuc}}$  and  $N_{\text{atk}}$  due to their smaller size, whereas in the case of  $N_{\text{acc}}$ , the calm winds had a lower effect due to their larger size (Tiwari et al., 2015). Even when the wind was calm, the dispersion of smaller particles occurred, finding the higher concentration under the local winds rotating from the S-W to the N-E direction where the monitoring site was located (Mohan & Mishra, 2022). In addition, a higher  $N_{\text{nuc}}$  concentration was observed under downwind conditions for the monitoring site. These findings show the role of traffic-related emission sources in the study area, with a higher impact during the day when the traffic emissions were greater than at night.

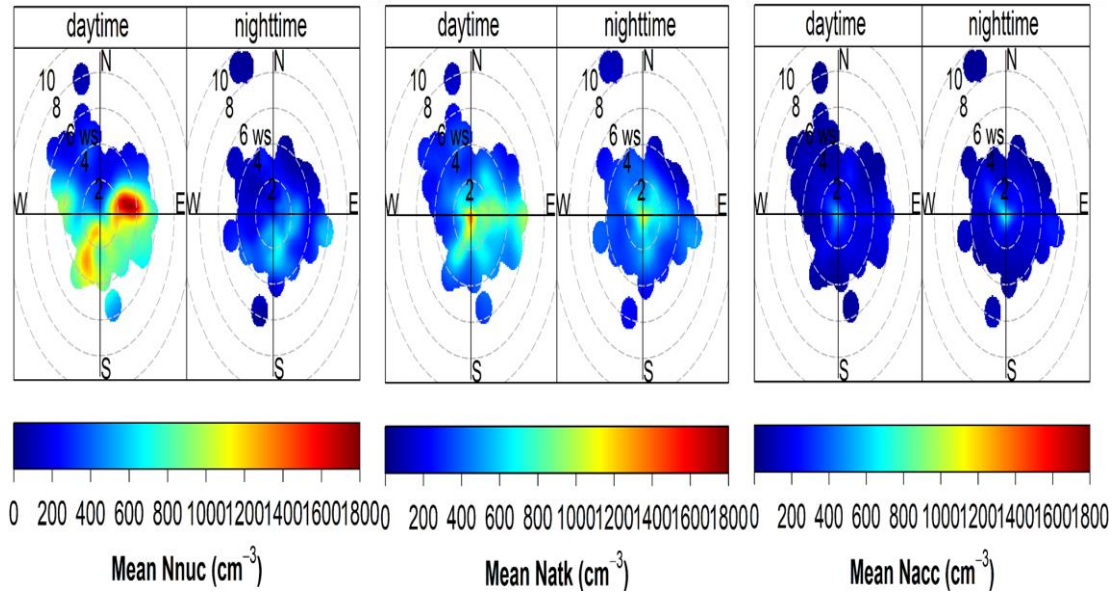


Figure 4.16. Polar plot represents the contributions of the different sources for  $N_{nuc}$ ,  $N_{atk}$  and  $N_{acc}$  at both scenarios (daytime and nighttime) in every month (from January to December) during 2022.

#### 4.7.2 Impact of meteorological conditions on particle number concentration during winter period

Bivariate polar plots have been analyzed to investigate the impact of wind direction and speed on the distribution of particle number sizes (Fig.4.17). The location's maximum average wind speed was roughly 6 m/s, and the highest particle concentrations were found during calm wind periods (less than 2 m/s). It was discovered that smaller particles were more significantly impacted by wind speed. Accordingly, the accumulation mode ( $N_{acc}$ ) was less affected by calm winds because of its bigger particle size, whereas the nucleation ( $N_{nuc}$ ) and accumulation ( $N_{atk}$ ) modes were affected by the wind because of their lower dimensions (Tiwari et al., 2015). Interestingly, smaller particles were scattered even in the presence of calm breezes, and concentrations were higher when local winds shifted from the southwest to the northeast, where the monitoring location is located (Mohan & Mishra, 2022). Except for the  $N_{acc}$  mode, which peaked at night, the maximum concentrations were seen during the day in December and January across all modes for the whole winter season. Additionally, at the monitoring location, the majority of the wind conditions were downwind. These findings highlight the importance of traffic-related emissions in the region, especially during the day when they were more noticeable than at night.

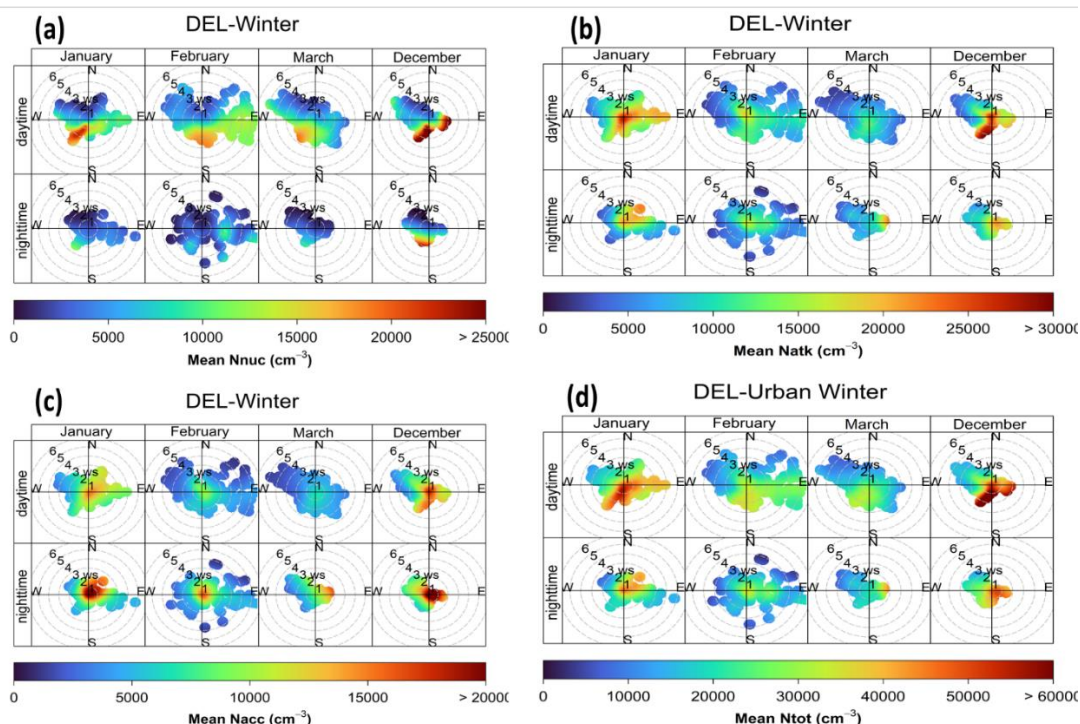


Figure 4.17. Polar plot represented the daytime and nighttime concentration of mode particles and total particles.

### 4.7.3 Role of wind speed and direction on particle dispersion in urban and background site

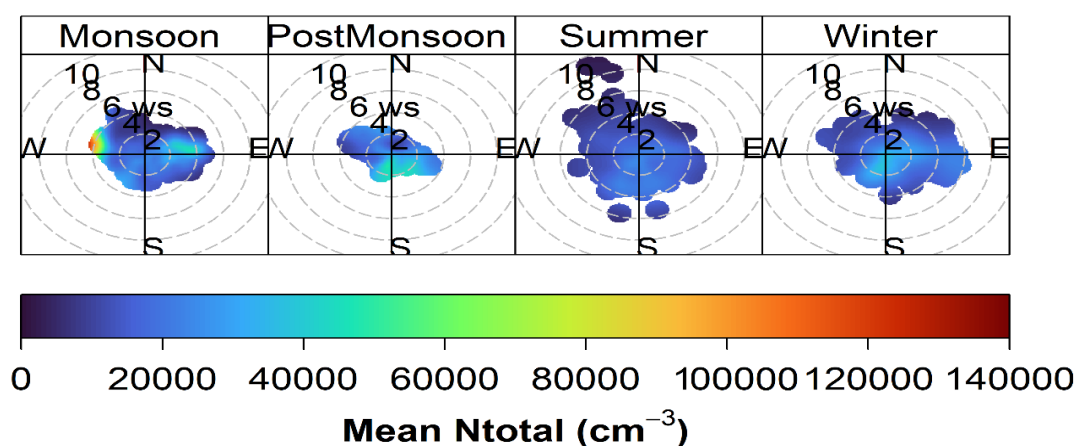
The wind speed and direction determine the pollutant's dispersion and rate from the sources to receptors. The urban site is surrounded by various buildings, which creates a shielding effect. Thus, the average wind speed was  $< 2$  m/s in all seasons, except for the post-monsoon season, with a similar wind direction in almost all seasons. In the post-monsoon season, the urban region receives an average wind speed throughout the season, ranging from 6 to 8 m/s. Similarly, the wind speed reached up to 10 m/s in the background site, but changes were found seasonally in the wind direction. Thus, particle dispersion occurs at a larger rate in this site during higher wind speeds, and the particle concentration lies between  $1.2$  and  $1.4 \times 10^3 \text{ cm}^{-3}$ .

The wind speed comparison between the urban and background sites showed a higher particle concentration in the background site, identifying an average wind speed of 2 to 3 m/s, while in the urban site, it was 1 to 2 m/s. The season-average wind speed was not more than 2 m/s in any season.



The mean  $N_{tot}$  may also increase based on the dispersion of pollutants from one region to another region due to the wind speed and direction. Calm winds ( $< 2$  m/s) led to less particle dispersion, oppositely with winds  $> 4$  m/s (Fig.4.18), being pollutants transported to the leeward side from the windward side. Other researchers have also stated similar kind of findings in their study (Mohan & Mishra, 2022; Şahin et al., 2022).

## DEL-Urban Region



## RNC-Background Region

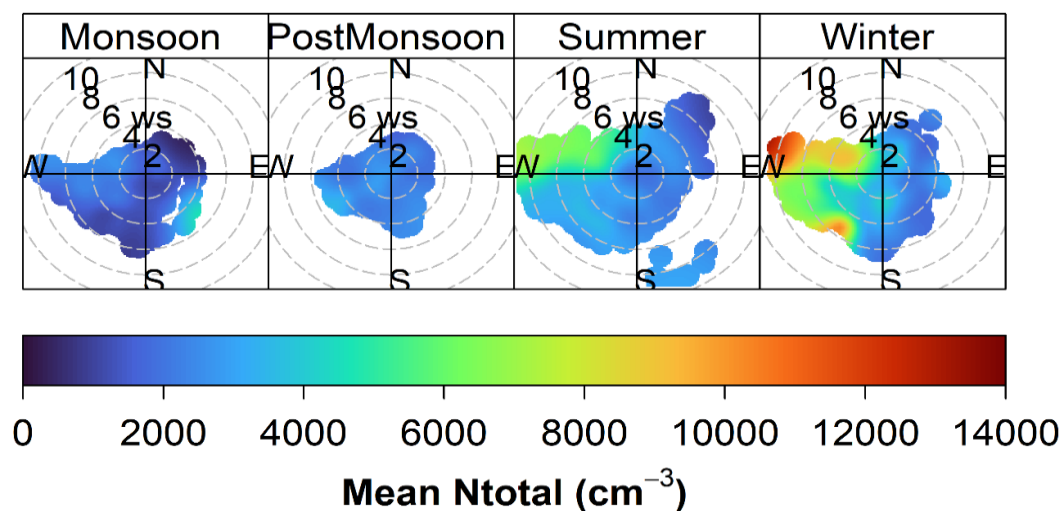


Figure 4.18. Polar cluster analysis of seasonal total particle concentration in the urban and background sites during different seasons.



#### **4.7.4 Long-range dispersion pattern in urban and background site**

The trajectory plot shows that the pollutants are not only generated from the local sources but also transported from long-range transportation. To analyse the impact of long-range transportation of pollutants from different faraway regions, the back trajectories were analysed for 2022 and 2017 in urban and background regions (Fig.4.19 & Fig.4.20). In the urban region of Delhi, the back trajectory shows that for most of the seasons, the winds are blown from the western side of the study location (Sharma et al., 2022). During the onset of winter, and post-monsoon season (October to March), most of the wind comes from the neighbouring states, namely Punjab and Haryana (~ 60 to 80%). This period is known for the crop residue burning period, where burning the remaining crop wastes brings large amounts of smoke particles to Delhi and causes smog formation. Severe air pollution events are attributed to the downwind movement of aerosols from biomass burning (Kanawade et al., 2020a).

In our study, the concentration of ultrafine particles was higher during the mentioned period. Around 82% of the winds come from the same direction possible, causing long-range transportation of aerosols apart from the local sources. Similarly, during summer, the winds are from Rajasthan, i.e., the westerly and north-westerly direction brings a significant amount of dust from the Thar desert that contributed to concentrations during the summer period (Banoo et al., 2022; Singh et al., 2020). However, from July to September, the wind pattern in the urban regions changes and the winds travel from the Arabian Sea or Bay of Bengal, i.e., from the southwestern coast. These winds are responsible for the precipitation in both the study regions, bringing many marine aerosols to the study location. The shift in the dispersion of wind patterns could be attributed to the dominant monsoon winds from the Indian Ocean.

In the background region, the wind pattern is more or less similar to the urban regions. The fascinating thing about the background region is that the hilly terrain restricts long-range transportation. At the same time, the regional wind sources contribute to around 50% of the wind in almost all the seasons in the background conditions (Fig.4.20). This analysis shows that the concentration of ultrafine particles is based on the long-range transportation of the winds and associated pollutants. Also, it varies from one geographical domain to another geographical condition, such as urban and background conditions.

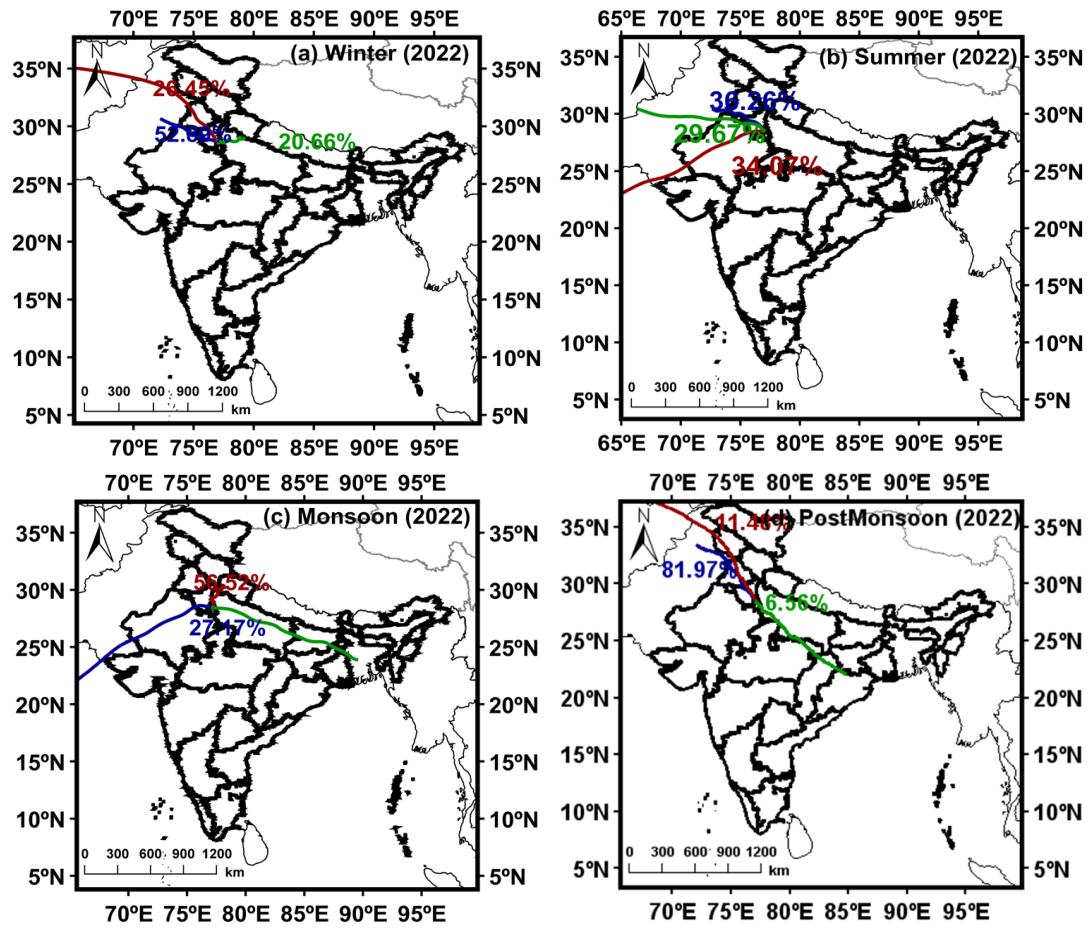


Figure 4.19. Back trajectory plots in urban site for the different seasons.

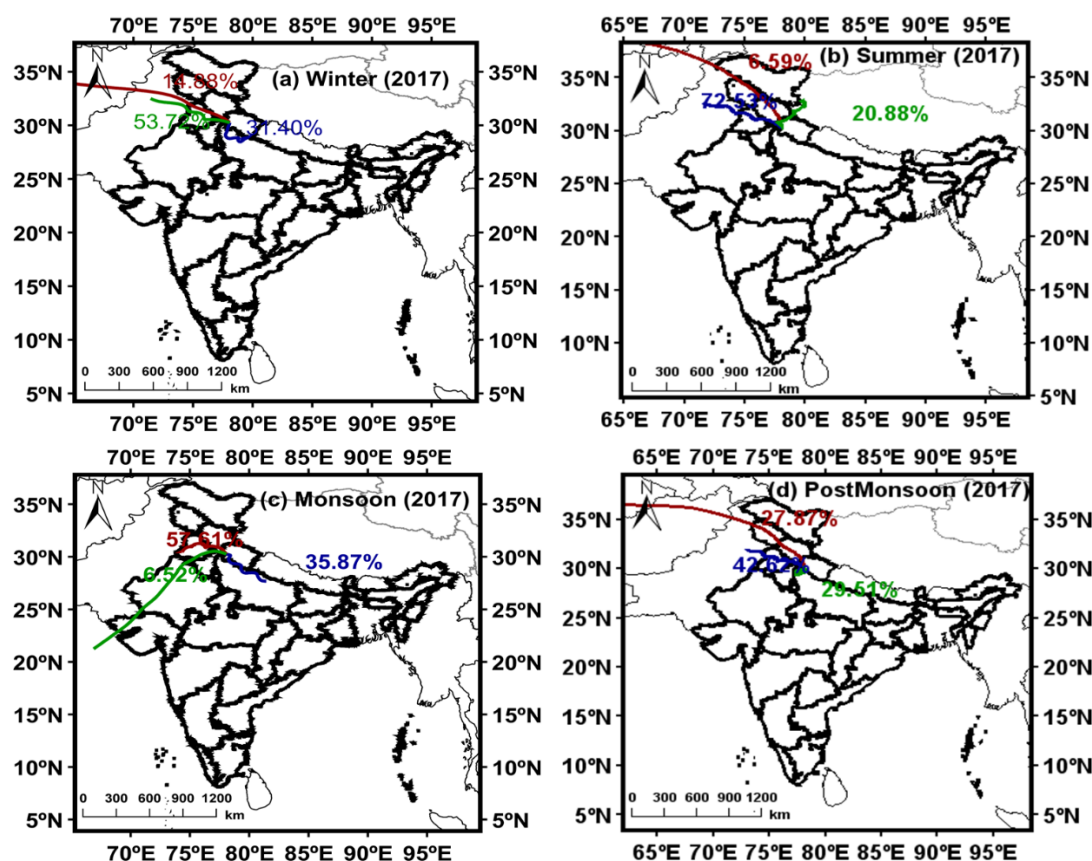


Figure 4.20. Back trajectory plots in background site for the different seasons.

#### 4.7.5 Diurnal variation of meteorological conditions in urban and background site

The existing meteorological conditions influence particle number size distributions, mainly relative humidity and temperature. Thus, the relative humidity played a crucial role in inducing the particle to undergo condensation and coagulation processes (Mohan et al., 2024a).

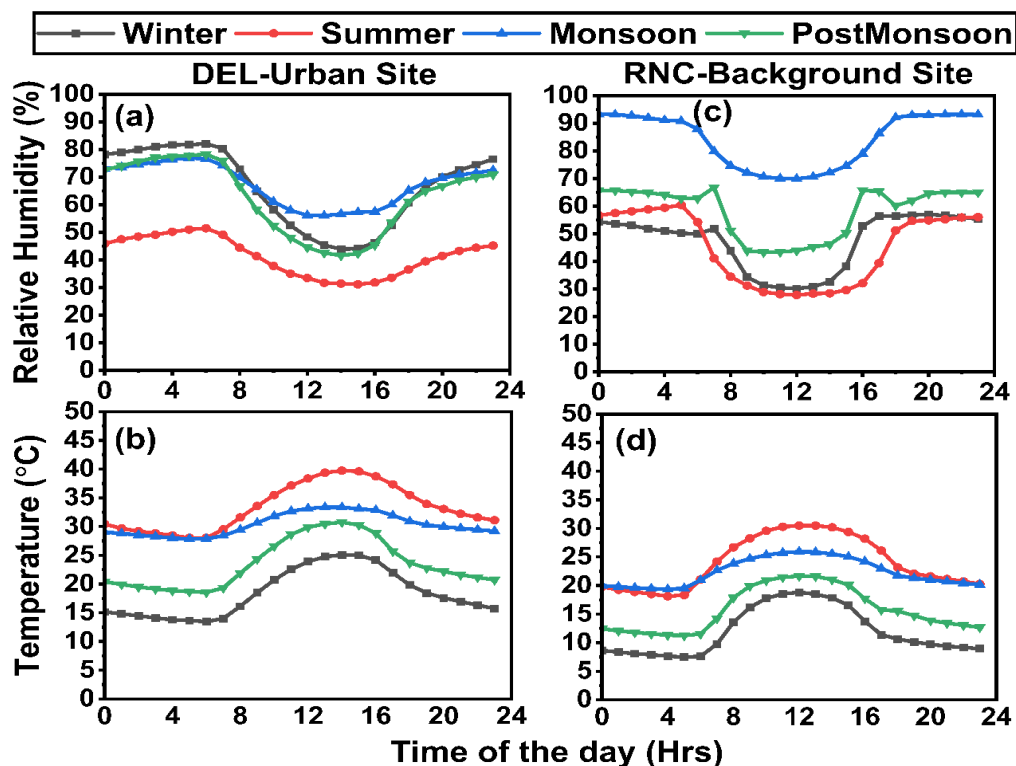


Figure 4.21. Diurnal variation of relative humidity and temperature in the urban and background sites during the different seasons.

In the urban site, the lowest mean temperature was registered during winter (18°C) and the highest during summer (33°C), reaching a maximum of ~46°C, while in the background site it was only 38°C (Fig.4.21, Fig.4.22 & Table 4.7). The relative humidity in the study sites was directly proportional to the particle concentration in the accumulation mode. The humidity >50% increased the possibility of coagulation and condensation of the lower-size particles ( $N_{nuc}$  and  $N_{atk}$ ) into accumulation mode particles, especially in the urban background. However, and although geographical characteristics in the background promoted the arrival of air masses with a higher humidity than in the urban site, particle coagulation and condensation processes were inhibited by their low concentration. In the urban site, even >70% humidity increased the particle condensation and coagulation; consequently, the accumulation-mode particles also increased (Mohan., et al., 2024a; Zhu et al., 2006).

Table 4.7. Seasonal-wise average statistical summary of temperature (T), relative humidity (RH), and wind speed (WS) in the urban and background sites during the study period.

		DEL-Urban Site			RNC-Background Site		
Season		RH (%)	T (°C)	WS (m/s)	RH (%)	T (°C)	WS (m/s)
Winter	Min	22.6	6.9	0.1	13.6	0.1	0.1
	Max	95.1	40.3	5.6	100.0	32.6	7.8
	Mean	66.3	18.4	1.3	47.2	12.0	2.3
	SD	18.7	7.2	0.9	17.1	5.7	1.3
Summer	Min	20.8	19.5	0.2	8.6	9.0	0.1
	Max	88.3	46.3	9.1	98.6	38.2	8.9
	Mean	41.5	33.3	1.6	44.5	24.2	3.0
	SD	13.4	5.1	0.9	21.1	5.4	1.8
Monsoon	Min	38.0	23.6	0.2	52.9	16.2	0.1
	Max	88.5	38.5	4.3	100.0	29.3	7.6
	Mean	67.5	30.3	1.5	84.0	22.4	2.2
	SD	11.4	3.1	0.7	11.9	2.7	1.4
Post Monsoon	Min	29.4	11.5	0.1	25.1	5.7	0.1
	Max	90.8	35.8	3.4	88.4	26.0	5.0
	Mean	62.8	23.5	0.9	58.3	15.7	2.0
	SD	15.7	5.4	0.6	12.8	4.9	0.8

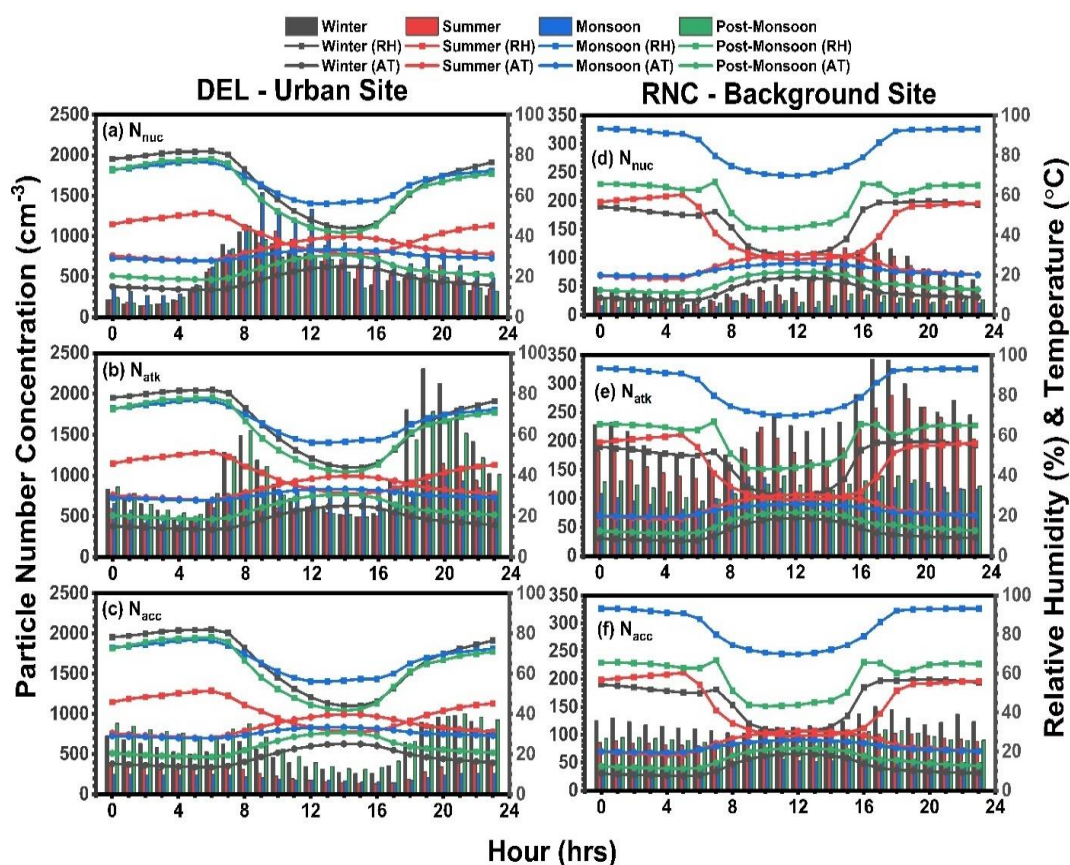


Figure 4.22. Diurnal variation of particle number concentrations and meteorology (temperature and relative humidity) in urban and background sites during different seasons.

#### 4.8 Role of new particle formation in urban microenvironment

##### 4.8.1 Overview of the new particle formation events

At this measurement site, the occurrences of new particle formation (NPF) events were significantly distinct, despite its closeness to a roadway. Over a comprehensive dataset spanning one year (365 days), a total of 23 NPF events, accounting for 6%, were recorded. In comparison, other research conducted in Delhi identified 17 NPF events over a period of 222 days (Jose et al., 2021), marking the lowest incidence in the context of long-term data. Additionally, Siingh et al. (2018) documented 109 NPF events from March 8, 2010, to December 31, 2012. During a two-month lockdown study, (Yadav et al., 2021) noted that the frequency of NPF events reached approximately 41%. On a global scale, Baalbaki et al. (2021) reported 207 event days, representing 56.7% of a one-year measurement campaign. In urban areas of Spain, approximately 23 events were observed (Casquero-Vera et al., 2020). The study also

noted 67 unidentified days (18%), approximately 257 non-event days (70%), and 18 days with no data (5%). Furthermore, over 20 years of observations at the SMEAR II station in a boreal forest revealed around 877 days classified as NPF events (Dada et al., 2017). Variations in the number of events can be attributed to several factors, including geographical influences, emission patterns, atmospheric aerosol loads, pre-existing aerosol particles, and critical considerations related to the classification methodology of NPF. The classification method for NPF events has been previously discussed in this study (see Chapter 3, Section 3.7.1).

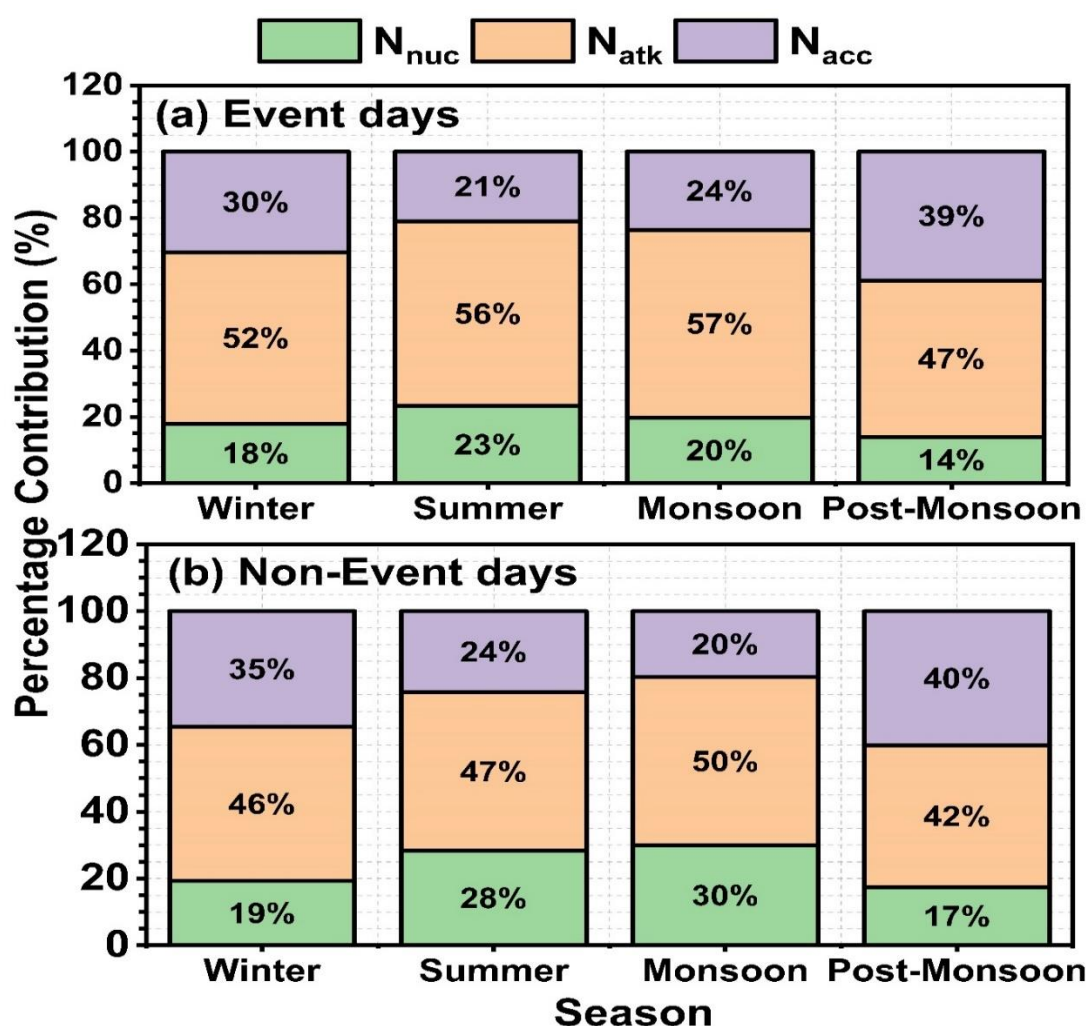


Figure 4.23. Percentage contribution represented the three different mode particles ( $N_{nuc}$ ,  $N_{atk}$ , and  $N_{acc}$ ) that contributed to total particle number concentration ( $N_{tot}$ ) during the event, and non-event.



In the analysis of event and non-event days, it was observed that the particle number concentration (PNC) was significantly higher on non-event days compared to event days, indicating a pronounced influence of anthropogenic activities during non-event periods (Rajagopal et al., 2024b, 2024a). Rajagopal et al. (2023) noted that PNC reached a concentration of  $10^5$  during pollution events in Delhi. Conversely, the maximum and minimum concentrations were recorded on event days in all three modes ( $N_{\text{nuc}}$ ,  $N_{\text{atk}}$ , and  $N_{\text{acc}}$ ), as well as in total concentration ( $N_{\text{tot}}$ ) and geometric mean diameter (GMD) in all seasons. This indicates that new particle formation (NPF) events, which involve the growth of new particles, contribute significantly to the increase in concentration from  $N_{\text{nuc}}$  to  $N_{\text{tot}}$ , including GMD. The contribution of ultrafine particles (UFP) to  $N_{\text{tot}}$  is relatively consistent at approximately 72% and 70% on event and non-event days, respectively. However, when the dynamics of particle size ranges are examined, the contribution of  $N_{\text{atk}}$  mode particles (25 nm to 100 nm) to  $N_{\text{tot}}$  is approximately 52% and 46%. This discrepancy can be attributed to the process of new particle growth (NPG), which facilitates the transition from smaller to larger particles (Fig.4.23).

#### **4.8.2 Nocturnal new particle events in Delhi**

The phenomenon of nocturnal new particle events in the atmospheric environment is infrequently observed globally. Recent studies have emerged, particularly in Delhi, India (Mishra et al., 2023; Sarangi et al., 2018). At our monitoring station located near a roadside, we identified rapid nocturnal particle growth events on two separate days out of a total of 23 events. These instances can be categorized as nocturnal particle events, marked by sustained growth that continued into the early hours of the subsequent day. Both events occurred in July, coinciding with the monsoon season. Fig.4.24. illustrates the typical days of nocturnal events, with the black cross symbol denoting the mode diameter of the particle number. On the days of these nocturnal events, the total growth rates recorded were  $4.3 \pm 0.8 \text{ nm h}^{-1}$  on July 06 and  $2.13 \pm 1.06 \text{ nm h}^{-1}$  on July 17 (Table 4.8). The mode diameter of the particle number increased from 10.23 to 78.76 nm and from 12.19 to 65.64 nm during the time intervals of 20:26 to 21:08 IST and 19:31 to 19:44 IST, respectively, over approximately 30 minutes and 15 minutes. This growth continued gradually until early



morning, reaching 101.25 nm at 05:18 hrs on July 07 and 95.85 nm at 04:07 hrs on July 17.

The newly generated particles exhibit a significant increase in particle number concentrations, as noted by Brines et al. (2015). Mishra et al. (2023) reported an increase in mass values during a nocturnal event. During this specific period, ammonia ( $\text{NH}_3$ ) levels, along with meteorological (sourced from the Central Pollution Control Board), parameters increased by approximately 34%, with mean concentrations increasing from  $53 \mu\text{g}/\text{m}^3$  on non-event days to  $71 \mu\text{g}/\text{m}^3$  on event days (Table 4.9). Among all seasons, the monsoon month recorded the highest  $\text{NH}_3$  concentrations, with an increase of around 34% during event days ( $63.8 \pm 16.4$ ), despite nocturnal events being observed exclusively in the monsoon season. This suggests that  $\text{NH}_3$  is a critical factor in the growth of particles during the nocturnal period. Xiao et al. (2021) highlighted that the occurrence of new particle formation (NPF) in polluted environments is often caused by the formation of sulfuric acid-base clusters, which are stabilized by amines, elevated ammonia levels, and low temperatures. Furthermore, Wang et al. (2022) indicated that the co-condensation of ammonia with nitric acid plays a role in the growth of newly formed particles. Additional research has established a link between NPF events and ammonia (Lehtipalo et al., 2018; Nursanto et al., 2023; Xiao et al., 2015). In urban settings, biomass combustion can significantly increase ammonia levels, which may play a key role in new particle formation by acting as a stabilizing agent for sulfuric acid clusters (Wang et al., 2023). The presence of ammonia facilitated the formation of new particles in almost 50% of the experiments conducted (Jorga et al., 2023).

Ammonia, a product of anthropogenic emissions, interacts with acidic pollutants, especially sulfur dioxide ( $\text{SO}_2$ ) and nitrogen oxides ( $\text{NO}_x$ ), leading to the formation of fine ammonium ( $\text{NH}_4^+$ ) aerosols. However, during the specific event period, there was no noticeable increase in  $\text{SO}_2$  and  $\text{NO}_x$  levels. This suggests that biomass burning may contribute to ammonia emissions from nearby residential areas or through cross-boundary transport. Additionally, the elevated humidity and temperature characteristics of the monsoon season can significantly affect atmospheric chemical reactions, facilitating the production of secondary aerosols from ammonia. The nocturnal growth of these aerosols is enhanced by favorable atmospheric

conditions, which include a marked decrease in solar radiation and reduced wind speeds, ranging from 0.6 to 1.6 m/s (minimum and maximum), with mean values of  $182 \text{ W/m}^2$  on non-event days compared to  $3.6 \text{ W/m}^2$  on event days, thereby promoting unhindered particle growth.

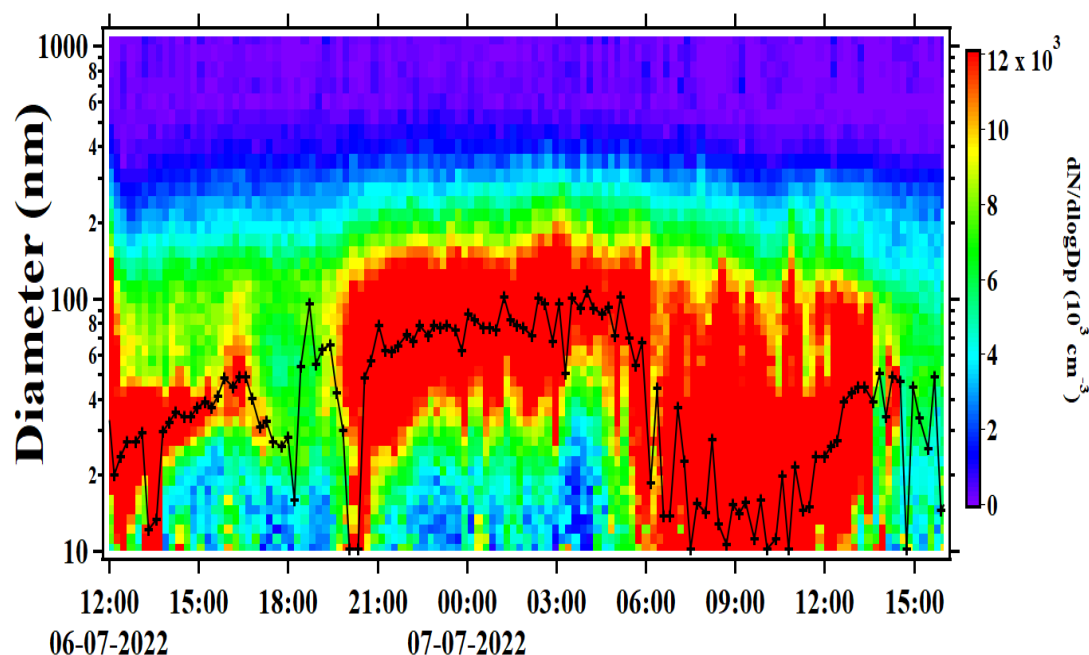


Figure 4.24. Typical nocturnal event of growth particles on 06 July 2022. The mode diameter of the particles is indicated by the black cross symbol.

Table 4.8. The growth rate for all event days during the monitoring period.

Season	Date	Growth Rate (GR) (nm/h)
Winter	27-Jan	$37.152 \pm 3.96$
	28-Feb	$7.13772 \pm 0.5688$
	02-Mar	$9.13536 \pm 0.6876$
	10-Mar	$7.28964 \pm 0.6552$
	11-Mar	$4.46544 \pm 0.34956$
	13-Mar	$7.28172 \pm 0.2358$
Summer	19-Apr	$7.61652 \pm 0.9$
	29-May	$4.38948 \pm 0.24804$
	22-Jun	$2.385648 \pm 0.17028$
Monsoon	06-Jul	$4.30272 \pm 0.8604$

	07-Jul	$5.049 \pm 0.26316$
	17-Jul	$2.137428 \pm 1.0692$
	19-Aug	$14.7402 \pm 1.8$
Post-Monsoon	01-Oct	$5.6394 \pm 0.3636$
	02-Oct	$5.36004 \pm 0.3924$
	04-Oct	$5.6754 \pm 0.20088$
	14-Nov	$6.50268 \pm 0.4896$
	15-Nov	$10.18332 \pm 0.5688$
	16-Nov	$11.42928 \pm 0.6516$

#### 4.8.3 Other new particle events in Delhi

In the investigation of new particle formation (NPF) events, a total of 23 occurrences were recorded, with the exception of 2 nocturnal events, indicating that approximately 21 events transpired during daylight hours (morning, noon, and late afternoon). Figure.4.25 illustrates the seasonal distribution of NPF events, with one event documented in each season. The occurrence of NPF events resulted in an increase in cloud condensation nuclei (CCN) number concentrations by a factor of 0.4 to 6 within the megacity of Beijing (Yue et al., 2011). The findings reveal a seasonal variation in NPF events, showing a greater frequency during the post-monsoon and winter seasons, each with 6 recorded events, followed by the monsoon season with 4 events and the summer season with 3 events. Table 4.8 provides a comprehensive overview of the specific event days across the seasons, along with their respective growth rates (GR).

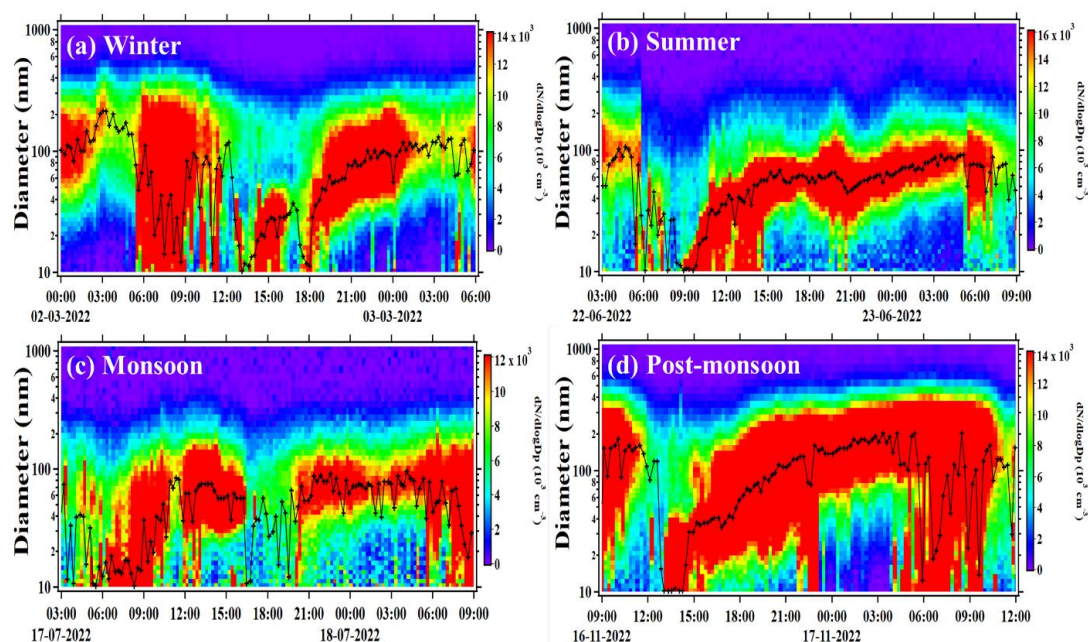


Figure 4.25. Each individual plot represents a new particle formation event occurring in each season. The black cross symbol represents the model diameter of the particles.

Table 4.9. Statistical mean concentration of gaseous precursors, and meteorological parameters in event and non-event.

Gaseous & Meteorological		Event				Non-Event			
		Winter	Summer	Monsoon	Post-Monsoon	Winter	Summer	Monsoon	Post-Monsoon
NO	Max	490.5	82.6	7.9	296.3	498.4	498.1	209.9	499.6
	Mean	40 ±	7.2 ±	3.3 ±	18.7 ±	46.9 ±	27 ±	7.9 ±	58.1 ±
	± SD	84.8	12.9	0.9	48.4	88.2	61.5	12.5	99.8
	Min	0.5	1.4	1.7	0.1	0.1	0.7	0.4	0.1
NO <sub>2</sub>	Max	60.5	50.4	27.9	72.9	136.8	163.4	90.4	195.8
	Mean	23.2 ±	14.8 ±	10.6 ±	23 ±	24.2 ±	26.2 ±	14.1 ±	31.2 ±
	± SD	15.4	13.6	6.4	14.8	16.1	21.6	8.4	21.7
	Min	3.5	0.6	3.0	3.2	1.0	0.1	1.2	1.9
NO <sub>x</sub>	Max	495.5	128.7	34.6	358.2	499.6	498.2	242.4	499.5
	Mean	61.5 ±	22 ±	13.9 ±	41.7 ±	69 ±	51.9 ±	22 ±	85.8 ±
	± SD	90.7	24.5	7	59.5	94.1	73.7	18.6	108.3

	Min	5.5	4.0	6.4	5.2	1.8	2.9	3.3	3.1
NH <sub>3</sub>	Max	75.3	68.5	116.6	73.5	208.0	239.3	203.9	456.8
	Mean	57.8 ±	56.7 ±	63.8 ±	51.1 ±	76.8 ±	64.8 ±	47 ±	59.6 ±
	± SD	6.2	6	16.4	9.8	25.8	19.8	14.2	23.8
	Min	28.3	39.0	33.9	34.9	9.7	0.2	19.5	19.8
SO <sub>2</sub>	Max	18.1	68.3	3.7	10.3	60.4	57.7	11.3	31.1
	Mean	9 ±	8.9 ±	2.4 ±	3.8 ±	6.2 ±	8.3 ±	2.3 ±	4 ±
	± SD	3.3	10.5	0.7	1.6	5.3	6.5	1	2.8
	Min	1.0	2.4	1.2	0.1	0.1	1.3	0.4	0.1
CO	Max	4.1	2.0	1.3	4.9	9.8	6.5	3.2	10.0
	Mean	1 ±	0.6 ±	0.7 ±	1.1 ±	1.3 ±	1 ±	0.8 ±	1.7 ±
	± SD	0.8	0.4	0.2	0.9	1.3	1	0.3	1.7
	Min	0.3	0.3	0.5	0.1	0.1	0.1	0.2	0.1
O <sub>3</sub>	Max	57.4	68.2	69.1	93.5	163.8	170.2	152.3	134.1
	Mean	21.6 ±	18.9 ±	6.4 ±	20.5 ±	20.4 ±	30.7 ±	9.6 ±	19.8 ±
	± SD	19.3	19.6	6.9	22.5	21.4	31.6	8.7	24.7
	Min	1.8	2.3	1.4	1.6	0.2	0.1	0.2	0.6
AT	Max	33.2	41.4	37.0	35.9	40.7	46.3	38.9	36.0
	Mean	22.1 ±	32.9 ±	32.3 ±	25.5 ±	17.8 ±	33.2 ±	30.3 ±	23.4 ±
	± SD	5.7	4.1	2	5.8	7.1	5.1	3.1	5.4
	Min	9.6	27.1	29.2	14.3	6.8	19.3	23.5	5.3
RH	Max	90.1	66.3	76.1	81.9	95.2	89.0	91.0	90.8
	Mean	61.3 ±	45.5 ±	65.1 ±	56.9 ±	68 ±	42 ±	67.6 ±	63.1 ±
	± SD	14.3	11.9	7.5	13.3	18.7	13.7	11.6	15.8
	Min	37.6	24.3	46.2	31.1	22.2	20.4	37.3	29.1
WS	Max	3.9	5.8	4.2	3.8	5.8	10.9	5.3	4.2
	Mean	1.6 ±	1.7 ±	1.5 ±	1.2 ±	1.3 ±	1.6 ±	1.5 ±	0.9 ±
	± SD	0.9	0.8	0.5	0.8	0.9	1	0.8	0.6
	Min	0.1	0.3	0.5	0.1	0.1	0.1	0.1	0.1
SR	Max	656.3	723.3	719.3	660.6	684.3	830.4	888.7	659.4
	Mean	119.5 ±	207.3 ±	68.7 ±	99.7 ±	112.7 ±	184.5 ±	145.7 ±	102.7 ±
	± SD	206.6	272.8	164.8	180.7	179.3	244.2	208.9	155.0
	Min	2.9	3.0	3.0	3.0	2.8	2.7	2.7	3.0

This phenomenon can be attributed to several factors. First, during winter and post-monsoon periods, the boundary layer height is low, resulting in the accumulation of aerosols and gases near the surface, creating conditions conducive to particle formation (Franco et al., 2022). Conversely, the monsoon season are characterized by increased precipitation, which effectively clear the atmosphere of aerosols and inhibit the growth of particles. Several studies have indicated that new particle formation (NPF) events are higher in summer compared to other seasons. However, the lowest frequency of NPF events was recorded in summer, which is consistent with the findings of Cyprus (Baalbaki et al., 2021). In addition, research conducted by Gani et al. (2020) on long-term particle number size distribution (PNSD) in Delhi revealed the absence of NPF during winter and autumn. However, NPF events have been frequently recorded in both winter (Kulmala et al., 2004; Sebastian et al., 2022), and autumn. This indicates that there is no seasonal pattern associated with NPF events (Dall'Osto et al., 2018; Şahin et al., 2022). Notably, most NPF events were detected during the daytime (Nursanto et al., 2023), which is consistent with the understanding that solar radiation is a major factor in particle formation. This process is particularly affected by photochemical reactions (Franco et al., 2022) that produce nucleating agents such as sulfuric acid and various organic compounds (Brines et al., 2015).

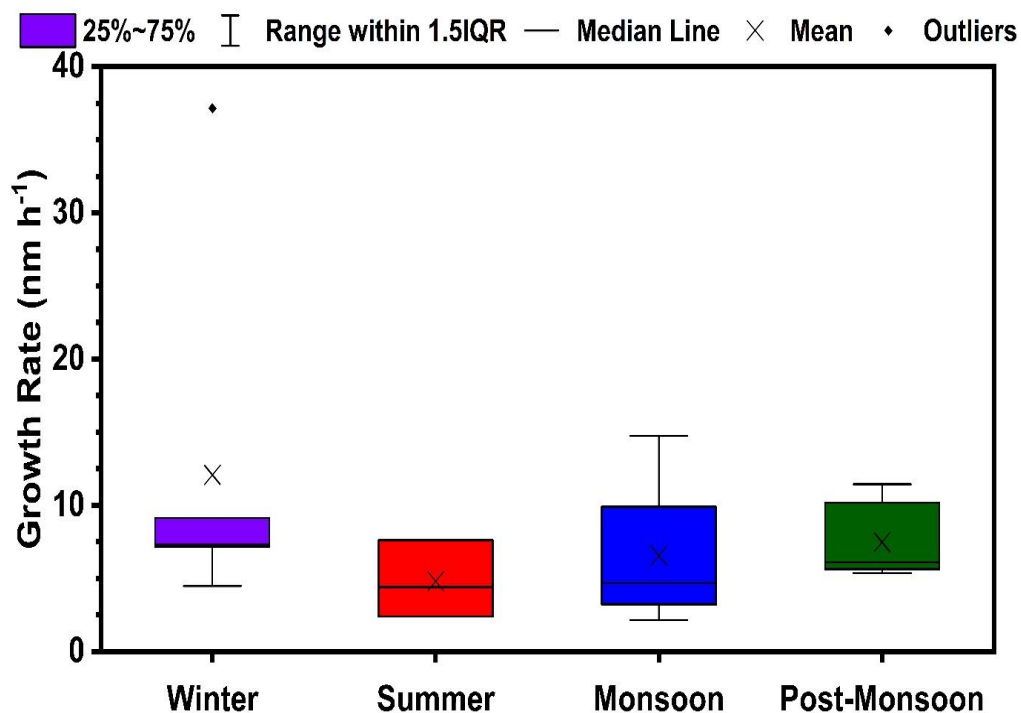


Figure 4.26. Box-wisher plot represented the growth rate of different seasons (Winter, Summer, Monsoon, and Post-Monsoon).

Table 4.10. Season-wise mean value of Growth Rate (GR), Condensation Sink (CS), and Coagulation Sink (CoagS).

Season	Growth Rate (GR)	Condensation Sink (CS)		Coagulation Sink (CoagS)
	(nm/h)	Event-day (s <sup>-1</sup> )	Non-Event day (s <sup>-1</sup> )	(s <sup>-1</sup> )
Winter	12.07698 ± 1.07616	0.055722 ± 0.023440	0.102092 ± 0.076062	5.96 x 10 <sup>-7</sup>
Summer	4.797216 ± 0.43944	0.039477 ± 0.015958	0.047202 ± 0.031820	2.68 x 10 <sup>-7</sup>
Monsoon	6.557337 ± 0.99819	0.037376 ± 0.010505	0.052338 ± 0.043846	2.44 x 10 <sup>-7</sup>
Post-Monsoon	7.46502 ± 0.44448	0.087404 ± 0.039698	0.125598 ± 0.076674	3.78 x 10 <sup>-7</sup>

The most significant growth rates were observed in winter ( $12.07 \pm 1.07 \text{ nm h}^{-1}$ ), followed by the post-monsoon period ( $7.46 \pm 0.4 \text{ nm h}^{-1}$ ), monsoon ( $6.55 \pm 0.9 \text{ nm h}^{-1}$ ), and summer ( $4.79 \pm 0.43 \text{ nm h}^{-1}$ ) as illustrated in Table 4.10 and Fig.4.26. The peak estimated condensation sink (cs) occurred during the post-monsoon season ( $0.087 \pm 0.039 \text{ s}^{-1}$ ), with winter ( $0.055 \pm 0.023440 \text{ s}^{-1}$ ), summer ( $0.039 \pm 0.015 \text{ s}^{-1}$ ), and monsoon ( $0.037 \pm 0.010 \text{ s}^{-1}$ ) following in that order. Notably, the CS values in Delhi were higher than those recorded in Pune ( $16.2 \times 10^{-3} \text{ s}^{-1}$ ) and Kanpur ( $33.3 \times 10^{-3} \text{ s}^{-1}$ ), although they are relatively consistent with the findings of a previous study conducted at this location (Yadav et al., 2021). The post-monsoon season exhibited both elevated particle concentrations and higher CS values. The post-monsoon period had a higher number of particles and larger sizes, which contributed to increased condensation sinking, while winter recorded the highest growth rate. This suggests that the presence of larger sized particles in the post-monsoon period may have inhibited formation rates while promoting particle growth compared to winter (Kanawade et al., 2014a).

Park et al. (2021) recorded a growth rate (GR) of  $6.95 \text{ nm h}^{-1}$  during the summer months on Bangnyeong Island, Korea. Similarly, Casquero-Vera et al. (2020) found growth rates of  $4.1$  and  $3.6 \text{ nm h}^{-1}$  at urban locations in Spain, classified as GR<sub>4-70</sub>. This hierarchy of growth rates indicates that winter conditions, characterized by low temperatures and high concentrations of precursor gases, are more favorable for rapid particle formation and growth than the hot summer months. The highest individual growth rate was observed on January 27<sup>th</sup> in winter, which may be due to stable atmospheric conditions and abundant precursor availability during cold periods. This was followed by a significant rate during the monsoon season on August 19<sup>th</sup>, which may have occurred during relatively dry periods. In addition, significant growth rates were recorded on November 15<sup>th</sup> and 16<sup>th</sup> during the post-monsoon season, due to moderate temperatures and relatively high concentrations of precursor gases, which facilitated significant particle formation and growth. The above dates showed growth rates greater than  $10 \text{ nm h}^{-1}$ , while the remaining days recorded growth rates ranging from  $2$  to  $9 \text{ nm h}^{-1}$  (Table 4.8). In Kanpur, particle growth rates varied from  $2.7$  to  $6.7 \text{ nm h}^{-1}$  as reported by Kanawade et al. (2014a). In November 2016, a significant episode of air pollution occurred in Delhi, during which new particle formation (NPF)



was suppressed. However, the co-condensation of water vapors generated from anthropogenic activities with water on existing primary particles resulted in a rapid increase in particle size (Kanawade et al., 2020b).

The lowest growth rates were observed on 17<sup>th</sup> July and 22<sup>rd</sup> June, which coincided with the monsoon and summer seasons. This phenomenon may be due to increased humidity levels and wet cleaning of particles, which reduced aerosol availability and inhibited the growth process. This study's findings indicate that the winter and post-monsoon periods are most conducive to particle growth, which may be influenced by factors such as low temperatures, high concentrations of precursor gases, and reduced atmospheric composition. In contrast, monsoon and summer periods show low particle growth, primarily due to increased humidity and wet cleaning effects.

#### **4.8.4 Diurnal variation in event and non-event days**

Analysis of diurnal variation provides valuable insights into the dynamics of air pollution. In this study, we examined the diurnal variation patterns of three particle modes ( $N_{nuc}$ ,  $N_{atk}$ , and  $N_{acc}$ ), as well as the total particle number concentration ( $N_{tot}$ ) and condensation sink (CS), for both event and non-event days, as depicted in Fig. 4.27. The diurnal variation of particle number concentrations on non-event days showed two major peaks, which is characteristic of the double whale pattern often observed in urban microenvironments (Mohan et al., 2024b). The initial peak occurred in the early morning hours (07:00 - 09:00 hrs), while the most pronounced second peak was observed in the evening (19:00 - 21:00 hrs) throughout the 24-hrs period (Fig.4.27b). These periods are generally associated with peak traffic conditions in urban settings.

A significant increase in particle number concentration was observed during this period. The increase in transport emissions, a major source of ultrafine particles produced in the atmosphere after being released into the engine or from the exhaust (Brines et al., 2015), is evident in the concentrations of  $N_{tot}$  and  $N_{atk}$  in urban environments. The typical diurnal variation pattern is interrupted by the frequent occurrence of new particle formation events. As depicted in the upper panels of Fig.4.27a, notable peaks in  $N_{nuc}$ ,  $N_{atk}$ , and  $N_{tot}$  are recorded during the early morning hour of 07:00 hrs during these event periods, with a subsequent peak occurring around

noon at 12:00 hrs. This suggests that the majority of these events are driven by photochemical reactions. In addition to new particle formation, subsequent aerosol dynamic processes also play a crucial role in shaping the observed particle number size distributions. Once nucleation occurs, condensational growth by low-volatility vapors (e.g., organics and sulfuric acid) and coagulation among freshly formed particles or with pre-existing aerosols drive the temporal evolution of particle sizes. These combined effects likely contribute to the shift of the dominant particle number mode from nucleation (<30 nm) to Aitken (30-100 nm) sizes as observed during the later part of the day. The specific timing and nature of these events are elaborated upon in the preceding sections. The timing variations of the new particle formation events are largely governed by photochemical processes and reduced condensation sink values, which facilitate the enhanced dispersion of existing particles.

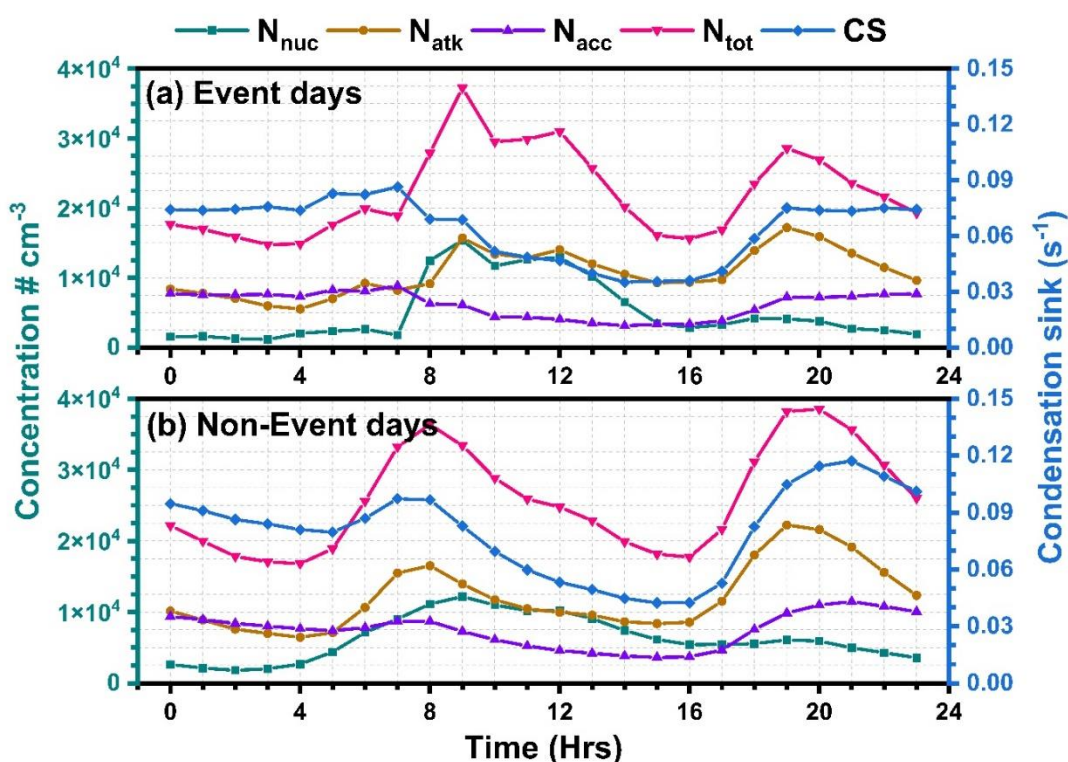


Figure 4.27. Diurnal profile represents the particle concentration during event and non-event periods (left-side axis), and condensation sink (right-side axis).

The findings of this study reveal a significant increase in  $N_{\text{nuc}}$  and  $N_{\text{tot}}$  at 07:00 hrs on event days. In addition, the peak shifted to the  $N_{\text{atk}}$  mode between approximately 08:00 and 09:00 hrs (Fig.4.27a), indicating that newly formed particles initially existed

as small entities ( $dp > 3$ ) before evolving into the  $N_{\text{atk}}$  mode and beyond (Dal Maso et al., 2005; Lee et al., 2019; Nursanto et al., 2023). This pattern suggests that new particle formation was initiated during this period, possibly influenced by favorable atmospheric or chemical conditions that promote nucleation. Notably, this surge in particle numbers was accompanied by a decrease in condensation sink (CS) values. In contrast, on non-event days, an opposite trend was observed, indicating less favorable conditions for new particle formation. Similar results were reported in a study in Shanghai, China, with high pollution levels (Yao et al., 2018).

The observed decrease in the condensation sink (CS) indicates a decrease in the ability of existing large particles to remove water vapor, which may facilitate the emergence of new particles. In general, high CS values inhibit nucleation by extracting condensable vapors; however, the low CS recorded at 07:00 hrs indicates a decrease in competition for these vapors, thereby facilitating the involvement of a larger number of nucleation particles. This inverse relationship between nucleation and CS in the early morning hours underscores the complex dynamics of atmospheric aerosol processes and indicates that diurnal variations play an important role in influencing particle growth and formation. More detailed analysis is necessary to elucidate the mechanisms underlying these findings, and we will relate these observations to meteorological parameters in the next section (4.6.5). The seasonal diurnal variation of event and non-event days was depicted in Fig.4.28.

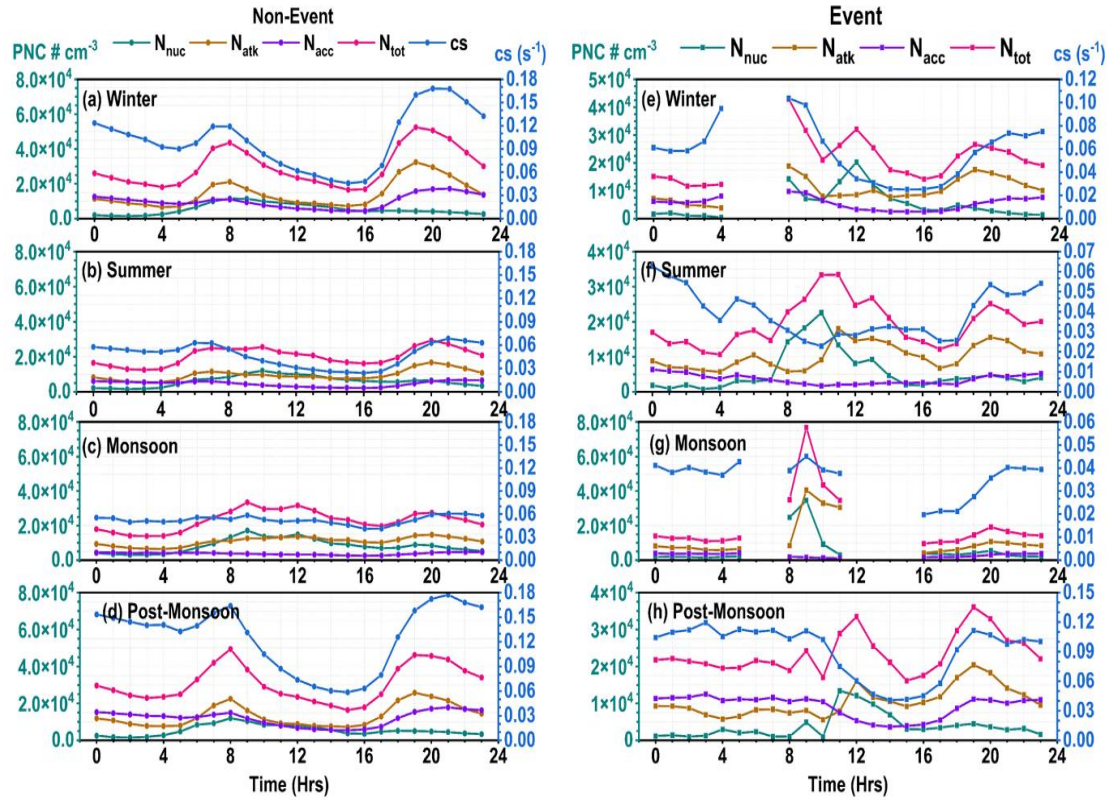


Figure 4.28. Diurnal variation shows four seasons (Winter, Summer, Monsoon, and Post-Monsoon) of non-event (a-d), and event (e-f) periods of particle number concentration (left-side), and condensation sink (right-side).

#### 4.8.5 Role of meteorological parameters in NPF event days

Meteorological parameters are important in the process of new particle formation (NPF). Variations in air mass can significantly affect NPF by modifying the concentrations of precursors and various meteorological factors, such as relative humidity (RH), air temperature (AT), and solar radiation (SR) (Park et al., 2021; Siingh et al., 2013). To investigate this relationship, we analyzed the correlation between wind speed (WS), wind direction (WD), and particle concentrations. Polar plot analysis indicated that on event days, wind speeds were predominantly low, typically ranging from 0 to 8 m/s in almost all seasons. In contrast, on non-event days, wind speeds were significantly higher, ranging from 0 to 12 m/s (Fig.4.29). This suggests that wind conditions are calm on event days, which may affect the dispersion of air pollutants in the region. The prevailing wind direction towards our monitoring site is predominantly from the northwest. Since the Badli industrial area is located in this direction, it is

likely that it contributes to the flow of rich atmospheric components, which aid in the formation of new particles.

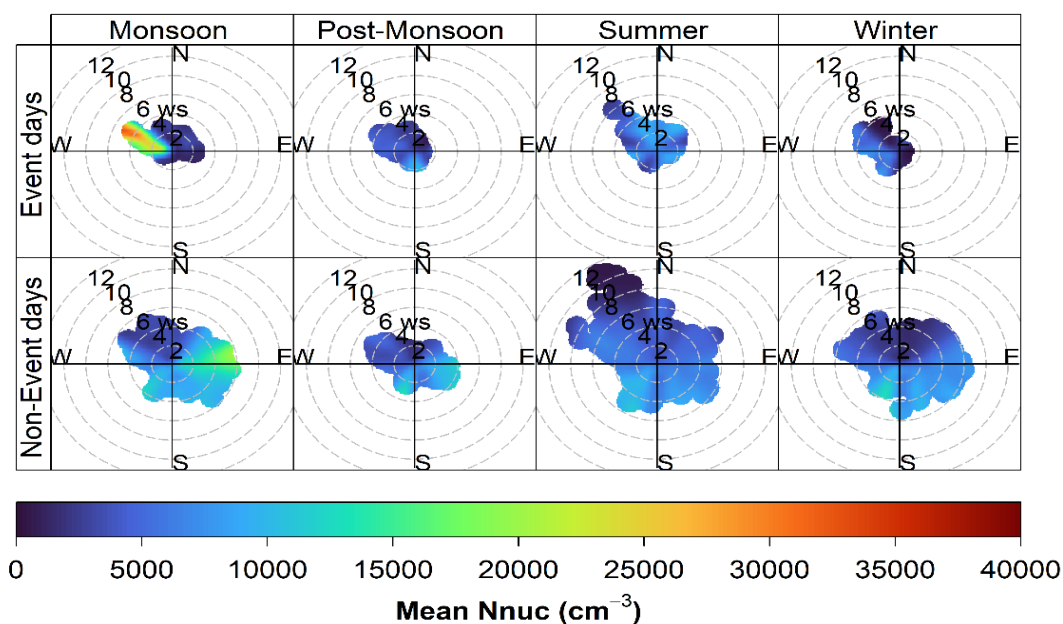


Figure 4.29. The polar plot represented the event and non-event days of  $N_{nuc}$  in different seasons (Winter, Summer, Monsoon, and Post-Monsoon).

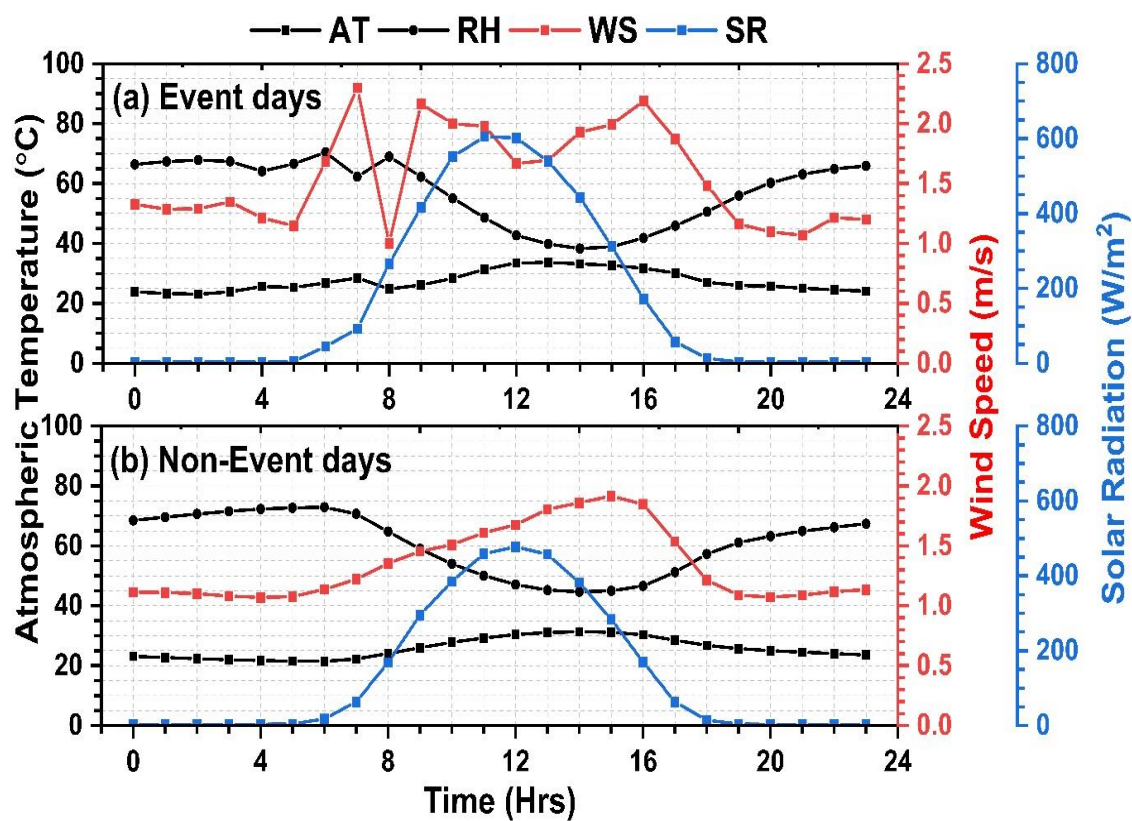


Figure 4.30. Diurnal plots represent the event and non-event periods of meteorological parameters. The left-side axis shows Relative Humidity (RH), and atmospheric Temperature (AT), The First right-side axis shows wind speed (WS), and the second right-side axis shows Solar Radiation (SR).

The diurnal variation in meteorological parameters such as wind speed, solar radiation (SR), air temperature (AT), and relative humidity (RH) exhibited distinct patterns. On days marked by significant events, solar radiation peaked at approximately  $800 \text{ W/m}^2$ , suggesting that enhanced solar radiation facilitated photochemical processes that contributed to new particle formation (Kanawade et al., 2014b; Kerminen et al., 2018; Yuan et al., 2015). Concurrently, air temperature increased while relative humidity experienced a sharp decline beginning at 07:00 hrs on these event days. The seasonal averages and standard deviations of gaseous precursors and meteorological parameters for both event and non-event days are presented in Table 4.9. Brines et al. (2015) noted that during peak traffic periods, aerosol size distributions are predominantly affected by traffic clusters (Fig.4.27b).

Nucleation clusters are notably present around midday (Fig.4.27a), especially under conditions of heightened temperature and solar radiation (Fig.4.30a). This observation indicates a transformation in atmospheric conditions, likely resulting from increased solar heating and alterations in wind patterns. As discussed in the preceding section, the levels of particle number concentration (PNC) on event days exhibited a similar diurnal trend, with a notable increase commencing around 07:00 hrs, which aligns with a decrease in relative humidity (RH) and an increase in air temperature (AT). This correlation implies that early morning fluctuations in meteorological factors, particularly temperature and humidity, play a crucial role in determining the concentration of airborne particles. Collectively, these findings underscore that event days, marked by reduced wind speeds and significant variations in solar radiation and temperature, create distinct atmospheric conditions that may facilitate the formation of new particles.

## **4.9 Episodic event during the monitoring period**

### **4.9.1 Introduction**

Diwali is one of the prominent festivals celebrated in India, characterized by the widespread use of firecrackers and the illumination of lamps across the nation each



year (Garg & Gupta, 2018; Yadav et al., 2019, 2022c). The firecrackers utilized during this festival are composed of various chemicals, including aluminum, sulfur, potassium nitrate, barium nitrate, charcoal, manganese, strontium nitrate, potassium, and iron dust powder (Nishanth et al., 2012; Perrino et al., 2011; Sateesh et al., 2018). The detonation of these firecrackers releases a range of atmospheric pollutants, such as particulate matter, ultrafine particles, gaseous emissions, and toxic metals, in substantial quantities (Izhar et al., 2018; Vaghmaria et al., 2018; Yerramsetti et al., 2013). These pollutants can linger in the atmosphere for several days, contributing to the development of hazardous smog (Cetin, 2015; Ertugrul et al., 2019; Ozenen Kavlak et al., 2021). The presence of these pollutants poses significant health risks (Kanawade et al., 2014a).

Delhi is recognized as one of the most urbanized cities, frequently facing pollution challenges. Throughout the majority of the year, the air quality in the city is categorized as poor (Agarwal et al., 2020; Mishra et al., 2016; Mohan & Mishra, 2022). The levels of air pollution consistently surpass national standards (Garg & Gupta, 2020; Goyal et al., 2021; Kanawade et al., 2020a). The Diwali festival typically occurs in October and November, coinciding with the onset of winter in Delhi (Ghei & Sane, 2018). In response to air quality concerns, the government has implemented several measures, including the Graded Response Action Plan (GRAP), an Odd-Even vehicle movement scheme (Mishra et al., 2019), and restrictions on the entry of diesel vehicles from other states. Additionally, the use of firecrackers during the festival has been prohibited (Parkhi et al., 2016; Sateesh et al., 2018; Yadav et al., 2022b). Emissions from Diwali celebrations release particles in both coarse and nano-sized ranges (Rajagopal et al., 2023). Given that human health is particularly susceptible to the effects of these emitted nanoparticles, it is essential to analyze exposure to these particles for a comprehensive health impact assessment (Cetin, 2015, 2016).

In light of the comprehensive prohibition of Diwali celebrations in 2022, this research was juxtaposed with the festivities of 2021. The investigation aims to elucidate the reduction in nanoparticle emissions during the cessation of firework displays. The study examined the concentration and temporal variations of nanoparticles, particularly those measuring between 10 nm and 1000 nm, during the Diwali festival in 2021 and 2022. This analysis aimed to evaluate the effects of the

firecracker ban on both particle number concentration and the concentration of inhalable particles over the two-year period. The ultrafine particles were categorized into three distinct sub-groups: Nucleation ( $N_{nuc}$  (10 to 30 nm)), Aitken ( $N_{atk}$  (30 to 100 nm)), and Accumulation mode ( $N_{acc}$  (100 to 1000 nm)). The study was carried out over a span of two successive years during the Diwali festival. In 2021, the festival (Diwali) occurred on November 4<sup>th</sup>, with Pre-Diwali defined as October 30<sup>th</sup> to November 3<sup>rd</sup>, and the Post-Diwali period from November 5<sup>th</sup> to 10<sup>th</sup>. In 2022, the Pre-Diwali period spanned from October 19<sup>th</sup> to 23<sup>rd</sup>, with Diwali on the 24<sup>th</sup>, followed by the Post-Diwali period from October 25<sup>th</sup> to 29<sup>th</sup>. Data collection took place over a span of 11 days in each year, with the first five days designated as the Pre-Diwali phase, followed by the day of Diwali, and concluding with the final five days categorized as the Post-Diwali phase. Approximately 94% of the data from 2021 was available for analysis, while 100% of the data from 2022 was accessible.

#### **4.9.2 Temporal variability of particle number concentration**

The temporal dynamics of particle number concentration (PNC) across three distinct size categories -  $N_{nuc}$  (10 nm to 30 nm),  $N_{atk}$  (30 nm to 100 nm), and  $N_{acc}$  (100 nm to 1000 nm) were examined during the Diwali celebrations of 2021 and 2022 (Fig.4.31a, b). This festive period is characterized by a significant surge in emissions over a brief timeframe. Analysis reveals that the particle concentrations in 2022 were lower than those in 2021, particularly for the  $N_{atk}$  and  $N_{acc}$  size ranges. Specifically, the average total particle concentration on Diwali day decreased from approximately  $3.8 \times 10^4 \text{ cm}^{-3}$  in 2021 to around  $3.1 \times 10^4 \text{ cm}^{-3}$  in 2022 (Table 4.11). This downward trend was also evident during the Pre- and Post-Diwali phases, with the Pre-Diwali concentration in 2022 recorded at  $2.9 \times 10^4 \text{ cm}^{-3}$ , compared to  $3.4 \times 10^4 \text{ cm}^{-3}$  in 2021 (Fig.4.31a). Similarly, the Post-Diwali concentrations ranged from  $3.0 \times 10^4 \text{ cm}^{-3}$  to  $3.7 \times 10^4 \text{ cm}^{-3}$ . The use of firecrackers in the city has faced increasing restrictions in recent years, culminating in a complete ban in 2022 due to deteriorating air quality following the festival. On Diwali day in 2022, the total PNC was notably lower than in 2021 (Fig.4.31b) (Table 4.11). Since 2021, the use of firecrackers has been limited, and in 2022, even online sales were prohibited, effectively eliminating their use. Before the implementation of the ban, significant concentrations of  $\text{PM}_{2.5}$ ,  $\text{PM}_{10}$ , and ultrafine particles (UFP's) were recorded in the region, as evidenced by various prior



studies that linked these emissions to the use of firecrackers. Typically, the Post-Diwali period exhibits higher particle concentrations than Diwali day itself (Fig.4.31a), a phenomenon attributed to the increased emissions on the festival day and the atmospheric conditions that facilitate prolonged particle accumulation. In 2021, the concentrations of particle numbers observed after Diwali were greater than those recorded during the Diwali festivities. However, in 2022, there was no significant variation in particle number concentrations when compared to Diwali day, suggesting a reduction in emissions associated with fireworks due to the implementation of a ban. These findings imply that the prohibition of firecrackers in the studied region has effectively diminished the release of anthropogenic aerosols resulting from fireworks. The day-wise variations in concentration, represented through Box plots for the periods D - 5 to D + 5 for both 2021 and 2022, are illustrated in (Fig.4.32).

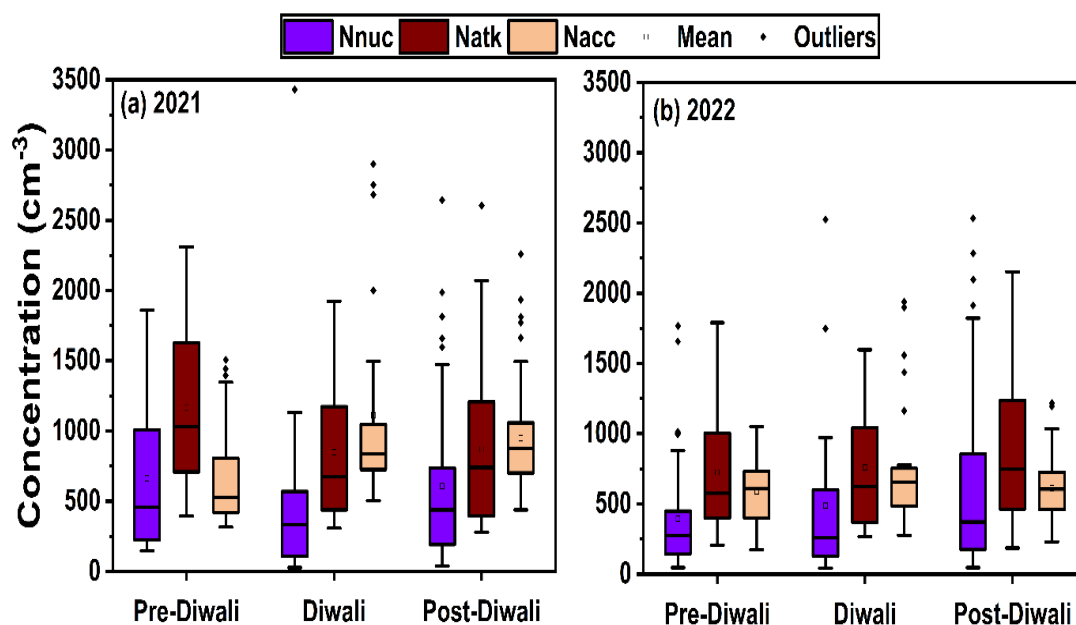


Figure 4.31. Box whisker plot represents the hourly mean concentration of  $N_{nuc}$  (10 nm to 30 nm),  $N_{atk}$  (30 nm to 100 nm), and  $N_{acc}$  (100 nm to 1000 nm) during Diwali 2021 (a), and Diwali 2022 (b).

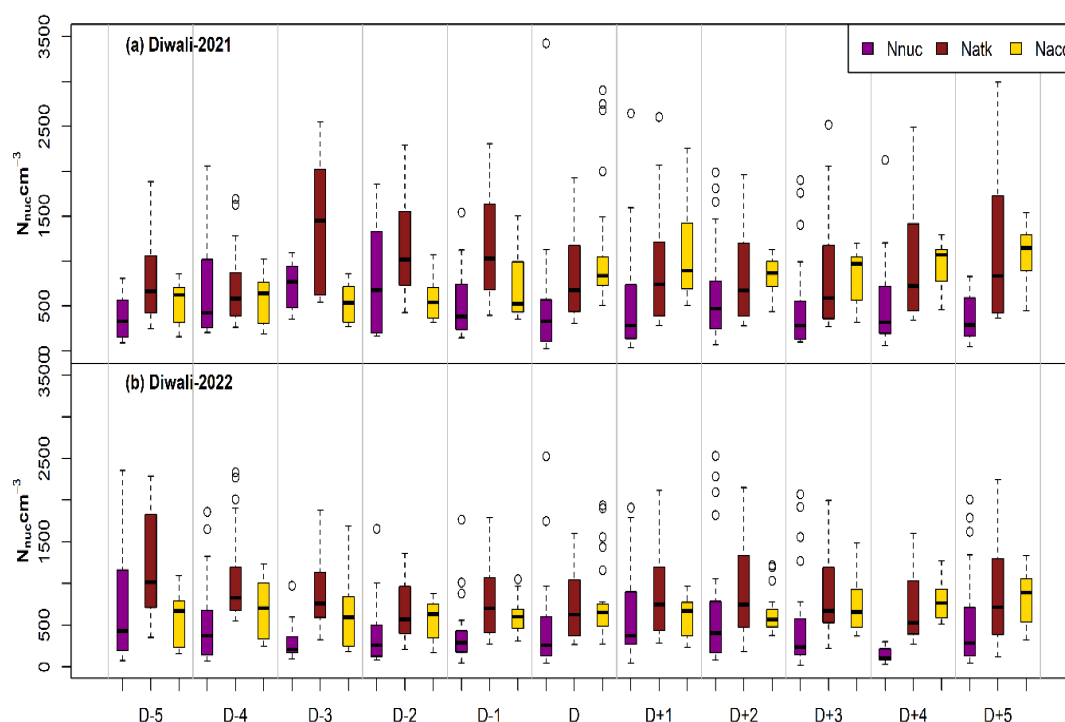


Figure 4.32. The daily variation in the hourly averaged concentrations of  $N_{nuc}$  (ranging from 10 nm to 30 nm),  $N_{atk}$  (spanning 30 nm to 100 nm), and  $N_{acc}$  (covering 100 nm to 1000 nm) during Diwali are presented for two distinct periods: (a) Diwali 2021, from October 30 to November 10, and (b) Diwali 2022, from October 19 to October 29.

### 4.9.3 Size-resolved particle distribution during Diwali

The log-normal distribution of particle number concentration for both Diwali periods is analyzed and illustrated in Fig.4.33. The size distribution of various size-resolved particles ranging from 10 nm to 1000 nm indicates a transition of particles across different size regimes, influenced by changes in emission sources. The size distribution observed in 2021 (Fig.4.33a), and 2022 (Fig.4.33b) reveals a progressive increase from smaller particles ( $N_{nuc}$ ) to larger ones ( $N_{acc}$ ). In 2021, the use of firecrackers was not entirely prohibited, leading to a noticeable level of firework activity, while in 2022, such activities were completely banned. The size distribution peaks during the Diwali period and the subsequent Post-Diwali phase in 2021 exhibit distinct patterns and peaks, indicative of emissions associated with Diwali celebrations. Conversely, the size distribution pattern in 2022 remains consistent

across all three Diwali periods, suggesting that the emission sources were stable and no new sources were introduced.

The emission patterns detected in a standard urban environment closely correspond to the concentration levels established in our study, which can be primarily ascribed to emissions from the transportation sector, in addition to other contributing sectors. In both years examined, the particle size distribution exhibits a significant peak in the accumulation mode ( $N_{acc}$ ). The concentration of  $N_{acc}$  particles arises from a combination of primary and secondary emissions, as well as various atmospheric processes affecting these particles. Notable changes in particle size distribution result from the incorporation of smaller particles into larger size categories through physiochemical processes influenced by climatic conditions (Kompalli et al., 2018; Moorthy et al., 2011). The festival of Diwali, occurring in winter, is characterized by elevated relative humidity and reduced wind speeds, which promote particle coagulation and consequently lead to the formation of larger particles. A detailed statistical overview for various timeframes within the study area is provided in Table 4.11.

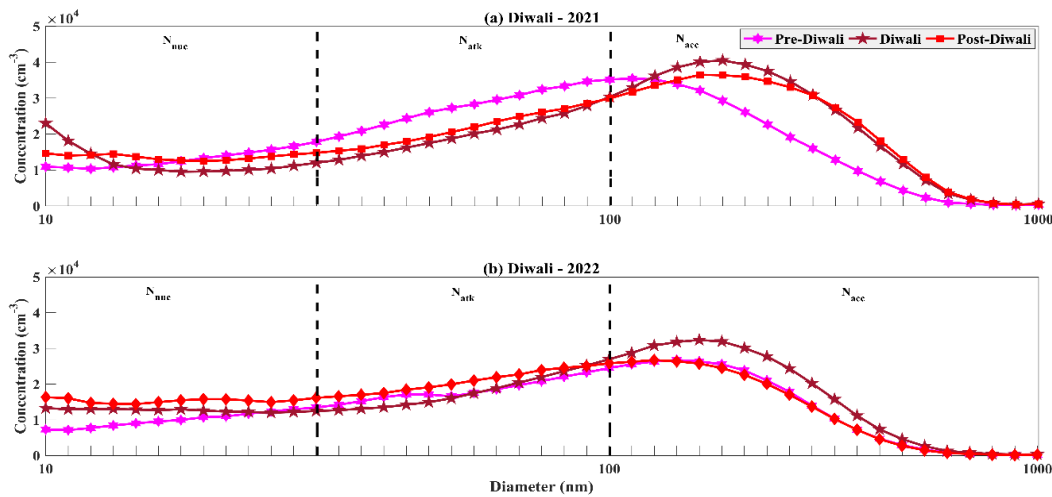


Figure 4.33. Particle number size distribution during Diwali 2021, and 2022.

Table 4.11. Statistical mean concentration of different mode particles ( $N_{nuc}$  (10 nm to 30 nm),  $N_{atk}$  (30 nm to 100 nm),  $N_{acc}$  (100 nm to 1000 nm),  $N_{total}$  (10 nm to 1000 nm), and Geometric Mean Diameter (GMD) during Diwali 2021, and 2022.

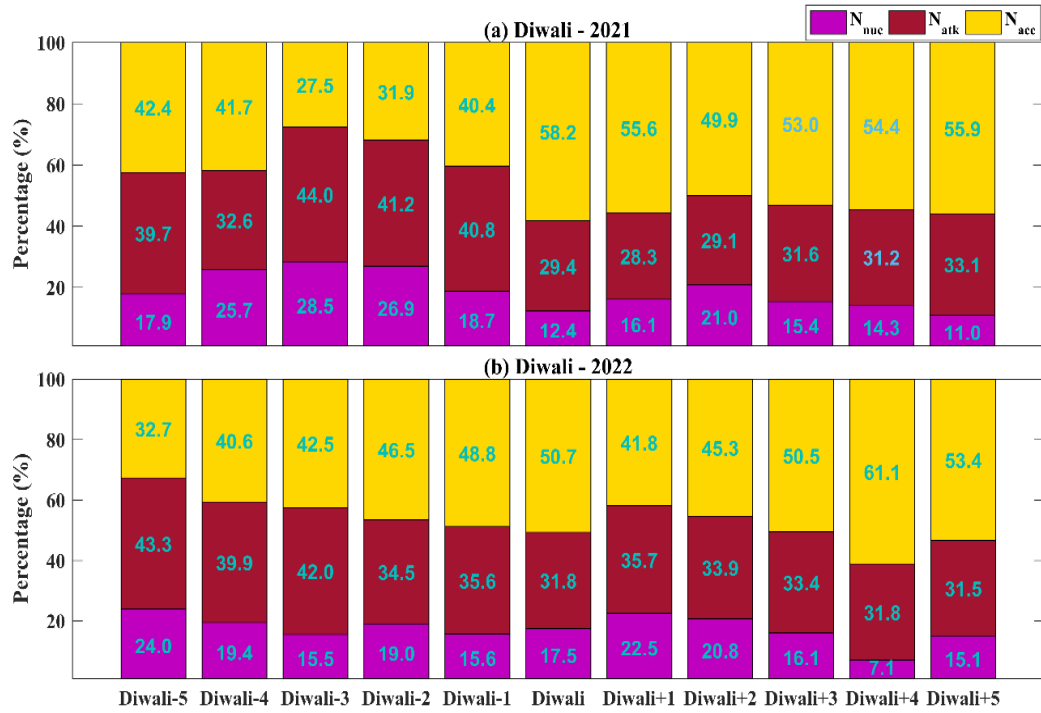
<b>Mode Particles</b>		<b>PD-21</b>	<b>D-21</b>	<b>PoD-21</b>	<b>PD-22</b>	<b>D-22</b>	<b>PoD-22</b>
<b>N<sub>nuc</sub></b>	Min	87	27	38	47	41	21
	Median	460	331	355	300	259	257
	Mean $\pm$ SD	606 $\pm$ 462	473 $\pm$ 689	514 $\pm$ 495	456 $\pm$ 448	487 $\pm$ 579	485 $\pm$ 574
	Max	2062	3428	2646	2354	2526	2532
<b>N<sub>atk</sub></b>	Min	249	308	273	208	266	120
	Median	847	675	712	780	624	685
	Mean $\pm$ SD	1023 $\pm$ 594	847 $\pm$ 481	942 $\pm$ 672	927 $\pm$ 536	759 $\pm$ 423	839 $\pm$ 533
	Max	2547	1924	2993	2332	1596	2247
<b>N<sub>acc</sub></b>	Min	158	506	317	157	276	230
	Median	580	837	979	621	654	681
	Mean $\pm$ SD	598 $\pm$ 278	111 $\pm$ 714	961 $\pm$ 337	619 $\pm$ 297	784 $\pm$ 469	718 $\pm$ 279
	Max	1505	2902	2258	1690	1938	1482
<b>N<sub>total</sub></b>	Min	8156	15120	11263	7511	10458	8241
	Median	32033	28749	32483	27057	25313	27732
	Mean $\pm$ SD	32550 $\pm$ 13957	38289 $\pm$ 23038	37203 $\pm$ 15796	29769 $\pm$ 13208	31115 $\pm$ 16603	30877 $\pm$ 15067
	Max	66314	95073	76588	67504	67710	74501
<b>GMD</b>	Min	35	47	44	28	31	38
	Median	74	119	99	81	93	99
	Mean $\pm$ SD	73 $\pm$ 20	114 $\pm$ 27	104 $\pm$ 31	83 $\pm$ 25	95 $\pm$ 25	98 $\pm$ 30
	Max	117	156	183	135	147	170

Note - PD – Pre-Diwali, D – Diwali, PoD - Post-Diwali, 21 - year 2021 and 22 - Year 2022.

#### 4.9.4 Different mode particle contribution to the total number particle concentration

The contribution of various size ranges to the overall particle number concentration is determined by the emissions from specific sources. Research indicates that emissions during Diwali predominantly occur in the size range exceeding 100 nm (Yadav et al., 2022a). Typically, in the Pre-Diwali period, the N<sub>atk</sub> mode (30 to 100 nm) exhibited a higher contribution, primarily attributed to vehicular emissions. However, on Diwali day, there was a notable decrease in the contribution from the N<sub>atk</sub> mode, reflecting the impact of Diwali-related sources on particle number concentration in 2021. In contrast, the situation in 2022 was different; the contribution of N<sub>atk</sub> mode

particles remained relatively stable throughout the period, with a slight reduction on Diwali day due to diminished vehicular activity compared to regular days, as indicated by Google Mobility data (Rajagopal et al., 2023). Rather than an increase in  $N_{acc}$  mode particles in 2022, there was a rise in the concentration of  $N_{nuc}$  particles, suggesting that the contribution from Diwali emissions was lower than in 2021. During the study period,  $N_{nuc}$  exhibited a contribution ranging from 17% to 28% in the Pre-Diwali phase, 12% during Diwali, and 11% to 21% in the Post-Diwali phase. In 2022,  $N_{nuc}$  contributions were recorded at 15% to 24% in the Pre-Diwali phase, 17% during Diwali, and 15% to 22% in the Post-Diwali phase. In contrast, the  $N_{atk}$  size range demonstrated a contribution of approximately 32% to 44% during the Pre-Diwali phase, followed by 29% during Diwali and 28% to 33% in the Post-Diwali phase in 2021. In 2022, the contributions for  $N_{atk}$  were 34% to 43% in the Pre-Diwali phase, 31% during Diwali, and 31% to 35% in the Post-Diwali phase. Notably, the  $N_{atk}$  size range exhibited minimal variation in concentration across both years. The  $N_{acc}$  mode particles displayed concentration levels ranging from 31% to 42% during Diwali, peaking at 58% on Diwali itself, and 49% to 55% in the Post-Diwali phase in 2021 (Fig.4.34). In 2022, the concentrations were recorded at 32% to 48% in the Pre-Diwali phase, 50% during Diwali, and 41% to 61% in the Post-Diwali phase. The percentage contributions of various size bins to the total particle concentration exhibited variability between 2021 and 2022, attributed to differences in sources and other influencing factors. The findings indicate a reduction in the average concentration of total particles in 2022, suggesting that the implementation of the firecracker ban policy effectively diminished particle number concentrations in the study area.



Note: Diwali - 5, Diwali - 4, Diwali - 3, Diwali - 2, and Diwali - 1 represent the pre-Diwali, and Diwali + 1, Diwali + 2, Diwali + 3, Diwali + 4, and Diwali + 5 represent the Post-Diwali.

Figure 4.34. Percentage contribution of mode particles ( $N_{\text{nuc}}$  (10 nm to 30 nm),  $N_{\text{atk}}$  (30 nm to 100 nm), and  $N_{\text{acc}}$  (100 nm to 1000 nm)) to total particles ( $N_{\text{tot}}$ ) during Diwali 2021, and 2022.

#### 4.9.5 Hourly analysis of particle contribution

The hourly contributions of various particle sizes to the overall particle concentration distinctly illustrate the emissions associated with Diwali on an hourly basis. It is evident that Diwali emissions are not uniformly distributed throughout the day; rather, numerous studies have indicated that these emissions are concentrated within a specific timeframe, during which there is a significant increase in emission levels (Khan et al., 2022; Shivani et al., 2019; Yerramsetti et al., 2013). This phenomenon predominantly occurs during the evening hours, extending from dusk until midnight. The hour-by-hour concentration data reflect the variations in particle sizes attributable to their respective sources. In 2021 (Fig.4.35), the evening of Diwali, specifically from 20:00 hours to the following morning, saw a substantial rise in the

concentration of accumulation mode particles, which escalated from approximately 54% in the evening to 83% by the next morning (Fig.4.35b-c). This significant change in concentration is mainly associated with emissions produced by the use of firecrackers during Diwali. Throughout the Diwali periods in both years, the meteorological conditions in the study area remained relatively consistent (Table 4.12), indicating that the observed concentration changes are largely attributable to the restrictions on emissions from firecrackers.

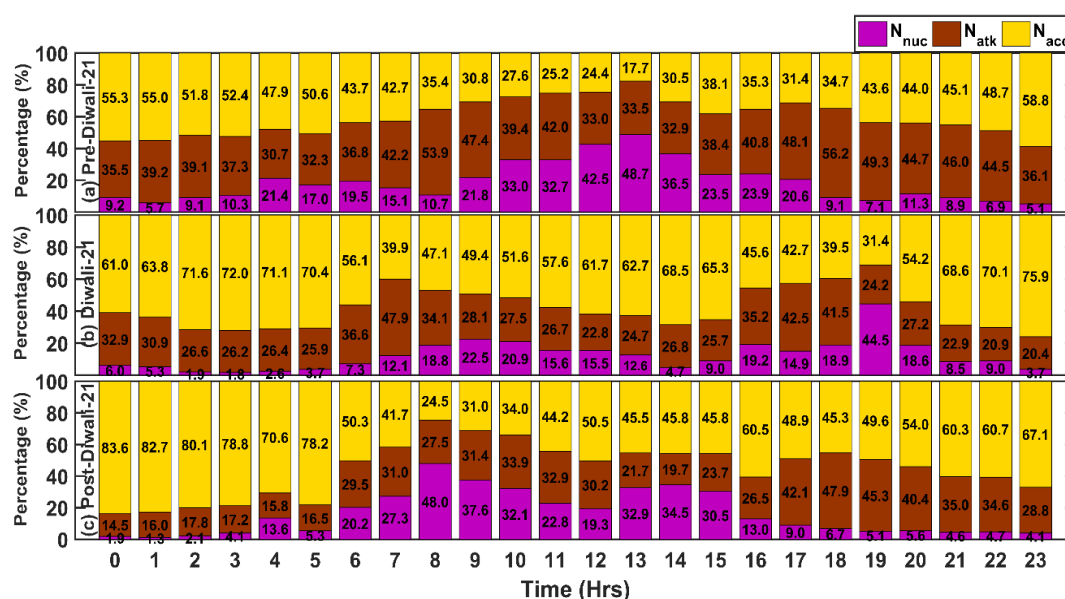


Figure 4.35. Hourly percentage contribution of three mode particles ( $N_{nuc}$  (10 nm to 30 nm),  $N_{atk}$  (30 nm to 100 nm), and  $N_{acc}$  (100 nm to 1000 nm)) to Total PNC on Pre-Diwali (a), Diwali (b), and Post-Diwali (c) during 2021.

Table 4.12 Average mean concentration of meteorological parameters (Ambient Temperature (AT), Relative Humidity (RH), and Solar Radiation (SR)) during Pre-Diwali, Diwali, and pre, Post-Diwali in 2021, and 2022.

Meteorological		PD-21	D-21	PoD-21	PD-22	D-22	PoD-22
AT (°C)	Min	20	20	19	18	17	16
	Median	24	23	22	24	22	22
	Mean $\pm$ SD	26 $\pm$ 5	25 $\pm$ 4	24 $\pm$ 4	26 $\pm$ 5	24 $\pm$ 5	24 $\pm$ 5
	Max	36	32	34	35	33	33
RH (%)	Min	25	41	29	33	36	34
	Median	58	78	68	60	62	69

	Mean $\pm$ SD	57 $\pm$ 17	71 $\pm$ 16	63 $\pm$ 14	57 $\pm$ 14	59 $\pm$ 14	63 $\pm$ 16
	Max	84	87	88	83	81	86
	Min	3	3	3	3	3	3
	Median	8	5	4	6	6	5
	Mean $\pm$ SD	152 $\pm$ 208	102 $\pm$ 148	115 $\pm$ 165	138 $\pm$ 198	132 $\pm$ 185	109 $\pm$ 165
<b>SR (w/m<sup>2</sup>)</b>	Max	644	413	519	550	499	496

In 2022 (Fig.4.36), the analysis of Diwali day on an hourly basis indicates that the prevalence of the accumulation mode ( $N_{acc}$ ) during the evening and the following morning was absent (Fig.4.36b-c), contrasting with observations from 2021. The concentration of the accumulation mode ( $N_{acc}$ ) was slightly elevated compared to other times of the day, attributed to minimal illegal firecracker usage and the impact of emissions from areas outside Delhi. Following the Diwali celebrations, the contribution of the nucleation mode ( $N_{nuc}$ ) was more closely associated with emissions from the transportation sector (Fig.4.36c). Throughout both the pre- and post-festival periods, increased human activity led to higher emissions within a specific size range, a trend consistent in both 2021 and 2022. The hour-wise contribution of nucleation mode ( $N_{nuc}$ ) particles during the period from 12 to 13 hrs on Diwali day also revealed a significant contribution, ranging from approximately 54 % to 62 % (Fig.4.36b) of particles in the nucleation size range. This increase is likely linked to the release of particles during the gas-to-particle conversion process, a natural phenomenon that occurs under specific conditions (Sebastian et al., 2021; Yadav et al., 2021; Yu et al., 2017).



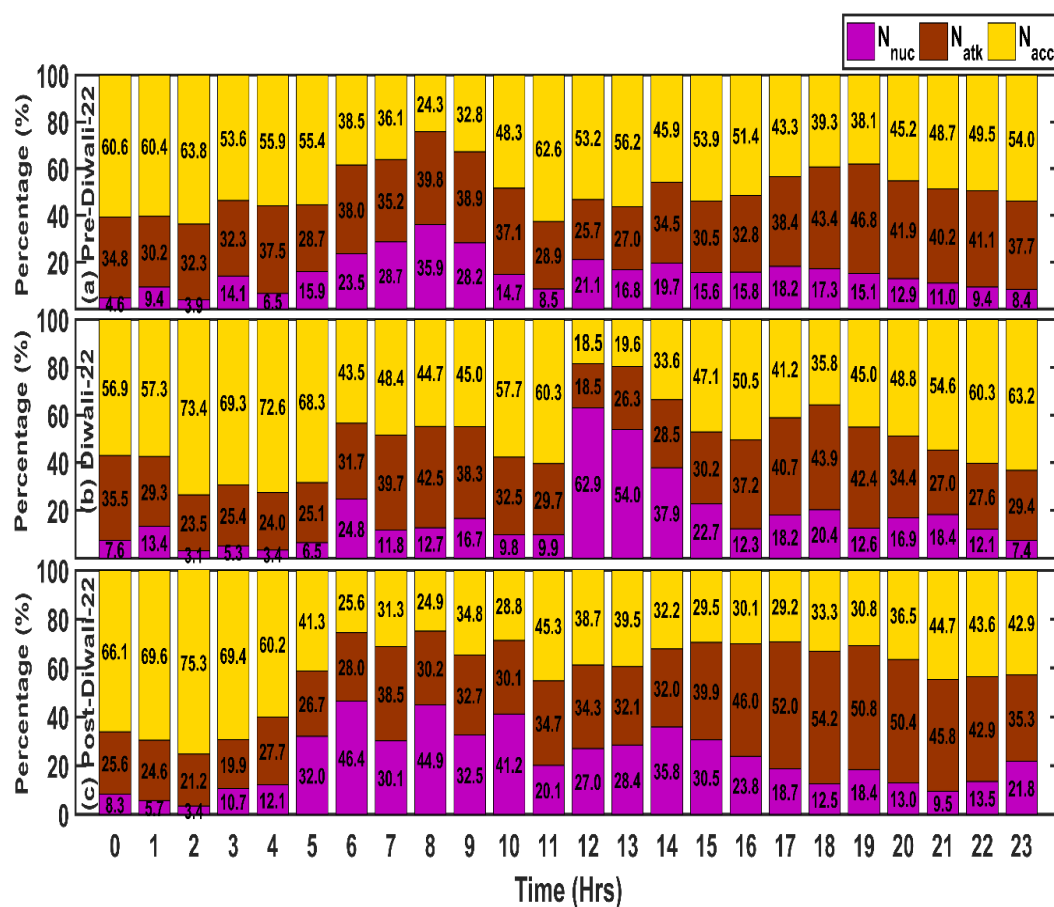


Figure 4.36. Hourly percentage contribution of three mode particles ( $N_{nuc}$  (10 nm to 30 nm),  $N_{atk}$  (30 nm to 100 nm), and  $N_{acc}$  (100 nm to 1000 nm)) to Total PNC a) Pre-Diwali, b) Diwali, and c) Post-Diwali during 2022.

#### 4.9.6 Percentage variations in size-resolved particle concentration

The comparison of particle concentration between 2022 and 2021 serves to elucidate the variations observed in 2022 (Fig.4.37). The analysis of percentage changes indicates a decline across all three size categories, ranging from nucleation to accumulation, in 2022. Notably, although the festival occurred on October 24, 2022, festivities commenced several days prior and extended a few days Post-Diwali. The data reveal a decrease in concentration during the Pre-Diwali (D - 1), Diwali (D), and Post-Diwali periods (D + 1, D + 2, and D + 3). On the day of Diwali in 2022, an increase in nucleation mode ( $N_{nuc}$ ) particles was observed, attributed to a burst of ultrafine particles (UFPs) resulting from diminished emissions associated with Diwali celebrations and other anthropogenic activities. Following the festival, specifically on D - 3, a resurgence in anthropogenic activities and vehicular emissions led to an

increase in accumulation mode ( $N_{atk}$ ) particles (Fig.4.37), with concentrations continuing to rise in subsequent days, such as D + 4 and D + 5 (Fig.4.37). The noted decline in concentration during the Diwali season can be attributed to the implementation of a ban on firecrackers in Delhi.

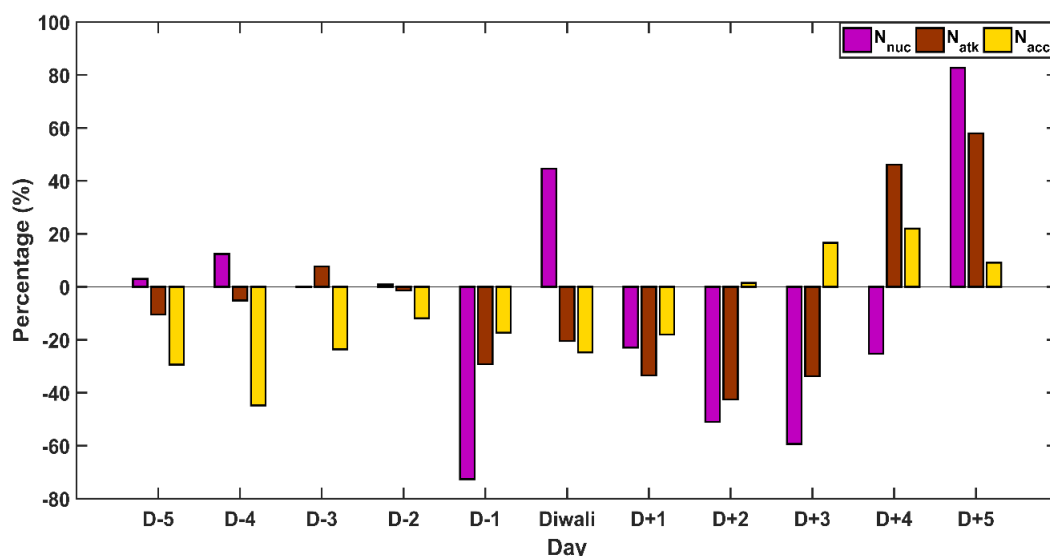


Figure 4.37. Percentage change of three different mode particles ( $N_{nuc}$  (10 nm to 30 nm),  $N_{atk}$  (30 nm to 100 nm), and  $N_{acc}$  (100 nm to 1000 nm)) in the year 2022 compared to 2021.

Note: D - 5, D - 4, D - 3, D - 2, and D - 1 represent the pre-Diwali, and D + 1, D + 2, D + 3, D + 4, and D + 5 represent the Post-Diwali.

#### 4.9.7 Diurnal variation of particle concentration

The diurnal variation of particles across various size ranges was examined during different hours of the day in the years 2021 and 2022. In 2021, both the pre- and post-Diwali periods exhibited elevated particle concentrations during the morning and evening peak hours (specifically, from 07 to 11, and 16 to 20) (Fig.4.38a, c) when compared to other times of the day. This fluctuation in concentration can be attributed to increased vehicular movement within the study area, a phenomenon commonly referred to as the double hump model, which is typical in urban environments. On the day of Diwali, the emission profile of the accumulation mode ( $N_{acc}$ ) was notably distinct from that observed in the Pre-Diwali, and Post-Diwali periods, indicating that emissions associated with Diwali significantly influence air quality (Fig.4.38a, c). A

marked change in concentration was particularly noted during the evening hours, coinciding with the customary bursting of firecrackers.

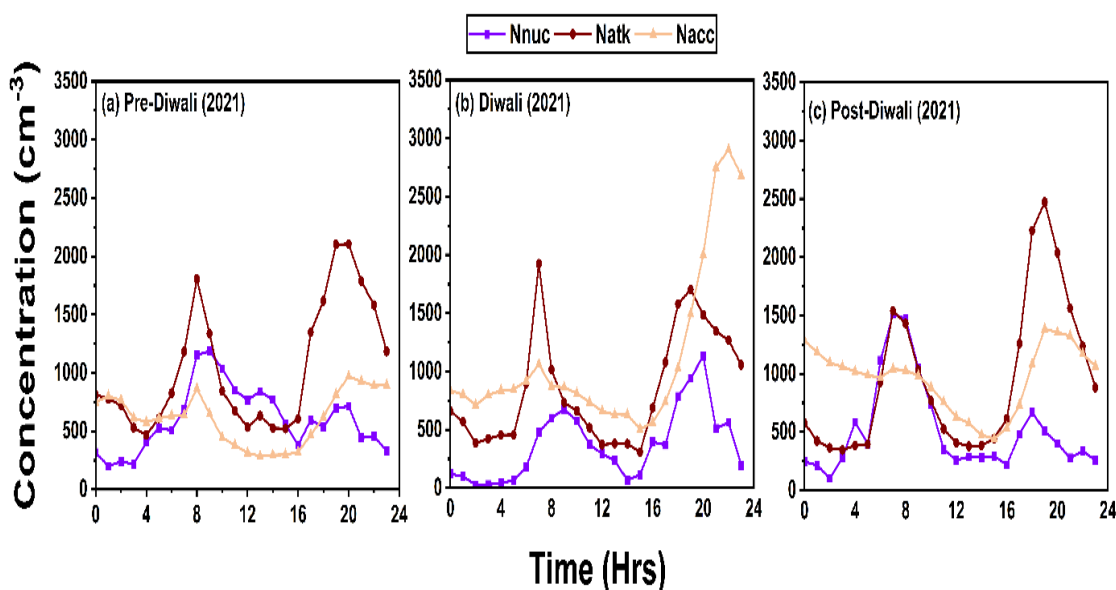


Figure 4.38. Diurnal variation of three mode particles ( $N_{nuc}$  (10 to 30 nm),  $N_{atk}$  (30 to 100 nm), and  $N_{acc}$  (100 to 1000 nm)) during three days (Pre-Diwali, Diwali, and Post-Diwali) in the year 2021.

The diurnal variation observed in 2022 indicates no significant alterations in concentration levels throughout the Pre-Diwali, Post-Diwali, and Diwali periods. The data indicates that the emission profiles have remained stable, implying that the ban on firecrackers successfully decreased emissions during Diwali in 2022 (Fig.4.39b). Notably, the concentration of  $N_{nuc}$  particles on Diwali day experiences an increase, attributed to the release of ultrafine particles, which is a consequence of the diminished levels of  $N_{atk}$  and  $N_{acc}$  mode particles. This trend is similarly observed during the Post-Diwali phase for both  $N_{nuc}$  and  $N_{atk}$  mode particles (Fig.4.39c). Furthermore, the emission profiles during the Pre-Diwali phase of 2022 are comparable to those recorded in the Pre-Diwali phase of the previous year (Fig.4.39a), indicating consistent emission scenarios during this period. Additional heat map analyses for the years 2021 and 2022 are available (Fig.4.40 a-f).

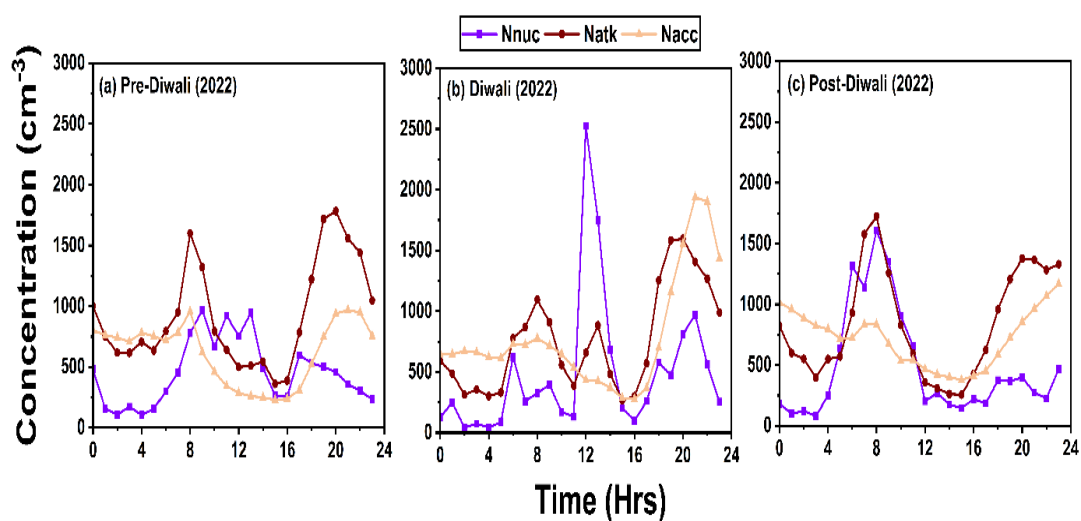


Figure 4.39. Diurnal variation of three mode particles ( $N_{nuc}$  (10 to 30 nm),  $N_{atk}$  (30 to 100 nm), and  $N_{acc}$  (100 to 1000 nm)) during three days (Pre-Diwali, Diwali, and Post-Diwali) in the year 2022.

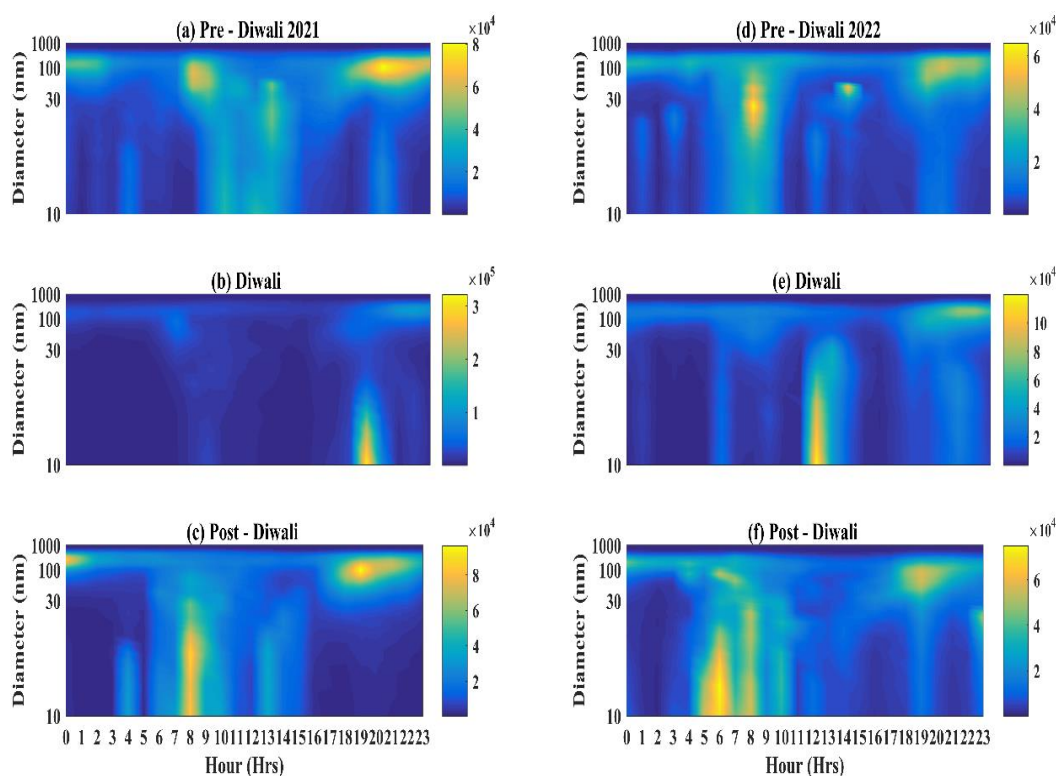


Figure 4.40. Analysis of heat maps depicting the distribution of size-resolved particles and geometric mean diameter (GMD) was conducted during Diwali 2021, spanning from October 30 to November 10, and in 2022, from October 19 to October 29.

#### 4.9.8 Exposure analysis

##### 4.9.8.1 Inhalable particle assessment

The inhalable particle number concentration serves as a metric for assessing the total quantity of particles inhaled by an individual at a specific moment. This concentration is calculated based on mathematical computations that consider both the Particle Number Concentration (PNC) and the rate of inhalation. The inhalation rate is influenced by the nature of physical activity increased physical exertion correlates with a higher inhalation rate, and conversely, reduced activity leads to a lower rate. According to the EPA Handbook (2011 edition), the average inhalation rate for adults aged 21 to 30 engaged in light physical activity is estimated to be  $12 \text{ cm}^3 \text{ min}^{-1}$  (Prabhu et al., 2019). The PNC is determined through direct measurement. Notably, nanoscale particles are capable of penetrating deeper into the pulmonary system compared to larger particulate matter due to their lower mass, which necessitates the use of the Inhalable Particle Number count for accurate deposition calculations. These calculations are governed by equation (1).

$$IPN(\text{min}^{-1}) = PNC(\text{cm}^{-3}) \times IR(\text{cm}^3 \text{min}^{-1}) \quad (4.1)$$

In 2021, during the pre-Diwali phase, the concentration of inhalable particulate matter (IPN) was notably elevated for  $N_{\text{atk}}$  particles, with values ranging from 0.8 to  $1.6 \times 10^7$  particles (Fig.4.41). However, during the Diwali celebration and the subsequent day ( $D + 1$ ), the concentration of  $N_{\text{acc}}$  particles increased significantly. Following this period, the concentrations of both  $N_{\text{atk}}$  and  $N_{\text{acc}}$  particles converged to similar levels during the later stages of the post-Diwali phase. In contrast, the year 2022 exhibited a lower overall inhalation concentration of particles, with a consistent pattern observed throughout the year. Specifically,  $N_{\text{atk}}$  particles maintained the highest concentration, followed by  $N_{\text{acc}}$  and then  $N_{\text{nuc}}$  particles. On Diwali day in 2021, the average inhalation rate of total particles per individual, assuming a constant inhalation rate of  $12 \text{ cm}^3 \text{ min}^{-1}$ , was recorded at 9.73 million particles per day, which decreased to 8.12 million particles per day in 2022. Notably, on Diwali day in 2022, the inhalation concentration further declined to approximately 1.6 million particles per day. In 2022, the inhalation concentration was decreased to 0.3 million particles per

minute, down from 0.4 million particles per minute in the previous year. This represents an approximate reduction of 18% in inhalation concentration when comparing 2022 to 2021. The elevated levels of inhalation have resulted in significant health consequences for the population. Exposure to these nanoparticles facilitates their deposition in the alveolar regions of the lungs (Hussein et al., 2022; Manojkumar et al., 2019). Such deposition occurs specifically within the alveolar sacs. Extended exposure to these particles is associated with serious health complications (Kwon et al., 2020; Schraufnagel, 2020). Due to their diminutive size, nanoparticles possess the ability to infiltrate both the skin and blood vessels (Møller et al., 2020). The primary health risks linked to exposure to these small nanoparticles include stroke, hypertension, and myocardial infarction (Gupta et al., 2020; Karl et al., 2020; Mao et al., 2020; Schraufnagel, 2020). Furthermore, these particles pose significant health threats to vulnerable populations, such as children and the elderly (Balakrishnan et al., 2019).

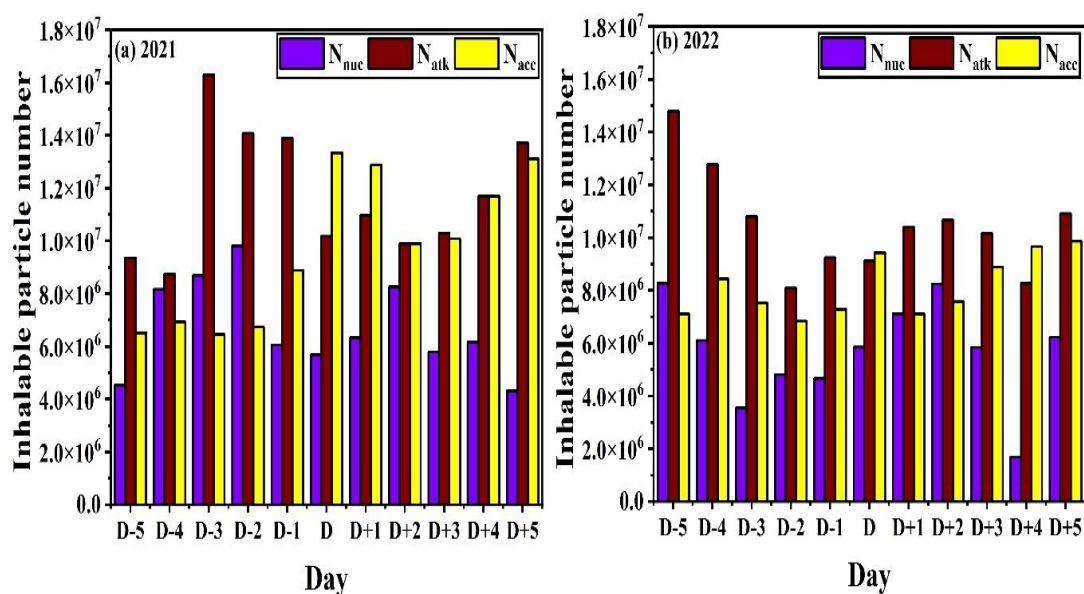


Figure 4.41. Total concentration of inhalable particles of varying sizes, specifically N<sub>nuc</sub> (ranging from 10 nm to 30 nm), N<sub>atk</sub> (from 30 nm to 100 nm), and N<sub>acc</sub> (spanning 100 nm to 1000 nm), was calculated for two distinct periods: (a) Diwali 2021, which occurred from October 30 to November 10, and (b) Diwali 2022, taking place from October 19 to October 29.

#### **4.10 Summary**

Chapter 4 presents the study's results and provides a detailed discussion of their significance in relation to the research objectives. The chapter elaborates on the collected data, highlighting key patterns, trends, and anomalies, and contrasts these findings with existing literature. Interpretations of the results are provided, emphasizing their implications for understanding ultrafine particles in urban environments. The discussion also addresses limitations of the study and suggests directions for future research.

Overall, Chapter 4 consolidates the core findings and analytical insights of the study, demonstrating how the results support, refine, or challenge the original hypotheses introduced in earlier chapters. This chapter sets the stage for Chapter 5 by presenting evidence-based conclusions, summarizing the broader implications of the study, and highlighting key recommendations for policy, practice, and future research, thereby ensuring a coherent transition from data interpretation to final conclusions.

## **CHAPTER - 5**

### **CONCLUSION**

#### **5.1 General**

The study comprehensively investigates various aspects of particle number size distribution (PNSD) and particle number concentration (PNC), including the influence of micrometeorological conditions on these parameters. It examines PNC and PNSD across different scenarios such as day and night cycles, seasonal variations (winter, summer, monsoon, and post-monsoon), and distinct geographical settings, including urban and background locations within a specific context. The study was conducted in two distinct microenvironments. The first region of study is the Delhi observatory (Inside the campus of Delhi Technological University), located in the northwest part of New Delhi (~223 m above the mean sea level (amsl)). This observatory is represented as an urban microenvironment. The monitoring was conducted from 01<sup>th</sup> January 2022 to 31<sup>st</sup> December 2022. The second location considered for the study is the Ranichauri Observatory, located in Tehri Garhwal district of Uttarakhand's, on the southern slope of the Western Himalaya (~1930 m above the mean sea level). This observatory is represented as a regional background microenvironment. The monitoring was conducted from 01<sup>th</sup> January 2017 to 31<sup>st</sup> December 2017. While during the monitoring period, the study also covered the episodic event like Diwali.

#### **5.2 Ultrafine particle number concentration during day and nighttime near selected urban roadside**

The study examines the 10.23-1090.21 nm aerosol number size distribution measurements conducted in the Delhi megacity's urban traffic corridor between 1<sup>st</sup> January 2022 to 31<sup>st</sup> December 2022. Taking into account the three size modes fractions ( $N_{nuc}$ ,  $N_{atk}$ , and  $N_{acc}$ ), the data set was examined for the various meteorological periods, as well as day and nighttime, sources, and emission types (from CNG, petrol, and diesel vehicle exhaust). Measurements of pollutants in a traffic corridor from January to December 2022 were examined using the mode sizes fractions ( $N_{nuc}$  (10 - 30 nm),  $N_{atk}$  (30 - 100 nm), and  $N_{acc}$  (100 - 1000 nm)) and the total particle concentration ( $N_{tot} < 1000$  nm). The terms  $N_{nuc}$  (10 - 30 nm) +  $N_{atk}$  (30 - 100 nm) refer to particles that are ultrafine (less than 100 nm).



- The contribution of  $N_{\text{nuc}}$  to the  $N_{\text{total}}$  reached a maximum of about 50% due to the direct fresh engine exhaust emissions during summer periods. Similarly,  $N_{\text{acc}}$  made a significant contribution (from 30 to 35%) to the  $N_{\text{total}}$  during the winter periods due to the effect of humidity on coagulation processes.
- The contribution of  $N_{\text{nuc}}$  is  $< 35\%$  throughout the year during nighttime due to the lower density of vehicles. Similarly, the  $N_{\text{acc}}$  mode particles contributed more during the nighttime due to the flow of heavy-duty vehicles.
- During daytime, the annual mean for  $N_{\text{nuc}}$ ,  $N_{\text{atk}}$ , and  $N_{\text{acc}}$  was 770, 846, and 313  $\text{cm}^{-3}$ , respectively, and during night, it was 353, 819, and 481  $\text{cm}^{-3}$ , respectively. Particle concentration for  $N_{\text{nuc}}$  and  $N_{\text{atk}}$  was higher during the day than at night, decreasing by approximately 45.84% and 4%, respectively.
- Regarding the  $N_{\text{acc}}$ , a contrary behavior was observed, around 34% higher at night than in the daytime. This indicated the significant role of vehicular sources in contributing to the aerosol particle concentration in this urban area.

### 5.2.1 Key takeaways from the results

- Ultrafine numbers are traffic-dominated, with  $N_{\text{atk}}$  leading  $N_{\text{tot}}$  year-round.
- Day favors fresh  $N_{\text{nuc}}$ , night shifts to  $N_{\text{acc}}$  via heavy-duty flow and weaker dilution.
- Summer boosts  $N_{\text{nuc}}$ , winter humidity grows  $N_{\text{acc}}$ , showing source–meteorology coupling.

## 5.3 Particle number concentration of ultrafine particles in urban and background regions

This study examined the differences in the concentration of ultrafine particle numbers between urban and background environments. The monitoring period spanned from January 1<sup>st</sup> 2017 to December 31<sup>st</sup> 2017 in background, and 1<sup>st</sup> January 2022 to 31<sup>st</sup> December 2022 in urban respectively. The study focused on total particle concentration ( $N_{\text{tot}} < 800 \text{ nm}$ ) and specific mode size fractions, including  $N_{\text{nuc}}$  (10 - 30 nm),  $N_{\text{atk}}$  (30 - 100 nm), and  $N_{\text{acc}}$  (100 - 800 nm). Ultrafine particles, defined as those smaller than 100 nm, are categorized as  $N_{\text{nuc}}$  (10 - 30 nm) plus  $N_{\text{atk}}$  (30 - 100 nm).

- The annual average  $N_{\text{tot}}$  in the urban site was  $2.5 \times 10^4 \text{ cm}^{-3}$ , and the concentration in the background site was  $2.9 \times 10^3 \text{ cm}^{-3}$ .

- Particle number concentration in the urban site was higher for  $N_{\text{atk}}$ , followed by  $N_{\text{nuc}}$  and  $N_{\text{acc}}$ , whereas in the background site, it was higher for  $N_{\text{atk}}$ , followed by  $N_{\text{nuc}}$  and  $N_{\text{acc}}$ .
- In both urban and background locations, the concentration of  $N_{\text{atk}}$  was found more in urban and background regions.
- The lowest concentration ( $6.4 \times 10^2 \text{ cm}^{-3}$ ) of  $N_{\text{atk}}$  was observed at the urban site during the summer, and at the background site during the monsoon season ( $1.09 \times 10^2 \text{ cm}^{-3}$ ).
- Urban regions with higher anthropogenic emissions, particularly from transportation sources, exhibit a peak around 80 to 90 nm. Similarly, at the background site, the size distribution changes gradually from smaller to larger sizes due to particle growth.
- The diurnal variation of particles in the urban site and background regions revealed the impact of anthropogenic sources, with transport emissions being higher during morning and evening peak hours.
- At the background site, particle concentration was high during the evening hours due to the accumulation of morning emissions throughout the study area.

### **5.3.1 Key takeaways from the results**

- Urban particle number levels exceeded background levels by approximately an order of magnitude, indicating strong anthropogenic control.
- Both peak at  $N_{\text{atk}}$ , urban modes center near 80-90 nm, while background spectra are smoothed by aging.
- Urban areas exhibit rush-hour bimodality; the background builds toward evening from daytime accumulation.

### **5.4 Role of micrometeorological parameters in urban and background ultrafine particle number concentration**

Apart from aerosol particle sources, local meteorological conditions, such as wind speed and relative humidity, also play a significant role in aerosol concentration, influencing the formation of secondary aerosol particles. During the study, the meteorological data were also collected from both urban and background sites.

- The average ( $\pm$ ) standard deviation for air temperature, wind speed, relative humidity, and solar radiation in urban areas was  $25.89 \pm 8.35$  °C,  $1.35 \pm 0.83$  m/s, and  $59.52 \pm 18.73$  %, while in background locations, these values were  $18.49 \pm 7.02$  °C,  $2.39 \pm 1.42$  m/s, and  $58.67 \pm 22.97$  %, respectively.
- The dispersion rate was higher for lower-size particles, such as  $N_{\text{nuc}}$ , even under calm wind conditions. At the same time, the larger particles, such as  $N_{\text{acc}}$  mode, were influenced by wind speed  $> 3$  m/s.
- The normalized aerosol number size distribution showed that particles in the ultrafine range, between 10 and 30 nm, dominated, corresponding to fresh engine emissions.
- The particle number size distribution was studied for relative humidity (RH) levels higher and lower than 70%. The size distribution of the particles showed a higher concentration around 100 nm when the RH was higher  $> 70\%$  due to the coagulation processes of the lower-size particles into larger ones. This led to an increase in the concentration of large particles, resulting in a decrease in the number of smaller particles and an increase in their total mass.
- At the urban site, the lowest mean temperature was recorded during winter (18 °C) and the highest during summer (33 °C), reaching a maximum of  $\sim 46$  °C, while in the background site, it was only 38 °C.
- The relative humidity in the study sites was directly proportional to the particle concentration in the accumulation mode. The humidity  $> 50$  % increased the possibility of coagulation and condensation of the lower-size particles ( $N_{\text{nuc}}$  and  $N_{\text{atk}}$ ) into accumulation mode particles, especially in the urban background.
- However, although geographical characteristics in the background promoted the arrival of air masses with a higher humidity than in the urban site, particle coagulation and condensation processes were inhibited by their low concentration. At the urban site, even  $>70\%$  increased particle condensation and coagulation; consequently, the accumulation-mode particles also increased.
- The annual wind speed in the urban site was  $< 2$  m/s and ranged from 6 to 10 m/s in the background site.

- The back-trajectory analysis showed that in both the study sites, during different seasons, wind pattern changes, especially the global wind direction, contributed to different types of particles originating from various sources such as burning, sand dust, and marine aerosols.
- During the winter onset and the post-monsoon period (October to March), a considerable proportion of the wind, approximately 60% to 80%, originates from adjacent states, notably Punjab and Haryana.
- Around 82% of the winds come from the same direction, causing long-range transportation of aerosols apart from the local sources. Similarly, during the summer, winds from Rajasthan, specifically from the westerly and north-westerly directions, carry a significant amount of dust from the Thar Desert, contributing to elevated concentrations during this period.
- However, from July to September, the wind pattern in the urban region changes, and the winds travel from the Arabian Sea or the Bay of Bengal, i.e., from the southwestern coast. These winds are responsible for the precipitation in both study regions, bringing many marine aerosols to the study location.
- The shift in wind patterns' dispersion could be attributed to the dominant monsoon winds from the Indian Ocean. In the background region, the wind pattern is generally similar to that in urban regions. The background region is characterized by hilly terrain, which restricts long-range transportation. At the same time, regional wind sources contribute to around 50% of the wind in almost all seasons under these background conditions.

#### **5.4.1 Key takeaways from the results**

- $N_{\text{nuc}}$  disperses even in calm air;  $N_{\text{acc}}$  scales with wind and higher RH via growth pathways.
- High RH shifts sizes toward ~100 nm, lowering the number but raising the mass via coagulation.
- Seasonal transport and terrain set mixtures: winter smoke and summer dust elevate UFP, hills limit long-range in the background.

### 5.5 Role of new particle formation in urban microenvironment

The characteristics of New Particle Formation (NPF) were investigated through measurements of particle size distribution ranging from 10 to 1000 nm at an urban site in Delhi, India. The analysis revealed that the highest total particle mean concentration, denoted as  $N_{\text{tot}}$ , followed the order of Post-Monsoon > Winter > Monsoon > Summer.

- The concentration of particle numbers was observed to be highest on non-event days in comparison to event days, indicating a significant influence of anthropogenic activities.
- On event days, the contribution of the  $N_{\text{atk}}$  mode (25 to 100 nm) to the total particle number concentration ( $N_{\text{tot}}$ ) was approximately 52%, while on non-event days, it was around 46%.
- Throughout the year, a total of 23 NFP Events, constituting 6% of the days, were identified, including 2 nocturnal and 21 midday occurrences. The diameter of the particle number mode increased from 10.23 nm to 101.25 nm and then to 95.85 nm.
- During these events, ammonia levels increased by approximately 34%, facilitating the growth of newly formed particles.
- In urban environments, biomass burning is a significant source of ammonia, which is essential for new particle formation as it stabilizes sulfuric acid clusters. The nocturnal growth of particles is enhanced by favorable atmospheric conditions, characterized by a notable decrease in wind speeds and solar radiation, which ranged from 0.6 to 1.6 m/s (minimum and maximum) and averaged 182 W/m<sup>2</sup> on non-event days, compared to 3.6 W/m<sup>2</sup> on event days, thereby promoting unhindered particle growth.
- The majority of the NPF events occurred during daylight hours, which is consistent with the influence of solar radiation on particle formation.
- This process is particularly driven by photochemical reactions that generate nucleating agents such as sulfuric acid and various organic compounds.
- Seasonally, the highest growth rates were observed in winter ( $12.07 \pm 1.07 \text{ nm h}^{-1}$ ), followed by post-monsoon ( $7.46 \pm 0.4 \text{ nm h}^{-1}$ ), monsoon ( $6.55 \pm 0.9 \text{ nm h}^{-1}$ ), and summer ( $4.79 \pm 0.43 \text{ nm h}^{-1}$ ).

- The growth rates varied between 2 to 37 nm h<sup>-1</sup>. The peak condensation sink (cs) was recorded during the post-monsoon season ( $0.087 \pm 0.039 \text{ s}^{-1}$ ), followed by winter ( $0.055 \pm 0.023440 \text{ s}^{-1}$ ), summer ( $0.039 \pm 0.015 \text{ s}^{-1}$ ), and monsoon ( $0.037 \pm 0.010 \text{ s}^{-1}$ ).
- Notably, the post-monsoon season exhibited both elevated particle number concentration (PNC) and higher cs values.
- Although the post-monsoon period had a greater concentration of particles, the larger sizes of these particles contributed to an increased condensation sink.
- Conversely, while winter demonstrated a higher growth rate, the estimated cs was greater during the post-monsoon. This suggests that the presence of larger pre-existing particles in the post-monsoon season may have inhibited formation rates while promoting particle growth.
- Notably, this rise in particle numbers was associated with a decrease in condensation sink (CS) values. Conversely, on non-event days, an inverse relationship was observed, suggesting conditions that are less conducive to new particle formation. Meteorological factors significantly influence new particle formation. On event days, wind speeds were predominantly lower, typically ranging from 0 to 8 m/s across most seasons.
- In contrast, non-event days experienced markedly higher wind speeds, ranging from 0 to 12 m/s. The prevailing winds predominantly originated from the northwest, facilitating new particle formation at the study site.

#### **5.5.1 Key takeaways from the results**

- NPF is episodic (~6% of days) and mainly occurs during midday, driving urban UFP peaks under photochemical conditions.
- Higher ammonia and lower condensation sinks enable growth from ~10 nm into the sub-100 nm range.
- Post-monsoon supports growth under high sink; winter shows the fastest growth rates.

#### **5.6 Particle number concentration during the diwali period**

During the Diwali festival, the city of Delhi faces significant air pollution challenges, particularly in the winter months. The ban on firecrackers is a measure

aimed at mitigating further emissions from fireworks. Initially, restrictions were placed on the sale and purchase of firecrackers, followed by regulations on the timing of their use. Subsequently, the introduction of green crackers was implemented to address concerns about air quality. These measures represent the earlier phases of the firecracker ban policy. This research examined particle number emissions during the 2022 Diwali celebrations, in comparison to the period prior to the firecracker ban in 2021. Data on particle number concentration were collected and analyzed across three size categories (10-30 nm, 30-100 nm, and 100-1000 nm) immediately before, during, and after the Diwali festival over two consecutive years.

- The average mean concentration of particles in 2022 decreased to approximately  $3.1 \times 10^4 \text{ cm}^{-3}$  from  $3.8 \times 10^4 \text{ cm}^{-3}$ . Notably, the particle size distribution did not exhibit any significant alterations on Diwali day in 2022, remaining below  $3 \times 10^4 \text{ cm}^{-3}$  throughout the observed period.
- The percentage reduction in particle concentration indicated a decrease of 20 to 22% for  $N_{\text{atk}}$  and  $N_{\text{acc}}$ . Conversely, the concentration of  $N_{\text{nuc}}$  increased on Diwali day, attributed to the natural gas to-particle conversion process, which falls outside the scope of this study.
- The concentration of  $N_{\text{acc}}$  mode particles on Diwali 2021 ranged from approximately 54% to 83% due to emissions associated with the festival. In contrast, this figure decreased to approximately 60% in 2022. The overall particle concentration was measured at  $10^4 \text{ cm}^{-3}$  in 2022, a decline from  $10^5 \text{ cm}^{-3}$  in the previous year.
- On Diwali day, exposure to nanoparticles was recorded at 9.73 million in 2021, which fell to 8.12 million in 2022. The observance of Diwali in 2022 alone resulted in a reduction of approximately 1.6 million particles, representing an 18% decrease in nanoparticle concentration, attributed to the enforcement of a ban on firecrackers.

#### **5.6.1 Key takeaways from the results**

- Firecracker curbs cut number exposure and mode concentrations, demonstrating policy impact.

- Residual signal shifts modes:  $N_{\text{atk}}$  and  $N_{\text{acc}}$  drop while  $N_{\text{nuc}}$  can rise via gas-to-particle conversion.

### 5.7 Importance of the study

The research indicates that the concentration of particles in an urban environment is approximately eight times greater than that found in background locations. In urban areas, the Aitken and Nucleation modes were the primary contributors to the overall particle concentration, whereas in background sites, the Aitken and Accumulation modes were more prevalent. The study presents several potential applications:

- The results assist in understanding the varying intensity and behavior of different sources throughout the day and night, which can inform policy development and decision-making aimed at improving air quality and addressing related health concerns.
- The results underscore the considerable influence of vehicle emissions on the production of ultrafine particles in urban environments, facilitating the identification of multiple sources and the execution of essential strategies to mitigate nanoparticle emissions and improve air quality.
- This study seeks to clarify the impact of different sources, meteorological variables, and geographical characteristics on the concentration, size distribution, and other essential factors required for understanding the dynamics of ultrafine particles (UFPs) in various environmental contexts.
- Future investigations can be carried out under varying environmental conditions to analyze the sources, concentration levels, and potential health effects associated with these UFPs.
- Urban environments pose a considerable threat regarding exposure to these particles. The probability of particle accumulation within the respiratory tract is affected by their concentration and properties, which can increase toxicity levels.
- The present research has the potential to offer significant insights into the evaluation of both long-term and short-term seasonal exposure. The concentrations obtained can be employed to simulate health effects, including pulmonary deposition.



- The study further emphasizes the importance of adopting mitigation strategies to improve air quality, as well as the need for policy-oriented initiatives that promote sustainability.
- This research aims to enhance the comprehension of the dimensions and numerical distribution of ultrafine particles (UFPs) in diverse environments, encompassing both urban and regional contexts, as well as various outdoor locations and seasonal variations.

### **5.8 Future prospects of the study**

The comprehensive study was conducted across various scenarios, including both day and night, different seasons (Winter, Summer, Monsoon, and Post-Monsoon), and diverse geographical settings such as urban areas and rural backgrounds in Delhi and Ranichauri. The results of this comprehensive research suggest several recommendations for future investigations.

- It is essential to implement long-term monitoring of ultrafine particles (UFP) at various locations within urban environments to better understand the sources of particle number concentration (PNC). Attention from both the public and policymakers is crucial regarding the issue of vehicular pollution.
- Additionally, further investigation is needed into the effects of UFP on human health, particularly when combined with exposure biomarkers, to establish a connection between passenger exposure variability and particle concentrations in public transportation settings.
- Future research could also focus on health risk assessments for school-aged children, as well as comparative evaluations of commuters' exposure to black carbon, precursor gases, and UFP in both urban and rural transport environments.

### **5.9 SDGs alignment**

Both studies play a crucial role in promoting the integration of Sustainable Development Goals (SDGs) through their focus on air quality management and public health. The research aligns with SDG 3 (Good Health and Well-being) by highlighting the health hazards associated with UFP exposure and recommending strategies for mitigation. It also reinforces SDG 11 (Sustainable Cities and Communities) by

recognizing the necessity for proper urban planning and improved transportation infrastructure approaches to reduce traffic-related emissions and enhance air quality in major cities like Delhi. Furthermore, the studies highlight the significance of SDG 13 (Climate Action) by presenting evidence about the environmental effects of vehicle emissions, advocating for stricter emission regulations, and sustainable transportation initiatives. By highlighting geographical disparities in air quality, the research also supports SDG 10 (Reduced Inequalities) by emphasizing the need for equitable access to clean air.

### **5.10 Summary**

Chapter 5 concludes the thesis by emphasizing the key findings in relation to the research objectives. The study quantified ultrafine particle (UFP) concentrations at a selected urban roadside during both day and nighttime, and compared these with urban background levels, considering the influence of micrometeorological parameters. The chapter also assessed the implications of UFP exposure on human health and the surrounding environment. Additionally, the study contributed to advancing selected Sustainable Development Goals (SDGs), demonstrating its broader societal relevance.

Overall, this chapter synthesizes the results presented in Chapter 4 and reflects on their significance, highlighting how the study addresses the research objectives outlined in Chapter 1. It also identifies limitations and proposes avenues for future research on ultrafine particles, ensuring that the thesis provides a coherent and actionable contribution to the field.

## References

- Abdel-Shafy, H. I., & Mansour, M. S. M. (2016). A review on polycyclic aromatic hydrocarbons: Source, environmental impact, effect on human health and remediation. *Egyptian Journal of Petroleum*, 25(1), 107–123. <https://doi.org/10.1016/j.ejpe.2015.03.011>
- Adam, M. G., Chiang, A. W. J., & Balasubramanian, R. (2020). Insights into characteristics of light absorbing carbonaceous aerosols over an urban location in Southeast Asia. *Environmental Pollution*, 257, 113425. <https://doi.org/10.1016/j.envpol.2019.113425>
- Afshari, A., Matson, U., & Ekberg, L. E. (2005). Characterization of indoor sources of fine and ultrafine particles: A study conducted in a full-scale chamber. *Indoor Air*, 15(2), 141–150. <https://doi.org/10.1111/j.1600-0668.2005.00332.x>
- Agarwal, A., Kaushik, A., Kumar, S., & Mishra, R. K. (2020). Comparative study on air quality status in Indian and Chinese cities before and during the COVID-19 lockdown period. *Air Quality, Atmosphere and Health*, 13(10), 1167–1178. <https://doi.org/10.1007/s11869-020-00881-z>
- Agarwal, R., & Aggarwal, S. G. (2023). A year-round study of ambient gaseous pollutants, their atmospheric chemistry and role in secondary particle formation at an urban site in Delhi. *Atmospheric Environment*, 295(December 2022), 119557. <https://doi.org/10.1016/j.atmosenv.2022.119557>
- Agudelo-Castañeda, D. M., Teixeira, E. C., Braga, M., Rolim, S. B. A., Silva, L. F. O., Beddows, D. C. S., Harrison, R. M., & Querol, X. (2019). Cluster analysis of urban ultrafine particles size distributions. *Atmospheric Pollution Research*, 10(1), 45–52. <https://doi.org/10.1016/j.apr.2018.06.006>
- Ali, M. U., Lin, S., Yousaf, B., Abbas, Q., Munir, M. A. M., Rashid, A., Zheng, C., Kuang, X., & Wong, M. H. (2022). Pollution characteristics, mechanism of toxicity and health effects of the ultrafine particles in the indoor environment: Current status and future perspectives. *Critical Reviews in Environmental Science and Technology*, 52(3), 436–473. <https://doi.org/10.1080/10643389.2020.1831359>
- Amato, F., Pandolfi, M., Moreno, T., Furger, M., Pey, J., Alastuey, A., Bukowiecki, N., Prevot, A. S. H., Baltensperger, U., & Querol, X. (2011). Sources and

- variability of inhalable road dust particles in three European cities. *Atmospheric Environment*, 45(37), 6777–6787.  
<https://doi.org/10.1016/j.atmosenv.2011.06.003>
- Amato, F., Pandolfi, M., Viana, M., Querol, X., Alastuey, A., & Moreno, T. (2009). Spatial and chemical patterns of PM<sub>10</sub> in road dust deposited in urban environment. *Atmospheric Environment*, 43(9), 1650–1659.  
<https://doi.org/10.1016/j.atmosenv.2008.12.009>
- Apte, J. S., Kirchstetter, T. W., Reich, A. H., Deshpande, S. J., Kaushik, G., Chel, A., Marshall, J. D., & Nazaroff, W. W. (2011). Concentrations of fine, ultrafine, and black carbon particles in auto-rickshaws in New Delhi, India. *Atmospheric Environment*, 45(26), 4470–4480.  
<https://doi.org/10.1016/j.atmosenv.2011.05.028>
- Austin, E., Xiang, J., Gould, T. R., Shirai, J. H., Yun, S., Yost, M. G., Larson, T. V., & Seto, E. (2021). Distinct ultrafine particle profiles associated with aircraft and roadway traffic. *Environmental Science and Technology*, 55(5), 2847–2858.  
<https://doi.org/10.1021/acs.est.0c05933>
- Azimi, P., & Stephens, B. (2020). A framework for estimating the US mortality burden of fine particulate matter exposure attributable to indoor and outdoor microenvironments. *Journal of Exposure Science and Environmental Epidemiology*, 30(2), 271–284. <https://doi.org/10.1038/s41370-018-0103-4>
- Baalbaki, R., Pikridas, M., Jokinen, T., Laurila, T., Dada, L., Bezantakos, S., Ahonen, L., Neitola, K., Maisser, A., Bimenyimana, E., Christodoulou, A., Unga, F., Savvides, C., Lehtipalo, K., Kangasluoma, J., Biskos, G., Petäjä, T., Kerminen, V. M., Sciare, J., & Kulmala, M. (2021). Towards understanding the characteristics of new particle formation in the Eastern Mediterranean. *Atmospheric Chemistry and Physics*, 21(11), 9223–9251.  
<https://doi.org/10.5194/acp-21-9223-2021>
- Babu, S. S., Kompalli, S. K., & Moorthy, K. K. (2016). Aerosol number size distributions over a coastal semi urban location: Seasonal changes and ultrafine particle bursts. *Science of the Total Environment*, 563–564, 351–365.  
<https://doi.org/10.1016/j.scitotenv.2016.03.246>
- Balakrishnan, K., Dey, S., Gupta, T., Dhaliwal, R. S., Brauer, M., Cohen, A. J.,

- Stanaway, J. D., Beig, G., Joshi, T. K., Aggarwal, A. N., Sabde, Y., Sadhu, H., Frostad, J., Causey, K., Godwin, W., Shukla, D. K., Kumar, G. A., Varghese, C. M., Muraleedharan, P., ... Dandona, L. (2019). The impact of air pollution on deaths, disease burden, and life expectancy across the states of India: the Global Burden of Disease Study 2017. *The Lancet Planetary Health*, 3(1), e26–e39. [https://doi.org/10.1016/S2542-5196\(18\)30261-4](https://doi.org/10.1016/S2542-5196(18)30261-4)
- Baldauf, R. W., Heist, D., Isakov, V., Perry, S., Hagler, G. S. W., Kimbrough, S., Shores, R., Black, K., & Brixey, L. (2013). Air quality variability near a highway in a complex urban environment. *Atmospheric Environment*, 64, 169–178. <https://doi.org/10.1016/j.atmosenv.2012.09.054>
- Banoo, R., Sharma, S. K., Vijayan, N., & Mandal, T. K. (2022). Assessment of Potential Source and the Source Region of Particulate Matter in an Urban Area of Delhi, India. *Aerosol Science and Engineering*, 6(3), 231–245. <https://doi.org/10.1007/s41810-022-00139-4>
- Baylon, P., Jaffe, D. A., Hall, S. R., Ullmann, K., Alvarado, M. J., & Lefer, B. L. (2018). Impact of Biomass Burning Plumes on Photolysis Rates and Ozone Formation at the Mount Bachelor Observatory. *Journal of Geophysical Research: Atmospheres*, 123(4), 2272–2284. <https://doi.org/10.1002/2017JD027341>
- Becker, S., & Soukup, J. M. (2003). Coarse (PM<sub>2.5-10</sub>), fine (PM<sub>2.5</sub>), and ultrafine air pollution particles induce/increase immune costimulatory receptors on human blood-derived monocytes but not on alveolar macrophages. *Journal of Toxicology and Environmental Health - Part A*, 66(9), 847–859. <https://doi.org/10.1080/15287390306381>
- Beig, G., Sahu, S. K., Singh, V., Tikle, S., Sobhana, S. B., Gargeva, P., Ramakrishna, K., Rathod, A., & Murthy, B. S. (2020). Objective evaluation of stubble emission of North India and quantifying its impact on air quality of Delhi. *Science of the Total Environment*, 709. <https://doi.org/10.1016/j.scitotenv.2019.136126>
- Bein, K. J., Zhao, Y., Johnston, M. V., & Wexler, A. S. (2008). Interactions between boreal wildfire and urban emissions. *Journal of Geophysical Research: Atmospheres*, 113(7), 1–17. <https://doi.org/10.1029/2007JD008910>
- Bekö, G., Kjeldsen, B. U., Olsen, Y., Schipperijn, J., Wierzbicka, A., Karottki, D. G., Toftum, J., Loft, S., & Clausen, G. (2015). Contribution of various

- microenvironments to the daily personal exposure to ultrafine particles: Personal monitoring coupled with GPS tracking. *Atmospheric Environment*, 110, 122–129. <https://doi.org/10.1016/j.atmosenv.2015.03.053>
- Belkacem, I., Khardi, S., Helali, A., Slimi, K., & Serindat, S. (2020). The influence of urban road traffic on nanoparticles: Roadside measurements. *Atmospheric Environment*, 242, 117786. <https://doi.org/10.1016/j.atmosenv.2020.117786>
- Bergbäck, B., Johansson, K., & Mohlander, U. (2001). Urban metal flows—A case study of Stockholm. Review and conclusions. *Water, Air, and Soil Pollution: Focus*, 1, 3–24. <http://link.springer.com/article/10.1023/A:1017531532576>
- Bhandari, S., Gani, S., Patel, K., Wang, D. S., Soni, P., Arub, Z., Habib, G., Apte, J. S., & Hildebrandt Ruiz, L. (2020). Sources and atmospheric dynamics of organic aerosol in New Delhi, India: Insights from receptor modeling. *Atmospheric Chemistry and Physics*, 20(2), 735–752. <https://doi.org/10.5194/acp-20-735-2020>
- Bougiatioti, A., Bezantakos, S., Stavroulas, I., Kalivitis, N., Kokkalis, P., Biskos, G., Mihalopoulos, N., Papayannis, A., & Nenes, A. (2016). Biomass-burning impact on CCN number, hygroscopicity and cloud formation during summertime in the eastern Mediterranean. *Atmospheric Chemistry and Physics*, 16(11), 7389–7409. <https://doi.org/10.5194/acp-16-7389-2016>
- Bran, S. H., & Srivastava, R. (2017). Investigation of PM<sub>2.5</sub> mass concentration over India using a regional climate model. *Environmental Pollution*, 224, 484–493. <https://doi.org/10.1016/j.envpol.2017.02.030>
- Brines, M., Dall'Osto, M., Beddows, D. C. S., Harrison, R. M., Gómez-Moreno, F., Núñez, L., Artíñano, B., Costabile, F., Gobbi, G. P., Salimi, F., Morawska, L., Sioutas, C., & Querol, X. (2015). Traffic and nucleation events as main sources of ultrafine particles in high-insolation developed world cities. *Atmospheric Chemistry and Physics*, 15(10), 5929–5945. <https://doi.org/10.5194/acp-15-5929-2015>
- Buenrostro Mazon, S., Kontkanen, J., Manninen, H. E., Nieminen, T., Kerminen, V. M., & Kulmala, M. (2016). A long-term comparison of nighttime cluster events and daytime ion formation in a boreal forest. *Boreal Environment Research*, 21(3–4), 242–261.

- Bukowiecki, N., Lienemann, P., Hill, M., Furger, M., Richard, A., Amato, F., Prévôt, A. S. H., Baltensperger, U., Buchmann, B., & Gehrig, R. (2010). PM<sub>10</sub> emission factors for non-exhaust particles generated by road traffic in an urban street canyon and along a freeway in Switzerland. *Atmospheric Environment*, 44(19), 2330–2340. <https://doi.org/10.1016/j.atmosenv.2010.03.039>
- Burkart, J., Willis, M. D., Bozem, H., Thomas, J. L., Law, K., Hoor, P., Aliabadi, A. A., Köllner, F., Schneider, J., Herber, A., Abbatt, J. P. D., & Richard Leaitch, W. (2017). Summertime observations of elevated levels of ultrafine particles in the high Arctic marine boundary layer. *Atmospheric Chemistry and Physics*, 17(8), 5515–5535. <https://doi.org/10.5194/acp-17-5515-2017>
- Burtscher, H., & Schüepp, K. (2012). The occurrence of ultrafine particles in the specific environment of children. *Paediatric Respiratory Reviews*, 13(2), 89–94. <https://doi.org/10.1016/j.prrv.2011.07.004>
- Businger, S., Huff, R., Pattantyus, A., Horton, K., Sutton, A. J., Elias, T., & Cherubini, T. (2015). Observing and forecasting vog dispersion from Kīlauea Volcano, Hawaii. *Bulletin of the American Meteorological Society*, 96(10), 1667–1686. <https://doi.org/10.1175/BAMS-D-14-00150.1>
- Cai, J., Chu, B., Yao, L., Yan, C., Heikkinen, L. M., Zheng, F., Li, C., Fan, X., Zhang, S., Yang, D., Wang, Y., Kokkonen, T. V., Chan, T., Zhou, Y., Dada, L., Liu, Y., He, H., Paasonen, P., Kujansuu, J. T., ... Daellenbach, K. R. (2020). Size-segregated particle number and mass concentrations from different emission sources in urban Beijing. *Atmospheric Chemistry and Physics*, 20(21), 12721–12740. <https://doi.org/10.5194/acp-20-12721-2020>
- Carn, S. A., Fioletov, V. E., Mclinden, C. A., Li, C., & Krotkov, N. A. (2017). A decade of global volcanic SO<sub>2</sub> emissions measured from space. *Scientific Reports*, 7, 1–12. <https://doi.org/10.1038/srep44095>
- Cash, J. M., Di Marco, C., Langford, B., Heal, M. R., Mandal, T. K., Sharma, S. K., Gurjar, B. R., & Nemitz, E. (2023). Response of organic aerosol to Delhi's pollution control measures over the period 2011–2018. *Atmospheric Environment*, 315(September), 120123. <https://doi.org/10.1016/j.atmosenv.2023.120123>
- Casquero-Vera, J. A., Lyamani, H., Dada, L., Hakala, S., Paasonen, P., Román, R.,

- Fraile, R., Petäjä, T., Olmo-Reyes, F. J., & Alados-Arboledas, L. (2020). New particle formation at urban and high-altitude remote sites in the south-eastern Iberian Peninsula. *Atmospheric Chemistry and Physics*, 20(22), 14253–14271. <https://doi.org/10.5194/acp-20-14253-2020>
- Cetin, M. (2015). Using GIS analysis to assess urban green space in terms of accessibility: Case study in Kutahya. *International Journal of Sustainable Development and World Ecology*, 22(5), 420–424. <https://doi.org/10.1080/13504509.2015.1061066>
- Cetin, M. (2016). Sustainability of urban coastal area management: A case study on Cide. *Journal of Sustainable Forestry*, 35(7), 527–541. <https://doi.org/10.1080/10549811.2016.1228072>
- Chan, L. Y., & Kwok, W. S. (2001). Roadside suspended particulates at heavily trafficked urban sites of Hong Kong - Seasonal variation and dependence on meteorological conditions. *Atmospheric Environment*, 35(18), 3177–3182. [https://doi.org/10.1016/S1352-2310\(00\)00504-5](https://doi.org/10.1016/S1352-2310(00)00504-5)
- Charron, A., Birmili, W., & Harrison, R. M. (2008). Fingerprinting particle origins according to their size distribution at a UK rural site. *Journal of Geophysical Research Atmospheres*, 113(7), 1–15. <https://doi.org/10.1029/2007JD008562>
- Chatain, M., Alvarez, R., Ustache, A., Rivière, E., Favez, O., & Pallares, C. (2021). Simultaneous roadside and urban background measurements of submicron aerosol number concentration and size distribution (In the range 20–800 nm), along with chemical composition in strasbourg, france. *Atmosphere*, 12(1). <https://doi.org/10.3390/ATMOS12010071>
- Chen, Y., Du, W., Shen, G., Zhuo, S., Zhu, X., Shen, H., Huang, Y., Su, S., Lin, N., Pei, L., Zheng, X., Wu, J., Duan, Y., Wang, X., Liu, W., Wong, M., & Tao, S. (2017). Household air pollution and personal exposure to nitrated and oxygenated polycyclic aromatics (PAHs) in rural households: Influence of household cooking energies. *Indoor Air*, 27(1), 169–178. <https://doi.org/10.1111/ina.12300>
- Chen, Y., Masiol, M., Squizzato, S., Chalupa, D. C., Zíková, N., Pokorná, P., Rich, D. Q., & Hopke, P. K. (2022). Long-term trends of ultrafine and fine particle number concentrations in New York State: Apportioning between emissions and dispersion. *Environmental Pollution*, 310(July).



<https://doi.org/10.1016/j.envpol.2022.119797>

- Cheung, H. C., Nie, C., Huang, M., Yang, T., Wang, H., Lee, C. S. L., Pei, C., Zhao, J., & Liang, B. (2022). Influence of Regional Pollution Outflow on Particle Number Concentration and Particle Size in Airshed of Guangzhou, South China. *Aerosol and Air Quality Research*, 22(9), 1–18. <https://doi.org/10.4209/aaqr.220097>
- Ciccone, G., Forastiere, F., Agabiti, N., Biggeri, A., Bisanti, L., Chellini, E., Corbo, G., Dell’Orco, V., Dalmaso, P., Volante, T. F., Galassi, C., Piffer, S., Renzoni, E., Rusconi, F., Sestini, P., & Viegi, G. (1998). Road traffic and adverse respiratory effects in children. SIDRIA Collaborative Group. *Occupational and Environmental Medicine*, 55(11), 771–778. <https://doi.org/10.1136/oem.55.11.771>
- Cincinelli, A., & Martellini, T. (2017). Indoor air quality and health. *International Journal of Environmental Research and Public Health*, 14(11). <https://doi.org/10.3390/ijerph14111286>
- Clifford, S., Mazaheri, M., Salimi, F., Ezz, W. N., Yeganeh, B., Low-Choy, S., Walker, K., Mengersen, K., Marks, G. B., & Morawska, L. (2018). Effects of exposure to ambient ultrafine particles on respiratory health and systemic inflammation in children. *Environment International*, 114(February), 167–180. <https://doi.org/10.1016/j.envint.2018.02.019>
- Collins, D. B., Burkart, J., Chang, R. Y. W., Lizotte, M., Boivin-Rioux, A., Blais, M., Mungall, E. L., Boyer, M., Irish, V. E., Massé, G., Kunkel, D., Tremblay, J. É., Papakyriakou, T., Bertram, A. K., Bozem, H., Gosselin, M., Levasseur, M., & Abbatt, J. P. D. (2017). Frequent ultrafine particle formation and growth in Canadian Arctic marine and coastal environments. *Atmospheric Chemistry and Physics*, 17(21), 13119–13138. <https://doi.org/10.5194/acp-17-13119-2017>
- Cooper, D. M., & Loxham, M. (2019). Particulate matter and the airway epithelium: The special case of the underground? *European Respiratory Review*, 28(153). <https://doi.org/10.1183/16000617.0066-2019>
- Cuesta-Mosquera, A. P., González-Duque, C. M., Velasco-García, M., & Aristizábal, B. H. (2018). Distribución Espacial De Concentraciones De So<sub>2</sub>, Nox Y O<sub>3</sub> En El Aire Ambiente De Manizales. *Revista Internacional de Contaminacion*

- Ambiental*, 34(3), 489–504. <https://doi.org/10.20937/RICA.2018.34.03.11>
- Cuesta-Mosquera, A. P., Wahl, M., Acosta-López, J. G., García-Reynoso, J. A., & Aristizábal-Zuluaga, B. H. (2020). Mixing layer height and slope wind oscillation: Factors that control ambient air SO<sub>2</sub> in a tropical mountain city. *Sustainable Cities and Society*, 52(May 2019), 101852. <https://doi.org/10.1016/j.scs.2019.101852>
- Dada, L., Lehtipalo, K., Kontkanen, J., Nieminen, T., Baalbaki, R., Ahonen, L., Duplissy, J., Yan, C., Chu, B., Petäjä, T., Lehtinen, K., Kerminen, V. M., Kulmala, M., & Kangasluoma, J. (2020). Formation and growth of sub-3-nm aerosol particles in experimental chambers. *Nature Protocols*, 15(3), 1013–1040. <https://doi.org/10.1038/s41596-019-0274-z>
- Dada, L., Okuljar, M., Shen, J., Olin, M., Wu, Y., Heimsch, L., Herlin, I., Kankaanrinta, S., Lampimäki, M., Kalliokoski, J., Baalbaki, R., Lohila, A., Petäjä, T., Maso, M. D., Duplissy, J., Kerminen, V. M., & Kulmala, M. (2023). The synergistic role of sulfuric acid, ammonia and organics in particle formation over an agricultural land. *Environmental Science: Atmospheres*, 3(8), 1195–1211. <https://doi.org/10.1039/d3ea00065f>
- Dada, L., Paasonen, P., Nieminen, T., Buenrostro Mazon, S., Kontkanen, J., Peräkylä, O., Lehtipalo, K., Hussein, T., Petäjä, T., Kerminen, V. M., Bäck, J., & Kulmala, M. (2017). Long-term analysis of clear-sky new particle formation events and nonevents in Hyytiälä. *Atmospheric Chemistry and Physics*, 17(10), 6227–6241. <https://doi.org/10.5194/acp-17-6227-2017>
- Dal Maso, M., Kulmala, M., Riipinen, I., Wagner, R., Hussein, T., Aalto, P. P., & Lehtinen, K. E. J. (2005). Formation and growth of fresh atmospheric aerosols: Eight years of aerosol size distribution data from SMEAR II, Hyytiälä, Finland. *Boreal Environment Research*, 10(5), 323–336.
- Dall'Osto, M., Beddows, D. C. S., Asmi, A., Poulain, L., Hao, L., Freney, E., Allan, J. D., Canagaratna, M., Crippa, M., Bianchi, F., De Leeuw, G., Eriksson, A., Swietlicki, E., Hansson, H. C., Henzing, J. S., Granier, C., Zemankova, K., Laj, P., Onasch, T., ... Harrison, R. M. (2018). Novel insights on new particle formation derived from a pan-european observing system. *Scientific Reports*, 8(1), 1–11. <https://doi.org/10.1038/s41598-017-17343-9>

- Dalmora, A. C., Ramos, C. G., Querol, X., Kautzmann, R. M., Oliveira, M. L. S., Taffarel, S. R., Moreno, T., & Silva, L. F. O. (2016). Nanoparticulate mineral matter from basalt dust wastes. *Chemosphere*, 144(2016), 2013–2017. <https://doi.org/10.1016/j.chemosphere.2015.10.047>
- Damayanti, S., & Harrison, R. M. (2022). *Long-term trends of Total Number Count and Black Carbon at Rural , Urban Background , and Urban Traffic Sites in the UK. September.*
- Damayanti, S., Harrison, R. M., Pope, F., & Beddows, D. C. S. (2023). Limited impact of diesel particle filters on road traffic emissions of ultrafine particles. *Environment International*, 174(March), 107888. <https://doi.org/10.1016/j.envint.2023.107888>
- Dandona, L., & Singh, G. (2021). Challenges in estimating the burden of neurological disorders across Indian states – Authors’ reply. *The Lancet Global Health*, 9(11), e1504. [https://doi.org/10.1016/S2214-109X\(21\)00412-5](https://doi.org/10.1016/S2214-109X(21)00412-5)
- Deng, C., Fu, Y., Dada, L., Yan, C., Cai, R., Yang, D., Zhou, Y., Yin, R., Lu, Y., Li, X., Qiao, X., Fan, X., Nie, W., Kontkanen, J., Kangasluoma, J., Chu, B., Ding, A., Kerminen, V. M., Paasonen, P., ... Jiang, J. (2020). Seasonal characteristics of new particle formation and growth in urban Beijing. *Environmental Science and Technology*, 54(14), 8547–8557. <https://doi.org/10.1021/acs.est.0c00808>
- Deng, C., Li, Y., Yan, C., Wu, J., Cai, R., Wang, D., Liu, Y., Kangasluoma, J., Kerminen, V. M., Kulmala, M., & Jiang, J. (2022). Measurement report: Size distributions of urban aerosols down to 1 nm from long-term measurements. *Atmospheric Chemistry and Physics*, 22(20), 13569–13580. <https://doi.org/10.5194/acp-22-13569-2022>
- Di Natale, F., & Carotenuto, C. (2015). Particulate matter in marine diesel engines exhausts: Emissions and control strategies. *Transportation Research Part D: Transport and Environment*, 40(600), 166–191. <https://doi.org/10.1016/j.trd.2015.08.011>
- Diapouli, E., Eleftheriadis, K., Karanasiou, A. A., Vratolis, S., Hermansen, O., Colbeck, I., & Lazaridis, M. (2011). Indoor and outdoor particle number and mass concentrations in Athens. Sources, sinks and variability of aerosol parameters. *Aerosol and Air Quality Research*, 11(6), 632–642.

<https://doi.org/10.4209/aaqr.2010.09.0080>

- Ding, K., Huang, X., Ding, A., Wang, M., Su, H., Kerminen, V. M., Petäjä, T., Tan, Z., Wang, Z., Zhou, D., Sun, J., Liao, H., Wang, H., Carslaw, K., Wood, R., Zuidema, P., Rosenfeld, D., Kulmala, M., Fu, C., ... Andreae, M. O. (2021). Aerosol-boundary-layer-monsoon interactions amplify semi-direct effect of biomass smoke on low cloud formation in Southeast Asia. *Nature Communications*, 12(1). <https://doi.org/10.1038/s41467-021-26728-4>
- Dinoi, A., Gulli, D., Weinhold, K., Ammoscato, I., Calidonna, C. R., Wiedensohler, A., & Contini, D. (2023). Characterization of ultrafine particles and the occurrence of new particle formation events in an urban and coastal site of the Mediterranean area. *Atmospheric Chemistry and Physics*, 23(3), 2167–2181. <https://doi.org/10.5194/acp-23-2167-2023>
- Donaldson, G. C., Seemungal, T. A. R., Bhowmik, A., & Wedzicha, J. A. (2008). Relationship between exacerbation frequency and lung function decline in chronic obstructive pulmonary disease (Thorax (2002) 57, (847-852)). *Thorax*, 63(8), 753. <https://doi.org/10.1136/thorax.57.10.847corr1>
- Dröge, J., Klingelhöfer, D., Braun, M., & Groneberg, D. A. (2024). Influence of a large commercial airport on the ultrafine particle number concentration in a distant residential area under different wind conditions and the impact of the COVID-19 pandemic. *Environmental Pollution*, 345(January). <https://doi.org/10.1016/j.envpol.2024.123390>
- Dumka, U. C., Kosmopoulos, P. G., Patel, P. N., & Sheoran, R. (2022). Can Forest Fires Be an Important Factor in the Reduction in Solar Power Production in India? *Remote Sensing*, 14(3), 14–23. <https://doi.org/10.3390/rs14030549>
- Dupuy, J. luc, Fargeon, H., Martin-StPaul, N., Pimont, F., Ruffault, J., Guijarro, M., Hernando, C., Madrigal, J., & Fernandes, P. (2020). Climate change impact on future wildfire danger and activity in southern Europe: a review. *Annals of Forest Science*, 77(2). <https://doi.org/10.1007/s13595-020-00933-5>
- Durant, A. J., Bonadonna, C., & Horwell, C. J. (2010). Atmospheric and environmental impacts of volcanic particulates. *Elements*, 6(4), 235–240. <https://doi.org/10.2113/gselements.6.4.235>
- Durant, A. J., Villarosa, G., Rose, W. I., Delmelle, P., Prata, A. J., & Viramonte, J. G.

- (2012). Long-range volcanic ash transport and fallout during the 2008 eruption of Chaitén volcano, Chile. *Physics and Chemistry of the Earth*, 45–46, 50–64. <https://doi.org/10.1016/j.pce.2011.09.004>
- Dutta, A., & Jinsart, W. (2022). Air pollution in Delhi, India: It's status and association with respiratory diseases. *PLoS ONE*, 17(9 September), 1–20. <https://doi.org/10.1371/journal.pone.0274444>
- Ehn, M., Thornton, J. A., Kleist, E., Sipilä, M., Junninen, H., Pullinen, I., Springer, M., Rubach, F., Tillmann, R., Lee, B., Lopez-Hilfiker, F., Andres, S., Acir, I. H., Rissanen, M., Jokinen, T., Schobesberger, S., Kangasluoma, J., Kontkanen, J., Nieminen, T., ... Mentel, T. F. (2014). A large source of low-volatility secondary organic aerosol. *Nature*, 506(7489), 476–479. <https://doi.org/10.1038/nature13032>
- English, P., Neutra, R., Scalf, R., Sullivan, M., Waller, L., & Zhu, L. (1999). Examining associations between childhood asthma and traffic flow using a geographic information system. *Environmental Health Perspectives*, 107(9), 761–767. <https://doi.org/10.1289/ehp.99107761>
- Ertugrul, M., Ozel, H. B., Varol, T., Cetin, M., & Sevik, H. (2019). Investigation of the relationship between burned areas and climate factors in large forest fires in the Çanakkale region. *Environmental Monitoring and Assessment*, 191(12). <https://doi.org/10.1007/s10661-019-7946-6>
- Eyring, V., Köhler, H. W., Lauer, A., & Lemper, B. (2005). Emissions from international shipping: 2. Impact of future technologies on scenarios until 2050. *Journal of Geophysical Research D: Atmospheres*, 110(17), 183–200. <https://doi.org/10.1029/2004JD005620>
- Filonchyk, M., Peterson, M. P., & Sun, D. (2022). Deterioration of air quality associated with the 2020 US wildfires. *Science of the Total Environment*, 826. <https://doi.org/10.1016/j.scitotenv.2022.154103>
- Flueckiger, A. C., & Petrucci, G. A. (2024). Effect of Relative Humidity on the Rate of New Particle Formation for Different VOCs. *Atmosphere*, 15(4). <https://doi.org/10.3390/atmos15040480>
- Forrister, H., Liu, J., Scheuer, E., Dibb, J., Ziemba, L., Thornhill, K. L., Anderson, B., Diskin, G., Perring, A. E., Schwarz, J. P., Campuzano-Jost, P., Day, D. A., Palm,

- B. B., Jimenez, J. L., Nenes, A., & Weber, R. J. (2015). Evolution of brown carbon in wildfire plumes. *Geophysical Research Letters*, 42(11), 4623–4630. <https://doi.org/10.1002/2015GL063897>
- Franck, U., Herbarth, O., Wehner, B., Wiedensohler, A., & Manjarrez, M. (2003). How do the indoor size distributions of airborne submicron and ultrafine particles in the absence of significant indoor sources depend on outdoor distributions? *Indoor Air*, 13(2), 174–181. <https://doi.org/10.1034/j.1600-0668.2003.00177.x>
- Franco, M. A., Ditas, F., Kremper, L. A., Machado, L. A. T., Andreae, M. O., Araújo, A., Barbosa, H. M. J., De Brito, J. F., Carbone, S., Holanda, B. A., Morais, F. G., Nascimento, J. P., Pöhlker, M. L., Rizzo, L. V., Sá, M., Saturno, J., Walter, D., Wolff, S., Pöschl, U., ... Pöhlker, C. (2022). Occurrence and growth of sub-50nm aerosol particles in the Amazonian boundary layer. *Atmospheric Chemistry and Physics*, 22(5), 3469–3492. <https://doi.org/10.5194/acp-22-3469-2022>
- Fujitani, Y., Kumar, P., Tamura, K., Fushimi, A., Hasegawa, S., Takahashi, K., Tanabe, K., Kobayashi, S., & Hirano, S. (2012). Seasonal differences of the atmospheric particle size distribution in a metropolitan area in Japan. *Science of the Total Environment*, 437, 339–347. <https://doi.org/10.1016/j.scitotenv.2012.07.085>
- Gani, S., Bhandari, S., Patel, K., Seraj, S., Soni, P., Arub, Z., Habib, G., Hildebrandt Ruiz, L., & Apte, J. S. (2020). Particle number concentrations and size distribution in a polluted megacity: The Delhi Aerosol Supersite study. *Atmospheric Chemistry and Physics*, 20(14), 8533–8549. <https://doi.org/10.5194/acp-20-8533-2020>
- Gani, S., Chambliss, S. E., Messier, K. P., Lunden, M. M., & Apte, J. S. (2021). Spatiotemporal profiles of ultrafine particles differ from other traffic-related air pollutants: Lessons from long-term measurements at fixed sites and mobile monitoring. *Environmental Science: Atmospheres*, 1(7), 558–568. <https://doi.org/10.1039/d1ea00058f>
- Ganteaume, A., Barbero, R., Jappiot, M., & Maillé, E. (2021). Understanding future changes to fires in southern Europe and their impacts on the wildland-urban interface. *Journal of Safety Science and Resilience*, 2(1), 20–29. <https://doi.org/10.1016/j.jnlssr.2021.01.001>

- Gao, J., Chai, F., Wang, T., Wang, S., & Wang, W. (2012). Particle number size distribution and new particle formation: New characteristics during the special pollution control period in Beijing. *Journal of Environmental Sciences*, 24(1), 14–21. [https://doi.org/10.1016/S1001-0742\(11\)60725-0](https://doi.org/10.1016/S1001-0742(11)60725-0)
- Garcia-Marlès, M., Lara, R., Reche, C., Pérez, N., Tobías, A., Savadkoohi, M., Beddows, D., Salma, I., Vörösmarty, M., Weidinger, T., Hueglin, C., Mihalopoulos, N., Grivas, G., Kalkavouras, P., Ondráček, J., Zíková, N., Niemi, J. V., Manninen, H. E., Green, D. C., ... Querol, X. (2024). Inter-annual trends of ultrafine particles in urban Europe. *Environment International*, 185(February). <https://doi.org/10.1016/j.envint.2024.108510>
- Garg, A., & Gupta, N. C. (2018). Episodic Levels of PM<sub>10</sub>, PM<sub>2.5</sub> and PM<sub>1</sub> during Diwali : A study in urban area of Delhi , India. *International Research Journal of Environmental Sciences*, 7(3), 25–30.
- Garg, A., & Gupta, N. C. (2020). Short-term variability on particulate and gaseous emissions induced by fireworks during Diwali celebrations for two successive years in outdoor air of an urban area in Delhi, India. *SN Applied Sciences*, 2(12), 1–14. <https://doi.org/10.1007/s42452-020-03906-5>
- Géhin, E., Ramalho, O., & Kirchner, S. (2008). Size distribution and emission rate measurement of fine and ultrafine particle from indoor human activities. *Atmospheric Environment*, 42(35), 8341–8352. <https://doi.org/10.1016/j.atmosenv.2008.07.021>
- Geiser, M., & Kreyling, W. G. (2010). Deposition and biokinetics of inhaled nanoparticles. *Particle and Fibre Toxicology*, 7(i), 1–17. <https://doi.org/10.1186/1743-8977-7-2>
- Ghei, D., & Sane, R. (2018). Estimates of air pollution in Delhi from the burning of firecrackers during the festival of Diwali. *PLoS ONE*, 13(8), 1–11. <https://doi.org/10.1371/journal.pone.0200371>
- Giemsä, E., Soentgen, J., Kusch, T., Beck, C., Münkler, C., Cyrys, J., & Pitz, M. (2021a). Influence of Local Sources and Meteorological Parameters on the Spatial and Temporal Distribution of Ultrafine Particles in Augsburg, Germany. *Frontiers in Environmental Science*, 8(September). <https://doi.org/10.3389/fenvs.2020.609846>

- Giemsma, E., Soentgen, J., Kusch, T., Beck, C., Münkkel, C., Cyrus, J., & Pitz, M. (2021b). Influence of Local Sources and Meteorological Parameters on the Spatial and Temporal Distribution of Ultrafine Particles in Augsburg, Germany. *Frontiers in Environmental Science*, 8(January), 1–18. <https://doi.org/10.3389/fenvs.2020.609846>
- Glencross, D. A., Ho, T. R., Camiña, N., Hawrylowicz, C. M., & Pfeffer, P. E. (2020). Air pollution and its effects on the immune system. *Free Radical Biology and Medicine*, 151(January), 56–68. <https://doi.org/10.1016/j.freeradbiomed.2020.01.179>
- Glossary on air pollution. (1980). In *Glossary on air pollution*. (Issue 9). [https://doi.org/10.1016/0160-4120\(81\)90119-7](https://doi.org/10.1016/0160-4120(81)90119-7)
- Goel, A., & Kumar, P. (2015). Characterisation of nanoparticle emissions and exposure at traffic intersections through fast-response mobile and sequential measurements. *Atmospheric Environment*, 107, 374–390. <https://doi.org/10.1016/j.atmosenv.2015.02.002>
- Gómez-Moreno, F. J., Pujadas, M., Plaza, J., Rodríguez-Maroto, J. J., Martínez-Lozano, P., & Artñano, B. (2011). Influence of seasonal factors on the atmospheric particle number concentration and size distribution in Madrid. *Atmospheric Environment*, 45(18), 3169–3180. <https://doi.org/10.1016/j.atmosenv.2011.02.041>
- González, Y., Rodríguez, S., Guerra García, J. C., Trujillo, J. L., & García, R. (2011). Ultrafine particles pollution in urban coastal air due to ship emissions. *Atmospheric Environment*, 45(28), 4907–4914. <https://doi.org/10.1016/j.atmosenv.2011.06.002>
- Goossens, J., Jonckheere, A. C., Dupont, L. J., & Bullens, D. M. A. (2021). Air pollution and the airways: Lessons from a century of human urbanization. *Atmosphere*, 12(7), 1–22. <https://doi.org/10.3390/atmos12070898>
- Goyal, P., Gulia, S., & Goyal, S. K. (2021). Identification of air pollution hotspots in urban areas - An innovative approach using monitored concentrations data. *Science of the Total Environment*, 798, 149143. <https://doi.org/10.1016/j.scitotenv.2021.149143>
- Größ, J., Hamed, A., Sonntag, A., Spindler, G., Elina Manninen, H., Nieminen, T.,



- Kulmala, M., Hörrak, U., Plass-Dülmer, C., Wiedensohler, A., & Birmili, W. (2018). Atmospheric new particle formation at the research station Melpitz, Germany: Connection with gaseous precursors and meteorological parameters. *Atmospheric Chemistry and Physics*, 18(3), 1835–1861. <https://doi.org/10.5194/acp-18-1835-2018>
- Guascito, M. R., Lionetto, M. G., Mazzotta, F., Conte, M., Giordano, M. E., Caricato, R., De Bartolomeo, A. R., Dinoi, A., Cesari, D., Merico, E., Mazzotta, L., & Contini, D. (2023). Characterisation of the correlations between oxidative potential and in vitro biological effects of PM10 at three sites in the central Mediterranean. *Journal of Hazardous Materials*, 448(December 2022), 130872. <https://doi.org/10.1016/j.jhazmat.2023.130872>
- Guo, L., Ma, Y., Tigabu, M., Guo, X., Zheng, W., & Guo, F. (2020). Emission of atmospheric pollutants during forest fire in boreal region of China. *Environmental Pollution*, 264, 114709. <https://doi.org/10.1016/j.envpol.2020.114709>
- Gupta, P., Satsangi, M., Satsangi, G. P., Jangid, A., Liu, Y., Pani, S. K., & Kumar, R. (2020). Exposure to respirable and fine dust particle over North-Central India: chemical characterization, source interpretation, and health risk analysis. *Environmental Geochemistry and Health*, 42(7), 2081–2099. <https://doi.org/10.1007/s10653-019-00461-w>
- Gurjar, B. R., Butler, T. M., Lawrence, M. G., & Lelieveld, J. (2008). Evaluation of emissions and air quality in megacities. *Atmospheric Environment*, 42(7), 1593–1606. <https://doi.org/10.1016/j.atmosenv.2007.10.048>
- Guttikunda, S. K., & Calori, G. (2013). A GIS based emissions inventory at 1 km × 1 km spatial resolution for air pollution analysis in Delhi, India. *Atmospheric Environment*, 67, 101–111. <https://doi.org/10.1016/j.atmosenv.2012.10.040>
- Guttikunda, S. K., & Gurjar, B. R. (2012). Role of meteorology in seasonality of air pollution in megacity Delhi, India. *Environmental Monitoring and Assessment*, 184(5), 3199–3211. <https://doi.org/10.1007/s10661-011-2182-8>
- Harrison, R. M., Beddows, D. C. S., Alam, M. S., Singh, A., Brean, J., Xu, R., Kotthaus, S., & Grimmond, S. (2019). Interpretation of particle number size distributions measured across an urban area during the FASTER campaign. *Atmospheric Chemistry and Physics*, 19(1), 39–55. <https://doi.org/10.5194/acp->

19-39-2019

- Harrison, R. M., & Harrison, R. M. (2020). Airborne particulate matter Author for correspondence : *Philosophical Transactions of the Royal Society A*, 378.
- Harrison, R. M., Rob Mackenzie, A., Xu, H., Alam, M. S., Nikolova, I., Zhong, J., Singh, A., Zeraati-Rezaei, S., Stark, C., Beddows, D. C. S., Liang, Z., Xu, R., & Cai, X. (2018). Diesel exhaust nanoparticles and their behaviour in the atmosphere. *Proceedings of the Royal Society A: Mathematical, Physical and Engineering Sciences*, 474(2220). <https://doi.org/10.1098/rspa.2018.0492>
- Harrison, R. M., Stedman, J., & Derwent, D. (2008). New Directions: Why are PM10 concentrations in Europe not falling? *Atmospheric Environment*, 42(3), 603–606. <https://doi.org/10.1016/j.atmosenv.2007.11.023>
- Hashad, K., Steffens, J. T., Baldauf, R. W., Heist, D. K., Deshmukh, P., & Zhang, K. M. (2024). Resolving the effect of roadside vegetation barriers as a near-road air pollution mitigation strategy. *Environmental Science: Advances*, 24(3). <https://doi.org/10.1039/d3va00220a>
- Hassan, S. K., El-Abssawy, A. A., & Khoder, M. I. (2015). Chemical Composition, Characterization and Factors Affecting Household Dust (<20 &#181;m) in Greater Cairo, Egypt. *Open Journal of Air Pollution*, 04(04), 184–197. <https://doi.org/10.4236/ojap.2015.44016>
- Hays, M. D., Fine, P. M., Geron, C. D., Kleeman, M. J., & Gullett, B. K. (2005). Open burning of agricultural biomass: Physical and chemical properties of particle-phase emissions. *Atmospheric Environment*, 39(36), 6747–6764. <https://doi.org/10.1016/j.atmosenv.2005.07.072>
- He, C., Morawska, L., Hitchins, J., & Gilbert, D. (2004). Contribution from indoor sources to particle number and mass concentrations in residential houses. *Atmospheric Environment*, 38(21), 3405–3415. <https://doi.org/10.1016/j.atmosenv.2004.03.027>
- Hodnebrog, O., Myhre, G., Forster, P. M., Sillmann, J., & Samset, B. H. (2016). Local biomass burning is a dominant cause of the observed precipitation reduction in southern Africa. *Nature Communications*, 7. <https://doi.org/10.1038/ncomms11236>
- Horwell, C. J., & Baxter, P. J. (2006). The respiratory health hazards of volcanic ash:

- A review for volcanic risk mitigation. *Bulletin of Volcanology*, 69(1), 1–24. <https://doi.org/10.1007/s00445-006-0052-y>
- Hussein, T., Al-Abdallat, A., Saleh, S. S. A., & Al-Kloub, M. (2022). Estimation of the Seasonal Inhaled Deposited Dose of Particulate Matter in the Respiratory System of Urban Individuals Living in an Eastern Mediterranean City. *International Journal of Environmental Research and Public Health*, 19(7). <https://doi.org/10.3390/ijerph19074303>
- Hussein, T., Dada, L., Hakala, S., Petäjä, T., & Kulmala, M. (2019). Urban aerosol particle size characterization in Eastern Mediterranean Conditions. *Atmosphere*, 10(11), 1–21. <https://doi.org/10.3390/atmos10110710>
- Hussein, T., Glytsos, T., Ondráček, J., Dohányosová, P., Ždímal, V., Hämeri, K., Lazaridis, M., Smolík, J., & Kulmala, M. (2006). Particle size characterization and emission rates during indoor activities in a house. *Atmospheric Environment*, 40(23), 4285–4307. <https://doi.org/10.1016/j.atmosenv.2006.03.053>
- Ibald-Mulli, A., Wichmann, H. E., Kreyling, W., & Peters, A. (2002). Epidemiological evidence on health effects of ultrafine particles. *Journal of Aerosol Medicine: Deposition, Clearance, and Effects in the Lung*, 15(2), 189–201. <https://doi.org/10.1089/089426802320282310>
- Isaxon, C., Gudmundsson, A., Nordin, E. Z., Lönnblad, L., Dahl, A., Wieslander, G., Bohgard, M., & Wierzbicka, A. (2015). Contribution of indoor-generated particles to residential exposure. *Atmospheric Environment*, 106, 458–466. <https://doi.org/10.1016/j.atmosenv.2014.07.053>
- Izhar, S., Rajput, P., & Gupta, T. (2018). Variation of particle number and mass concentration and associated mass deposition during Diwali festival. *Urban Climate*, 24(October), 1027–1036. <https://doi.org/10.1016/j.uclim.2017.12.005>
- Jeong, C. H., Traub, A., & Evans, G. J. (2017). Exposure to ultrafine particles and black carbon in diesel-powered commuter trains. *Atmospheric Environment*, 155, 46–52. <https://doi.org/10.1016/j.atmosenv.2017.02.015>
- Jorga, S. D., Florou, K., Patoulias, D., & Pandis, S. N. (2023). New particle formation and growth during summer in an urban environment: a dual chamber study. *Atmospheric Chemistry and Physics*, 23(1), 85–97. <https://doi.org/10.5194/acp-23-85-2023>

- Jose, S., Mishra, A. K., Lodhi, N. K., Sharma, S. K., & Singh, S. (2021). Characteristics of Aerosol Size Distributions and New Particle Formation Events at Delhi: An Urban Location in the Indo-Gangetic Plains. *Frontiers in Earth Science*, 9(December), 1–12. <https://doi.org/10.3389/feart.2021.750111>
- Joshi, M., Khan, A., Anand, S., & Sapra, B. K. (2016). Size evolution of ultrafine particles: Differential signatures of normal and episodic events. *Environmental Pollution*, 208, 354–360. <https://doi.org/10.1016/j.envpol.2015.10.001>
- Kalaiarasan, G., Kumar, P., Tomson, M., Zavala-Reyes, J. C., Porter, A. E., Young, G., Sephton, M. A., Abubakar-Waziri, H., Pain, C. C., Adcock, I. M., Mumby, S., Dilliway, C., Fang, F., Arcucci, R., & Chung, K. F. (2024). Particle Number Size Distribution in Three Different Microenvironments of London. *Atmosphere*, 15(1). <https://doi.org/10.3390/atmos15010045>
- Kalkavouras, P., Bougiatioti, A., Grivas, G., Stavroulas, I., Kalivitis, N., Liakakou, E., Gerasopoulos, E., Pilinis, C., & Mihalopoulos, N. (2020). On the regional aspects of new particle formation in the Eastern Mediterranean: A comparative study between a background and an urban site based on long term observations. *Atmospheric Research*, 239(August 2019), 104911. <https://doi.org/10.1016/j.atmosres.2020.104911>
- Kamara, A. A., & Harrison, R. M. (2021). Analysis of the air pollution climate of a central urban roadside supersite: London, Marylebone Road. *Atmospheric Environment*, 258(May), 118479. <https://doi.org/10.1016/j.atmosenv.2021.118479>
- Kanawade, V. P., Srivastava, A. K., Ram, K., Asmi, E., Vakkari, V., Soni, V. K., Varaprasad, V., & Sarangi, C. (2020a). What caused severe air pollution episode of November 2016 in New Delhi? *Atmospheric Environment*, 222(November 2016), 117125. <https://doi.org/10.1016/j.atmosenv.2019.117125>
- Kanawade, V. P., Srivastava, A. K., Ram, K., Asmi, E., Vakkari, V., Soni, V. K., Varaprasad, V., & Sarangi, C. (2020b). What caused severe air pollution episode of November 2016 in New Delhi? *Atmospheric Environment*, 222(November 2019), 117125. <https://doi.org/10.1016/j.atmosenv.2019.117125>
- Kanawade, V. P., Tripathi, S. N., Bhattu, D., & Shamjad, P. M. (2014). Sub-micron particle number size distributions characteristics at an urban location, Kanpur, in

- the Indo-Gangetic Plain. *Atmospheric Research*, 147–148, 121–132. <https://doi.org/10.1016/j.atmosres.2014.05.010>
- Kanawade, V. P., Tripathi, S. N., Chakraborty, A., & Yu, H. (2020). Chemical characterization of sub-micron aerosols during new particle formation in an urban atmosphere. *Aerosol and Air Quality Research*, 20(6), 1294–1305. <https://doi.org/10.4209/aaqr.2019.04.0196>
- Kanawade, V. P., Tripathi, S. N., Siingh, D., Gautam, A. S., Srivastava, A. K., Kamra, A. K., Soni, V. K., & Sethi, V. (2014). Observations of new particle formation at two distinct Indian subcontinental urban locations. *Atmospheric Environment*, 96, 370–379. <https://doi.org/10.1016/j.atmosenv.2014.08.001>
- Karl, M., Pirjola, L., Karppinen, A., Jalkanen, J. P., Ramacher, M. O. P., & Kukkonen, J. (2020). Modeling of the concentrations of ultrafine particles in the plumes of ships in the vicinity of major harbors. *International Journal of Environmental Research and Public Health*, 17(3), 1–24. <https://doi.org/10.3390/ijerph17030777>
- Kaskaoutis, D. G., Petrinoli, K., Grivas, G., Kalkavouras, P., Tsagkaraki, M., Tavernaraki, K., Papoutsidaki, K., Stavroulas, I., Paraskevopoulou, D., Bougiatioti, A., Liakakou, E., Rashki, A., Sotiropoulou, R. E. P., Tagaris, E., Gerasopoulos, E., & Mihalopoulos, N. (2024). Impact of peri-urban forest fires on air quality and aerosol optical and chemical properties: The case of the August 2021 wildfires in Athens, Greece. *Science of the Total Environment*, 907(July 2023), 168028. <https://doi.org/10.1016/j.scitotenv.2023.168028>
- Kasper, A., Aufdenblatten, S., Forss, A., Mohr, M., & Burtscher, H. (2007). Particulate Emissions from a Low-Speed Marine Diesel Engine. *Aerosol Science and Technology*, 41(1), 24–32. <https://doi.org/10.1080/02786820601055392>
- Kecorius, S., Kivekäs, N., Kristensson, A., Tuch, T., Covert, D. S., Birmili, W., Lihavainen, H., Hyvärinen, A. P., Martinsson, J., Sporre, M. K., Swietlicki, E., Wiedensohler, A., & Ulevicius, V. (2016). Significant increase of aerosol number concentrations in air masses crossing a densely trafficked sea area. *Oceanologia*, 58(1), 1–12. <https://doi.org/10.1016/j.oceano.2015.08.001>
- Kerminen, V. M., Chen, X., Vakkari, V., Petäjä, T., Kulmala, M., & Bianchi, F. (2018). Atmospheric new particle formation and growth: Review of field observations.

- Environmental Research Letters*, 13(10). <https://doi.org/10.1088/1748-9326/aadf3c>
- Keuken, M. P., Moerman, M., Zandveld, P., Henzing, J. S., & Hoek, G. (2015). Total and size-resolved particle number and black carbon concentrations in urban areas near Schiphol airport (the Netherlands). *Atmospheric Environment*, 104, 132–142. <https://doi.org/10.1016/j.atmosenv.2015.01.015>
- Khan, T., Lawrence, A., Dwivedi, S., Arif, S., Dwivedi, S., Upadhyay, A., Abraham, A., & Roberts, V. (2022). Air Pollution Trend and Variation during a Mega Festival of Firecrackers (Diwali) in Context to COVID-19 Pandemic. *Asian Journal of Atmospheric Environment*, 16(3). <https://doi.org/10.5572/ajae.2022.016>
- Kim, S. Y., Bechle, M., Hankey, S., Sheppard, L., Szpiro, A. A., & Marshall, J. D. (2020). Concentrations of criteria pollutants in the contiguous U.S., 1979 – 2015: Role of prediction model parsimony in integrated empirical geographic regression. *PLoS ONE*, 15(2), 1–21. <https://doi.org/10.1371/journal.pone.0228535>
- Kittelson, D., Khalek, I., McDonald, J., Stevens, J., & Giannelli, R. (2022). Particle emissions from mobile sources: Discussion of ultrafine particle emissions and definition. *Journal of Aerosol Science*, 159(October 2021), 105881. <https://doi.org/10.1016/j.jaerosci.2021.105881>
- Klemm, O., Ahrens, A., Arnschuld, M., Bethke, R., Berger, D. F., Blankenhau, K., Blauth, L., Breuer, B., Buchholz, S., Burek, F., Ehrnsperger, L., Funken, S., Henninger, E., Hohl, J., Jöllenbeck, N., Kirgasser, P., Kuhls, M., Paas, B., Roters, L. A., ... Schlüter, H. (2022). The Impact of Traffic and Meteorology on Urban Particle Mass and Particle Number Concentrations: Student-Led Studies Using Mobile Measurements before, during, and after the COVID-19 Pandemic Lockdowns. *Atmosphere*, 13(1), 1–16. <https://doi.org/10.3390/atmos13010062>
- Klepeis, N. E., Nelson, W. C., Ott, W. R., Robinson, J. P., Tsang, A. M., Switzer, P., Behar, J. V, Hern, C., & Engelmann, W. H. (2001). *Klepeis2001.Pdf. September 1998*.
- Kodros, J. K., Volckens, J., Jathar, S. H., & Pierce, J. R. (2018). Ambient Particulate Matter Size Distributions Drive Regional and Global Variability in Particle

- Deposition in the Respiratory Tract. *GeoHealth*, 2(10), 298–312. <https://doi.org/10.1029/2018GH000145>
- Kompalli, S. K., Babu, S. S., Udayasoorian, C., & Jayabalakrishnan, R. M. (2018). Role of anthropogenic emissions and meteorology on ultrafine particle bursts over a high altitude site in Western Ghats during pre-monsoon. *Journal of Atmospheric and Solar-Terrestrial Physics*, 179, 378–388. <https://doi.org/10.1016/j.jastp.2018.09.001>
- Kompalli, S. K., Nair, V. S., Jayachandran, V., Gogoi, M. M., & Babu, S. S. (2020). Particle number size distributions and new particle formation events over the northern Indian Ocean during continental outflow. *Atmospheric Environment*, 238, 117719. <https://doi.org/10.1016/j.atmosenv.2020.117719>
- Kontkanen, J., Deng, C., Fu, Y., Dada, L., Zhou, Y., Cai, J., Daellenbach, K. R., Hakala, S., Kokkonen, T. V., Lin, Z., Liu, Y., Wang, Y., Yan, C., Petäjä, T., Jiang, J., Kulmala, M., & Paasonen, P. (2020). Size-resolved particle number emissions in Beijing determined from measured particle size distributions. *Atmospheric Chemistry and Physics*, 20(19), 11329–11348. <https://doi.org/10.5194/acp-20-11329-2020>
- Krecl, P., Johansson, C., Norman, M., Silvergren, S., Burman, L., Mollinedo, E. M., & Targino, A. C. (2024a). Long-term trends of black carbon and particle number concentrations and their vehicle emission factors in Stockholm. *Environmental Pollution*, 347(February). <https://doi.org/10.1016/j.envpol.2024.123734>
- Krecl, P., Johansson, C., Norman, M., Silvergren, S., Burman, L., Mollinedo, E. M., & Targino, A. C. (2024b). Long-term trends of black carbon and particle number concentrations and their vehicle emission factors in Stockholm. *Environmental Pollution*, 347(January). <https://doi.org/10.1016/j.envpol.2024.123734>
- Kronbauer, M. A., Izquierdo, M., Dai, S., Waanders, F. B., Wagner, N. J., Mastalerz, M., Hower, J. C., Oliveira, M. L. S., Taffarel, S. R., Bizani, D., & Silva, L. F. O. (2013). Geochemistry of ultra-fine and nano-compounds in coal gasification ashes: A synoptic view. *Science of the Total Environment*, 456–457, 95–103. <https://doi.org/10.1016/j.scitotenv.2013.02.066>
- Kulkarni, S. H., Ghude, S. D., Jena, C., Karumuri, R. K., Sinha, B., Sinha, V., Kumar, R., Soni, V. K., & Khare, M. (2020). How Much Does Large-Scale Crop Residue

- Burning Affect the Air Quality in Delhi? *Environmental Science & Technology*, 54(8), 4790–4799. <https://doi.org/10.1021/acs.est.0c00329>
- Kulmala, M., Petäjä, T., Nieminen, T., Sipilä, M., Manninen, H. E., Lehtipalo, K., Dal Maso, M., Aalto, P. P., Junninen, H., Paasonen, P., Riipinen, I., Lehtinen, K. E. J., Laaksonen, A., & Kerminen, V. M. (2012). Measurement of the nucleation of atmospheric aerosol particles. *Nature Protocols*, 7(9), 1651–1667. <https://doi.org/10.1038/nprot.2012.091>
- Kulmala, M., Vehkamäki, H., Petäjä, T., Dal Maso, M., Lauri, A., Kerminen, V. M., Birmili, W., & McMurry, P. H. (2004). Formation and growth rates of ultrafine atmospheric particles: A review of observations. *Journal of Aerosol Science*, 35(2), 143–176. <https://doi.org/10.1016/j.jaerosci.2003.10.003>
- Kumar, P., Gurjar, B. R., Nagpure, A. S., & Harrison, R. M. (2011). Preliminary estimates of nanoparticle number emissions from road vehicles in megacity Delhi and associated health impacts. *Environmental Science and Technology*, 45(13), 5514–5521. <https://doi.org/10.1021/es2003183>
- Kumar, P., Morawska, L., Birmili, W., Paasonen, P., Hu, M., Kulmala, M., Harrison, R. M., Norford, L., & Britter, R. (2014). Ultrafine particles in cities. *Environment International*, 66, 1–10. <https://doi.org/10.1016/j.envint.2014.01.013>
- Kumar, P., Robins, A., Vardoulakis, S., & Britter, R. (2010). A review of the characteristics of nanoparticles in the urban atmosphere and the prospects for developing regulatory controls. *Atmospheric Environment*, 44(39), 5035–5052. <https://doi.org/10.1016/j.atmosenv.2010.08.016>
- Kumar, P., Wiedensohler, A., Birmili, W., Quincey, P., & Hallquist, M. (2016). Ultrafine Particles Pollution and Measurements. In *Comprehensive Analytical Chemistry* (Vol. 73). Elsevier Ltd. <https://doi.org/10.1016/bs.coac.2016.04.004>
- Kumar, R. R., Soni, V. K., & Jain, M. K. (2020). Evaluation of spatial and temporal heterogeneity of black carbon aerosol mass concentration over India using three year measurements from IMD BC observation network. *Science of the Total Environment*, 723, 138060. <https://doi.org/10.1016/j.scitotenv.2020.138060>
- Kwon, H. S., Ryu, M. H., & Carlsten, C. (2020). Ultrafine particles: unique physicochemical properties relevant to health and disease. *Experimental and Molecular Medicine*, 52(3), 318–328. <https://doi.org/10.1038/s12276-020-0405->



- Lazaridis, M., Latos, M., Aleksandropoulou, V., Hov, O., Papayannis, A., & Tørseth, K. (2008). Contribution of forest fire emissions to atmospheric pollution in Greece. *Air Quality, Atmosphere and Health*, 1(3), 143–158. <https://doi.org/10.1007/s11869-008-0020-0>
- Lee, S. H., Gordon, H., Yu, H., Lehtipalo, K., Haley, R., Li, Y., & Zhang, R. (2019). New Particle Formation in the Atmosphere: From Molecular Clusters to Global Climate. *Journal of Geophysical Research: Atmospheres*, 124(13), 7098–7146. <https://doi.org/10.1029/2018JD029356>
- Lehtipalo, K., Yan, C., Dada, L., Bianchi, F., Xiao, M., Wagner, R., Stolzenburg, D., Ahonen, L. R., Amorim, A., Baccarini, A., Bauer, P. S., Baumgartner, B., Bergen, A., Bernhammer, A. K., Breitenlechner, M., Brilke, S., Buchholz, A., Mazon, S. B., Chen, D., ... Worsnop, D. R. (2018). Multicomponent new particle formation from sulfuric acid, ammonia, and biogenic vapors. *Science Advances*, 4(12), 1–10. <https://doi.org/10.1126/sciadv.aau5363>
- Leizel Madueño, Simonas Kecorius, Jakob Löndahl, Jürgen Schnelle-Kreis, Alfred Wiedensohler, and Pöhlker, M. (n.d.). 2022 *A novel in-situ method to determine.pdf*.
- Li Ma, Ying Zhang, Zhuohui Lin, Ying Zhou, Chao Yan, Yusheng Zhang, Wenshuo Zhou, Wei Ma, Chenjie Hua, Xiaoxiao Li, Chenjuan Deng, Yu Qi, Lubna Dada, Hongyan Li, Federico Bianchi, Tuukka Petaj, Juha Kangasluoma, Jingkun Jiang, Sijin Liu, Tareq Hussein, Ma, Y. L. (n.d.). 2022 *Deposition potential of 0.003–10 µm ambient particles in the humidified.pdf*.
- Li, Q. Q., Guo, Y. T., Yang, J. Y., & Liang, C. S. (2023). Review on main sources and impacts of urban ultrafine particles: Traffic emissions, nucleation, and climate modulation. *Atmospheric Environment: X*, 19(March), 100221. <https://doi.org/10.1016/j.aeaoa.2023.100221>
- Liang, C. S., Wu, H., Li, H. Y., Zhang, Q., Li, Z., & He, K. Bin. (2020). Efficient data preprocessing, episode classification, and source apportionment of particle number concentrations. *Science of the Total Environment*, 744, 1–17. <https://doi.org/10.1016/j.scitotenv.2020.140923>
- Lingard, J. J. N., Agus, E. L., Young, D. T., Andrews, G. E., & Tomlin, A. S. (2006).

- Observations of urban airborne particle number concentrations during rush-hour conditions: Analysis of the number based size distributions and modal parameters. *Journal of Environmental Monitoring*, 8(12), 1203–1218. <https://doi.org/10.1039/b611479b>
- Liu, T., Marlier, M. E., DeFries, R. S., Westervelt, D. M., Xia, K. R., Fiore, A. M., Mickley, L. J., Cusworth, D. H., & Milly, G. (2018). Seasonal impact of regional outdoor biomass burning on air pollution in three Indian cities: Delhi, Bengaluru, and Pune. *Atmospheric Environment*, 172(September 2017), 83–92. <https://doi.org/10.1016/j.atmosenv.2017.10.024>
- Ljungman, P. L. S., Andersson, N., Stockfelt, L., Andersson, E. M., Sommar, J. N., Eneroth, K., Gidhagen, L., Johansson, C., Lager, A., Leander, K., Molnar, P., Pedersen, N. L., Rizzuto, D., Rosengren, A., Segersson, D., Wennberg, P., Barregard, L., Forsberg, B., Sallsten, G., ... Pershagen, G. (2019). Long-term exposure to particulate air pollution, black carbon, and their source components in relation to ischemic heart disease and stroke. *Environmental Health Perspectives*, 127(10), 1–11. <https://doi.org/10.1289/EHP4757>
- Longo, B. M., Rossignol, A., & Green, J. B. (2008). Cardiorespiratory health effects associated with sulphurous volcanic air pollution. *Public Health*, 122(8), 809–820. <https://doi.org/10.1016/j.puhe.2007.09.017>
- Longo, B. M., & Yang, W. (2008). Acute bronchitis and volcanic air pollution: A community-based cohort study at Kilauea Volcano, Hawai'i, USA. *Journal of Toxicology and Environmental Health - Part A: Current Issues*, 71(24), 1565–1571. <https://doi.org/10.1080/15287390802414117>
- Lorelei de Jesus, A., Thompson, H., Knibbs, L. D., Kowalski, M., Cyrus, J., Niemi, J. V., Kousa, A., Timonen, H., Luoma, K., Petäjä, T., Beddows, D., Harrison, R. M., Hopke, P., & Morawska, L. (2020). Long-term trends in PM<sub>2.5</sub> mass and particle number concentrations in urban air: The impacts of mitigation measures and extreme events due to changing climates. *Environmental Pollution*, 263. <https://doi.org/10.1016/j.envpol.2020.114500>
- Losacco, C., & Perillo, A. (2018). Particulate matter air pollution and respiratory impact on humans and animals. *Environmental Science and Pollution Research*, 25(34), 33901–33910. <https://doi.org/10.1007/s11356-018-3344-9>

- Machaczka, O., Jirik, V., Brezinova, V., Vrtkova, A., Miturova, H., Riedlova, P., Dalecka, A., Hermanova, B., Slachtova, H., Siemiatkowski, G., Osrodka, L., & Sram, R. J. (2021). Evaluation of fine and ultrafine particles proportion in airborne dust in an industrial area. *International Journal of Environmental Research and Public Health*, 18(17). <https://doi.org/10.3390/ijerph18178915>
- Manisalidis, I., Stavropoulou, E., Stavropoulos, A., & Bezirtzoglou, E. (2020). Environmental and Health Impacts of Air Pollution: A Review. *Frontiers in Public Health*, 8(February), 1–13. <https://doi.org/10.3389/fpubh.2020.00014>
- Manojkumar, N., Srimuruganandam, B., & Shiva Nagendra, S. M. (2019). Application of multiple-path particle dosimetry model for quantifying age specified deposition of particulate matter in human airway. *Ecotoxicology and Environmental Safety*, 168(October 2018), 241–248. <https://doi.org/10.1016/j.ecoenv.2018.10.091>
- Mao, M., Zhang, X., Shao, Y., & Yin, Y. (2020). Spatiotemporal variations and factors of air quality in urban central china during 2013–2015. *International Journal of Environmental Research and Public Health*, 17(1). <https://doi.org/10.3390/ijerph17010229>
- Marabini, L., Ozgen, S., Turacchi, S., Aminti, S., Arnaboldi, F., Lonati, G., Fermo, P., Corbella, L., Valli, G., Bernardoni, V., Dell'Acqua, M., Vecchi, R., Becagli, S., Caruso, D., Corrado, L. G., & Marinovich, M. (2017). Ultrafine particles (UFPs) from domestic wood stoves: genotoxicity in human lung carcinoma A549 cells. *Mutation Research - Genetic Toxicology and Environmental Mutagenesis*, 820(June), 39–46. <https://doi.org/10.1016/j.mrgentox.2017.06.001>
- Marval, J., & Tronville, P. (2022). Ultrafine particles: A review about their health effects, presence, generation, and measurement in indoor environments. *Building and Environment*, 216(December 2021), 108992. <https://doi.org/10.1016/j.buildenv.2022.108992>
- Mayer, K. J., Wang, X., Santander, M. V., Mitts, B. A., Sauer, J. S., Sultana, C. M., Cappa, C. D., & Prather, K. A. (2020). Secondary Marine Aerosol Plays a Dominant Role over Primary Sea Spray Aerosol in Cloud Formation. *ACS Central Science*, 6(12), 2259–2266. <https://doi.org/10.1021/acscentsci.0c00793>
- Mazaheri, M., Lin, W., Clifford, S., Yue, D., Zhai, Y., Xu, M., Rizza, V., & Morawska,

- L. (2019). Characteristics of school children's personal exposure to ultrafine particles in Heshan, Pearl River Delta, China – A pilot study. *Environment International*, 132(August), 105134. <https://doi.org/10.1016/j.envint.2019.105134>
- Mazaheri, M., Reche, C., Rivas, I., Crilley, L. R., Álvarez-Pedrerol, M., Viana, M., Tobias, A., Alastuey, A., Sunyer, J., Querol, X., & Morawska, L. (2016). Variability in exposure to ambient ultrafine particles in urban schools: Comparative assessment between Australia and Spain. *Environment International*, 88, 142–149. <https://doi.org/10.1016/j.envint.2015.12.029>
- McCawley, M. A., Berakis, M. T., & Kent, M. S. (2001). Ultrafine Beryllium Number Concentration as a Possible Metric for Chronic Beryllium Disease Risk. *Applied Occupational and Environmental Hygiene*, 16(5), 631–638. <https://doi.org/10.1080/10473220120812>
- Mcguinness, D. (2008). Integrating Inter-disciplinary Science Data with Semantic. *Integration The Vlsi Journal*, May.
- Mejía, J. F., Choy, S. L., Mengersen, K., & Morawska, L. (2011). Methodology for assessing exposure and impacts of air pollutants in school children: Data collection, analysis and health effects - A literature review. *Atmospheric Environment*, 45(4), 813–823. <https://doi.org/10.1016/j.atmosenv.2010.11.009>
- Meskhidze, N., Jaimes-Correa, J. C., Petters, M. D., Royalty, T. M., Phillips, B. N., Zimmerman, A., & Reed, R. (2019). Possible Wintertime Sources of Fine Particles in an Urban Environment. *Journal of Geophysical Research: Atmospheres*, 124(23), 13055–13070. <https://doi.org/10.1029/2019JD031367>
- Miezite, L. E., Ameztegui, A., De Cáceres, M., Coll, L., Morán-Ordóñez, A., Vega-García, C., & Rodrigues, M. (2022). Trajectories of wildfire behavior under climate change. Can forest management mitigate the increasing hazard? *Journal of Environmental Management*, 322(March). <https://doi.org/10.1016/j.jenvman.2022.116134>
- Mikkonen, S., Németh, Z., Varga, V., Weidinger, T., Leinonen, V., Yli-Juuti, T., & Salma, I. (2020). Decennial time trends and diurnal patterns of particle number concentrations in a central European city between 2008 and 2018. *Atmospheric Chemistry and Physics*, 20(20), 12247–12263. <https://doi.org/10.5194/acp-20->

12247-2020

- Mishra, R. K., Pandey, A., Pandey, G., & Kumar, A. (2019). The effect of odd-even driving scheme on PM 2.5 and PM 1.0 emission. *Transportation Research Part D: Transport and Environment*, 67(January), 541–552. <https://doi.org/10.1016/j.trd.2019.01.005>
- Mishra, R. K., Shukla, A., Parida, M., & Pandey, G. (2016). Urban roadside monitoring and prediction of CO, NO<sub>2</sub> and SO<sub>2</sub> dispersion from on-road vehicles in megacity Delhi. *Transportation Research Part D: Transport and Environment*, 46(2), 157–165. <https://doi.org/10.1016/j.trd.2016.03.019>
- Mishra, S., Tripathi, S. N., Kanawade, V. P., Haslett, S. L., Dada, L., Ciarelli, G., Kumar, V., Singh, A., Bhattu, D., Rastogi, N., Daellenbach, K. R., Ganguly, D., Gargava, P., Slowik, J. G., Kulmala, M., Mohr, C., El-Haddad, I., & Prevot, A. S. H. (2023). Rapid night-time nanoparticle growth in Delhi driven by biomass-burning emissions. *Nature Geoscience*, 16(3), 224–230. <https://doi.org/10.1038/s41561-023-01138-x>
- Mogno, C., Palmer, P. I., Marvin, M. R., Sharma, S., Chen, Y., & Wild, O. (2023). Road transport impact on PM<sub>2.5</sub> pollution over Delhi during the post-monsoon season. *Atmospheric Environment: X*, 17(August 2022), 100200. <https://doi.org/10.1016/j.aeaoa.2022.100200>
- Mohan, V., & Kumar, R. (2022). A picture of Delhi 's regional air quality during diminished anthropogenic activities in the COVID - 19 era Indian Council of Medical Research. *Arabian Journal of Geosciences*, 2, 1–14. <https://doi.org/10.1007/s12517-022-10567-8>
- Mohan, V., Kumar Soni, V., & Kumar Mishra, R. (2024). Analysing the impact of day-night road traffic variation on ultrafine particle number size distribution and concentration at an urban site in the megacity Delhi. *Atmospheric Pollution Research*, 15(4), 102065. <https://doi.org/10.1016/j.apr.2024.102065>
- Mohan, V., & Mishra, R. K. (2022). A picture of Delhi's regional air quality during diminished anthropogenic activities in the COVID-19 era. *Arabian Journal of Geosciences*, 15(15), 1–14. <https://doi.org/10.1007/s12517-022-10567-8>
- Mohan, V., Soni, V. K., & Mishra, R. K. (2024). Geographical variability of ultrafine particle concentrations in urban and background regions in India. *Urban Climate*,

- 56(May), 102066. <https://doi.org/10.1016/j.uclim.2024.102066>
- Møller, K. L., Brauer, C., Mikkelsen, S., Bonde, J. P., Loft, S., Helweg-Larsen, K., & Thygesen, L. C. (2020). Cardiovascular disease and long-term occupational exposure to ultrafine particles: A cohort study of airport workers. *International Journal of Hygiene and Environmental Health*, 223(1), 214–219. <https://doi.org/10.1016/j.ijheh.2019.08.010>
- Mönkkönen, P., Koponen, I. K., Lehtinen, K. E. J., Uma, R., Srinivasan, D., Hämeri, K., & Kulmala, M. (2004). Death of nucleation and Aitken mode particles: Observations at extreme atmospheric conditions and their theoretical explanation. *Journal of Aerosol Science*, 35(6), 781–787. <https://doi.org/10.1016/j.jaerosci.2003.12.004>
- Mönkkönen, P., Uma, R., Srinivasan, D., Koponen, I. K., Lehtinen, K. E. J., Hämeri, K., Suresh, R., Sharma, V. P., & Kulmala, M. (2004). Relationship and variations of aerosol number and PM10 mass concentrations in a highly polluted urban environment - New Delhi, India. *Atmospheric Environment*, 38(3), 425–433. <https://doi.org/10.1016/j.atmosenv.2003.09.071>
- Moorthy, K. K., Sreekanth, V., Prakash Chaubey, J., Gogoi, M. M., Suresh Babu, S., Kumar Kompalli, S., Bagare, S. P., Bhatt, B. C., Gaur, V. K., Prabhu, T. P., & Singh, N. S. (2011). Fine and ultrafine particles at a near-free tropospheric environment over the high-altitude station Hanle in the Trans-Himalaya: New particle formation and size distribution. *Journal of Geophysical Research Atmospheres*, 116(20), 1–12. <https://doi.org/10.1029/2011JD016343>
- Morawska, L., Ayoko, G. A., Bae, G. N., Buonanno, G., Chao, C. Y. H., Clifford, S., Fu, S. C., Hänninen, O., He, C., Isaxon, C., Mazaheri, M., Salthammer, T., Waring, M. S., & Wierzbicka, A. (2017). Airborne particles in indoor environment of homes, schools, offices and aged care facilities: The main routes of exposure. *Environment International*, 108(April), 75–83. <https://doi.org/10.1016/j.envint.2017.07.025>
- Morawska, L., He, C., Johnson, G., Guo, H., Uhde, E., & Ayoko, G. (2009). Ultrafine particles in indoor air of a school: Possible role of secondary organic aerosols. *Environmental Science and Technology*, 43(24), 9103–9109. <https://doi.org/10.1021/es902471a>

- Moreno-Ríos, A. L., Tejeda-Benítez, L. P., & Bustillo-Lecompte, C. F. (2022). Sources, characteristics, toxicity, and control of ultrafine particles: An overview. *Geoscience Frontiers*, 13(1). <https://doi.org/10.1016/j.gsf.2021.101147>
- Muñoz-Salazar, J. I., Raga, G. B., Yakobi-Hancock, J., Kim, J. S., Rosas, D., Caudillo, L., Alvarez-Ospina, H., & Ladino, L. A. (2020). Ultrafine aerosol particles in the western Caribbean: A first case study in Merida. *Atmospheric Pollution Research*, 11(10), 1767–1775. <https://doi.org/10.1016/j.apr.2020.07.008>
- Nair, V. S., Moorthy, K. K., & Babu, S. S. (2013). Influence of continental outflow and ocean biogeochemistry on the distribution of fine and ultrafine particles in the marine atmospheric boundary layer over Arabian Sea and Bay of Bengal. *Journal of Geophysical Research Atmospheres*, 118(13), 7321–7331. <https://doi.org/10.1002/jgrd.50541>
- Nim, N., Morris, J., Tekasakul, P., & Dejchanchaiwong, R. (2023). Fine and ultrafine particle emission factors and new diagnostic ratios of PAHs for peat swamp forest fires. *Environmental Pollution*, 335(July), 122237. <https://doi.org/10.1016/j.envpol.2023.122237>
- Nirwan, N., Siddiqui, A., Kannemadugu, H. baba shaeb, Chauhan, P., & Singh, R. P. (2024). Determining hotspots of gaseous criteria air pollutants in Delhi airshed and its association with stubble burning. *Scientific Reports*, 14(1), 1–16. <https://doi.org/10.1038/s41598-023-51140-x>
- Nishanth, T., Praseed, K. M., Rathnakaran, K., Satheesh Kumar, M. K., Ravi Krishna, R., & Valsaraj, K. T. (2012). Atmospheric pollution in a semi-urban, coastal region in India following festival seasons. *Atmospheric Environment*, 47, 295–306. <https://doi.org/10.1016/j.atmosenv.2011.10.062>
- Noble, C. A., Mukerjee, S., Gonzales, M., Rodes, C. E., Lawless, P. A., Natarajan, S., Myers, E. A., Norris, G. A., Smith, L., Özkaynak, H., & Neas, L. M. (2003). Continuous measurement of fine and ultrafine particulate matter, criteria pollutants and meteorological conditions in urban El Paso, Texas. *Atmospheric Environment*, 37(6), 827–840. [https://doi.org/10.1016/S1352-2310\(02\)00935-4](https://doi.org/10.1016/S1352-2310(02)00935-4)
- Nursanto, F. R., Meinen, R., Holzinger, R., Krol, M. C., Liu, X., Dusek, U., Henzing, B., & Fry, J. L. (2023). What chemical species are responsible for new particle formation and growth in the Netherlands? A hybrid positive matrix factorization

- (PMF) analysis using aerosol composition (ACSM) and size (SMPS). *Atmospheric Chemistry and Physics*, 23(17), 10015–10034. <https://doi.org/10.5194/acp-23-10015-2023>
- Olin, M., Patoulias, D., Kuuluvainen, H., Niemi, J. V., Rönkkö, T., Pandis, S. N., Riipinen, I., & Dal Maso, M. (2022). Contribution of traffic-originated nanoparticle emissions to regional and local aerosol levels. *Atmospheric Chemistry and Physics*, 22(2), 1131–1148. <https://doi.org/10.5194/acp-22-1131-2022>
- Oliveira, M., Costa, S., Vaz, J., Fernandes, A., Slezakova, K., Delerue-Matos, C., Teixeira, J. P., Carmo Pereira, M., & Morais, S. (2020). Firefighters exposure to fire emissions: Impact on levels of biomarkers of exposure to polycyclic aromatic hydrocarbons and genotoxic/oxidative-effects. *Journal of Hazardous Materials*, 383(March 2019). <https://doi.org/10.1016/j.jhazmat.2019.121179>
- Oosterlee, A., Drijver, M., Lebre, E., & Brunekreef, B. (1996). Chronic respiratory symptoms in children and adults living along streets with high traffic density. *Occupational and Environmental Medicine*, 53(4), 241–247. <https://doi.org/10.1136/oem.53.4.241>
- Ostro, B., Hu, J., Goldberg, D., Reynolds, P., Hertz, A., Bernstein, L., & Kleeman, M. J. (2015). Associations of mortality with long-term exposures to fine and ultrafine particles, species and sources: Results from the California teachers study Cohort. *Environmental Health Perspectives*, 123(6), 549–556. <https://doi.org/10.1289/ehp.1408565>
- Ott, W. R., Wallace, L. A., McAteer, J. M., & Hildemann, L. M. (2017). Fine and ultrafine particle exposures on 73 trips by car to 65 non-smoking restaurants in the San Francisco Bay Area. *Indoor Air*, 27(1), 205–217. <https://doi.org/10.1111/ina.12292>
- Ou, J., Hu, Q., Liu, H., Xu, S., Wang, Z., Ji, X., Wang, X., Xie, Z., & Kang, H. (2021). Exploring the impact of new particle formation events on PM<sub>2.5</sub> pollution during winter in the Yangtze River Delta, China. *Journal of Environmental Sciences (China)*, 111, 75–83. <https://doi.org/10.1016/j.jes.2021.01.005>
- Ozenen Kavlak, M., Cabuk, S. N., & Cetin, M. (2021). Development of forest fire risk map using geographical information systems and remote sensing capabilities:



- Ören case. *Environmental Science and Pollution Research*, 28(25), 33265–33291. <https://doi.org/10.1007/s11356-021-13080-9>
- P. Biswas, & C. W. (2005). Nanoparticles and the environment. *Journal of the Air and Waste Management Association*, 55(6), 708–746. <https://doi.org/10.1080/10473289.2005.10464656>
- Pandey, A., Brauer, M., Cropper, M. L., Balakrishnan, K., Mathur, P., Dey, S., Turkgulu, B., Kumar, G. A., Khare, M., Beig, G., Gupta, T., Krishnankutty, R. P., Causey, K., Cohen, A. J., Bhargava, S., Aggarwal, A. N., Agrawal, A., Awasthi, S., Bennitt, F., ... Dandona, L. (2021). Health and economic impact of air pollution in the states of India: the Global Burden of Disease Study 2019. *The Lancet Planetary Health*, 5(1), e25–e38. [https://doi.org/10.1016/S2542-5196\(20\)30298-9](https://doi.org/10.1016/S2542-5196(20)30298-9)
- Pant, P., Shukla, A., Kohl, S. D., Chow, J. C., Watson, J. G., & Harrison, R. M. (2015). Characterization of ambient PM<sub>2.5</sub> at a pollution hotspot in New Delhi, India and inference of sources. *Atmospheric Environment*, 109, 178–189. <https://doi.org/10.1016/j.atmosenv.2015.02.074>
- Paraskevopoulou, D., Bougiatioti, A., Stavroulas, I., Fang, T., Lianou, M., Liakakou, E., Gerasopoulos, E., Weber, R., Nenes, A., & Mihalopoulos, N. (2019). Yearlong variability of oxidative potential of particulate matter in an urban Mediterranean environment. *Atmospheric Environment*, 206(August 2018), 183–196. <https://doi.org/10.1016/j.atmosenv.2019.02.027>
- Park, J. U., Kim, H. J., Choi, J., Park, J. S., Heo, J., & Kim, S. W. (2021). Observation of aerosol size distribution and new particle formation under different air masses arriving at the northwesternmost South Korean island in the Yellow Sea. *Atmospheric Research*, 255(February), 105537. <https://doi.org/10.1016/j.atmosres.2021.105537>
- Parkhi, N., Chate, D., Ghude, S. D., Peshin, S., Mahajan, A., Srinivas, R., Surendran, D., Ali, K., Singh, S., Trimbake, H., & Beig, G. (2016). Large inter annual variation in air quality during the annual festival “Diwali” in an Indian megacity. *Journal of Environmental Sciences (China)*, 43, 265–272. <https://doi.org/10.1016/j.jes.2015.08.015>
- Peng, J. F., Hu, M., Wang, Z. B., Huang, X. F., Kumar, P., Wu, Z. J., Guo, S., Yue, D.

- L., Shang, D. J., Zheng, Z., & He, L. Y. (2014). Submicron aerosols at thirteen diversified sites in China: Size distribution, new particle formation and corresponding contribution to cloud condensation nuclei production. *Atmospheric Chemistry and Physics*, 14(18), 10249–10265. <https://doi.org/10.5194/acp-14-10249-2014>
- Perrino, C., Tiwari, S., Catrambone, M., Torre, S. D., Rantica, E., & Canepari, S. (2011). Chemical characterization of atmospheric PM in Delhi, India, during different periods of the year including Diwali festival. *Atmospheric Pollution Research*, 2(4), 418–427. <https://doi.org/10.5094/APR.2011.048>
- Petzold, A., & Schönlinner, M. (2004). Multi-angle absorption photometry - A new method for the measurement of aerosol light absorption and atmospheric black carbon. *Journal of Aerosol Science*, 35(4), 421–441. <https://doi.org/10.1016/j.jaerosci.2003.09.005>
- Pipal, A. S., Jan, R., Satsangi, P. G., Tiwari, S., & Taneja, A. (2014). Study of surface morphology, elemental composition and origin of atmospheric aerosols (PM<sub>2.5</sub> and PM<sub>10</sub>) over Agra, India. *Aerosol and Air Quality Research*, 14(6), 1685–1700. <https://doi.org/10.4209/aaqr.2014.01.0017>
- Pirhadi, M., Mousavi, A., Sowlat, M. H., Janssen, N. A. H., Cassee, F. R., & Sioutas, C. (2020). Relative contributions of a major international airport activities and other urban sources to the particle number concentrations (PNCs) at a nearby monitoring site. *Environmental Pollution*, 260, 114027. <https://doi.org/10.1016/j.envpol.2020.114027>
- Pohl, H. R., & Abadin, H. G. (2008). Chemical mixtures: Evaluation of risk for child-specific exposures in a multi-stressor environment. *Toxicology and Applied Pharmacology*, 233(1), 116–125. <https://doi.org/10.1016/j.taap.2008.01.015>
- Popovicheva, O., Kistler, M., Kireeva, E., Persiantseva, N., Timofeev, M., Kopeikin, V., & Kasper-Giebl, A. (2014). Physicochemical characterization of smoke aerosol during large-scale wildfires: Extreme event of August 2010 in Moscow. *Atmospheric Environment*, 96(August 2011), 405–414. <https://doi.org/10.1016/j.atmosenv.2014.03.026>
- Posner, L. N., & Pandis, S. N. (2015). Sources of ultrafine particles in the Eastern United States. *Atmospheric Environment*, 111, 103–112.

<https://doi.org/10.1016/j.atmosenv.2015.03.033>

- Prabhu, V., Prakash, J., Soni, A., Madhwal, S., & Shridhar, V. (2019). Atmospheric aerosols and inhalable particle number count during Diwali in Dehradun. *City and Environment Interactions*, 2, 100006. <https://doi.org/10.1016/j.cacint.2019.100006>
- Presto, A. A., Saha, P. K., & Robinson, A. L. (2021). Past, present, and future of ultrafine particle exposures in North America. *Atmospheric Environment: X*, 10, 100109. <https://doi.org/10.1016/j.aeaoa.2021.100109>
- Pullabhotla, H. K., & Souza, M. (2022). Air pollution from agricultural fires increases hypertension risk. *Journal of Environmental Economics and Management*, 115(July 2021), 102723. <https://doi.org/10.1016/j.jeem.2022.102723>
- Pushpawela, B., Jayaratne, R., & Morawska, L. (2018). Differentiating between particle formation and growth events in an urban environment. *Atmospheric Chemistry and Physics*, 18(15), 11171–11183. <https://doi.org/10.5194/acp-18-11171-2018>
- Quang, T. N., He, C., Morawska, L., & Knibbs, L. D. (2013). Influence of ventilation and filtration on indoor particle concentrations in urban office buildings. *Atmospheric Environment*, 79, 41–52. <https://doi.org/10.1016/j.atmosenv.2013.06.009>
- Querol, X., Alastuey, A., Rodriguez, S., Plana, F., Mantilla, E., & Ruiz, C. R. (2001). Monitoring of PM<sub>10</sub> and PM<sub>2.5</sub> around primary particulate anthropogenic emission sources. *Atmospheric Environment*, 35(5), 845–858. [https://doi.org/10.1016/S1352-2310\(00\)00387-3](https://doi.org/10.1016/S1352-2310(00)00387-3)
- Rajagopal, K., Mohan, V., & Kumar, R. (2024). Are Delhi residents exposed to lesser particle number concentration due to the firework ban in the city? *Air Quality, Atmosphere & Health*, 0123456789. <https://doi.org/10.1007/s11869-024-01532-3>
- Rajagopal, K., Ramachandran, S., & Mishra, R. K. (2023). Roadside measurements of nanoparticles and their dynamics in relation to traffic sources in Delhi: Impact of restrictions and pollution events. *Urban Climate*, 51(August), 101625. <https://doi.org/10.1016/j.uclim.2023.101625>
- Rajagopal, K., Ramachandran, S., & Mishra, R. K. (2024a). Seasonal variation of

- particle number concentration in a busy urban street with exposure assessment and deposition in human respiratory tract. *Chemosphere*, 366(April), 143470. <https://doi.org/10.1016/j.chemosphere.2024.143470>
- Rajagopal, K., Ramachandran, S., & Mishra, R. K. (2024b). Size resolved particle contribution to vehicle induced ultrafine particle number concentration in a metropolitan curbside region. *Atmospheric Environment*, 337(May), 120773. <https://doi.org/10.1016/j.atmosenv.2024.120773>
- Ramírez, O., da Boit, K., Blanco, E., & Silva, L. F. O. (2020). Hazardous thoracic and ultrafine particles from road dust in a Caribbean industrial city. *Urban Climate*, 33(April), 100655. <https://doi.org/10.1016/j.uclim.2020.100655>
- Reche, C., Viana, M., Rivas, I., Bouso, L., Àlvarez-Pedrerol, M., Alastuey, A., Sunyer, J., & Querol, X. (2014). Outdoor and indoor UFP in primary schools across Barcelona. *Science of the Total Environment*, 493, 943–953. <https://doi.org/10.1016/j.scitotenv.2014.06.072>
- Rivas-Ubach, A., Liu, Y., Steiner, A. L., Sardans, J., Tfaily, M. M., Kulkarni, G., Kim, Y. M., Bourriane, E., Paša-Tolić, L., Peñuelas, J., & Guenther, A. (2019). Atmoscometabolomics: a novel atmospheric particle chemical characterization methodology for ecological research. *Environmental Monitoring and Assessment*, 191(2). <https://doi.org/10.1007/s10661-019-7205-x>
- Rivas, I., Viana, M., Moreno, T., Pandolfi, M., Amato, F., Reche, C., Bouso, L., Àlvarez-Pedrerol, M., Alastuey, A., Sunyer, J., & Querol, X. (2014). Child exposure to indoor and outdoor air pollutants in schools in Barcelona, Spain. *Environment International*, 69, 200–212. <https://doi.org/10.1016/j.envint.2014.04.009>
- Robock, A. (2000). Ice Eruptions. *Reviews of Geophysics*, 1998, 191–219.
- Rose, C., Collaud Coen, M., Andrews, E., Lin, Y., Bossert, I., Lund Myhre, C., Tuch, T., Wiedensohler, A., Fiebig, M., Aalto, P., Alastuey, A., Alonso-Blanco, E., Andrade, M., Artinano, B., Arsov, T., Baltensperger, U., Bastian, S., Bath, O., Beukes, J. P., ... Laj, P. (2021). Seasonality of the particle number concentration and size distribution: A global analysis retrieved from the network of Global Atmosphere Watch (GAW) near-surface observatories. *Atmospheric Chemistry and Physics*, 21(22), 17185–17223. <https://doi.org/10.5194/acp-21-17185-2021>

- Rossignol, S., Rio, C., Ustache, A., Fable, S., Nicolle, J., Môme, A., D'Anna, B., Nicolas, M., Leoz, E., & Chiappini, L. (2013). The use of a housecleaning product in an indoor environment leading to oxygenated polar compounds and SOA formation: Gas and particulate phase chemical characterization. *Atmospheric Environment*, 75, 196–205. <https://doi.org/10.1016/j.atmosenv.2013.03.045>
- Ruellan, S., & Cachier, H. (2001). Characterisation of fresh particulate vehicular exhausts near a Paris high flow road. *Atmospheric Environment*, 35(2), 453–468. [https://doi.org/10.1016/S1352-2310\(00\)00110-2](https://doi.org/10.1016/S1352-2310(00)00110-2)
- Saha, P. K., Robinson, E. S., Shah, R. U., Zimmerman, N., Apte, J. S., Robinson, A. L., & Presto, A. A. (2018). Reduced Ultrafine Particle Concentration in Urban Air: Changes in Nucleation and Anthropogenic Emissions. *Environmental Science and Technology*, 52(12), 6798–6806. <https://doi.org/10.1021/acs.est.8b00910>
- Şahin, Ü. A., Harrison, R. M., Alam, M. S., Beddows, D. C. S., Bousiotis, D., Shi, Z., Crilley, L. R., Bloss, W., Brean, J., Khanna, I., & Verma, R. (2022). Measurement report: Interpretation of wide-range particulate matter size distributions in Delhi. *Atmospheric Chemistry and Physics*, 22(8), 5415–5433. <https://doi.org/10.5194/acp-22-5415-2022>
- Sahu, S. K., Beig, G., & Parkhi, N. S. (2011). Emissions inventory of anthropogenic PM<sub>2.5</sub> and PM<sub>10</sub> in Delhi during Commonwealth Games 2010. *Atmospheric Environment*, 45(34), 6180–6190. <https://doi.org/10.1016/j.atmosenv.2011.08.014>
- Saliba, G., Chen, C. L., Lewis, S., Russell, L. M., Quinn, P. K., Bates, T. S., Bell, T. G., Lawler, M. J., Saltzman, E. S., Sanchez, K. J., Moore, R., Shook, M., Rivellini, L. H., Lee, A., Baetge, N., Carlson, C. A., & Behrenfeld, M. J. (2020). Seasonal Differences and Variability of Concentrations, Chemical Composition, and Cloud Condensation Nuclei of Marine Aerosol Over the North Atlantic. *Journal of Geophysical Research: Atmospheres*, 125(19), 1–24. <https://doi.org/10.1029/2020JD033145>
- Salthammer, T., Uhde, E., Schripp, T., Schieweck, A., Morawska, L., Mazaheri, M., Clifford, S., He, C., Buonanno, G., Querol, X., Viana, M., & Kumar, P. (2016). Children's well-being at schools: Impact of climatic conditions and air pollution.

- Environment International*, 94, 196–210.  
<https://doi.org/10.1016/j.envint.2016.05.009>
- Sarangi, B., Aggarwal, S. G., & Gupta, P. K. (2015). A simplified approach to calculate particle growth rate due to self-coagulation, scavenging and condensation using SMPS measurements during a particle growth event in New Delhi. *Aerosol and Air Quality Research*, 15(1), 166–179.  
<https://doi.org/10.4209/aaqr.2013.12.0350>
- Sarangi, B., Aggarwal, S. G., Kunwar, B., Kumar, S., Kaur, R., Sinha, D., Tiwari, S., & Kawamura, K. (2018). Nighttime particle growth observed during spring in New Delhi: Evidences for the aqueous phase oxidation of SO<sub>2</sub>. *Atmospheric Environment*, 188, 82–96. <https://doi.org/10.1016/j.atmosenv.2018.06.018>
- Sateesh, M., Soni, V. K., & Raju, P. V. S. (2018). Effect of Diwali Firecrackers on Air Quality and Aerosol Optical Properties over Mega City (Delhi) in India. *Earth Systems and Environment*, 2(2), 293–304. <https://doi.org/10.1007/s41748-018-0054-x>
- Saxena, P., Sonwani, S., Srivastava, A., Jain, M., Srivastava, A., Bharti, A., Rangra, D., Mongia, N., Tejan, S., & Bhardwaj, S. (2021). Impact of crop residue burning in Haryana on the air quality of Delhi, India. *Heliyon*, 7(5), e06973. <https://doi.org/10.1016/j.heliyon.2021.e06973>
- Schäfer, K., Thomas, W., Peters, A., Ries, L., Obleitner, F., Schnelle-Kreis, J., Birmili, W., Diemer, J., Fricke, W., Junkermann, W., Pitz, M., Emeis, S., Forkel, R., Suppan, P., Flentje, H., Gilge, S., Wichmann, H. E., Meinhardt, F., Zimmermann, R., ... Cyrys, J. (2011). Influences of the 2010 Eyjafjallajökull volcanic plume on air quality in the northern Alpine region. *Atmospheric Chemistry and Physics*, 11(16), 8555–8575. <https://doi.org/10.5194/acp-11-8555-2011>
- Schraufnagel, D. E. (2020). The health effects of ultrafine particles. *Experimental and Molecular Medicine*, 52(3), 311–317. <https://doi.org/10.1038/s12276-020-0403-3>
- Sebastian, M., Kanawade, V. P., Soni, V. K., Asmi, E., Westervelt, D. M., Vakkari, V., Hyvärinen, A. P., Pierce, J. R., & Hooda, R. K. (2021a). New Particle Formation and Growth to Climate-Relevant Aerosols at a Background Remote Site in the Western Himalaya. *Journal of Geophysical Research: Atmospheres*,

126(7). <https://doi.org/10.1029/2020JD033267>

- Sebastian, M., Kanawade, V. P., Soni, V. K., Asmi, E., Westervelt, D. M., Vakkari, V., Hyvärinen, A. P., Pierce, J. R., & Hooda, R. K. (2021b). New Particle Formation and Growth to Climate-Relevant Aerosols at a Background Remote Site in the Western Himalaya. *Journal of Geophysical Research: Atmospheres*, 126(7), 1–16. <https://doi.org/10.1029/2020JD033267>
- Sebastian, M., Kompalli, S. K., Kumar, V. A., Jose, S., Babu, S. S., Pandithurai, G., Singh, S., Hooda, R. K., Soni, V. K., Pierce, J. R., Vakkari, V., Asmi, E., Westervelt, D. M., Hyvärinen, A. P., & Kanawade, V. P. (2022). Observations of particle number size distributions and new particle formation in six Indian locations. *Atmospheric Chemistry and Physics*, 22(7), 4491–4508. <https://doi.org/10.5194/acp-22-4491-2022>
- Sharma, N. L., Kuniyal, J. C., Singh, M., Negi, A. K., Singh, K., & Sharma, P. (2009). Number concentration characteristics of ultrafine aerosols (atmospheric nanoparticles/aitken nuclei) during 2008 over western Himalayan region, Kullu-Manali, India. *Indian Journal of Radio and Space Physics*, 38(6), 326–337.
- Sharma, N. L., Kuniyal, J. C., Singh, M., Sharma, P., Chand, K., Negi, A. K., Sharma, M., & Thakur, H. K. (2011). Atmospheric ultrafine aerosol number concentration and its correlation with vehicular flow at two sites in the western Himalayan region: Kullu-Manali, India. *Journal of Earth System Science*, 120(2), 281–290. <https://doi.org/10.1007/s12040-011-0046-9>
- Sharma, P., Peshin, S. K., Soni, V. K., Singh, S., Beig, G., & Ghosh, C. (2022). Seasonal dynamics of particulate matter pollution and its dispersion in the city of Delhi, India. *Meteorology and Atmospheric Physics*, 134(2), 1–18. <https://doi.org/10.1007/s00703-021-00852-8>
- Shivani, Gadi, R., Saxena, M., Sharma, S. K., & Mandal, T. K. (2019). Short-term degradation of air quality during major firework events in Delhi, India. *Meteorology and Atmospheric Physics*, 131(4), 753–764. <https://doi.org/10.1007/s00703-018-0602-9>
- Siingh, D., Gautam, A. S., Buchunde, P. S., & Kamra, A. K. (2018). Classification of the new particle formation events observed at a tropical site, Pune, India. *Atmospheric Environment*, 190(January), 10–22.

<https://doi.org/10.1016/j.atmosenv.2018.07.025>

Siingh, D., Gautam, A. S., Kamra, A. K., & Komsaare, K. (2013). Nucleation events for the formation of charged aerosol particles at a tropical station - Preliminary results. *Atmospheric Research*, 132–133, 239–252. <https://doi.org/10.1016/j.atmosres.2013.05.024>

Silva, L. F. O., Hower, J. C., Izquierdo, M., & Querol, X. (2010). Complex nanominerals and ultrafine particles assemblages in phosphogypsum of the fertilizer industry and implications on human exposure. *Science of the Total Environment*, 408(21), 5117–5122. <https://doi.org/10.1016/j.scitotenv.2010.07.023>

Silva, L. F. O., Pinto, D., Neckel, A., Oliveira, M. L. S., & Sampaio, C. H. (2020). Atmospheric nanocompounds on Lanzarote Island: Vehicular exhaust and igneous geologic formation interactions. *Chemosphere*, 254, 126822. <https://doi.org/10.1016/j.chemosphere.2020.126822>

Singh, J., Gupta, P., Gupta, D., Verma, S., Prakash, D., & Payra, S. (2020). Fine particulate pollution and ambient air quality: A case study over an urban site in Delhi, India. *Journal of Earth System Science*, 129(1). <https://doi.org/10.1007/s12040-020-01495-w>

Sipilä, M., Sarnela, N., Neitola, K., Laitinen, T., Kemppainen, D., Beck, L., Duplissy, E. M., Kuittinen, S., Lehmusjärvi, T., Lampilahti, J., Kerminen, V. M., Lehtipalo, K., Aalto, P. P., Keronen, P., Siivola, E., Rantala, P. A., Worsnop, D. R., Kulmala, M., Jokinen, T., & Petäjä, T. (2021). Wintertime subarctic new particle formation from Kola Peninsula sulfur emissions. *Atmospheric Chemistry and Physics*, 21(23), 17559–17576. <https://doi.org/10.5194/acp-21-17559-2021>

Slezakova, K., de Oliveira Fernandes, E., & Pereira, M. do C. (2019). Assessment of ultrafine particles in primary schools: Emphasis on different indoor microenvironments. *Environmental Pollution*, 246, 885–895. <https://doi.org/10.1016/j.envpol.2018.12.073>

Solomon, P. A. (2019). *An Overview of Ultrafine*. May 2012.

Soppa, V. J., Shinnawi, S., Hennig, F., Sasse, B., Hellack, B., Kaminski, H., Quass, U., Schins, R. P. F., Kuhlbusch, T. A. J., & Hoffmann, B. (2019). Effects of short-term exposure to fine and ultrafine particles from indoor sources on arterial



- stiffness – A randomized sham-controlled exposure study. *International Journal of Hygiene and Environmental Health*, 222(8), 1115–1132. <https://doi.org/10.1016/j.ijheh.2019.08.002>
- Sörme, L., Bergbäck, B., & Lohm, U. (2001). Goods in the anthroposphere as a metal emission source. A case study of Stockholm, Sweden. *Water, Air, & Soil Pollution: Focus*, 1(3), 213–227. <http://dx.doi.org/10.1023/A:1017516523915>
- Srivastava, A. K., Tiwari, S., Devara, P. C. S., Bisht, D. S., Srivastava, M. K., Tripathi, S. N., Goloub, P., & Holben, B. N. (2011). Pre-monsoon aerosol characteristics over the Indo-Gangetic Basin: Implications to climatic impact. *Annales Geophysicae*, 29(5), 789–804. <https://doi.org/10.5194/angeo-29-789-2011>
- Stacey, B. (2019). Measurement of ultrafine particles at airports: A review. *Atmospheric Environment*, 198(July 2018), 463–477. <https://doi.org/10.1016/j.atmosenv.2018.10.041>
- Stohl, A., Berg, T., Burkhardt, J. F., Fjæraa, A. M., Forster, C., Herber, A., Hov, Lunder, C., McMillan, W. W., Oltmans, S., Shiobara, M., Simpson, D., Solberg, S., Stebel, K., Ström, J., Tørseth, K., Treffeisen, R., Virkkunen, K., & Yttri, K. E. (2007). Arctic smoke - Record high air pollution levels in the European Arctic due to agricultural fires in Eastern Europe in spring 2006. *Atmospheric Chemistry and Physics*, 7(2), 511–534. <https://doi.org/10.5194/acp-7-511-2007>
- Su, S., Lv, T., Lai, Y., Mu, J., Ge, Y., & Giechaskiel, B. (2021). Particulate emissions of heavy duty diesel engines measured from the tailpipe and the dilution tunnel. *Journal of Aerosol Science*, 156(March), 105799. <https://doi.org/10.1016/j.jaerosci.2021.105799>
- Sun, J., Birmili, W., Hermann, M., Tuch, T., Weinhold, K., Spindler, G., Schladitz, A., Bastian, S., Löschau, G., Cyrys, J., Gu, J., Flentje, H., Briel, B., Asbach, C., Kaminski, H., Ries, L., Sohmer, R., Gerwig, H., Wirtz, K., ... Wiedensohler, A. (2019). Variability of black carbon mass concentrations, sub-micrometer particle number concentrations and size distributions: results of the German Ultrafine Aerosol Network ranging from city street to High Alpine locations. *Atmospheric Environment*, 202(December 2018), 256–268. <https://doi.org/10.1016/j.atmosenv.2018.12.029>
- Takegawa, N., Murashima, Y., Fushimi, A., Misawa, K., Fujitani, Y., Saitoh, K., &

- Sakurai, H. (2021). Characteristics of sub-10 nm particle emissions from in-use commercial aircraft observed at Narita International Airport. *Atmospheric Chemistry and Physics*, 21(2), 1085–1104. <https://doi.org/10.5194/acp-21-1085-2021>
- Talukdar, S., Tripathi, S. N., Lalchandani, V., Rupakheti, M., Bhowmik, H. S., Shukla, A. K., Murari, V., Sahu, R., Jain, V., Tripathi, N., Dave, J., Rastogi, N., & Sahu, L. (2021). Air pollution in new delhi during late winter: An overview of a group of campaign studies focusing on composition and sources. *Atmosphere*, 12(11), 1–22. <https://doi.org/10.3390/atmos12111432>
- Tang, T., Hurraß, J., Gminski, R., & Mersch-Sundermann, V. (2012). Fine and ultrafine particles emitted from laser printers as indoor air contaminants in German offices. *Environmental Science and Pollution Research*, 19(9), 3840–3849. <https://doi.org/10.1007/s11356-011-0647-5>
- Teixeira, J., Sousa, G., Azevedo, R., Almeida, A., Delerue-Matos, C., Wang, X., Santos-Silva, A., Rodrigues, F., & Oliveira, M. (2024). Characterization of Wildland Firefighters' Exposure to Coarse, Fine, and Ultrafine Particles; Polycyclic Aromatic Hydrocarbons; and Metal(loid)s, and Estimation of Associated Health Risks. *Toxics*, 12(6), 1–22. <https://doi.org/10.3390/toxics12060422>
- Textor, C., Graf, H. F., Herzog, M., Oberhuber, J. M., Rose, W. I., & Ernst, G. G. J. (2006). Volcanic particle aggregation in explosive eruption columns. Part I: Parameterization of the microphysics of hydrometeors and ash. *Journal of Volcanology and Geothermal Research*, 150(4), 359–377. <https://doi.org/10.1016/j.jvolgeores.2005.09.007>
- Thén, W., & Salma, I. (2022). Particle Number Concentration: A Case Study for Air Quality Monitoring. *Atmosphere*, 13(4), 1–16. <https://doi.org/10.3390/atmos13040570>
- Tiotiu, A. I., Novakova, P., Nedeva, D., Chong-Neto, H. J., Novakova, S., Steiropoulos, P., & Kowal, K. (2020). Impact of air pollution on asthma outcomes. *International Journal of Environmental Research and Public Health*, 17(17), 1–29. <https://doi.org/10.3390/ijerph17176212>
- Tiwari, S., Pandithurai, G., Attri, S. D., Srivastava, A. K., Soni, V. K., Bisht, D. S.,

- Anil Kumar, V., & Srivastava, M. K. (2015). Aerosol optical properties and their relationship with meteorological parameters during wintertime in Delhi, India. *Atmospheric Research*, 153, 465–479. <https://doi.org/10.1016/j.atmosres.2014.10.003>
- Trechera, P., Garcia-Marlès, M., Liu, X., Reche, C., Pérez, N., Savadkoohi, M., Beddows, D., Salma, I., Vörösmarty, M., Casans, A., Casquero-Vera, J. A., Hueglin, C., Marchand, N., Chazeau, B., Gille, G., Kalkavouras, P., Mihalopoulos, N., Ondracek, J., Zikova, N., ... Querol, X. (2023). Phenomenology of ultrafine particle concentrations and size distribution across urban Europe. *Environment International*, 172(January). <https://doi.org/10.1016/j.envint.2023.107744>
- Trejos, E. M., Silva, L. F. O., Hower, J. C., Flores, E. M. M., González, C. M., Pachón, J. E., & Aristizábal, B. H. (2021). Volcanic emissions and atmospheric pollution: A study of nanoparticles. *Geoscience Frontiers*, 12(2), 746–755. <https://doi.org/10.1016/j.gsf.2020.08.013>
- Tremper, A. H., Jephcote, C., Gulliver, J., Hibbs, L., Green, D. C., Font, A., Priestman, M., Hansell, A. L., & Fuller, G. W. (2022). Sources of particle number concentration and noise near London Gatwick Airport. *Environment International*, 161(November 2021), 107092. <https://doi.org/10.1016/j.envint.2022.107092>
- Tu, J. (2023). *Determining emitted particle number size distributions in Helsinki from ambient measurements*. 64.
- Tuovinen, S., Kontkanen, J., Cai, R., & Kulmala, M. (2021). Condensation sink of atmospheric vapors: The effect of vapor properties and the resulting uncertainties. *Environmental Science: Atmospheres*, 1(7), 543–557. <https://doi.org/10.1039/d1ea00032b>
- Tyukavina, A., Potapov, P., Hansen, M. C., Pickens, A. H., Stehman, S. V., Turubanova, S., Parker, D., Zalles, V., Lima, A., Kommareddy, I., Song, X. P., Wang, L., & Harris, N. (2022). Global Trends of Forest Loss Due to Fire From 2001 to 2019. *Frontiers in Remote Sensing*, 3(March), 1–20. <https://doi.org/10.3389/frsen.2022.825190>
- Ubaid Ali, M., Liu, G., Yousaf, B., Ullah, H., Irshad, S., Ahmed, R., Hussain, M., &

- Rashid, A. (2019). Evaluation of floor-wise pollution status and deposition behavior of potentially toxic elements and nanoparticles in air conditioner dust during urbanistic development. *Journal of Hazardous Materials*, 365(July 2018), 186–195. <https://doi.org/10.1016/j.jhazmat.2018.11.005>
- Vaattovaara, P., Huttunen, P. E., Yoon, Y. J., Joutsensaari, J., Lehtinen, K. E. J., O'Dowd, C. D., & Laaksonen, A. (2006). The composition of nucleation and Aitken modes particles during coastal nucleation events: Evidence for marine secondary organic contribution. *Atmospheric Chemistry and Physics*, 6(12), 4601–4616. <https://doi.org/10.5194/acp-6-4601-2006>
- Vaghmaria, N., Mevada, N., & Maliakal, J. (2018). Impact of Diwali festival on aerosol optical properties over an Urban city, Ahmedabad (India). *Aerosol and Air Quality Research*, 18(2), 522–532. <https://doi.org/10.4209/aaqr.2017.04.0124>
- Van De Beek, E., Kerckhoffs, J., Hoek, G., Sterk, G., Meliefste, K., Gehring, U., & Vermeulen, R. (2021). Spatial and Spatiotemporal Variability of Regional Background Ultrafine Particle Concentrations in the Netherlands. *Environmental Science and Technology*, 55(2), 1067–1075. <https://doi.org/10.1021/acs.est.0c06806>
- Venn, A. J., Lewis, S. A., Cooper, M., Hubbard, R., & Britton, J. (2002). Living near a main road and the risk of wheezing illness in children. *American Journal of Respiratory and Critical Care Medicine*, 164(12), 2177–2180. <https://doi.org/10.1164/ajrccm.164.12.2106126>
- Viitanen, A. K., Uuksulainen, S., Koivisto, A. J., Hämeri, K., & Kauppinen, T. (2017). Workplace measurements of ultrafine particles-A literature review. *Annals of Work Exposures and Health*, 61(7), 749–758. <https://doi.org/10.1093/annweh/wxx049>
- Vörösmarty, M., Hopke, P. K., & Salma, I. (2024). Attribution of aerosol particle number size distributions to main sources using an 11-year urban dataset. *Atmospheric Chemistry and Physics*, 24(9), 5695–5712. <https://doi.org/10.5194/acp-24-5695-2024>
- Vu, T. V., Delgado-Saborit, J. M., & Harrison, R. M. (2015). Review: Particle number size distributions from seven major sources and implications for source

- apportionment studies. *Atmospheric Environment*, 122, 114–132. <https://doi.org/10.1016/j.atmosenv.2015.09.027>
- Wake, D., Mark, D., & Northage, C. (2002). Ultrafine aerosols in the workplace. *Annals of Occupational Hygiene*, 46, 235–238. <https://doi.org/10.1093/annhyg/46.suppl-1.235>
- Wallace, L. (2009). *Ultrafine Particles : A Review*. March, 1–116.
- Wallace, L., & Ott, W. (2011). Personal exposure to ultrafine particles. *Journal of Exposure Science and Environmental Epidemiology*, 21(1), 20–30. <https://doi.org/10.1038/jes.2009.59>
- Wang, D., Guo, H., & He, C. (2017). An investigation on particle emission from a new laser printer using an environmental chamber. *Indoor and Built Environment*, 26(8), 1144–1154. <https://doi.org/10.1177/1420326X16665160>
- Wang, K., Ma, X., Tian, R., & Yu, F. (2023). Analysis of new particle formation events and comparisons to simulations of particle number concentrations based on GEOS-Chem-advanced particle microphysics in Beijing, China. *Atmospheric Chemistry and Physics*, 23(7), 4091–4104. <https://doi.org/10.5194/acp-23-4091-2023>
- Wang, M., Xiao, M., Bertozzi, B., Marie, G., Rörup, B., Schulze, B., Bardakov, R., He, X. C., Shen, J., Scholz, W., Marten, R., Dada, L., Baalbaki, R., Lopez, B., Lamkaddam, H., Manninen, H. E., Amorim, A., Ataei, F., Bogert, P., ... Donahue, N. M. (2022). Synergistic HNO<sub>3</sub>–H<sub>2</sub>SO<sub>4</sub>–NH<sub>3</sub> upper tropospheric particle formation. *Nature*, 605(7910), 483–489. <https://doi.org/10.1038/s41586-022-04605-4>
- Wang, Q., Huo, J., Chen, H., Duan, Y., Fu, Q., Sun, Y., Zhang, K., Huang, L., Wang, Y., Tan, J., Li, L., Wang, L., Li, D., George, C., Mellouki, A., & Chen, J. (2023). Traffic, marine ships and nucleation as the main sources of ultrafine particles in suburban Shanghai, China. *Environmental Science: Atmospheres*, 3(12), 1805–1819. <https://doi.org/10.1039/d3ea00096f>
- Wang, Y., Henning, S., Poulain, L., Lu, C., Stratmann, F., Wang, Y., Niu, S., Pöhlker, M. L., Herrmann, H., & Wiedensohler, A. (2022). Aerosol activation characteristics and prediction at the central European ACTRIS research station of Melpitz, Germany. *Atmospheric Chemistry and Physics*, 22(24), 15943–15962.

<https://doi.org/10.5194/acp-22-15943-2022>

- Weichenthal, S., Dufresne, A., Infante-Rivard, C., & Joseph, L. (2007). Indoor ultrafine particle exposures and home heating systems: A cross-sectional survey of Canadian homes during the winter months. *Journal of Exposure Science and Environmental Epidemiology*, 17(3), 288–297. <https://doi.org/10.1038/sj.jes.7500534>
- Westerling, A. L., Hidalgo, H. G., Cayan, D. R., & Swetnam, T. W. (2006). Warming and earlier spring increase Western U.S. forest wildfire activity. *Science*, 313(5789), 940–943. <https://doi.org/10.1126/science.1128834>
- Westerling, A. L. R. (2016). Increasing western US forest wildfire activity: Sensitivity to changes in the timing of spring. *Philosophical Transactions of the Royal Society B: Biological Sciences*, 371(1696). <https://doi.org/10.1098/rstb.2015.0178>
- WHO. (2014). Health-related Millennium Development Goals. In *World Health Organization* (Vol. 1, Issue 22 Jan).
- WHO. (2016). WORLD HEALTH STATISTICS - MONITORING HEALTH FOR THE SDGs. *World Health Organization*, 1.121.
- WHO. (2020). Division of Country Health Policies and Systems, WHO Regional Office for Europe. *World Health Organization*. <http://apps.who.int/bookorders>.
- Wierzbicka, A., Bohgard, M., Pagels, J. H., Dahl, A., Löndahl, J., Hussein, T., Swietlicki, E., & Gudmundsson, A. (2015). Quantification of differences between occupancy and total monitoring periods for better assessment of exposure to particles in indoor environments. *Atmospheric Environment*, 106, 419–428. <https://doi.org/10.1016/j.atmosenv.2014.08.011>
- Won, S. R., Shim, I. K., Kwon, M., Ji, H. A., Park, K. soo, & Ghim, Y. S. (2020). Particle number size distributions generated by different Korean pork cooking methods. *Air Quality, Atmosphere and Health*, 13(7), 807–813. <https://doi.org/10.1007/s11869-020-00837-3>
- Wong, J. P. S., Tsagkaraki, M., Tsiodra, I., Mihalopoulos, N., Violaki, K., Kanakidou, M., Sciare, J., Nenes, A., & Weber, R. J. (2019). Atmospheric evolution of molecular-weight-separated brown carbon from biomass burning. *Atmospheric Chemistry and Physics*, 19(11), 7319–7334. <https://doi.org/10.5194/acp-19->

7319-2019

- Wu, T., & Boor, B. E. (2021). Urban aerosol size distributions: A global perspective. *Atmospheric Chemistry and Physics*, 21(11), 8883–8914. <https://doi.org/10.5194/acp-21-8883-2021>
- Xiao, M., Hoyle, C. R., Dada, L., Stolzenburg, D., Kürten, A., Wang, M., Lamkaddam, H., Garmash, O., Mentler, B., Molteni, U., Baccarini, A., Simon, M., He, X. C., Lehtipalo, K., Ahonen, L. R., Baalbaki, R., Bauer, P. S., Beck, L., Bell, D., ... Dommen, J. (2021). The driving factors of new particle formation and growth in the polluted boundary layer. *Atmospheric Chemistry and Physics*, 21(18), 14275–14291. <https://doi.org/10.5194/acp-21-14275-2021>
- Xiao, S., Wang, M. Y., Yao, L., Kulmala, M., Zhou, B., Yang, X., Chen, J. M., Wang, D. F., Fu, Q. Y., Worsnop, D. R., & Wang, L. (2015). Strong atmospheric new particle formation in winter in urban Shanghai, China. *Atmospheric Chemistry and Physics*, 15(4), 1769–1781. <https://doi.org/10.5194/acp-15-1769-2015>
- Yadav, R., Beig, G., & Jaaffrey, S. N. A. (2014). The linkages of anthropogenic emissions and meteorology in the rapid increase of particulate matter at a foothill city in the Arawali range of India. *Atmospheric Environment*, 85, 147–151. <https://doi.org/10.1016/j.atmosenv.2013.09.007>
- Yadav, R., Nagori, A., Mukherjee, A., Singh, V., Lodha, R., Kabra, S. K., Yadav, G., Saini, J. K., Singhal, K. K., Jat, K. R., Madan, K., George, M. P., Mani, K., Mrigpuri, P., Kumar, R., Guleria, R., Pandey, R. M., Sarin, R., & Dhaliwal, R. S. (2021). Effects of ambient air pollution on emergency room visits of children for acute respiratory symptoms in Delhi, India. *Environmental Science and Pollution Research*, 28(33), 45853–45866. <https://doi.org/10.1007/s11356-021-13600-7>
- Yadav, R., Sahu, L. K., Jaaffrey, S. N. A., & Beig, G. (2014). Temporal variation of Particulate Matter (PM) and potential sources at an urban site of Udaipur in Western India. *Aerosol and Air Quality Research*, 14(6), 1613–1629. <https://doi.org/10.4209/aaqr.2013.10.0310>
- Yadav, S. K., Kompalli, S. K., Gurjar, B. R., & Mishra, R. K. (2021). Aerosol number concentrations and new particle formation events over a polluted megacity during the COVID-19 lockdown. *Atmospheric Environment*, 259(May), 118526. <https://doi.org/10.1016/j.atmosenv.2021.118526>

- Yadav, S. K., Kumar, M., Sharma, Y., Shukla, P., Singh, R. S., & Banerjee, T. (2019). Temporal evolution of submicron particles during extreme fireworks. *Environmental Monitoring and Assessment*, 191(9). <https://doi.org/10.1007/s10661-019-7735-2>
- Yadav, S. K., Mishra, R. K., & Gurjar, B. R. (2022a). Assessment of the effect of the judicial prohibition on firecracker celebration at the Diwali festival on air quality in Delhi, India. *Environmental Science and Pollution Research*, 29(57), 86247–86259. <https://doi.org/10.1007/s11356-021-17695-w>
- Yadav, S. K., Mishra, R. K., & Gurjar, B. R. (2022b). Fireworks induced quasi-ultrafine particle number concentration and size-resolved elemental distribution in megacity Delhi. *Arabian Journal of Geosciences*, 15(1), 1–13. <https://doi.org/10.1007/s12517-021-09385-1>
- Yadav, S. K., Mishra, R. K., & Gurjar, B. R. (2022c). Ultrafine particle number concentration and its size distribution during Diwali festival in megacity Delhi, India: Are ‘green crackers’ safe? *Journal of Environmental Management*, 317(July 2021), 115459. <https://doi.org/10.1016/j.jenvman.2022.115459>
- Yadav, S. K., Sharma, R., Kumar, S., Agarwal, A., Mohan, V., Mishra, R. K., & Shukla, A. (2021). Urban air pollution reduction: evidence from phase-wise analysis of COVID-19 pandemic lockdown. *Arabian Journal of Geosciences*, 14(14). <https://doi.org/10.1007/s12517-021-07777-x>
- Yang, S., Lau, W. K. M., Ji, Z., Dong, W., & Yang, S. (2022). Impacts of radiative effect of pre-monsoon biomass burning aerosols on atmospheric circulation and rainfall over Southeast Asia and southern China. *Climate Dynamics*, 59(1–2), 417–432. <https://doi.org/10.1007/s00382-021-06135-7>
- Yang, Z., He, Z., Zhang, K., Zeng, L., & de Nazelle, A. (2021). Investigation into Beijing commuters’ exposure to ultrafine particles in four transportation modes: bus, car, bicycle and subway. *Atmospheric Environment*, 266(August), 118734. <https://doi.org/10.1016/j.atmosenv.2021.118734>
- Yao, L., Garmash, O., Bianchi, F., Zheng, J., Yan, C., Kontkanen, J., Junninen, H., Mazon, S. B., Ehn, M., Paasonen, P., Sipilä, M., Wang, M., Wang, X., Xiao, S., Chen, H., Lu, Y., Zhang, B., Wang, D., Fu, Q., ... Wang, L. (2018). Atmospheric new particle formation from sulfuric acid and amines in a Chinese megacity.



- Science*, 361(6399), 278–281. <https://doi.org/10.1126/science.aao4839>
- Yerramsetti, V. S., Sharma, A. R., Gauravarapu Navlur, N., Rapolu, V., Dhulipala, N. S. K. C., & Sinha, P. R. (2013). The impact assessment of Diwali fireworks emissions on the air quality of a tropical urban site, Hyderabad, India, during three consecutive years. *Environmental Monitoring and Assessment*, 185(9), 7309–7325. <https://doi.org/10.1007/s10661-013-3102-x>
- Yu, F., Luo, G., Arjunan Nair, A., Schwab, J. J., Sherman, J. P., & Zhang, Y. (2020). Wintertime new particle formation and its contribution to cloud condensation nuclei in the Northeastern United States. *Atmospheric Chemistry and Physics*, 20(4), 2591–2601. <https://doi.org/10.5194/acp-20-2591-2020>
- Yu, H., Ren, L., & Kanawade, V. P. (2017). New Particle Formation and Growth Mechanisms in Highly Polluted Environments. *Current Pollution Reports*, 3(4), 245–253. <https://doi.org/10.1007/s40726-017-0067-3>
- Yuan, Q., Yang, L., Dong, C., Yan, C., Meng, C., Sui, X., & Wang, W. (2015). Particle physical characterisation in the Yellow River Delta of Eastern China: number size distribution and new particle formation. *Air Quality, Atmosphere and Health*, 8(5), 441–452. <https://doi.org/10.1007/s11869-014-0293-4>
- Yue, D. L., Hu, M., Zhang, R. Y., Wu, Z. J., Su, H., Wang, Z. B., Peng, J. F., He, L. Y., Huang, X. F., Gong, Y. G., & Wiedensohler, A. (2011). Potential contribution of new particle formation to cloud condensation nuclei in Beijing. *Atmospheric Environment*, 45(33), 6070–6077. <https://doi.org/10.1016/j.atmosenv.2011.07.037>
- Yusuf, A. A., Yahyah, H., Farooq, A. A., Buyondo, K. A., Olupot, P. W., Nura, S. S., Sanni, T., Hannington, T., Ukundimana, Z., Hassan, A. S., Mundu, M. M., Samede, S. S., Makeri, Y. A., & Selvam, M. D. (2021). Characteristics of ultrafine particle emission from light-vehicle engine at city transport-speed using after-treatment device fueled with n-butanol-hydrogen blend. *Case Studies in Chemical and Environmental Engineering*, 3(January), 100085. <https://doi.org/10.1016/j.cscee.2021.100085>
- Zauli Sajani, S., Ricciardelli, I., Trentini, A., Bacco, D., Maccone, C., Castellazzi, S., Lauriola, P., Poluzzi, V., & Harrison, R. M. (2015). Spatial and indoor/outdoor gradients in urban concentrations of ultrafine particles and PM<sub>2.5</sub> mass and

- chemical components. *Atmospheric Environment*, 103, 307–320. <https://doi.org/10.1016/j.atmosenv.2014.12.064>
- Zhang, Q., Gangupomu, R. H., Ramirez, D., & Zhu, Y. (2010). Measurement of ultrafine particles and other air pollutants emitted by cooking activities. *International Journal of Environmental Research and Public Health*, 7(4), 1744–1759. <https://doi.org/10.3390/ijerph7041744>
- Zhang, T., Zhu, Z., Gong, W., Xiang, H., & Fang, R. (2016). Characteristics of fine particles in an urban atmosphere—relationships with meteorological parameters and trace gases. *International Journal of Environmental Research and Public Health*, 13(8), 1–16. <https://doi.org/10.3390/ijerph13080807>
- Zhang, T., Zhu, Z., Gong, W., Xiang, H., Li, Y., & Cui, Z. (2016). Characteristics of ultrafine particles and their relationships with meteorological factors and trace gases in Wuhan, Central China. *Atmosphere*, 7(8). <https://doi.org/10.3390/atmos7080096>
- Zhang, Y., Du, W., Wang, Y., Wang, Q., Wang, H., Zheng, H., Zhang, F., Shi, H., Bian, Y., Han, Y., Fu, P., Canonaco, F., Prévôt, A. S. H., Zhu, T., Wang, P., Li, Z., & Sun, Y. (2018). Aerosol chemistry and particle growth events at an urban downwind site in North China Plain. *Atmospheric Chemistry and Physics*, 18(19), 14637–14651. <https://doi.org/10.5194/acp-18-14637-2018>
- Zhang, Y. L., & Cao, F. (2015). Fine particulate matter (PM 2.5) in China at a city level. *Scientific Reports*, 5(2014), 1–12. <https://doi.org/10.1038/srep14884>
- Zhao, B., Fast, J. D., Donahue, N. M., Shrivastava, M., Schervish, M., Shilling, J. E., Gordon, H., Wang, J., Gao, Y., Zaveri, R. A., Liu, Y., & Gaudet, B. (2021). Impact of Urban Pollution on Organic-Mediated New-Particle Formation and Particle Number Concentration in the Amazon Rainforest. *Environmental Science and Technology*, 55(8), 4357–4367. <https://doi.org/10.1021/acs.est.0c07465>
- Zhao, J., Birmili, W., Hussein, T., Wehner, B., & Wiedensohler, A. (2021). Particle number emission rates of aerosol sources in 40 German households and their contributions to ultrafine and fine particle exposure. *Indoor Air*, 31(3), 818–831. <https://doi.org/10.1111/ina.12773>
- Zhao, J., Birmili, W., Wehner, B., Daniels, A., Weinhold, K., Wang, L., Merkel, M.,

- Kecorius, S., Tuch, T., Franck, U., Hussein, T., & Wiedensohler, A. (2020). Particle mass concentrations and number size distributions in 40 homes in germany: Indoor-to-outdoor relationships, diurnal and seasonal variation. *Aerosol and Air Quality Research*, 20(3), 576–589. <https://doi.org/10.4209/aaqr.2019.09.0444>
- Zhao, Y., Wang, F., & Zhao, J. (2015). Size-Resolved Ultrafine Particle Deposition and Brownian Coagulation from Gasoline Vehicle Exhaust in an Environmental Test Chamber. *Environmental Science and Technology*, 49(20), 12153–12160. <https://doi.org/10.1021/acs.est.5b02455>
- Zheng, T., Wang, H. W., Li, X. B., Peng, Z. R., & He, H. Di. (2021). Impacts of traffic on roadside particle variations in varied temporal scales. *Atmospheric Environment*, 253(October 2020), 118354. <https://doi.org/10.1016/j.atmosenv.2021.118354>
- Zhou, Y., Dada, L., Liu, Y., Fu, Y., Kangasluoma, J., Chan, T., Yan, C., Chu, B., Daellenbach, K. R., Bianchi, F., Kokkonen, T. V., Liu, Y., Kujansuu, J., Kerminen, V. M., Petäjä, T., Wang, L., Jiang, J., & Kulmala, M. (2020). Variation of size-segregated particle number concentrations in wintertime Beijing. *Atmospheric Chemistry and Physics*, 20(2), 1201–1216. <https://doi.org/10.5194/acp-20-1201-2020>
- Zhu, A., Xu, H., Deng, J., Ma, J., & Hua, S. (2022). Instant and delayed effects of March biomass burning aerosols over the Indochina Peninsula. *Atmospheric Chemistry and Physics*, 22(23), 15425–15447. <https://doi.org/10.5194/acp-22-15425-2022>
- Zhu, Y., Hinds, W. C., Kim, S., Shen, S., & Sioutas, C. (2002). Study of ultrafine particles near a major highway with heavy-duty diesel traffic. *Atmospheric Environment*, 36(27), 4323–4335. [https://doi.org/10.1016/S1352-2310\(02\)00354-0](https://doi.org/10.1016/S1352-2310(02)00354-0)
- Zhu, Y., Hinds, W. C., Shen, S., & Sioutas, C. (2004). Seasonal trends of concentration and size distribution of ultrafine particles near major highways in Los Angeles. *Aerosol Science and Technology*, 38(SUPPL. 1), 5–13. <https://doi.org/10.1080/02786820390229156>
- Zhu, Y., Kuhn, T., Mayo, P., & Hinds, W. C. (2006). Comparison of daytime and

nighttime concentration profiles and size distributions of ultrafine particles near a major highway. *Environmental Science and Technology*, 40(8), 2531–2536.  
<https://doi.org/10.1021/es0516514>

Zimmerman, A., Petters, M. D., & Meskhidze, N. (2020). Observations of new particle formation, modal growth rates, and direct emissions of sub-10 nm particles in an urban environment. *Atmospheric Environment*, 242(August), 117835.  
<https://doi.org/10.1016/j.atmosenv.2020.117835>

**VIGNESH.M,**  
S/O B. MOHAN,  
5/133, Kilcowhatty Village,  
Muthorai Post,  
The Nilgiri's - 643 004.  
Mobile no: +91-9894796137.



E-Mail ID: [vikiviki93@gmail.com](mailto:vikiviki93@gmail.com)

### **EXECUTIVE SUMMARY**

Pursuing Ph.D. in the Department of Environmental Engineering at Delhi Technological University, Delhi, India, since 25<sup>th</sup> August 2020.

### **OBJECTIVE**

Seeking a challenging position in the field of Engineering and Research with an organization of repute, where I can utilize my skills and enhance my knowledge to add value and grow with the organization.

### **EDUCATIONAL QUALIFICATIONS**

<b>Academic Qualification</b>	<b>Institution</b>	<b>Percentage Obtained</b>	<b>Year of Passing</b>
Ph.D. (Environmental Engineering)	Delhi Technological University, Delhi.	-	Thesis submitted
M.E (Environmental Engineering)	Erode Sengunthar Engineering College, Thudupathi.	81%	2017
B.E (Environmental Engineering)	Park College of Technology, Coimbatore.	63.5%	2015
HSLC	St.Joseph's Higher Secondary School, Ooty.	66.5%	2011
SSLC	Government Higher Secondary School, Karuvalur.	68%	2009

Ph.D. Thesis title “A COMPARATIVE STUDY ON SIZE SEGREGATED ULTRAFINE PARTICLE CONCENTRATION AND ITS TEMPORAL DISTRIBUTION IN URBAN AND BACKGROUND REGIONS”.

### **LIST OF PUBLICATIONS**

#### **International Journals**

- (1) Kanagaraj Rajagopal, **Vignesh Mohan**, Monika Sharma, Shailendra Kumar Yadav, Veerendra Sahu, Rajeev Kumar Mishra, Sneha Gautam, Bhola Ram Gurjar & Prashant Kumar (2025). “Impact of the odd-even scheme on particulate matter reduction in Delhi traffic intersections”. Particulate Science and Technology. <https://doi.org/10.1080/02726351.2025.2558979>.
- (2) **Vignesh Mohan**, Rajeev Kumar Mishra, Vijay Kumar Soni (2024). “Air Quality Analysis in Desert Region in the Northern State of India: GIS Based Approach”. Journal of the Indian Society of Remote Sensing. <https://doi.org/10.1007/s12524-024-02073-z>.
- (3) **Vignesh Mohan**, Vijay Kumar Soni, Rajeev Kumar Mishra (2024). “Geographical variability of ultrafine particle concentrations in urban and background regions in India”. Urban Climate. <https://doi.org/10.1016/j.uclim.2024.102066>.
- (4) Kanagaraj Rajagopal, **Vignesh Mohan**, Rajeev Kumar Mishra (2024). “Are Delhi residents exposed to lesser particle number concentration due to the firework ban in the city?”. Air Quality, Atmosphere & Health. <https://doi.org/10.1007/s11869-024-01532-3>.
- (5) **Vignesh Mohan**, Vijay Kumar Soni, Rajeev Kumar Mishra (2024). “Analysing the impact of day-night road traffic variation on ultrafine particle number size distribution and concentration at an urban site in the megacity Delhi”. Atmospheric Pollution Research. <https://doi.org/10.1016/j.apr.2024.102065>.
- (6) **Vignesh Mohan**, Rajeev Kumar Mishra (2022). “A picture of Delhi’s regional air quality during diminished anthropogenic activities in the COVID era”. Arabian Journal of Geosciences. <https://doi.org/10.1007/s12517-022-10567-8>.
- (7) Shailendra Kumar Yadav, Raghav Sharma, Sankalp Kumar, Aviral Agarwal, **Vignesh Mohan**, Rajeev Kumar Mishra, Ankita Shukla (2021). “Urban air pollution reduction: evidence from phase-wise analysis of COVID-19 pandemic lockdown”. Arabian Journal of Geosciences. <https://doi.org/10.1007/s12517-021-07777-x>.

## **PROCEEDINGS**

(1) **Vignesh Mohan**, Rajeev Kumar Mishra, and Vijay Kumar Soni. "Seasonal and Temporal Distribution of Urban Fine Particulates and Associated Health Risk Analysis: A Long-Term Measurement (2018-2020) Analysis in Megacity Delhi". Select Proceedings of the 8th Indian International Conference on Air Quality Management (IICAQM 2023). [https://doi.org/10.1007/978-981-96-2359-4\\_15](https://doi.org/10.1007/978-981-96-2359-4_15).

## **THRUST AREAS OF RESEARCH**

1. Ultrafine Particles
2. New Particle Formation
3. Climate Change
4. Health Risk Assessment
5. Air Quality Modelling
6. Urban Air Pollution Monitoring

## **EXPERIENCE**

- (1) I have worked on the Project entitled **"Air Quality, Sustainable Cities & Transport"** as an intern at the World Resources Institute (WRI).
- (2) I have worked on the Project entitled **"Proxy Relationship of Ultrafine Particles Number Concentration, New Particle Formation and Its Growth Rate in Transport Microenvironment in Delhi"** funded by the Central Pollution Control Board (CPCB).
- (3) I have worked on the Project entitled **"Air Pollution Study during Odd-Even Scheme in Delhi"** funded by Delhi Technological University (DTU).
- (4) I have worked at **Vocon Manufacturing Private Limited**.
- (5) I worked on Air and Noise pollution monitoring during Diwali, organized by the **Tamil Nadu Pollution Control Board (TNPCB)**, Coimbatore.

## **ACADEMIC ACTIVITIES/SEMINAR**

- (1) Participated in the online training program on **"Indoor Air Pollution and its Effect on Women and Children's Health in India"** on 27 Sep 2021, organized by the **National Institute of Disaster Management, Ministry of Home Affairs, Govt. of India**, in collaboration with **WRI India**.
- (2) Participated in a national-level technical mini project contest cum science expo in TRP Engineering College, Trichy.

(3) Activities on the **Greenz Association** function held at Park College of Technology.

(4) I attended the seminar on **Carbon Sequestration and Global Climate Change** held at **Park College of Technology**.

(5) I attended the seminar on Industrial Symbiosis: **How to Conduct the IS Research in India**, funded by USAID under the PEER-PIRE project PP26, held at Park College of Technology

### **STRENGTHS AND SKILLS**

Well acquainted with software like

- R-Software
- Matlab Software
- Origin Pro
- GIS
- Python
- Technical skills in air and noise monitoring
- Modelling

**(VIGNESH M)**